

---

# **Functional Stability of Plant Peroxioredoxins**

---

## **Dissertation**

Zur Erlangung des Akademischen Grades  
Doktor der Naturwissenschaften (Dr. rer. nat.)

Fakultät für Biologie  
Universität Bielefeld

vorgelegt von  
**Simone Jacob**  
aus Rinteln

## Table of contents

Summary	I
Zusammenfassung	III
Abbreviations	V
<b>1. Introduction</b>	<b>1</b>
1.1. Reactive oxygen and nitrogen species – mechanisms and sites of ROS and RNS generation	1
1.1.1. Reactive oxygen species (ROS) and reactive nitrogen species (RNS)	1
1.1.2. ROS and RNS are generated at different subcellular sites	4
1.1.3. Consequences of ROS and RNS formation	6
1.2. Detoxification of ROS – the antioxidative network in plants	8
1.2.1. Non-enzymatic antioxidants	9
1.2.2. Enzymatic antioxidants	11
1.3. Peroxiredoxins	12
1.3.1. Peroxiredoxins in plants	14
1.3.2. Type II peroxiredoxins	18
1.3.3. 2-Cysteine peroxiredoxins	19
1.3.4. Structural analyses of peroxiredoxins	21
1.4. Aims of this work	22
<b>2. Materials and Methods</b>	<b>24</b>
2.1. Plant growth and material	24
2.1.1. Plant material	24
2.1.2. Plant growth	24
2.1.2.1. Soil culture	24
2.1.2.2. MS plates	24
2.1.2.3. Sterilisation of seeds	25
2.1.3. Stress experiments	25
2.1.3.1. Ion leakage measurements	26
2.2. Molecular biological methods	26
2.2.1. Isolation of genomic DNA	26
2.2.2. RNA isolation and cDNA synthesis	27
2.2.3. Polymerase chain reaction (PCR)	28
2.2.3.1. Genomic PCR for identification of homozygous T-DNA insertion lines	29
2.2.3.2. Semi quantitative RT-PCR	30
2.2.3.3. Phusion PCR	30
2.2.3.4. Site directed mutagenesis	31
2.2.4. Agarose gel electrophoresis	32
2.2.5. Cloning and transformation into <i>E. coli</i>	33
2.2.5.1. Introduction of restriction sites	33
2.2.5.2. Purification of amplified DNA fragments by agarose gel electrophoresis	33
2.2.5.3. Digestion of DNA fragments	34
2.2.5.4. Ligation	35
2.2.5.5. TOPO cloning	35
2.2.5.6. Transformation of bacterial strains	35
2.2.5.7. LB medium and agar plates	36

2.2.5.8.	Colony PCR	36
2.2.5.9.	Overnight cultures and glycerol stock solutions of bacteria cultures	37
2.2.5.10.	Isolation of plasmids	37
2.2.5.11.	Analytical digestion	38
2.2.5.12.	Sequencing	38
2.3.	Protein biochemical methods	39
2.3.1.	Heterologous expression in <i>E. coli</i> and purification of recombinant protein	39
2.3.1.1.	Expression in <i>E. coli</i> M15 or BL21	39
2.3.1.2.	Purification of recombinant protein	39
2.3.2.	Protein extraction from <i>A. thaliana</i> plant material	40
2.3.3.	Quantification of protein content with the BioRad protein assay	41
2.3.4.	SDS polyacrylamide gel electrophoresis	41
2.3.5.	Coomassie staining of polyacrylamide (PAA) gels	42
2.3.6.	Silver staining of polyacrylamide gels	42
2.3.7.	Storage and drying of PAA-gels	43
2.3.8.	Detection of proteins by Western blot analysis	43
2.3.8.1.	Transfer of proteins onto a nitrocellulose membrane	43
2.3.8.2.	Dot Blot analysis	44
2.3.8.3.	Ponceau S staining	44
2.3.8.4.	Immunodetection of immobilised proteins with specific antibodies	44
2.3.8.5.	Detection of proteins with chemiluminescence	45
2.3.8.6.	Protein detection with NBT/BCIP staining	45
2.3.8.7.	‘Stripping’ of nitrocellulose membranes	46
2.3.9.	In-gel tryptic digest and mass spectrometric analysis	46
2.3.10.	Oxidation and overoxidation of 2-Cys Prx	47
2.4.	Biochemical methods	47
2.4.1.	Thioredoxin dependent peroxiredoxin activity assay	47
2.4.2.	Peroxiredoxin activity assay with xylenol orange assay	47
2.4.3.	DNA cleavage assay	48
2.5.	Surface plasmon resonance	49
2.6.	Labelling of protein cysteinyl variants with gold colloids	49
3.	<b>Results and Discussion</b>	51
3.1.	Establishment of <i>Arabidopsis thaliana</i> 2-cysteine peroxiredoxin A as a model protein for time-resolved dynamical x-ray imaging – modifications and prerequisites to enable visualisation of conformational changes	51
3.1.1.	Design and generation of functional 2-Cys Prx cysteinyl variants	53
3.1.1.1.	Generation of different 2-Cys Prx cysteinyl variants	53
3.1.1.2.	Generation of 2-Cys Prx cysteinyl variants – optimisation of expression and purification	57
3.1.1.3.	2-Cys Prx cysteinyl variants show functionality in spite of exchanged amino acids	60
3.1.2.	His-tagging of 2-Cys Prx enables long-term immobilisation on Ni-NTA surface	62
3.1.3.	Binding of gold colloids to 2-Cys Prx cysteinyl variants	64
3.1.3.1.	Conjugation of 15 nm gold crystals to 2-Cys Prx variant Lys174	65
3.1.3.2.	Gold-labelling of different 2-Cys Prx variants with 5 nm gold colloids	66
3.1.3.3.	Gold labelling of 2-Cys Prx variants – optimisation of conditions improves binding specificity	68

3.1.4.	Characterisation of x-ray induced damage to 2-Cys Prx conformation and function	73
3.1.4.1.	Short term irradiation had no impact on 2-Cys Prx amount and functionality	73
3.1.4.2.	Long time irradiation revealed partial modification of 2-Cys Prx aggregation pattern	76
3.1.4.3.	Inhibition of 2-Cys Prx functions upon long term irradiation	84
3.1.4.4.	Augmented x-ray damage on structural and functional features of 2-Cys Prx in presence of gold colloids	89
3.1.4.5.	Long term irradiation in presence of scavengers exhibited a decrease of irradiation induced damage especially on structural level	96
3.1.4.6.	Conclusion on damage development during x-ray treatment of 2-Cys Prx	100
3.1.5.	Establishment of 2-Cys Prx as a model protein for dynamical x-ray imaging: concluding remarks	101
3.2.	Biochemical characterisation of cytosolic PrxII B and PrxII C and their differentiation	102
3.2.1.	Peroxide detoxification by PrxII B and PrxII C	102
3.2.2.	Determination of crucial catalytic parameters of PrxII B and PrxII C – maximum velocity ( $v_{\max}$ ) and the Michaelis-Menten constant ( $K_M$ )	103
3.2.3.	Substrate specificity of PrxII B and PrxII C	108
3.2.4.	Search for <i>in vivo</i> regenerators of PrxII B and PrxII C	111
3.2.5.	Differential regulation of PrxII B and PrxII C transcript levels	113
3.2.6.	Future perspectives	117
4.	<b>Literatur</b>	120

## Appendices

- Appendix A
- Appendix B
- Appendix C

## Summary

In their natural environment plants are exposed to a multitude of external influences resulting in the disturbance of metabolic processes which may elicit redox imbalances and electron transfer reactions to molecular oxygen. The resulting generation of reactive oxygen species (ROS) represents an oxidative threat to the cell. An elaborated network of antioxidants counteracts the development of oxidative stress. A very tight control of ROS is also important in context of their additional signalling role in a variety of plant functions. One component of this complex system are the peroxiredoxins (Prx), a ubiquitous superfamily of peroxidases, with members of the subgroups of 2-Cys Prx and type II Prx being in focus of the present work.

A comparative characterisation of cytosolic PrxII B and PrxII C was performed in order to get insight into the functional stability and the biochemical differences between these highly homologous isoforms. In comparison to other Prxs, both cytosolic isoforms, especially PrxII C, exhibited remarkably high reaction velocities for conversion of peroxides with dithiothreitol (DTT) as artificial electron donor. The relative turnover of various substrates revealed preference towards small peroxides, a characteristic that was more pronounced for PrxII B with exclusive conversion of hydrogen peroxide (H<sub>2</sub>O<sub>2</sub>) and tertiary butylhydroperoxide (t-BOOH). The employment of different regeneration systems resulted in activities of PrxII B and PrxII C in presence of thioredoxin (Trx) and glutaredoxin (Grx). *In vitro*, Trx enabled higher activity of PrxII B than of PrxII C, whereas Grx-dependent peroxidase function was more enhanced with PrxII C. The cytosolic Grx CxxC4 allowed for the regeneration of both Prxs but not the cytosolic Grx CxxC10 or two chloroplastidic Grxs. A bioinformatic analysis also indicated a relationship between both components of the thiol-disulfide redox network since PrxII B and PrxII C/D transcripts were co-regulated with those of specific members of these protein families. Moreover, the differentiation of both cytosolic isoforms could be substantiated by means of an additional *in silico* analysis of publicly available expression data. The comparison of transcript regulation during different developmental states, in various organs and tissues as well as in dependence of a multitude of exogenous stimuli revealed differential regulation patterns for PrxII B and PrxII C/D.

The impairment of functional stability, which was observed during concentration-dependent measurements of the cytosolic type II Prx activities, might tentatively be interpreted to indicate a function of PrxII B and PrxII C in signal transduction. The inhibition of catalytic activity is hypothesised to be due to overoxidation and provides for a regulatory mechanism to control the high peroxidatic potential of PrxII B and

PrxII C. Consequently, this redox-dependent modulation might allow for a function as peroxide sensor and therefore facilitates signals via influencing levels of ROS.

Besides a functional characterisation of Prxs, it is important for a mechanistic understanding of catalytic functions to determine structural properties with a special focus on analysis of conformational dynamics and involved transition steps. In this context dynamical imaging via diffracted x-ray tracking (DXT) provides a new tool to investigate the complex conformational changes with high spatial and time resolution. The chloroplastidic 2-Cys Prx undergoes the necessary structural alterations that are important for its proper functionality. To establish a protein for dynamical imaging via x-ray dependent techniques, various prerequisites have to be fulfilled. Their analysis was the subject of the present work. Particular attention was given to the characterisation of functional stability of 2-Cys Prx upon x-ray treatment.

In this context, amino acid variants of 2-Cys Prx were generated by site-directed mutagenesis. The modified but still functional proteins on the one hand enabled the stable immobilisation on a Ni-NTA surface by its N-terminally fused His-tag as visualised by surface plasmon resonance (SPR). On the other hand, a stable interaction of gold-nanocrystals with introduced thiol-groups of the variants was investigated as another necessity to visualise conformational changes via DXT. The specificity of binding events could be considerably increased by supplementing the binding reaction buffer with additives. The supplements minimised the unspecific hydrophobic interactions significantly. As another very important aspect, irradiation impacts on different biochemical properties of 2-Cys Prx were characterised. Besides a dose-dependency of the occurring impairments, two different amino acids could be tentatively assigned as primary sites of damage. Tyrosine residues can be hypothesised to be responsible for structural impairments that were manifested by formation of higher molecular aggregates at the expense of monomeric 2-Cys Prx. In contrast, impacts on functional features as peroxidase activity and DNA protection from ROS-mediated cleavage were likely due to modification of cysteinyl residues. Overall, the 2-Cys Prx exhibited a remarkably high stability to x-ray treatment. These characteristics underlined its suitability as candidate to be used for dynamical imaging via DXT. Furthermore, radiation-mediated damaging effects could be alleviated by adding scavenging molecules.

## Zusammenfassung

Pflanzen sind in ihrer natürlichen Umgebung einer Vielzahl von biotischen und abiotischen Einflüssen ausgesetzt, die zu einer Störung ihres Metabolismus führen und ihre „Fitness“ beeinträchtigen können. Damit einhergehende metabolische Redox-Ungleichgewichte sowie die Übertragung von Elektronen auf molekularen Sauerstoff führen zu einer vermehrten Bildung reaktiver Sauerstoffspezies (ROS). Der resultierende oxidative Stress stellt eine Bedrohung für die Funktionalität der Zelle dar und erfordert ein umfangreiches Netzwerk an Antioxidantien, die den schädigenden Einflüssen entgegenwirken. Eine effiziente Kontrolle der ROS-Konzentrationen ist darüber hinaus von besonderer Bedeutung, da diese Moleküle ebenfalls eine Rolle in zellulären Signalgebungsprozessen spielen und ihnen in diesem Zusammenhang regulatorische Funktionen in verschiedensten Stoffwechselwegen *in planta* zugewiesen werden konnten. Ein wichtiger Bestandteil des antioxidativen Systems sind die Peroxiredoxine (Prx) als eine Familie ubiquitär vorkommender Peroxidasen.

Mitglieder zweier Untergruppen, der 2-Cys Prx-e und Typ II Prx-e, stehen im Fokus dieser Arbeit. Hierbei wurde eine vergleichende Charakterisierung der cytosolischen PrxII B und PrxII C durchgeführt, um Einblicke in ihre funktionale Stabilität zu erhalten sowie um eine biochemische Unterscheidung zwischen diesen sehr homologen Isoformen zu erreichen. Verglichen mit anderen Prx-en wiesen beide Peroxidasen, insbesondere das PrxII C, für Prx-e außergewöhnlich hohe Reaktionsgeschwindigkeiten beim Umsatz von Peroxidsubstraten mit Dithiothreitol (DTT) als artifiziellem Elektronendonator auf. Der Umsatz verschiedener Substrate zeigte eine Spezifität beider Prx-e für einfache Peroxide, die im Fall von PrxII B ein sehr eingeschränktes Spektrum von lediglich Wasserstoffperoxid ( $H_2O_2$ ) und tertiärem Butylhydroperoxid (t-BOOH) aufwies. Beide Prx-e zeigten enzymatische Aktivität in Gegenwart von Thioredoxin (Trx) und Glutaredoxin (Grx). In *in vitro*-Analysen erwies sich *E. coli*-TrxA als ein effizienterer Elektronendonator für PrxII B als für PrxII C, wohingegen die Grx-abhängige Peroxidasefunktion für PrxII C höher war. Allerdings konnte lediglich für das cytosolische Grx CxxC4 eine Regeneration der untersuchten Prx-e gezeigt werden, nicht aber für das Grx CxxC10 als weiterem cytosolischem Vertreter dieser Proteinfamilie. Auch eine bioinformatische Koexpressions-Analyse deutete auf eine Wechselwirkung beider Systeme hin, da spezifische Mitglieder dieser Proteinfamilien auf Transkriptionsebene eine signifikante Koregulation mit PrxII C/D aufwiesen. Darüber hinaus zeigten weitere *in silico*-Analysen frei zugänglicher Expressionsdaten eine isoformspezifische Regulation. So konnten Unterschiede in der Transkriptregulation von PrxII B und C beispielsweise in verschiedenen Entwicklungsstadien, unterschiedlichen Geweben und Organen sowie in Abhängigkeit verschiedener exogener Reize beobachtet werden.

Aufgrund der funktionellen Instabilität der cytosolischen Typ II Prx-e, gezeigt durch Substrat-abhängige Inhibition, wird für PrxII B und PrxII C eine Funktion in signalgebenden Prozessen postuliert. Eine Überoxidation der katalytischen Thiole könnte ursächlich an dieser Inaktivierung beteiligt sein und somit einen Regulationsmechanismus zur Modulation der hohen Peroxidaseaktivität darstellen. Diese redox-abhängige Veränderung könnte ein erster Hinweis auf eine Funktion von PrxII B und PrxII C im  $H_2O_2$ -*Signalling* sein.

Neben der Charakterisierung von Prx-Funktionen ist auch die Untersuchung struktureller Eigenschaften speziell in Hinblick auf Konformationsänderungen von großer Bedeutung. In diesem Zusammenhang stellt das so genannte *Dynamical Imaging* basierend auf Beugung und Detektion von Röntgenstrahlen (*Diffraction x-ray tracking: DXT*) eine neue Technik dar, die die Visualisierung von Konformationsübergängen mit hoher Zeit- und Ortsauflösung ermöglichen könnte. Da bekannt ist, dass das 2-Cys Prx in seinem katalytischen Zyklus wesentliche Änderungen auf struktureller Ebene durchführt, sollte seine Eignung für das DXT-Verfahren geprüft werden. Um eine solche Technik zu etablieren, bedarf es verschiedener Voraussetzungen, deren Charakterisierung Gegenstand der vorliegenden Arbeit war. Hierbei wurde ein besonderes Augenmerk auf die Untersuchung der funktionellen Stabilität von 2-Cys Prx während der Behandlung mit Röntgenstrahlen gelegt.

In diesem Zusammenhang wurden bifunktionale Varianten von 2-Cys Prx mittels ortsgerechter Mutagenese erzeugt. Diese speziellen funktionalen Proteine ermöglichten einerseits die stabile Immobilisierung auf einer Ni-NTA-Oberfläche durch den N-terminal fusionierten His-Tag. Andererseits wurde eine feste Bindung von Gold-Nanokristallen an Thiolgruppen dieser Varianten untersucht, eine Notwendigkeit zur Visualisierung von Konformationsänderungen durch DXT. Hierbei konnte die Spezifität der Bindungen durch Zugabe verschiedener Additive deutlich erhöht und hydrophobe Wechselwirkungen konnten stark reduziert werden. Als besonders wichtiger Aspekt wurden Einflüsse von Röntgenstrahlung auf biochemische Eigenschaften von 2-Cys Prx charakterisiert. Neben einer Dosis-abhängigen Beeinträchtigung konnten zusätzlich zwei Aminosäuren als primäre Ziele für die beobachtete Schädigung postuliert werden. Eine Beeinträchtigung von Tyrosinen könnte für strukturelle Veränderungen wie die Entstehung hochmolekularer Aggregate auf Kosten von 2-Cys Prx Monomeren verantwortlich sein. Negative Auswirkungen auf funktionelle Eigenschaften wie Peroxidaseaktivität und DNA-Schutzfunktion kann vermutlich geschädigten Cysteinen zugeordnet werden kann. Trotz der zu beobachtenden Beeinträchtigung zeigte sich eine außergewöhnlich hohe funktionelle und strukturelle Stabilität von 2-Cys Prx, was für eine besonders gute Eignung dieses Proteins für DXT-Anwendungen spricht. Darüber hinaus konnte durch Zugabe von Radikalfängern eine Abmilderung der Röntgenschädigungseffekte erzeugt werden.

## Abbreviations

°C	degree centigrade
μ	mikro
1-Cys Prx	1-cysteine peroxiredoxin
<sup>1</sup> O <sub>2</sub>	singlet oxygen
2-Cys Prx	2-cysteine peroxiredoxin
a	adenine
Å	Ångström
<i>A. thaliana</i>	<i>Arabidopsis thaliana</i>
Abs	absorption
APX	ascorbate peroxidase
Asc	ascorbate
Asp	aspartate
At	<i>Arabidopsis thaliana</i>
BAP 1	BONZAI-associated protein 1
BCIP	5-bromo-4-chloro-3-indolylphosphate
bp	basepair
BSA	bovine serum albumine
c	cytosine
CAT	catalase
cDNA	copy DNA
Chl	chlorophyll
COOH	cumene hydroperoxide
Cu	copper
Cyp	cyclophilin
Cys	cysteine
ddH <sub>2</sub> O	twice deionised H <sub>2</sub> O
DKS	aspartate-lysine-serine
DMSO	dimethyl sulfoxide
DNA	desoxyribonucleic acid
DTT	dithiotreitol
DXT	diffracted x-ray tracking
<i>E. coli</i>	<i>Escherichia coli</i>
Fer1	ferritin 1-precursor
g	acceleration due to gravity
g	guanine
GPX	glutathione peroxidase
GR	glutathione reductase
Grx	glutaredoxin
GSH	reduced glutathione
GSSG	reduced glutathione
H <sub>2</sub> O	water
H <sub>2</sub> O <sub>2</sub>	hydrogen peroxide
His	histidine
IPTG	isopropyl β-D-thiogalactopyranoside
kDa	kilodalton
K <sub>M</sub>	Michaelis-Menten constant
LB	Luria Bertani

---

Lys	lysine
m	milli
M	molar
MCO	metal catalysed oxidation
Met	methionine
min	minute
Mn	manganese
MV	methyl viologen
n	nano
NADPH	reduced form of nicotinamide adenine dinucleotide phosphate
NBT	nitrotetrazolium blue
Ni-NTA	nickel-nitrilotriacetic acid
NO	nitric oxide
O <sub>2</sub>	dioxygen
O <sub>2</sub> <sup>•-</sup>	superoxide radical anion
OH <sup>•</sup>	hydroxyl radical
ONOO <sup>-</sup>	peroxynitrite
overox	overoxidised
ox	oxidised
PAA	polyacrylamide
PCR	polymerase chain reaction
Prdx	human/mammalian prx
Prx	peroxiredoxin
Prx II	peroxiredoxin of type II
Prx Q	peroxiredoxin Q
PSI, II	photosystem I, II
red	reduced
RNA	ribonucleic acid
RNS	reactive nitrogen species
ROS	reactive oxygen species
SDS-PAGE	sodium dodecyl sulfate polyacrylamide gel electrophoresis
Ser	serine
SOD	superoxide dismutase
SPR	surface plasmon resonance
t	thymine
t-BOOH	tertiary butylhydroperoxide
T-DNA	transfer DNA
TEM	transmission electron microscopy
TR	thioredoxin reductase
Trx	thioredoxin
type II Prx	type II peroxiredoxin
V <sub>max</sub>	maximum velocity
Zn	zinc

## **1. Introduction**

In their natural environment plants are exposed to a variety of biotic and abiotic influences. These external factors can lead to the disturbance of important cellular metabolic processes and therefore can ultimately affect plant growth, development, and reproduction. The underlying mechanisms of these effects are predominantly based on imbalances in the redox and osmotic state. The former effect often results from an enhancement of electron transfer for instance on molecular oxygen and thereby to the generation of reactive oxygen species (ROS) (Scandalios, 1993). Plant cells are particularly prone to these mechanisms – especially due their photosynthetic capacity, their aerobic lifestyle and the corresponding presence of oxygen within the cellular environment. Metabolism under optimum conditions leads to the formation of reactive species, as electron leakage from electron transport chains within the different organelles and in membranes results in reduction of molecular oxygen (for review see Apel and Hirt, 2004). Changing environment triggered by different abiotic or biotic conditions can enhance ROS generation and consequently creates an additional oxidative threat (Mittler et al., 1999). ROS play a dual role in cell metabolism since they facilitate oxidative damage and are important in signal transduction processes. Therefore, a tight control of these reactive species in every cellular compartment is of utmost importance (Dat et al., 2000). To achieve both, the maintenance of a low steady state level of reactive species and the suppression of the formation of high ROS rates during stress situations, an elaborated network of regulatory mechanisms and antioxidants is essential (Møller, 2001; Gechev et al., 2006). An important component of the evolved complex system of non-enzymatic and enzymatic antioxidants is the protein family of peroxiredoxins (Prx) being in focus of the present work.

### **1.1. Reactive oxygen and nitrogen species – mechanisms and sites of ROS and RNS generation**

#### **1.1.1. Reactive oxygen species (ROS) and reactive nitrogen species (RNS)**

Due to its electron configuration molecular oxygen in its ground state, i.e. dioxygen (O<sub>2</sub>), is relatively inert and cannot easily abstract electrons from other molecules except

for those which also have two single electrons in parallel spin in outer orbitals or highly reactive electrons of suitable redox potential (Scandalios, 2005). ROS generation from molecular oxygen occurs via two distinct mechanisms. On the one hand physical activation can take place by the transfer of energy. This is mediated by photosensitisers like e.g. chlorophyll, which are able to harvest light energy and subsequently energise  $O_2$  to the considerably more reactive form singlet oxygen ( $^1O_2$ ) (Telfer et al., 1994). On the other hand, chemical activation occurs via the transfer of electrons to dioxygen, leading in dependence on the number of transferred electrons to the successive generation of superoxide anion radical ( $O_2^{\cdot-}$ ), hydrogen peroxide ( $H_2O_2$ ), and hydroxyl radical ( $OH^{\cdot}$ ) (Desikan et al., 2005). The latter can be generated in the presence of catalytic redox active metal ions by an interaction of  $O_2^{\cdot-}$  with  $H_2O_2$  or stoichiometric metal oxidation (Korytowski et al., 1987). The partially reduced oxygen derivatives exhibit a much higher reactivity towards many cellular compounds than molecular oxygen itself and therefore facilitate oxidative damage when produced in excess (Asada and Takahashi, 1987). To achieve a complete reduction from  $O_2$  to water, four electrons are required (Scandalios, 2002 a).

**Tab. 1.1: Compilation of important ROS of plant cells** with their basic biochemical properties and the antioxidants leading to their detoxification. Abbreviations:  $^1O_2$  = singlet oxygen,  $O_2^{\cdot-}$  = superoxide anion radical,  $H_2O_2$  = hydrogen peroxide,  $OH^{\cdot}$  = hydroxyl radical, Asc = ascorbate, SOD = superoxide dismutase, CAT = catalase, PRX = peroxiredoxin, GRX = glutaredoxin, TRX = thioredoxin, POX = peroxidase, GSH = glutathione. References: <sup>a</sup>Møller et al., 2007; <sup>b</sup>Foyer and Noctor, 2005; <sup>c</sup>Smirnoff, 2000.

	Half life <sup>a</sup>	Distance travelled <sup>a</sup>	Redox potential <sup>b</sup>	Concentration range <sup>b</sup>	Detoxification <sup>c</sup>
$^1O_2$	1 $\mu$ s	30 nm	-	-	Carotenes Tocopherol
$O_2^{\cdot-}$	1 $\mu$ s	30 nm	+ 0.94 V	< 1 nM	SOD
$H_2O_2$	1 ms	1 $\mu$ m	+ 0.54 V	1-100 $\mu$ M	CAT, APX, PRX, GRX, TRX, POX, Asc/GSH-cycle
$OH^{\cdot}$	1 ns	1 nm	+ 2.20 V	negligible	-

As a consequence of their chemical properties, ROS exhibit distinct characteristics like mean half life, mean diffusion distance or midpoint redox potential (Tab. 1.1) which all are linked to differences in their reactivity. This in turn modifies their damaging potentials when it comes to the interaction with other molecules in the surrounding

medium.  $^1\text{O}_2$  for instance displays a high specificity towards certain amino acids, such as histidine, methionine, and tryptophan and was described to cause lipid peroxidation within cellular environment (Knox and Dodge, 1985). Chemical and physicochemical studies suggest  $\text{O}_2^{\cdot-}$  to be relatively inert for a molecule with an unpaired electron, as its chief reaction is its own dismutation (Sawyer and Valentine, 1981; Babior, 1997; compare section 1.2.2). Deleterious effects that can directly be attributed to  $\text{O}_2^{\cdot-}$  are primarily related to the metal-catalysed generation of  $\text{OH}^{\cdot}$  in the presence of  $\text{H}_2\text{O}_2$  (Fridovich, 1986).  $\text{H}_2\text{O}_2$  has a low reactivity and shows no radical properties due to its electron configuration (Salin, 1988). Its toxicity is mostly exerted via oxidation of thiol-groups (Dat et al., 2000). The most reactive molecule among the different reactive oxygen intermediates is  $\text{OH}^{\cdot}$ , which consequently in a highly indiscriminate way attacks the first available substrate at its site of generation and therefore has the potential to inflict extensive damage (Scandalios, 2005).

To complete the picture of reactive intermediates within the network of oxidative stress and signal transduction pathways, another kind of reactive species has to be mentioned: the reactive nitrogen species (RNS) (Pauly et al., 2006). Their major compound nitric oxide (NO) exists in three interchangeable forms according to the gain or loss of electrons, namely the gaseous free radical ( $\text{NO}^{\cdot}$ ), the nitrosonium cation ( $\text{NO}^+$ ), and the nitroxyl radical ( $\text{NO}^-$ ) (Wojtaszek, 2000). Due to its characteristics as a free radical, NO has a short half life of just a few seconds and typically reacts with  $\text{O}_2$  upon formation of nitrogen dioxide ( $\text{NO}_2$ ), which rapidly degrades to nitrite and nitrate within an aqueous environment (Neill et al., 2003; Neill et al., 2008). Alternatively, NO may be rapidly converted to peroxynitrite ( $\text{ONOO}^-$ ) by reacting with  $\text{O}_2^{\cdot-}$  if both generation sites are in very close proximity (Yamasaki, 2005). The reaction takes place with an almost diffusion-controlled rate constant of  $1.9 \times 10^{10} \text{ M}^{-1} \text{ s}^{-1}$  (Kissner et al., 1997; Klotz, 2002).  $\text{ONOO}^-$  itself is an extremely short-lived RNS with a half life of less than 10 ms *in vivo* and a high potential to damage cellular compounds (Yeo et al., 2008; Denicola et al., 1998). In contrast to the just described rapid conversions in an oxygen-rich environment, NO could also be shown to remain considerably more stable upon hypoxic conditions, allowing for long-distance transport of this molecule (Yamasaki, 2005).

### 1.1.2. ROS and RNS are generated at different subcellular sites

As the presence of molecular oxygen in cells of aerobic organisms is unavoidable, the possibilities for electron leakage with subsequent transfer to oxygen are numerous and consequently, many sites of ROS generation can be found throughout the plant cell (Niyogi, 1999; Turrens, 2003; del Rio et al., 2002; compare Fig. 1.1).

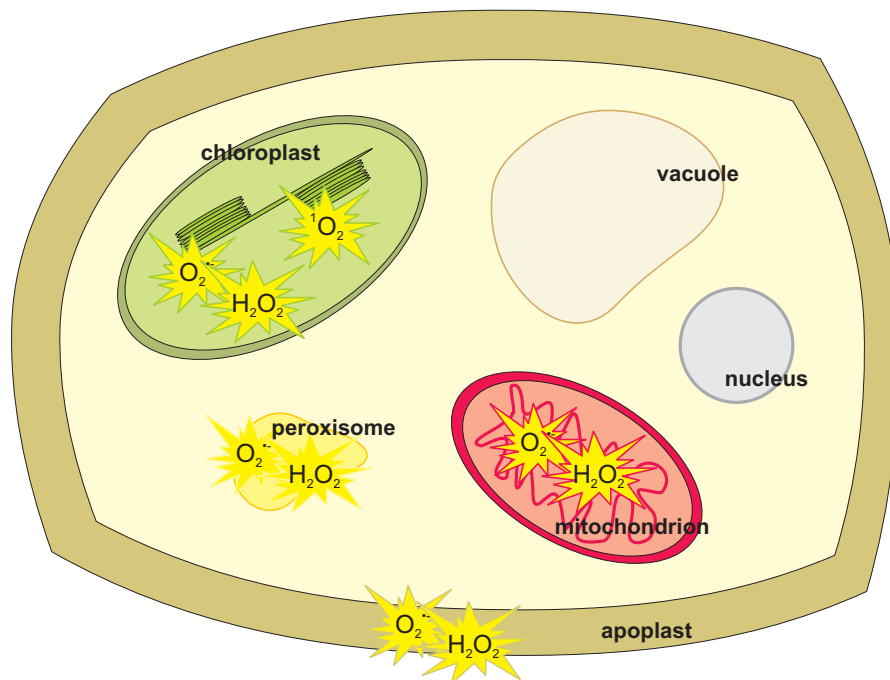


**Fig. 1.1: Schematic depiction of the most important ROS generation sites within the different compartments of the plant cell.** Size and number of organelles are not scaled. Abbreviations:  $^1\text{O}_2$  = singlet oxygen,  $\text{O}_2^{\cdot-}$  = superoxide anion radical,  $\text{H}_2\text{O}_2$  = hydrogen peroxide,  $\text{OH}^{\cdot}$  = hydroxyl radical.

In this context particular attention has to be given to the chloroplast as it contains different sites for ROS generation and is one of the main sources for these reactive intermediates, especially in the light (Foyer and Noctor, 2003). On the one hand, chlorophyll (Chl) molecules are essential participants of light harvesting and electron transfer reactions during photosynthesis (Niyogi, 1999). Due to intersystem crossings, triplet Chl ( $^3\text{Chl}$ ) may be generated from the excited singlet state ( $^1\text{Chl}$ ) if this cannot dissipate its energy (Knox and Dodge, 1985). Consequently, the considerably longer-lived  $^3\text{Chl}$  can interact with  $\text{O}_2$  to produce  $^1\text{O}_2$ . Because of a longer average life time of  $^1\text{Chl}$  in photosystem II (PSI)-associated light harvesting complexes (LHC) in comparison to PSI LHC, the potential of  $^1\text{O}_2$  generation is higher in PSII (Niyogi, 1999; Telfer et al., 1994). Furthermore,  $^1\text{O}_2$  generation can be facilitated by intermediates of chlorophyll biosynthesis, such as protoporphyrin IX and

protochlorophyllide, acting as potent photosensitisers (Tanaka and Tanaka, 2006; Meskauskiene et al., 2001). On the other hand, electron transfer reactions to molecular oxygen take place at the PS I acceptor side of the photosynthetic electron transport chain (PET). This photoreduction occurs via the Mehler reaction and leads to the formation of  $O_2^{\bullet -}$  which can subsequently be metabolised to  $H_2O_2$  (Mehler, 1951; Asada, 2006).

A second major mechanism of ROS generation in plants is linked to the photorespiration in green plant tissue. As a consequence of oxygenase function of RubisCO within the chloroplast, glycolate is translocated to the peroxisome where  $H_2O_2$  release takes place during oxidation of glycolate to glyoxylate catalysed by glycolate oxidase as part of the photorespiratory cycle (Wingler et al., 2000; Apel and Hirt, 2004). With  $10,000 \text{ nmol m}^{-2} \text{ s}^{-1}$  in mesophyll cells of C3-plants, the yield of generation of this ROS is very high (Foyer and Noctor, 2003).

But photorespiration in green tissue is not the only mechanism for  $H_2O_2$  generation within the peroxisome. Peroxisomes are probably the major producing sites of intracellular  $H_2O_2$  (del Rio et al., 2006). In general, the peroxisome is an organelle with an oxidative type of metabolism (del Rio et al., 2002), containing several flavin oxidases leading to the enzymatic generation of  $O_2^{\bullet -}$  at different sites (Corpas et al., 2001). In leaf peroxisomes, the matrix-localised enzyme xanthine oxidase (XOD) is responsible for the generation of  $O_2^{\bullet -}$  which by superoxide dismutases (SOD) is subsequently converted to  $H_2O_2$  and  $O_2$  (Scandalio et al., 1988). Furthermore, the peroxisomal membrane contains a small electron transport chain which was demonstrated to be responsible for  $O_2^{\bullet -}$  generation in dependence of NAD(P)H supply (López-Huertas et al., 1999, Corpas et al., 2001). Additionally, a special type of peroxisome – the glyoxysome – is the predominant location for  $\beta$ -oxidation of fatty acids and consequently another source of  $H_2O_2$  as a by-product of the corresponding reactions (Corpas et al., 2001).

Similar to the chloroplast, the mitochondrial metabolism releases ROS as consequence of reduction of molecular oxygen due to the presence of the mitochondrial electron transport chain (mETC) (Møller, 2001). The respiratory mETC contains several sites facilitating the electron transfer on  $O_2$  that results in  $O_2^{\bullet -}$ -generation. Involved are different redox-centers with a standard redox-potential sufficiently negative for such an electron transport (Turrens, 2003). The two major production sites are the flavoprotein-containing NADH dehydrogenase (complex I) and the ubisemiquinone-oxidase in

complex III (cytochrome b/c1 complex) (Turrens, 1997). Due to the function of mitochondrial Mn-SOD, released  $O_2^{\cdot-}$  is rapidly converted to  $H_2O_2$  (Jackson et al., 1978).

Besides their generation during normal metabolism ROS are produced in some enzyme catalysed reactions. For instance, NADPH oxidases, associated with the plasma membranes of plant cells, or cell wall bound peroxidases generate  $O_2^{\cdot-}$  and  $H_2O_2$ , respectively. Both were described to play a crucial role in context of hypersensitive response and pathogen defence (Lamb and Dixon, 1997).

Like in the case of ROS, there are also different sites of RNS formation in the cell. NO formation takes place in the cytosol, chloroplast, mitochondrion, peroxisome, apoplast, and nucleus (Crawford, 2006; Vanin et al., 2004; Planchet and Kaiser, 2006; del Rio et al., 2006; Bethke et al., 2004; Wendehenne et al., 2001). Since RNS generation sites mostly coincide with release of ROS in the cell, subsequent production of further reactive species by cross reaction of ROS with NO is unavoidable, as e.g. ONOO<sup>-</sup> formation (Wilson et al., 2008). Whereas in animal cells, NO is produced by nitric oxide synthetases (NOS), catalysing the conversion of L-arginine to L-citrullin and NO, mechanisms of NO generation in plants are not ultimately clarified. Up to now, two enzymatic pathways could be identified either utilising L-arginine or nitrate as substrate, namely nitrate reductase (NR) and a plant NOS-like enzyme, respectively (Besson-Bard et al., 2008).

### **1.1.3. Consequences of ROS and RNS formation**

As briefly mentioned before, ROS are assigned a dual function not only in damage development upon oxidative stress but also as signalling molecules (Dat et al., 2000). If produced in high concentrations, ROS oxidise different macromolecules within the cell in an uncontrolled manner. Detrimental ROS effects on DNA are manifold; they include deletions, mutations, or translocations, but also single strand breakage and cross-linking (Dizdaroglu, 2005; Scandalios, 2005). Also within proteins, there are different sites particularly prone to damage via ROS; oxidation of different amino acids such as tyrosine, cysteine, methionine, and histidine result in cross-linking events (Stadtman, 1992) which consequently cause degradation of the affected proteins (Fucci et al., 1983). Furthermore, ROS can oxidise unsaturated fatty acids in membranes. Such generation of lipid peroxides impairs membrane functions with the concomitant loss of

membrane integrity (Bowler et al., 1991). Thus, the modification of DNA, proteins, and lipids may cause cellular dysfunction and can ultimately induce cell death (Scandalios, 2005; Berlett and Stadtman, 1987; Taylor et al., 2002).

Due to the just described characteristics, ROS were traditionally considered as harmful, although in recent years, it could be shown that they have an important role in a variety of signal transduction pathways (Vranova et al., 2002; Miller et al., 2008). Their function as secondary messengers depends on a preferential and highly affine interaction with cellular sensors in order to specifically regulate diverse biological processes. Via exhibiting differential regulatory mechanisms on the levels of transcription, translation or post-translational processes they are able to modulate biotic and abiotic stress responses, growth and hormone signalling, as well as development and programmed cell death (Kovtun et al., 2000; Torres et al., 2002; Pei et al., 2000; Apel and Hirt, 2004). As the generation of different ROS is often linked very tightly to each other as described above, it is often difficult to discriminate between effects of particular species *in vivo*. Nevertheless, experimental data obtained with specific effectors and by genetic approaches have enabled to assign roles to specific ROS and RNS in signal transduction which will be described in the following. The signalling role of H<sub>2</sub>O<sub>2</sub> has been broadly investigated (Slesak et al., 2007; Vandenameele et al., 2003; Vanderauwera et al., 2005; Rentel and Knight, 2004) and numerous involvements could be established, such as in pathogen defence, wound response, or abscisic acid-induced stomatal closure (Mittler et al., 1999; Orozco-Cardenas and Ryan, 1999; Kwak et al., 2003). In addition to its role as defence signal molecule H<sub>2</sub>O<sub>2</sub> also functions in normal growth and development (Quan et al., 2008). For O<sub>2</sub><sup>•-</sup> the different roles in signal transduction are only slowly emerging. Besides an often described function in pathogen defence and programmed cell death (PCD) (Jabs et al., 1996 and 1997; Wisniewski et al., 1999; Overmyer et al., 2000), a recent study with transgenic potato plants displays a regulatory role in plant growth and tuber development (Kim et al., 2007). This is the first report showing an influence of O<sub>2</sub><sup>•-</sup> on gibberellin levels by varying the expression of genes within the biosynthetic pathways of this plant hormone. Another aspect that has to be taken into consideration when it comes to the signalling functions of O<sub>2</sub><sup>•-</sup> is its reaction with NO to yield ONOO<sup>-</sup>. Interestingly, ONOO<sup>-</sup> does not act as a signal for cell death in plants, as is described for the animal system (Delledonne et al., 2001). In modification to its function in animal cells plant ONOO<sup>-</sup> is hypothesised to have intrinsic signalling functions (Neill et al., 2008). Especially in regard to its ability to

cause protein nitration at tyrosine residues (Saito et al., 2006; Romero-Puertas et al., 2007), ONOO<sup>-</sup> is proposed to play an important physiological and signalling role. Also NO itself is an important signalling molecule. Besides its function in modulating disease resistance (Romero-Puertas et al., 2004; Delledonne et al., 2001), its various physiological roles include regulation of development such as leaf extension and root growth as well as the delay of leaf senescence and fruit maturation and regulation of stomatal closure (Neill et al., 2002 and 2003). Furthermore, a general involvement in signalling pathways could be shown as for instance an activation of mitogen activated protein (MAP) kinase cascades was observed (Pagnussat et al., 2002) as well as a transcript regulation of genes being important for synthesis and response to jasmonic acid (Orozco-Cardenas and Ryan, 2002).

## **1.2. Detoxification of ROS – the antioxidative network in plants**

Due to their dual role in both oxidative stress and signal transduction pathways, the tight control of ROS is of utmost importance. Therefore cells contain a very complex network of enzymatic and non-enzymatic components counteracting ROS accumulation in order to avoid oxidative stress which occurs as a consequence of progressive imbalance between levels of antioxidants and ROS (Scandalios, 2002 b; compare Fig. 1.2). The antioxidative system provides a powerful tool to regulate the turnover of reactive intermediates in order to achieve appropriate adjustments in context of gene expression, metabolism and physiology via their signalling functions (Foyer and Noctor, 2005).

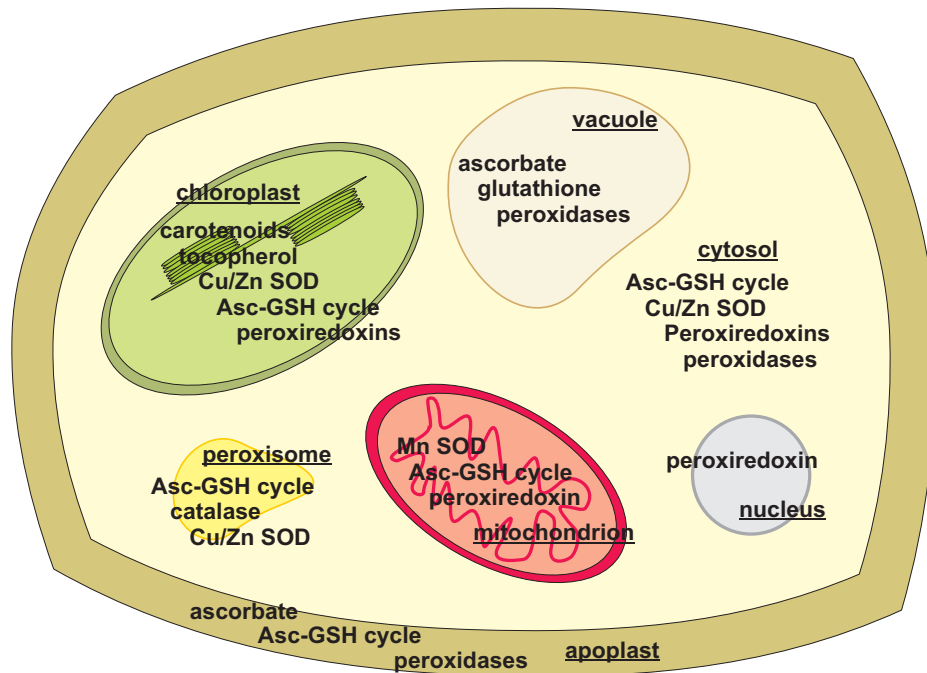


**Fig. 1.2: Schematic depiction of the components of the antioxidative system within the different compartments of the plant cell** (modified according to Scandalios, 2005). Abbreviations: Asc = ascorbate, GSH = glutathione, SOD = superoxide dismutase with its different isoforms according to the indicated co-factors Cu = copper, Zn = zinc, Mn = manganese. Size and number of organelles are not scaled.

### 1.2.1. Non-enzymatic antioxidants

Besides tocopherols, flavonoids, some alkaloids, and carotenoids (Apel and Hirt, 2004), plant cells contain also proline and amines as low-molecular weight antioxidants (Sharma and Dietz, 2006). However, ascorbate (Asc) and glutathione (GSH) constitute the two main redox-buffers in the aqueous phases of the cell (Noctor and Foyer, 1998). The congruent role in membranes is played by tocopherols and carotenoids. Asc and GSH accumulate to millimolar concentrations (Pignocchi and Foyer, 2003; Renneberg, 1982), with variations depending on tissue and physiological state (Noctor and Foyer, 1998). Additionally, the ratio of reduced and oxidised GSH allows for a tentative description of the thiol redox status of the cell which is a decisive parameter for protein functionality. Under non-stress situations the cell reduction state was described to be around 95 % (Wormuth et al., 2007); life cell imaging with the redox-sensitive fluorescent protein roGFP even suggests a reduction state of 99 % (Meyer et al., 2007). Whereas GSH acts as redox mediator in the whole cell, Asc is especially important for signalling events in just a few compartments (Foyer and Noctor, 2005). The reduction state of Asc plays an important role for instance in apoplast metabolism and plant

defence responses (Horemans et al., 2000). Ascorbate is an important reactant for  $\text{H}_2\text{O}_2$  detoxification, tocopherylradical reduction and within the xanthophyll cycle.

The reduced form of glutathione (GSH) exists as the thiol-tripeptide  $\gamma$ -glutamyl-L-cysteinyl-glycine ( $\gamma$ -Glu-Cys-Gly), which is interchangeable with its oxidised form, the glutathione disulfide GSSG (Noctor and Foyer, 1998). This is formed either as a consequence of direct interaction with ROS or following electron transfer reactions to glutaredoxins (Grx) which among other reactions is linked to type II peroxiredoxin activity (Lemaire, 2004; Finkemeier et al., 2005). It furthermore facilitates glutathionylation, a special posttranslational modification to regulate protein function and protecting them from irreversible oxidation (Lemaire, 2004). This modification could be shown for instance to modulate activities of glyceraldehyde-3-phosphate dehydrogenase and thioredoxin f (Michelet et al., 2005; Zaffagnini et al., 2007). Besides its role in protection and defence as well as in maintaining the major reservoir of non-protein sulphur within the cell, it is a precursor of phytochelatins involved in heavy metal detoxification and substrate for glutathione-S-transferase (GST) (Noctor et al., 2002).

Due to its capacity to detoxify  $^1\text{O}_2$ ,  $\text{O}_2^{\cdot-}$ , and  $\text{HO}^{\cdot}$  ascorbate (Asc) acts as primary antioxidant (Smirnoff, 2000). As powerful secondary antioxidant it is involved in the regeneration of oxidised  $\alpha$ -tocopherol and is a co-factor of violaxanthine deepoxidase (Padh et al., 1990). Apoplastic Asc is considered to function as counterpart for ROS arising from exposure to atmospheric pollutants like ozone (Polle et al., 1995; Luwe, 1996). Additionally it is implicated in various other functions such as regulation of the cell cycle (Kerk and Feldman, 1995) or an involvement in root elongation and cell wall extension (Cordoba-Pedregosa et al., 1996; Takahama and Oniki, 1994).

Moreover, Asc and GSH are employed as co-substrates within the ascorbate-glutathione cycle, also known as Halliwell-Asada cycle (Foyer and Halliwell, 1976). In a cyclic turnover of Asc and GSH this pathway enables the detoxification of  $\text{H}_2\text{O}_2$  (Asada, 1992). During its cyclic utilisation, Asc is oxidised to monodehydroascorbate (MDHA) during the conversion of  $\text{H}_2\text{O}_2$  catalysed by ascorbate peroxidase (APX). A further oxidation of MDHA leads to the formation of dehydroascorbate (DHA). Regeneration of these oxidised forms of Asc is provided by the enzymes monodehydroascorbate reductase or dehydroascorbate reductase, with the former being NADPH dependent and the latter utilising GSH as reductant. GSH itself is regenerated by NADPH dependent glutathione reductase (GR) (Foyer and Noctor, 2000)

### 1.2.2. Enzymatic antioxidants

As part of the first line of defence, superoxide dismutase (SOD) is a powerful enzyme to convert two molecules of  $O_2^{\cdot-}$  by dismutation to  $H_2O_2$  and  $O_2$ . It accelerates this otherwise spontaneous reaction by several orders of magnitude. Whereas  $O_2^{\cdot-}$  spontaneously disproportionates to  $H_2O_2$  and  $O_2$  with a rate constant of about  $2 \times 10^5 M^{-1}s^{-1}$  at neutral pH (Barbior, 1997; Fridovich, 1975), the presence of SOD enhances this rate constant to about  $2 \times 10^9 M^{-1}s^{-1}$  at pH 7.4 being very near to diffusion limitation (Fridovich, 1975). This reaction mechanism follows a cyclic reduction and oxidation of the transition metal ion localised within the active site of the enzyme (McCord and Fridovich, 1969). Unlike many other organisms, plants contain multiple isoforms of this enzyme (Scandalios, 1993); in *A. thaliana* for instance eight genes code for SODs which are present at all subcellular generation sites of  $O_2^{\cdot-}$  (Mittler et al., 2004). This is a crucial prerequisite for  $O_2^{\cdot-}$  detoxification, as this charged molecule is not able to cross phospholipid membranes – consequently it has to be removed directly at its site of generation (Takahashi and Asada, 1983). The family of SODs is subdivided according to the kind of metal co-factor utilised by the enzyme, which may be Cu/Zn, Fe, or Mn, as well as based on subcellular localisation (Alscher et al., 2002; compare Fig. 1.2).

Within the plant cell, there are several enzymes that allow for an efficient removal of  $H_2O_2$ . As part of the Asc-GSH cycle, ascorbate peroxidase (APX) catalyses the initial detoxification step of  $H_2O_2$ , supported by coordinated activities of different additional enzymes (compare section 1.2.1.). Thereby, the APX is among the primary  $H_2O_2$ -scavenging enzymes of both, the cytosol and especially the chloroplast (Asada, 1992). The genome of *A. thaliana* contains nine different APX isoforms, which either remain in the cytosol or are distributed among almost all compartments of the cell (Mittler et al., 2004). Within the chloroplast, three different isoenzymes are found: the thylakoid-bound tAPX, the stromal sAPX, and a third one found in the thylakoid lumen (Davletova et al., 2005).

A second protein family involved in  $H_2O_2$  detoxification are the catalases (CAT). These heme-containing enzymes are ubiquitous among aerobic eukaryotes and also catalyse the turnover of  $H_2O_2$  to oxygen and water (Feierabend, 2005). In *A. thaliana* three genes were identified, which code for individual isoforms able to assemble to at least six different homo- and heteromeric conformations of these tetrameric enzymes (Frugoli et

al., 1996). Catalases are localised in peroxisomes but exhibit differences in the tissue specific distribution (Frugoli et al., 1996).

Members of the protein-family of peroxiredoxins (Prx) are ubiquitous non-heme containing peroxidases, which are also known as thioredoxin peroxidases (TPX) or thiol specific antioxidants (TSA) (Chae et al., 1993; Hofmann et al., 2002). Their conserved cysteine residues allow for a detoxification of a variety of substrates such as  $\text{H}_2\text{O}_2$ , different other alkyl peroxides as well as  $\text{ONOO}^-$  (Chae et al., 1994; Lim et al., 1993; Jacobsen et al., 1989; König et al., 2003; Dietz et al., 2006; Bryk et al., 2000). According to the number and localisation of these conserved cysteine residues within their primary structure, four different subgroups can be distinguished, namely 1-Cys Prx, 2-Cys Prx, Prx Q, and type II Prx (Dietz, 2003 a). Just recently, the plant glutathione peroxidase (GPX) family was assigned to be a fifth subgroup of Prx as they also display a thioredoxin-dependent function and reveal similarity to Prx (Navrot et al., 2006).

The coordinated function of the just described components of the antioxidative network is of particular importance to prevent the generation of  $\text{HO}^\bullet$  by maintaining very low steady-state levels of  $\text{O}_2^{\bullet-}$  and  $\text{H}_2\text{O}_2$  as  $\text{HO}^\bullet$  exhibits an extraordinary high reactivity and is therefore highly toxic (Mittler and Poulos, 2005). Furthermore, this elaborated network is necessary to control signalling pathways that utilise  $\text{O}_2^{\bullet-}$ ,  $\text{H}_2\text{O}_2$ , and  $^1\text{O}_2$ , as these are known to play a critical role in various signal transduction processes involved in stress response, growth, development and many more functional processes (Apel and Hirt, 2004).

### 1.3. Peroxiredoxins

As mentioned before, peroxiredoxins (Prx) constitute a superfamily of non-heme containing peroxidases (Dietz, 2003 a). Peroxiredoxins are evolutionary old proteins present in prokaryotes, archaea, and eukaryotes and thus comprise members throughout all kingdoms (Hofmann et al., 2002; Stork et al., 2008; Wood et al., 2003 a). Since the first characterisation of a member of this protein family in the yeast *Saccharomyces cerevisiae* (Kim et al., 1988), a constantly rising number of Prx was identified and a broad spectrum of functions could be assigned to these proteins. The importance of Prx enzymes is underlined by their high abundance and involvement in multiple cellular

processes (Peltier et al., 2002; Sweetlove et al., 2002; Dietz et al., 2006). Their importance becomes particularly apparent in context of the causative participation of ROS in various diseases described for the mammalian/human system, ranging from neurodegenerative diseases (like Alzheimer's or Parkinson's disease) and neuroinflammatory disorders (e. g. multiple sclerosis) to cancer or arteriosclerosis (for review see Valko et al., 2007). In this context, for instance mice with genetically inactivated peroxiredoxin 6 (Prdx 6: Prdx is used as abbreviation for human/mammalian Prx) were investigated. The mouse line was not impaired in its development however the lack of Prdx 6 entailed a considerably higher susceptibility towards oxidative stress (Wang et al., 2003). Furthermore, the *knockout* mouse revealed a considerably shorter life span during hyperoxia treatment favouring ROS generation in the lung. In contrast, an over-expression of Prdx 6 protected from hyperoxia-mediated injury of the lung (Wang et al., 2004). In case of neurodegenerative disorders, brain region- and disease-specific expression patterns as determined with different proteomics approaches revealed an up-regulation of human Prdx 1 and Prdx 2 (for review see Hattori and Oikawa, 2007). A corresponding increase of Prdx expression and the ability to maintain these proteins in the reduced state could be attributed to neuroprotective mechanisms at least in case of Alzheimer's disease (Cumming et al., 2007). Additionally, Prdx isoforms play an important role in cancer development, as they are often highly expressed in these proliferative tissues and may determine their stress tolerance (Shen and Nathan, 2002). They have been shown to act on the one hand as 'tumor preventers' as mice lacking Prdx 1 died premature, whereas on the other hand the expression of Prdx led to the scavenging of ROS within the cells supporting tumor survival (for review see Neumann and Fang, 2007; Park et al., 2000). The latter reveals a role of specific Prx as potential therapeutic targets, as a decrease of for instance Prdx 2 sensitises tumors in respect of oxidative stress (Smith-Pearsons et al., 2008; Shen and Nathan, 2002; Zhang et al., 1997). Besides their function in antioxidative defence during various diseases (Penna et al., 2008; Nagy et al., 2006; Kim et al., 2000; Zhao et al., 2008), they also are involved in different signal transduction processes, as for instance in apoptosis and cell viability (Chang et al., 2004; Zhou et al., 2000; Zhou et al., 2002).

These findings exemplarily demonstrate the great importance of this protein family in vertebrates. Many other reports relate Prx to functions in redox regulation, antioxidant defence and signalling of different organisms.

### 1.3.1. Peroxiredoxins in plants

Phylogenetic and biochemical analyses revealed the presence of five distinct groups of thioredoxin dependent peroxidases within *A. thaliana*, which is presumably also true for all photosynthetic eukaryotic organisms (Rouhier and Jacquot, 2005). Four of these groups contain the strictly conserved catalytic cysteine within a conserved amino acid environment and are subdivided according to the absence or presence of a second cysteine and its localisation: 1-Cys Prx, 2-Cys Prx, type II Prx and Prx Q (Dietz, 2003 a; compare Fig. 1.3). The fifth one is represented by the GPX family (compare section 1.2.2) that also contains conserved cysteines but at different positions (Navrot et al., 2006; Rouhier and Jacquot, 2005; compare Fig. 1.3).

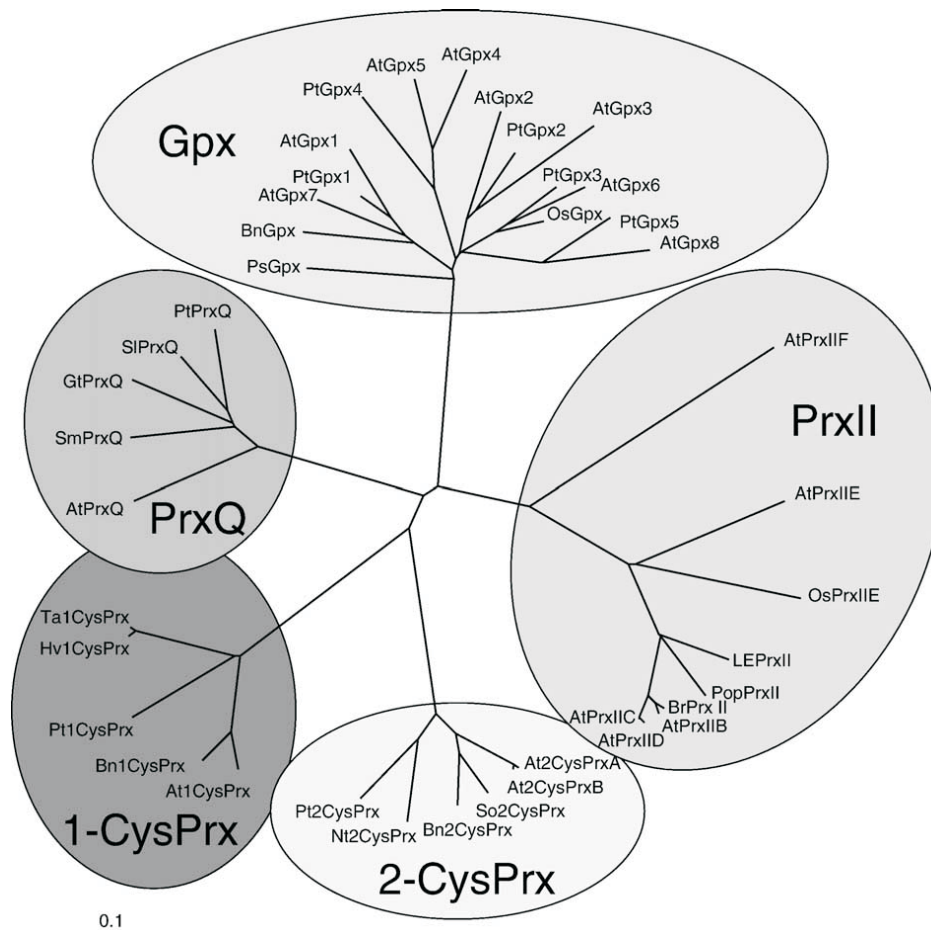


**Fig. 1.3: Phylogenetic tree of Prx.** Members of different plant species are subdivided into the five subgroups of Prx superfamily (from Rouhier and Jacquot, 2005, the tree was constructed using ClustalW). At = *Arabidopsis thaliana*, Bn = *Brassica napus*, Br = *Brassica rapa*, Gt = *Gentiana triflora*, Hv = *Hordeum vulgare*, Le = *Lycopersicon esculentum*, Nt = *Nicotiana tabacum*, Os = *Oryza sativa*, Ps = *Pisum sativum*, Pt = *Populus trichocarpa*, Sl = *Sedum lineare*, Sm = *Suaeda maritima* subsp. *salsa*, Ta = *Triticum aestivum*.

The genome of *A. thaliana* codes for ten Prx as well as eight GPX genes (Dietz, 2003 a; Rouhier and Jacquot, 2005) which are targeted to different cellular compartments. Besides two chloroplastidic 2-Cys Prx (isoforms 2-Cys Prx A and B), the chloroplastidic Prx Q and the nucleus localised 1-Cys Prx, the largest subgroup in *A. thaliana* with six identified genes are the type II Prx (Baier and Dietz, 1999 a; Lamkemeyer et al., 2006; Stacy et al., 1999; Dietz et al., 2002; Dietz, 2003 a). In addition to one member each being located in the chloroplast (PrxII E) and the mitochondrion (PrxII F), three of these Prx are localised in the cytosol, namely PrxII B, PrxII C and PrxII D (König et al., 2003; Bréhélin et al., 2003; Dietz, 2003 a; Finkemeier et al., 2005; Krufft et al., 2001). The expression of a sixth type II Prx – the PrxII A – could not be detected up to now and therefore it is assumed to be a pseudogene (Dietz, 2003 a).

A very important feature common to all Prx is their catalytic activity. It is based on thiol residues and therefore independent of any prosthetic group – supporting the functional stability of these enzymes (Chae et al., 1993; Hofmann et al., 2002). They all contain a catalytic triade, consisting besides the catalytic cysteine of the highly conserved amino acids threonine (Thr) and arginine (Arg). The Thr-residue is responsible for positioning of the thiol whereas the Arg-residue stabilises the thiolate to provide peroxidase activity (Noguera-Mazon et al., 2006). As already mentioned, Prx exhibit a broad substrate specificity ranging from detoxification of hydrogen peroxide, different alkyl hydroperoxides and lipid peroxides to the turnover of peroxynitrite (Flohé et al., 2000; Rouhier et al., 2004; Bryk et al., 2000). In general, the reaction mechanism of these peroxidases comprises three different steps: the oxidation, derivatisation, and regeneration (Hofmann et al., 2002; compare Fig. 1.4). The first step of the catalytic cycle is initiated by the nucleophilic attack of the peroxide substrate by the thiolate group of the catalytic cysteine, which results in its oxidation to the sulfenic acid derivative (Wood et al., 2003 b; compare Fig. 1.4). A second sulfhydryl group is employed to resolve the sulphenic acid under formation of a disulfide bridge releasing a water molecule. Differences are revealed among the different Prx subgroups (compare Fig. 1.4 B, C, D and E). The disulfide bridge is either formed intramolecularly with the second highly conserved cysteine residue in the same molecule as it is known for Prx Q and type II Prx or an intermolecular disulfide bridge is established between the catalytic cysteine of one monomer and the resolving one of the second monomer and leads to the formation of a homodimer (2-Cys Prx) (Horling et al., 2002; Hirotsu et al., 1999;

fully oxidise the 2-Cys Prx dimer with two disulfide bridges, two substrate molecules must be detoxified.

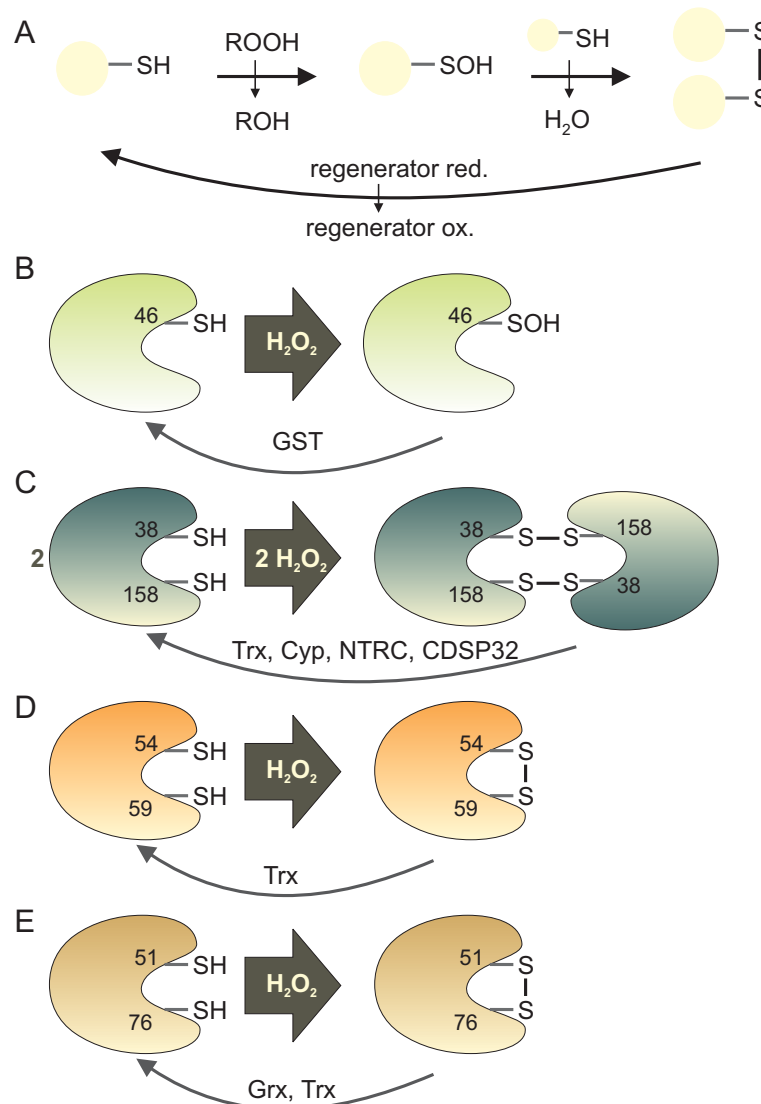


**Fig. 1.4: Schematic depiction of catalytic cycles during  $\text{H}_2\text{O}_2$  detoxification of members according to the different Prx subgroups.** Reaction mechanisms are depicted A) as a general mechanism and with regenerators for the different subgroups B) 1-Cys Prx, C) 2-Cys Prx, D) Prx Q, and E) Type II Prx. The given numbers indicate the position of cysteines in the amino acid sequence of each Prx type from *A. thaliana* without signal peptide that participate in the catalytic cycle (modified after Horling et al., 2002). Abbreviations: CDSP32 = chloroplastidic drought-induced stress protein of 32 kDa (Trx), Cyp = cyclophilin, Grx = glutaredoxin, GST = glutathione-S-transferase,  $\text{H}_2\text{O}_2$  = hydrogen peroxide, ox. = oxidised, red. = reduced, -SH = thiol group, -SOH = sulfenic acid, S-S = disulfide bond, Trx = thioredoxin,

Dependent on the Prx subgroup electron donors responsible for the re-reduction during catalytic cycle range from glutaredoxins, thioredoxins, glutathione, NADPH-dependent

Dependent on the Prx subgroup electron donors responsible for the re-reduction during catalytic cycle range from glutaredoxins, thioredoxins, glutathione, NADPH-dependent thioredoxin reductase C (NTRC), CDSP32, to cyclophilins (Chevallet et al., 2003; Collin et al., 2003; Finkemeier et al., 2005; Laxa et al., 2007; Rouhier et al., 2001; Pérez-Ruiz et al., 2006; Broin and Rey, 2003; compare Fig. 1.4). Even the low-molecular weight antioxidant ascorbate was described just recently as regeneration partner for 1-Cys Prx (Monteiro et al., 2007). With this set of Prx, cells contain an extensive repertoire and capacity for peroxide detoxification. The chloroplastidic 2-Cys Prx were assigned to an important role in alternative water-water cycle detoxifying  $H_2O_2$  in the chloroplast besides the ascorbate-dependent water-water cycle employing APX (Dietz et al., 2002; Dietz et al., 2006). However, this protein family was also shown to display an important function in signal transduction pathways as Prx modulate redox-dependent signalling cascades and function as binding partners e.g. of cyclophilins (Dietz, 2003 a; Dietz, 2007): Signalling functions of Prdx 1 to 6 are known from mammalian/human system (Hofmann et al. 2002; compare section 1.3). Signalling functions can be realised via various mechanisms. The immediately obvious mechanism is linked to the  $H_2O_2$  detoxification capacity. As already described in section 1.1.3, this ROS executes a signalling effect in various cellular processes (Slesak et al., 2007). A modulation of cellular  $H_2O_2$  concentrations by Prx affects the subsequent signalling events. In addition, lipid peroxide concentrations may be controlled by Prx-mediated decomposition (Romero-Puertas et al., 2007; Finkemeier et al., 2005; Rouhier et al., 2004). The resulting impact on oxylipins formed from lipid peroxides (Baier and Dietz, 1999 b) may affect plant responses via modification of gene expression (Schilmiller and Howe, 2005). Also  $ONOO^-$  as implicated in different signalling pathways (Delledonne et al., 2001 and 2002; compare section 1.1.3).  $ONOO^-$  is reduced by different Prx (Bryk et al., 2000; Dubuisson et al., 2004; Romero-Puertas et al., 2007) and therefore might be involved in Prx-mediated signalling events. Additional mechanisms are achieved in concert with other proteins. During their catalytic cycle Prx obtain their electrons for re-reduction from interacting thiol proteins, thereby affecting their redox state. As Prx have a high affinity to peroxides and their regenerators themselves have regulatory function, they may act as peroxide sensors transmitting information to other thiol proteins (Dietz, 2003 b). Furthermore chaperone function and alteration of conformational states in a redox-dependent manner are two well-established properties of Prx and provide the possibility to alter transmittance of cell signals by binding of

Although members of all different Prx subgroups have important functions in antioxidant defence and/or signalling, the following introductory sections predominantly focus on *A. thaliana* type II Prx and 2-Cys Prx since both are object of the present work.

### 1.3.2. Type II peroxiredoxins

Type II Prx – as encoded by multiple genes – are the largest subgroup of these peroxidases in plants (Bréhélin et al., 2003). They were discovered in 1998 and 1999, about ten years after the first description of the 2-Cys Prx (Kim et al., 1988) and were initially named atypical 2-Cys Prx (Godon et al., 1998; Jeong et al., 1999; Verdoucq et al., 1999; Yamashita et al., 1999; Choi et al., 1999). In contrast to plants, the mammalian system contains just one gene of this type, namely Prdx 5 (Knoops et al., 1999). Type II Prx were characterised in many organisms throughout all kingdoms, both *in vitro* with heterologously expressed protein and *in vivo* (Banmeyer et al., 2004; Hosoya-Matsuda et al., 2005; Lim et al., 1998; Baker and Poole, 2003; Kropotov et al., 1999; Barranco-Medina et al., 2006; Horling et al., 2002; Finkemeier et al., 2005). It was shown that during their catalytic cycle type II Prx interact with either glutaredoxins (Grx) or thioredoxins (Trx), or both, as well as with GSH (Bréhélin et al., 2003; Rouhier et al., 2001; Hosoya-Matsuda et al., 2005; Finkemeier et al., 2005; Gama et al., 2008). Furthermore, gene expression studies revealed a high responsiveness of this class of Prx to a multitude of treatments (Horling et al., 2002 and 2003; Pena-Ahumada et al., 2006). Except for an up-regulation in high light, chloroplastic PrxII E exhibits mostly down-regulations like under salt stress (Horling et al., 2002 and 2003). Mitochondrial PrxII F preferentially responds to cadmium treatment (Finkemeier et al., 2005). In contrast, cytosolic type II Prx transcripts are very responsive and up-regulated upon various stress conditions, as shown for e. g. sodium chloride, diamide, H<sub>2</sub>O<sub>2</sub>, and cold (Horling et al., 2002 and 2003; Ströher et al., 2009).

Type II Prx additionally reveal an organ specific distribution as shown by means of transcript analysis and reporter gene expression in different plant organs (Bréhélin et al., 2003). PrxII E and PrxII F are expressed ubiquitously in every tissue, which is also true for PrxII B. In contrast, PrxII C and PrxII D are preferentially transcribed in floral tissues, especially in pollen. These results on transcript level are confirmed by promoter-GUS experiments and Western blot analysis employing different antibodies in

combination with protein extracts from different tissues for selected type II Prx (Bréhélin et al., 2003).

### 1.3.3. 2-Cysteine peroxiredoxins

Proteins of the subgroup of 2-Cys Prx are described throughout all kingdoms and are denominated with several synonyms, for instance AhpC in the bacterial system (alkylhydroperoxide reductase subunit C) (Parsonage et al., 2005; Jacobson et al., 1989), TSA from yeast (thiol specific antioxidant) (Chae et al., 1993; Kristensen et al., 1999) or the HBP in rat (heme-binding protein) (Hirotsu et al., 1999). The first plant 2-Cys Prx was discovered in barley and was designated BAS1 (Baier and Dietz, 1996 and 1997), followed by cloning and characterisation of 2-Cys Prx from other plant species in the following years (Berberich et al., 1998; Cheong et al., 1999; Horling et al., 2001). In *A. thaliana* two isoforms of these Prx are encoded in the genome and are both targeted to the chloroplast, namely 2-Cys Prx A and 2-Cys Prx B (Horling et al., 2003; Dietz et al., 2006). Whereas the localisation in the chloroplast is an important characteristic of this type of Prx in plants, other organisms such as vertebrates reveal a distribution of 2-Cys Prx throughout all different cell compartments (Immenschuh et al., 1995; Chae et al., 1993; Rabilloud et al., 1995; Wood et al., 2003 a).

2-Cys Prx as functional proteins adopt a variety of aggregation states (compare Fig. 1.5). A well-described biochemical feature is the interconversion of these different aggregates as a consequence of redox state. The monomer as the smallest unit represents the reduced and overoxidised state of the protein, with the latter being produced upon highly oxidising conditions when the thiol-groups of the cysteinyl residues form the sulfinic acid derivative (Jang et al., 2006). Monomers do not exist *in vivo*, the minimal unit is the dimer. Dimers assemble to oligomerised forms which are favoured under reducing and overoxidising conditions (König et al., 2003; Schröder et al., 2000; Wood et al., 2003 b). The dimers assemble to donut-like decameric structure via hydrogen bonds, salt bridges or hydrophobic interactions (Alphey et al., 2000; Wood et al., 2003 b). The oxidised form exists as dimer linked via one or two disulfide bonds, with both monomers orientated in a head-to-tail structure (Wood et al., 2003 b; Hirotsu et al., 1999). Certain conditions of the protein environment like e. g. high or low ionic strength as well as low pH promote the formation of oligomers (König et al., 2002; Kitano et al., 1999; Kristensen et al., 1999). Furthermore, aggregation of 2-Cys Prx occurs in a concentration dependent manner as shown by isothermal titration

calorimetry studies: below a critical transition concentration of about  $1 \mu\text{mol l}^{-1}$  the reduced protein exists as a dimer while above this concentration the decamer is stably build (Barranco-Medina et al., 2008 a). Even the formation of higher molecular aggregates has been described *in vitro*, as reports exist of double and triple stacks of bovine 2-Cys Prx SP-22 as well as dodecahedral structures (Gourlay et al., 2003; Meissner et al., 2006; compare Fig. 1.5).

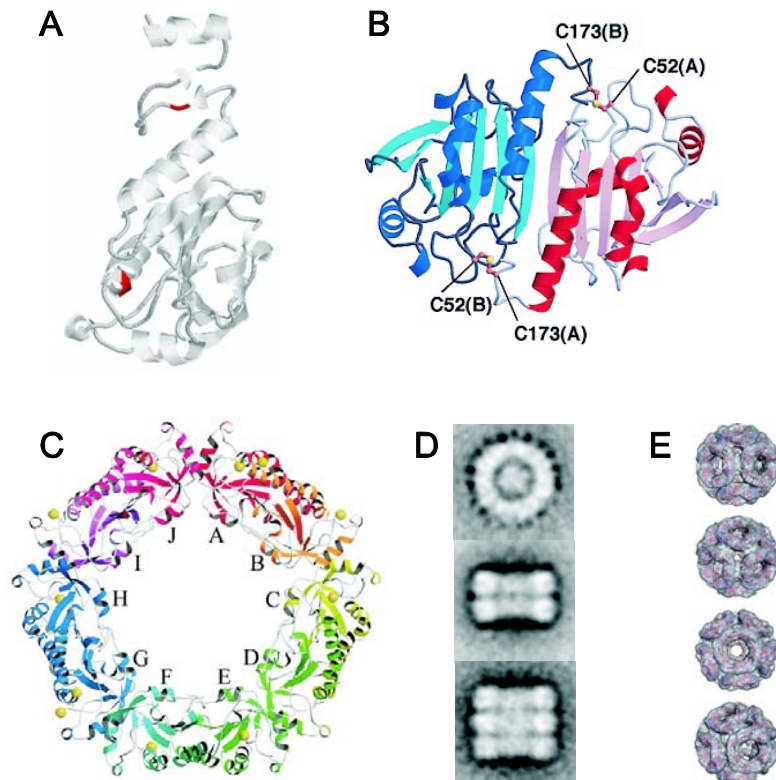


**Fig. 1.5: Depiction of different aggregation states of 2-Cys Prx.** A) Monomeric form of *A. thaliana* (3D-ribbon structure presentation generated with RasMol software on basis of 1qmvG, sequence identity: 63.5 %), red = conserved cysteine residues. B) Crystal structure of dimeric HBP 23 from *Rattus norvegicus* arranged in a head-to-tail orientation, with both monomers depicted in different colours (A = red, B = blue) (from Hirotsu et al., 1999). C) Crystal structure of TryP, a 2-Cys Prx from *Crithidia fasciculata* as reduced decamer with monomers depicted in different colours (from Alphey et al., 2000). D) Decameric toroid with double and triple stacks of bovine 2-Cys Prx SP-22 visualised via transmission electron microscopy (TEM) (from Gourlay et al., 2003). E) Dodecahedral structure of human 2-Cys Prx visualised as 3D-reconstruction after TEM (from Meissner et al., 2006). The different conformational states are not drawn to scale.

Apart from their diverse structural appearances, 2-Cys Prx also reveal different functional properties that have been extensively studied. First of all, 2-Cys Prx exhibits

catalytic activity in detoxification towards various substrates, as there are hydrogen peroxide, different alkyl hydroperoxides, phospholipid peroxides, and cholesterol peroxides (König et al., 2003; Nogoceke et al., 1997; Hillas et al., 2000; Wood et al., 2003 b). Additionally, the turnover of peroxyxynitrite has been described (Bryk et al., 2000; Wong et al., 2002; Trujillo et al., 2004). Re-reduction during the catalytic cycle is provided by the Trx/TR system, NTRC as well as GSH (Collin et al., 2003; Parsonage et al., 2005; Sekiya et al., 2006; Pérez-Ruiz et al., 2004; Sayed and Williams, 2004). An additional aspect connected to this detoxification capacity of certain ROS is the DNA protective function within a metal catalysed oxidation system. This function has been shown for 2-Cys Prx from different organisms, amongst them 2-Cys Prx from *A. thaliana* (Chauhan and Mande, 2002; Bernier-Villamor et al., 2004; Rho et al., 2006; Laxa et al., 2007).

Beyond that, 2-Cys Prx function as chaperones and are involved in different signalling processes (Wood et al., 2002; Jang et al., 2004; Baier and Dietz, 1999).

#### **1.3.4. Structural analyses of peroxiredoxins**

From the beginning of structural analyses of Prx, not only protein directly purified from tissue or defined cells was analysed, but a considerable number of studies was performed with protein obtained via molecular cloning and heterologous expression in suitable systems like *E. coli*. In addition to the high amount of purified recombinant protein, this also offers the possibility of comparative studies with wild-type and site-directed mutated variants altered in particular regions of the protein.

A very important role in the investigation of structural features of this superfamily of peroxidases is the transmission electron microscopy (TEM). Especially in the beginnings of structural investigations this method allowed for detailed insights into the larger aggregation forms. Besides the resolution of decameric arrangement of human 2-Cys Prx (Prdx 2) from erythrocytes (Schröder et al., 1999 and 2000) also high-order association states of oligomerisation (Gourlay et al., 2003) could be visualised, which could be improved in combination with techniques like 3D-modelling (Meissner et al., 2006).

Also x-ray crystallography is an important technique during investigation of structural features of Prx, as it allows for a more detailed insight compared to TEM via enabling even atomic resolutions of the structure. The first Prx crystal structure analysed was a human 2-Cys Prx (Choi et al., 1998). Furthermore x-ray crystallographic studies

visualised protein aggregates, for instance oxidised dimers of 2-Cys Prx with intermolecular disulfide bridges (Hirotsu et al., 1999; Schröder et al., 2000) as well as the intramolecular bond occurring during catalytic cycle of type II Prx (Declercq et al., 2001).

X-ray analysis of protein crystals provides static information of the atomic structure. Other techniques need to be deployed to understand dynamic features of protein functions. Prx, especially 2-Cys Prx, adopt different aggregation states (König et al., 2002; Wood et al., 2003 b) and thus undergo conformational changes during the catalytic cycle (Wood et al., 2003 b). Therefore it is of special interest to visualise these alterations for instance by means of dynamical imaging via diffracted x-ray tracking (DXT) (compare section 3.1).

#### **1.4. Aims of this work**

Prx display diverse functions in plant cells and tissues regarding detoxification of ROS and RNS as well as the involvement in various signalling pathways. Despite the progress made in understanding Prx function, open questions arise concerning structural dynamics and functional differentiation of highly similar isoforms.

In order to achieve a characterisation of a certain protein of interest, it is important to perform both, a functional and a structural analysis. To achieve the latter the utilisation of x-rays within different techniques is of significance and plays an important role when it comes to the analysis of single conversion steps within the process of conformational changes. 2-Cys Prx is an ideal candidate for the visualisation of such alterations because of its various conformational states that either occurs on the level of the dimer or higher aggregation state level (König et al., 2002; Wood et al., 2002). Although experimental evidence exists for single conformational states, especially the transition forms are not analysed in detail due to the limitations of available techniques, mostly elucidating static protein forms. Dynamical imaging via diffracted x-ray tracking (DXT) provides a new tool for a deeper insight into mechanisms of structural interconversions (compare section 3.1). The establishment of a certain protein for dynamical imaging via x-ray dependent techniques relies on various properties as prerequisites. The aim of the present work was to characterise 2-Cys Prx in respect to these features.

In addition to the technical prerequisites to enable DXT, the functionality of 2-Cys Prx has to be assured, as irradiation-mediated damage of proteins is an important topic brought more and more into focus of attention (Garman and McSweeney, 2007). In this context, detailed descriptions of such protein damage are scarce and mostly incorporated into crystallographic analyses up to now (Leiros et al., 2001; Ravelli and McSweeney, 2000). Therefore this study also focused on structural and functional impairments by x-rays on 2-Cys Prx stability.

Of further interest within this work was the investigation of functional stability of cytosolic type II Prx and the differentiation between those isoforms sharing a very high sequence homology. An incorporation of the data obtained from functional characterisation into data derived from a bioinformatic analysis was furthermore expected to give first insights into the involvement of these Prx in the antioxidative system of the cell versus a role in signal transduction.

## 2. Materials and Methods

### 2.1 Plant growth and material

#### 2.1.1 Plant material

In general plants of *Arabidopsis thaliana* (ecotype Columbia-0) were used during this work. In addition to wild type plants, different T-DNA insertion lines from the SALK collection (Alonso et al., 2003) were investigated as listed in Table 2.1

**Tab. 2.1: List of transgenic lines of *Arabidopsis thaliana* used in this study.** Given are SALK code numbers and affected genes of the utilised lines as well as the origin of the lines.

Gene	Line	Origin
PrxII B	SALK_009604	SALK collection
PrxII C	SALK_069621	SALK collection
PrxII D	SALK_138035	SALK collection

#### 2.1.2 Plant growth

##### 2.1.2.1 Soil culture

Plants were grown on an autoclaved soil mixture of Frühstorfer Pikiererde Klocke P, perlite and vermiculite in a ratio 2:1:1 in controlled conditions with a day-night-cycle of 10 h light (100-120  $\mu\text{mol quanta s}^{-1}$ , 23 °C) and 14 h of dark (18 °C) with an average humidity of 50 %. After sowing of the seeds, stratification for 48 h at 4 °C enabled a synchronised germination.

##### 2.1.2.2 MS plates

Seedlings were germinated and grown on  $\frac{1}{2}$  MS medium (Murashige and Skoog, 1962) in petri dishes, 100 ml medium containing 0,215 g MS (Duchefa, Haarlem, Netherlands) and 0,44 g of phytigel (Sigma, Germany). After adjusting the pH to 5.7 with KOH, the medium was autoclaved for sterilisation. For screening of SALK

T-DNA insertion lines, kanamycin was added to the medium to a final concentration of  $25 \mu\text{g ml}^{-1}$ . After sowing of the seeds, they were likewise stratified at  $4 \text{ }^{\circ}\text{C}$  for 48 h.

### 2.1.2.3 Sterilisation of seeds

Before sowing on MS plates (see 2.1.2.2) *A. thaliana* seeds were surface sterilised in order to avoid contamination. A first incubation for five minutes with 70 % (v/v) ethanol/0.1 % (w/v) SDS was followed by 15 minutes shaking in 20 % (v/v) commercial bleach containing 0.1 % (w/v) SDS. The seeds were washed four to six times with sterile ddH<sub>2</sub>O to remove residual sterilising reagent.

### 2.1.3 Stress experiments

Different effectors were analysed for their effects on transcript regulations during short term experiments with leaf discs harvested from four week old plants. The excised leaf discs of 0.3 cm in diameter were infiltrated for  $3 \times 2$  min with effector-containing solution and incubated for four hours under climate chamber conditions (see 2.1.2.1). Additional to effector treatments, leaf discs were exposed to high light for four hours ( $800 \mu\text{mol quanta m}^{-2} \text{ s}^{-1}$ ). On the other hand physiological parameters such as ion leakage (2.1.3.1) were quantified in the T-DNA insertion lines in comparison to wild type plants as consequence of methyl viologen (MV) treatment as described in the following. A compilation of utilised stress conditions and performed analyses is given in Table 2.2.

**Tab. 2.2: Compilation of the different stress experiments comparatively performed with wild type and the cytosolic type II Prx T-DNA insertion lines.** Described are the treatments and their duration additionally to the performed analyses.

Treatment	Concentration	Duration	Additional information
H <sub>2</sub> O <sub>2</sub>	10 mM	4 h	Leaf discs, transcript analysis
NaCl	50 mM	4 h	
High light	$800 \mu\text{mol quanta m}^{-2} \text{ s}^{-1}$	4 h	
MV	1 $\mu\text{M}$	16 h	Leaf discs, leakage measurement

### **2.1.3.1 Ion leakage measurements**

Application of methyl viologen (MV) in the light results in generation of ROS in the chloroplast with subsequent lipid peroxidation. The resulting loss of membrane integrity causes leakage of cell contents to the surrounding medium (Harris and Dodge, 1972). The electrolyte loss leads to an increase of conductance of the medium. Therefore ion leakage provides insight into antioxidative capacity of plants.

Leaf discs of 0.5 cm in diameter were excised from four week old plants and placed in single wells of a microtiter plate, each containing 1 ml of either 1  $\mu$ M MV or water as control. After infiltration for 3 $\times$ 2 min and subsequent incubation for 18 h under continuous light, leaf discs were transferred to 1 ml of fresh ddH<sub>2</sub>O and heated for 30 min at 95 °C to achieve a release of the remaining cell contents. Prior to leakage measurement with a conductivity meter (EC/TDS/SALT Testr low<sup>+</sup>, Eutech Instruments, Nijkerk, Netherlands), the samples were centrifuged for 5 min (RT, 13,000xg). The ion leakage as consequence of differential treatment was given as percentage of whole ion content of the cell, which was calculated from conductivities of experimental solution and boiled leaf solution. As additional control, a set of leaf discs was incubated with MV in the dark.

## **2.2 Molecular biological methods**

### **2.2.1 Isolation of genomic DNA**

The isolation of genomic DNA from green plant material of Arabidopsis was conducted according to Edwards et al. (1991). The plant material was homogenised in a reaction tube with a micro pestle, followed by addition of 500  $\mu$ l Edwards extraction buffer. The samples were thoroughly mixed by shaking for 5 s and subsequently centrifuged for two minutes at room temperature (13,000xg). 300  $\mu$ l of the supernatant were transferred to a new reaction tube and mixed with 310  $\mu$ l isopropanol for DNA precipitation. After incubation for 2 min (RT), the samples were centrifuged (7 min, RT, 13,000xg). The obtained DNA sediment was air dried for 5-10 min and finally resuspended in 100  $\mu$ l of sterile water.

---

**Edwards extraction buffer**

---

200 mM Tris-HCl, pH 7,5

250 mM NaCl

25 mM EDTA

0.5 % (v/v) SDS

---

**2.2.2 RNA isolation and cDNA synthesis**

Whole RNA was isolated from Arabidopsis leaf discs after the short term stress experiments (see 2.1.3). Plant material was frozen in liquid nitrogen and homogenised upon continuous supply with liquid nitrogen to avoid thawing of the samples. After transfer to a 2 ml reaction tube, the homogenised leaf material was supplemented with 0.5 ml RNA lysis buffer and thoroughly mixed. Subsequently, 0.5 ml phenol and 0.5 ml of chloroform-isoamylalcohol (24:1) were added and again the solution was mixed. After centrifugation for 5 min (4 °C, 13,000xg) the aqueous phase was collected and additional extraction steps were performed, using a 25:24:1 mixture of phenol, chloroform, and isoamylalcohol and subsequently chloroform-isoamylalcohol. The supernatant from the following centrifugation (3 min, 4 °C, 13,000xg) was supplemented with 0.5 ml of isopropanol for precipitation of nucleic acids at 4 °C for 1 h. The resulting sediment after 15 min centrifugation (4 °C, 13,000xg) was resuspended in ¼ volume 8 M LiCl and ¾ volumes of sterile ddH<sub>2</sub>O in order to precipitate RNA during incubation of the samples for 2 h on ice. Following further centrifugation (10 min, 4 °C, 13,000xg), the resulting RNA sediments were washed with 70 % (v/v) ethanol. After its removal, the sediment was air dried and subsequently dissolved in 25-50 µl of sterile ddH<sub>2</sub>O.

Residual DNA was removed by treatment with DNaseI (Promega, Mannheim, Germany). Prior to cDNA synthesis, DNase was inactivated by adding DNase STOP solution (Promega, Mannheim, Germany) and incubating for 20 min at 70 °C with subsequent freezing in liquid nitrogen. 2 µl oligo-dT primers at 0.5 µg/µl concentration were added and samples were incubated for 10 min at 70 °C with subsequent chilling on ice for 5 min. The reverse transcription reaction was performed with the enzyme MMLV (moloney-murine-leukemia virus) RT (reverse transcriptase) II [H-] (Promega, Mannheim, Germany) at 42 °C for 65 min. This reaction was terminated by incubation for 15 min at 70 °C.

RNA lysis buffer
100 mM Tris-HCl, pH 8.5
25 mM EDTA
25 mM EGTA
100 mM $\beta$ -Mercaptoethanol
2 % (w/v) SDS

### 2.2.3 Polymerase chain reaction (PCR)

Polymerase chain reaction (PCR) is a technique enabling a fast and specific amplification of defined DNA fragments by application of a continuous repetition of defined temperature cycles allowing for template denaturation, primer annealing and elongation of the product (for a typical PCR reaction protocol see Tab. 2.3). The reaction requires the presence of excess amounts of forward and reverse primer, deoxyribonucleotide triphosphates (dNTPs),  $MgCl_2$  as co-factor, and template DNA additional to polymerase buffer. In this work, the elongation was catalysed by the heat stable Taq DNA-polymerase.

**Tab. 2.3: Typical PCR reaction protocol.** Displayed are the different functional steps of a typical PCR reaction with the number of cycles, their temperatures and durations.

No. of cycles	Function	Temperature [ $^{\circ}C$ ]	Time [min]
1	denaturation	94	3:00
27-45	denaturation	94	0:30
	primer annealing	variable	0:45
	elongation	72	1:00
1	elongation	72	5:00

To carry out PCR analysis, the annealing temperature of the utilised primers to the DNA template had to be optimised. Therefore gradient PCRs were performed, using 20  $\mu$ l reactions (see Tab. 2.4) within a typical PCR reaction protocol (see Tab. 2.3) with variable annealing temperatures during the second step. For DNA fragments exceeding the size of 1 kb, the elongation time of the programme was increased, as the

polymerisation rate of the utilised Taq only allows for amplification of about 1 kb-fragments per minute.

**Tab. 2.4: Composition of a 20 µl PCR reaction.** Displayed are the different compounds with their concentrations and volumes within a typical 20 µl PCR reaction.

Component [Concentration]	Volume [µl]
Primer forward [10 pmol/µl]	0.4
Primer reverse [10 pmol/µl]	0.4
dNTPs [10 mM each]	0.4
MgCl <sub>2</sub> [25 mM]	1.28
TAQ buffer [10×]	2
Taq polymerase	1
DNA template	X
sterile H <sub>2</sub> O	14.52-X

#### 10×TAQ buffer

250 mM Tris-HCl, pH 8.4

500 mM KCl

15 mM MgSO<sub>4</sub>

#### 2.2.3.1 Genomic PCR for identification of homozygous T-DNA insertion lines

SALK lines were screened for homozygous T-DNA insertions by utilisation of different primer combinations. A first PCR confirmed the existence of the insertion by a primer pair specific for kanamycin resistance gene (Kan-F and Kan-R) localised in the T-DNA sequence. Furthermore the combination of a T-DNA specific (LBa1) and a gene specific primer was applied to prove the predicted site of insertion. As this gives no insight into heterozygosity or homozygosity of the insertion, additionally primers were used flanking the insertion site. While a heterozygous integration of the T-DNA would result in the amplification of a product, no amplicate would be obtained in the case of a homozygous insertion. See Appendix A for primer sequences and annealing temperatures.

### 2.2.3.2 Semi quantitative RT-PCR

Reverse transcriptase (RT) PCR allows for semiquantitative comparison of gene expression patterns for instance of differentially treated plant material or different transgenic lines. Firstly, cDNA was tested for lack of genomic DNA with the primer combination 2-CP-F and 2-CP-R being specific for 2-Cys Prx (At3g11630) and generating a fragment of 1117 bp size with introns and with 551 bp length if genomic DNA was absent. To adjust cDNA amounts of different samples, a standardisation on actin-2 (At5g09810) was performed, which was shown to be constitutively expressed, independent of plant tissue or effector treatment (Kreuzer et al., 1999). For primer combinations, annealing temperatures and numbers of cycles of analysed genes see Appendix B, the applied PCR reaction protocol is described in Tab. 2.5. Reaction cycles were optimised in order to visualise differences between the samples. The separation of PCR products was performed on 2 % (w/v) agarose gels for 10 min at 120 V (compare 2.2.4).

**Tab. 2.5: PCR reaction protocol for RT-PCR.** Annealing temperatures and the number of reaction cycles depended on the amplified gene.

No. of cycles	Temperature [°C]	Time [min]
1	94	3:00
27-45	94	0:15
	variable	0:30
	72	0:45
1	72	0:01

### 2.2.3.3 Phusion PCR

The utilisation of Phusion polymerase (Finnzymes, Espoo, Finland) as a different DNA-polymerase was necessary to reduce error probability during amplification as it has proof-reading function. Due to the characteristics of Phusion polymerase, both PCR reaction and PCR protocol had to be adjusted as displayed in Tab. 2.6 and Tab. 2.7, respectively. In case of problematic amplification of the fragment, DMSO was added to the PCR reaction with a concentration of up to 3 % (v/v).

**Tab. 2.6: Composition of a 50  $\mu$ l PCR reaction.** Displayed are the different compounds with their concentrations and volumes added to a typical 50  $\mu$ l PCR reaction containing Phusion polymerase.

Component [Concentration]	Volume [ $\mu$ l]
Primer forward [10 pmol/ $\mu$ l]	1.5
Primer reverse [10 pmol/ $\mu$ l]	1.5
dNTPs [10 mM each]	1
GC buffer [5 $\times$ ]	10
Phusion polymerase	0.5
DNA template	X
sterile H <sub>2</sub> O	35.5-X

**Tab. 2.7: PCR reaction protocol for PCR with Phusion polymerase.** Annealing temperatures and the number of reaction cycles depend on the amplified gene.

No. of cycles	Temperature [ $^{\circ}$ C]	Time [min]
1	98	0:30
27-45	98	0:10
	variable	0:30
	72	0:45
1	72	10:00

#### 2.2.3.4 Site directed mutagenesis

Site directed mutagenesis is a powerful approach to introduce point mutations in a given DNA sequence. During this work, the method was applied to exchange amino acids of interest in the protein 2-Cys Prx A. The technique utilises a set of four primers for a first amplification of two fragments: one containing the point mutation in the sequence of its reverse and one in the forward primer. In both PCR reactions the second primer was the corresponding gene specific one. For the following PCR, 60 ng of both fragments served as template and amplification was performed with both gene specific primers. As the region of the introduced point mutation is complementary in both fragments, a hybridisation of these parts allows for amplification of the whole length product with the introduced mutation. For amplification of the product 50  $\mu$ l reactions were used as

displayed in Table 2.9 within a PCR reaction protocol as shown in Table 2.8. For primer sequences as well as annealing temperatures see Appendix C.

**Tab. 2.8: Typical PCR reaction protocol for amplification of high fragment amounts.** Displayed are the different functional steps of a typical PCR reaction with the number of cycles, their temperatures and durations.

No. of cycles	Temperature [°C]	Time [min]
1	94	3:00
45	94	0:30
	variable	0:45
	72	1:00
1	72	5:00

**Tab. 2.9: Composition of 50 µl PCR reaction.** Displayed are the different compounds with their concentrations and volumes within a typical 50 µl PCR reaction.

Component [concentration]	Volume [µl]
Primer forward [10 pmol/µl]	2.0
Primer reverse [10 pmol/µl]	2.0
dNTPs [10 mM each]	1.0
MgCl <sub>2</sub> [25 mM]	3.6
TAQ buffer [10×]	5
Taq polymerase	1
DNA template	X
sterile H <sub>2</sub> O	34.4-X

#### 2.2.4 Agarose gel electrophoresis

An electrophoretic separation of DNA fragments according to their size was performed on 1-2 % (w/v) agarose gels. Agarose (Roth, Karlsruhe, Germany) was dissolved in 1×TAE buffer with 5 µg ml<sup>-1</sup> ethidium bromide (Roth, Karlsruhe, Germany) for visualisation of DNA. 6×DNA loading buffer was added to the samples prior to loading on the gel and separation was performed at constant voltage of 120 V. Detection of DNA via the intercalating substance ethidium bromide was performed with the help of a UV-light box in combination with a CCD-camera (INTAS, Göttingen, Germany) at

312 nm. For estimation of fragment size or amount of the amplificate 1kB ladder (Invitrogen, Karlsruhe, Germany) or low mass ladder (Invitrogen, Karlsruhe, Germany) were loaded, respectively.

<b>50×TAE buffer</b>
2 M Tris-acetate, pH 7.5
50 mM EDTA

<b>6×DNA loading buffer</b>
30 % (v/v) Glycerol
0.25 % (w/v) Bromophenol blue
0.25 % (w/v) Xylene cyanol

## **2.2.5 Cloning and transformation into *E. coli***

### **2.2.5.1 Introduction of restriction sites**

For heterologous expression of specific proteins, the gene products of interest were cloned in a vector N-terminally attaching the nucleotide sequence of a 6×histidin (His) tag. Therefore it was necessary to introduce restriction sites flanking the coding sequence which was done by PCR with cDNA as template and primers containing these restriction sequences. For primer design it was taken into account that the products had to be in frame after ligation into the vector. Furthermore, the fragment was analysed with the “NEBcutter” software (<http://tools.neb.com/NEBcutter2/index.php>) to exclude the possibility that the restriction enzyme digests the fragment itself. PCR amplification of the products containing restriction sites at both ends was performed in a 50 µl reaction (see Tab. 2.9) following the protocol displayed in Table 2.8 with the primers listed in Appendix C.

### **2.2.5.2 Purification of amplified DNA fragments by agarose gel electrophoresis**

The purification of amplified DNA fragments after separation in agarose gels was performed with the ‘Wizard<sup>®</sup> SV Gel and PCR Clean Up System’ (Promega, Mannheim, Germany) according to the manufacturer’s manual. Different to the

instructions, DNA was not eluted with nuclease free water but with sterile 10 mM Tris-HCl, pH 6.8.

### 2.2.5.3 Digestion of DNA fragments

Restriction site mediated cloning of PCR products necessitates the digestion of both, fragment and vector with the required restriction enzymes. The components needed for such a reaction are listed in Tab. 2.10. Depending on the restriction enzymes used, different buffer conditions were applied as recommended by the manufacturer. The combination of restriction enzymes and used buffers (New England Biolabs, Ipswich, MA) can be found in Tab. 2.11. For PCR products and vectors, different volumes were used for the digestion reaction (25  $\mu$ l of amplificate or 10  $\mu$ l of plasmid, respectively).

**Tab. 2.10: Composition of 50  $\mu$ l digestion reaction.** Displayed are the components of a 50  $\mu$ l digestion reaction containing two restriction enzymes.

Component [Concentration]	Volume [ $\mu$ l]
PCR product/vector	X
Restriction enzyme I	1
Restriction enzyme II	1
Restriction buffer [10 $\times$ ]	5
BSA	0.8
Sterile ddH <sub>2</sub> O	42.2-X

**Tab. 2.11: Restriction enzymes and corresponding restriction buffers utilised during this work.** Displayed are the buffer conditions being required for double digests.

Combination of restriction enzymes	Recommended buffers
BamHI/SacI	NEB1 + BSA
BamHI/KpnI	NEB1 + BSA

The digestion reactions were incubated for 2 h at 37 °C. Afterwards 6 $\times$ DNA loading buffer was added and the samples were loaded on an agarose gel. After the separation the DNA purification was performed as described in 2.2.5.2.

#### 2.2.5.4 Ligation

Digested and purified PCR products and vectors were ligated over night at 16 °C with T4-DNA Ligase (New England Biolabs, Ipswich, MA). Components of the ligation reaction generally were 7 µl of PCR product, 1 µl vector, 1 µl T4-DNA ligase buffer [10×] and 1 µl of T4-DNA ligase. In this work, fragments were cloned into pQE-30 vector.

#### 2.2.5.5 TOPO cloning

In order to achieve an introduction in pEXP5-NT/Topo<sup>®</sup>-vector, the DNA fragment of interest was amplified with Phusion-PCR (compare section 2.2.3.3) and a subsequent incubation with Taq polymerase at 72 °C for 10 min provided for A-overhang (Tab. 2.12). This A-overlap enables an easy ligation catalysed by the topoisomerase which is covalently bound to the 3'-phosphate of the vector's T-overhang.

**Tab. 2.12: Composition of reaction mixture to introduce A-overhang.** Displayed are the components of a 10 µl reaction.

Component [concentration]	Volume [µl]
dNTPs [10 mM each]	0.4
MgCl <sub>2</sub> [25 mM]	0.6
TAQ buffer [10×]	1
Taq polymerase	0.4
PCR product	7.6

Subsequently, 2 µl of this reaction mixture was added to 0.5 µl salt solution and 0.5 µl pEXP5-NT/Topo<sup>®</sup>-vector and incubated for 15 to 30 min at room temperature.

#### 2.2.5.6 Transformation of bacterial strains

For transformation of DNA-fragments, competent *E. coli* cells (strains DH5α for uptake of the construct, or BL21(DE3)pLysS as expression strain) were first thawed on ice. 2-5 µl of ligation reaction were added to 25 µl of bacteria and incubated for 30 min on ice. Subsequently, heat shock was performed by exposing the bacteria for 30 s to 42 °C, followed by a short incubation on ice (for 2-3 min) and addition of 250 µl SOC medium. In the following, bacteria were shaken for 1 h at 37 °C (140 rpm) for recovery,

and they were finally plated on LB agar plates (see 2.2.5.7) containing  $100 \mu\text{g ml}^{-1}$  of ampicillin.

<b>SOC medium</b>
2 % (w/v) Tryptone
0.5 % (w/v) Yeast extract
10 mM NaCl
2.5 mM KCl
10 mM $\text{MgCl}_2$
10 mM $\text{MgSO}_4$
20 mM Glucose

#### **2.2.5.7 LB medium and agar plates**

Bacteria were grown in Luria Bertani (LB) medium containing antibiotics to avoid unspecific growth in the cultures. Medium for agar plates contained 1.5 % (w/v) agar and after melting in the microwave, antibiotics were added and medium was poured into Petri dishes under sterile conditions to avoid contamination.

<b>LB medium</b>
1 % (w/v) Tryptone
1 % (w/v) NaCl
0.5 % (w/v) Yeast extract

#### **2.2.5.8 Colony PCR**

A first screening of the grown bacterial colonies after plating on selective media was performed by colony PCR (for PCR programme see Tab. 2.13). This technique allows for verifying of fragment insertion and furthermore gives hints on the direction the insert was ligated into the vector. Therefore grown colonies were resuspended in  $30 \mu\text{l}$  sterile ddH<sub>2</sub>O.  $5 \mu\text{l}$  of suspension was used as template for a PCR reaction with a specific set of primers. Gene specific primers were utilised to prove the presence of the whole fragment, while additionally a combination of a vector located forward primer

and a gene specific reverse primer only amplified products in case of correct orientation of the inserted fragments.

**Tab. 2.13: Typical colony PCR reaction protocol.** Displayed are the different functional steps of a typical colony PCR reaction with the number of cycles, their temperatures and durations.

No. of cycles	Temperature [°C]	Time [min]
1	94	5:00
45	94	1:00
	variable	1:00
	72	1:30
1	72	5:00

#### 2.2.5.9 Overnight cultures and glycerol stock solutions of bacteria cultures

4.5 ml of LB medium (2.2.5.7) were inoculated with resuspended bacteria cells from single colonies carrying the correct insertion of the fragment of interest. LB medium contained  $100 \mu\text{g ml}^{-1}$  ampicillin for selection and bacteria were grown over night at  $37^\circ\text{C}$  with continuous shaking (140 rpm). For storage of bacteria strains, 800  $\mu\text{l}$  of the cultures were supplemented with 200  $\mu\text{l}$  of glycerol, frozen in liquid nitrogen, and transferred to  $-80^\circ\text{C}$ .

#### 2.2.5.10 Isolation of plasmids

Isolation of plasmids by a miniprep procedure was performed with the ‘Wizard<sup>®</sup> Plus SV Miniprep DNA purification system’ (Promega, Mannheim, Germany) according to the manufacturer’s manual. Elution was not performed as described in the protocol but with sterile 10 mM Tris-HCl, pH 6.8.

The isolated plasmids were quantified by agarose gel electrophoresis with DNA low mass ladder (Invitrogen, Karlsruhe, Germany). Furthermore PCR with primer combinations according to the colony PCR recipe (2.2.5.8) and 1  $\mu\text{l}$  of plasmid as template and/or analytical digestion (2.2.5.11) was performed in order to verify correct insertion of the fragment.

### 2.2.5.11 Analytical digestion

Analytical digestion was performed with restriction enzymes corresponding to the introduced restriction sites bordering the fragment sequence (see 2.2.5.1 and Tab. 2.11). 20 µl digestion reactions (see Tab. 2.14) were incubated at 37 °C for two hours. Subsequently they were supplemented with 6×DNA loading buffer and separated on an agarose gel in order to check for the size of the introduced fragment.

**Tab. 2.14: Composition of a 20 µl digestion reaction.** Displayed are the components of a 20 µl digestion reaction containing two restriction enzymes. For combination of enzymes and buffers compare Tab. 2.11.

Component [Concentration]	Volume [µl]
Plasmid	X (200 ng)
Restriction enzyme I	0.5
Restriction enzyme II	0.5
Restriction buffer [10×]	2
BSA	0.3
Sterile water	16.7-X

### 2.2.5.12 Sequencing

Sequence analysis of cloned fragments was performed by the company MWG Biotech (Martinsried, Germany) or by the CeBiTec sequencing facility at Bielefeld University. The obtained sequences were aligned with the original sequences of the introduced fragments utilising the publicly available programme ClustalW (<http://www.ebi.ac.uk/clustalW/>). Furthermore the obtained nucleic acid sequences were translated into the corresponding amino acids using the ExPASy translate tool (<http://www.expasy.ch/tools/dna.html>) to verify the inserted sequence being in frame with the fused 6×His tag and the initiation site of translation. In case of the correct sequence inserted in frame, plasmids were used for transformation of *E. coli* strain BL21 for subsequent expression and purification (2.3.1) of the recombinant protein.

## 2.3 Protein biochemical methods

### 2.3.1 Heterologous expression in *E. coli* and purification of recombinant protein

#### 2.3.1.1 Expression in *E. coli* M15 or BL21

*E. coli* M15 or BL21 cells were grown in 150 ml LB cultures containing the selection marker ampicillin with a final concentration of  $100 \mu\text{g ml}^{-1}$ . Following overnight incubation at  $37^\circ\text{C}$  with continuous shaking (140 rpm) these cultures were used to inoculate 1 l expression cultures that were supplemented with ampicillin at a concentration of  $100 \mu\text{g ml}^{-1}$ . Bacteria cultures were grown at  $37^\circ\text{C}$  to an  $\text{OD}_{600}$  of 0.6 to 0.8. Protein synthesis was induced by addition of isopropyl- $\beta$ -D-thiogalactopyranoside (IPTG) to the medium to a final concentration of 0.1 or 0.4 mM depending on the expressed protein. Cells were harvested after 4 h by centrifugation at 5,000 rpm for 15 min at  $4^\circ\text{C}$ . The sediment was stored at  $-20^\circ\text{C}$  until purification. Prior to the first large scale expression of each protein, test expressions were performed in order to optimise protein yield by application of different concentrations of IPTG, variation of the expression time, and testing different BL21 stock cultures.

#### 2.3.1.2 Purification of recombinant protein

For purification the harvested bacteria cells (see 2.3.1.1) were thoroughly resuspended in lysis buffer and subsequently sonicated using 3 cycles of 10 s each at 200 W (Sonoplus Bandelin electronics, Berlin, Germany) on ice. Lysozyme (Roth, Karlsruhe, Germany) was added to a final concentration of  $1 \text{ mg ml}^{-1}$  and the cells were shaken for 1 h at  $4^\circ\text{C}$  and again sonicated. In order to remove cell debris, the sample was centrifuged at 15,000 rpm at  $4^\circ\text{C}$  for 30 min. The obtained supernatant was loaded on a nickel-nitrilotriacetic acid (NTA) column (Quiagen, Hilden, Germany) previously equilibrated with about 20 ml of lysis buffer and shaken for 1 h at  $4^\circ\text{C}$ . Washing of the loaded resin with 50 ml of washing buffer I and 50 ml of washing buffer II was followed by removal of the proteins from the column with elution buffer containing imidazole. The protein containing fractions measured at 280 nm were pooled and dialysed against 40 mM  $\text{K-P}_i$  buffer, pH 7.0 for removal of imidazole. After dialysis, protein content was measured with the BioRad protein assay (see 2.3.3) and the solution was aliquoted, shock frozen in liquid nitrogen, and stored at  $-80^\circ\text{C}$ .

---

**Lysis buffer**


---

50 mM NaH<sub>2</sub>PO<sub>4</sub>  
 300 mM NaCl  
 10 mM Imidazole  
 20 mM β-Mercaptoethanol  
 pH adjusted to 8.0 (NaOH)

---

<b>Washing buffer I</b>	<b>Washing buffer II</b>
50 mM NaH <sub>2</sub> PO <sub>4</sub>	50 mM NaH <sub>2</sub> PO <sub>4</sub>
300 mM NaCl	300 mM NaCl
20 mM Imidazole	20 % (v/v) Glycerol
20 mM β-Mercaptoethanol	40 mM Imidazole
	20 mM β-Mercaptoethanol
pH adjusted to 8.0 (NaOH)	pH adjusted to 8.0 (NaOH)

---



---

**Elution buffer**


---

50 mM NaH<sub>2</sub>PO<sub>4</sub>  
 300 mM NaCl  
 250 mM Imidazole  
 20 mM β-Mercaptoethanol  
 pH adjusted to 8.0 (NaOH)

---

### 2.3.2 Protein extraction from *A. thaliana* plant material

For extraction of *Arabidopsis thaliana* proteins, either leaves or whole seedlings were homogenised with a micropestle in a 1.5 ml reaction tube. One leaf or 5-10 seedlings were supplemented with 300 µl of extraction buffer (0.5 M Tris-HCl, pH 6.8) and quartz sand. After thorough grinding, the extract was centrifuged at maximum speed (10 min, 4 °C) and the supernatant was transferred to a fresh reaction tube. Protein content was measured with the BioRad protein assay (see 2.3.3) and the extracts were stored at -20 °C.

### 2.3.3 Quantification of protein content with the BioRad protein assay

The amount of protein in extracts or solutions was measured using the BioRad reagent (Bio-Rad Laboratories, Munich, Germany) according to the manufacturer's manual. This detection method employs the dye Coomassie Brilliant Blue G250 that forms complexes with hydrophobic and aromatic amino acids in acidic conditions (Bradford, 1976) causing a red shift from 470 nm to 595 nm. 200  $\mu$ l reactions contained 40  $\mu$ l of BioRad reagent and 2-5  $\mu$ l of protein solution replenished to the final volume with ddH<sub>2</sub>O. After 5 min of incubation at room temperature the absorption at 595 nm was measured with a microplate autoreader (PowerWave<sup>TM</sup> 200, BIOTEK Instruments, Bad Friedrichshall, Germany,) and processed with the KC4<sup>TM</sup> software. For standardisation, different amounts of bovine serum albumin (BSA) were used.

### 2.3.4 SDS polyacrylamide gel electrophoresis

SDS polyacrylamide gel electrophoresis (SDS-PAGE) is a technique that allows for separation of proteins according to their apparent molecular masses. Prior to separation protein loading buffer was added to the samples, the contained anionic detergent SDS binds to hydrophobic parts of the proteins and adds a rather uniform negative charge. Furthermore, for reducing the sample, dithiothreitol (DTT) was added to the loading buffer in order to reduce disulfide bridges. In combination with heating for 5-10 min which causes denaturation of tertiary and quaternary structures, an electrophoretic mobility according to the protein molecular mass within an electric field is achieved. Gel electrophoresis was performed according to Dietz and Bogorad (1987) on a 12 % (w/v) polyacrylamide (PAA) gel with a 6 % (w/v) stacking gel and a discontinuous Tris-HCl/glycine buffer system. The detection of proteins was subsequently performed either via Coomassie or silver staining (2.3.5 or 2.3.6, respectively) or by Western blot analysis was performed for antibody-mediated detection of specific antigens (2.3.8). Dependent on the detection method, different protein markers were loaded to estimate protein size. For Coomassie and silver staining 'PageRuler<sup>TM</sup> Unstained Protein Ladder' (Fermentas, St. Leon-Rot, Germany) was used, in case of Western blot analysis PageRuler<sup>TM</sup> Prestained Protein Ladder' (Fermentas, St. Leon-Rot, Germany) was applied.

If indicated, other reducing or denaturing conditions for instance  $\beta$ -mercaptoethanol ( $\beta$ -ME) or urea, respectively, were applied to the protein loading buffer.

---

**4×Protein loading buffer**


---

200 mM Tris-HCl, pH 8.8

40 % (v/v) Glycerol

8 % (w/v) SDS

0.04 % (w/v) Bromophenol blue

<b>6 % stacking gel</b>	<b>12 % separation gel</b>
25 % (v/v) 0.5 M Tris-HCl pH 6.8	25 % (v/v) 1.5 M Tris-HCl pH 8.8
5.84 % (w/v) Acrylamide	12.17 % (w/v) Acrylamide
0.16 % (w/v) Bisacrylamide	0.33 % (w/v) Bisacrylamide
0.1 % (w/v) AMPS	0.04 % (w/v) AMPS
0.1 % (v/v) TEMED	0.03 % (v/v) TEMED

---



---

**1×Reservoir buffer**


---

1.44 % (w/v) Glycine

3.03 % (w/v) Tris

0.1 % (w/v) SDS

**2.3.5 Coomassie staining of polyacrylamide (PAA) gels**

The staining of protein gels with the dye Coomassie brilliant blue enables visualisation of protein amounts of at least 1 µg per band. The staining solution contained 0.1 % (w/v) Coomassie brilliant blue R250 in 40 % (v/v) ethanol, and 10 % (v/v) acetic acid and the gels were incubated for about one hour at room temperature. Destaining of the polyacrylamide (PAA) gels was performed according to Miller et al. (2006).

**2.3.6 Silver staining of polyacrylamide gels**

A protein detection method with a much higher sensitivity than the Coomassie staining (2.3.5) is the treatment with silver nitrate solution. This detection is based on a complexation of Ag<sup>+</sup>-ions with the amino acid residues glutamate, aspartate, and cysteine allowing for visualisation of the protein bands upon treatment with alkaline formaldehyde as this leads to reduction of Ag<sup>+</sup>-ions to elementary silver. The staining procedure was performed as described by Blum et al. (1987).

### **2.3.7 Storage and drying of PAA-gels**

Silver or Coomassie stained PAA gels were dried for storage. The gels were shortly equilibrated in 'drying solution' containing 3 % (v/v) glycerol and 30 % (v/v) methanol to be subsequently dried at air between two uncoated cellophane foils that had also been soaked in the same solution.

### **2.3.8 Detection of proteins by Western blot analysis**

For Western blot analysis SDS-PAGE was performed as described before (see 2.3.4). Transfer of proteins and immunoblot analysis via different visualisation techniques are described in the following sections.

#### **2.3.8.1 Transfer of proteins onto a nitrocellulose membrane**

The technique of Western blotting allows for the transfer of proteins onto a nitrocellulose membrane for subsequent detection of specific proteins by antigen-antibody complex formation. Following SDS-PAGE, the separated proteins were transferred from the gel to the solid support membrane using the blotting device Fastblot B44 (Whatman/Biometra) which allows semi-dry blotting by applying an electric field. The blot consisted of different buffer-soaked layers of filter papers (Whatman GB002, Hartenstein, Würzburg, Germany) as well as the PAA-gel and the nitrocellulose membrane (Schleicher&Schuell, Dassel, Germany) as recommended by the manufacturer. A single layer of filter paper soaked with 10×anode buffer was placed directly on the anode. This was followed by two layers with 1×anode buffer soaked filter paper, the membrane, the PAA gel and finally three layers of cathode buffer soaked filter paper. The duration of the transfer process depends on the size of proteins. To allow for transfer also of higher mass proteins, 30-40 min of blotting time was selected at a current of 2.0 mA per cm<sup>2</sup> of membrane area.

Application of an electric field resulted in the transfer of the proteins from the PAA-gel to the membrane where they were immobilised. The presence of methanol in the blotting buffers served on the one hand for activation of protein binding sites on the membrane and on the other hand for weakening the bonds between proteins and SDS which is essential for the blotting procedure. Furthermore it was important to equilibrate the membrane in 1×anode buffer and PAA-gel in cathode buffer prior to blotting procedure to maintain conductivity of the system.

<b>10×Anode buffer</b>	<b>Cathode buffer</b>
300 mM Tris	40 mM ε-Aminocaproic acid
15 % (v/v) Methanol	20 mM Tris
	15 % (v/v) Methanol
pH adjusted to 9.4	pH adjusted to 9.4

### 2.3.8.2 Dot Blot analysis

During dot blot analysis, protein solution was spotted directly on a nitrocellulose membrane (Schleicher&Schuell, Dassel, Germany) circumventing the voltage-driven transfer of proteins (2.3.8.1). Protein spots were allowed to dry on the membrane with subsequent antibody detection being performed as described in the following (2.3.8.4 to 2.3.8.6). In contrast to Western blot analysis, this method only allows for the detection of the presence of a certain protein and gives no insights into the conformational state and apparent size of the protein.

### 2.3.8.3 Ponceau S staining

After protein transfer onto the nitrocellulose membrane, the membrane was incubated with Ponceau S solution (Applichem, Darmstadt, Germany). This procedure allows for qualitative verification of the performed electro-transfer by reversible binding of the dye to the protein. The membrane was incubated for 2-5 min with the staining solution and subsequently washed in ddH<sub>2</sub>O until protein bands were clearly visible. After documentation the residual dye was removed by washing in 1×TBST.

<b>10×TBS</b>	<b>1×TBST</b>
0.5 M Tris	10 % (v/v) 10×TBS
1.5 M NaCl	0.05% (v/v) Tween 20
pH adjusted to 7.5	

### 2.3.8.4 Immunodetection of immobilised proteins with specific antibodies

After Ponceau S staining (2.3.8.3), the membrane was shaken for one hour at room temperature in blocking solution (1 % (w/v) milk powder (Bio-Magermilchpulver,

Heirler, Germany) in 1×TBST) to block free protein binding sites of the membrane in order to avoid unspecific binding of antibody molecules to the membrane during the following treatment. The incubation with the specific antibody (diluted 1:5,000 or 1:10,000 in blocking solution) was performed either for 3 h at room temperature with constant shaking or over night at 4 °C. Washing steps were performed with 1×TBST for 3×5 min. The subsequent detection with secondary antibodies took place either by chemiluminescence (2.3.8.5) or NBT/BCIP staining (2.3.8.6). The selection of the secondary antibody depended on the detection method as described in the following.

### **2.3.8.5 Detection of proteins with chemiluminescence**

Horseradish peroxidase conjugated to goat anti-rabbit IgG (Sigma, Seelze, Germany) was utilised for visualisation of antigen-antibody complexes (2.3.8.4). The membrane was incubated for 30 min in a 1:6,000 dilution (in blocking solution). Subsequently the membrane was washed 3×5 min in 1×TBST in order to avoid background development by unspecifically bound secondary antibody. During the following treatment with ‘Supersignal<sup>®</sup> West Pico Chemiluminescence Substrate’ (Thermo Scientific, Rockford, USA) oxidation of the luminol substrate led to the emission of light which allows for detection of signals by x-ray film (X-Ray XBA, photochemische Werke, Berlin, Germany).

### **2.3.8.6 Protein detection with NBT/BCIP staining**

Another detection method for immobilised proteins on a nitrocellulose membrane is the staining with NBT (nitrotetrazolium blue) and BCIP (5-bromo-4-chloro-3-indolylphosphate). The membrane which was washed after incubation with the primary antibody (see 2.3.8.4) was incubated for 45 min with a 1:6,000 dilution of secondary goat anti-rabbit antibody with conjugated alkaline phosphatase (Sigma, Seelze, Germany) in blocking solution. Subsequently the membrane was washed 3×5 min with 1×TBST and equilibrated for 20 min in carbonate buffer. The staining reaction, that is catalysed by alkaline phosphatase and produces a blue product in presence of NBT and BCIP, was performed in the dark with detection solution. The colour development was continued until bands were clearly visible. The staining reaction was stopped by removal of detection buffer and several washing steps with deionised H<sub>2</sub>O.

---

<b>Carbonate buffer</b>
-------------------------

---

100 mM Carbonate

1 mM MgCl<sub>2</sub>

---

<b>NBT stock solution</b>	<b>BCIP stock solution</b>
---------------------------	----------------------------

---

15 mg/ml NBT

30 mg/ml BCIP

Dissolved in 70 % dimethylformamide    Dissolved in 100 % dimethylformamide

---

<b>Detection buffer</b>
-------------------------

---

0.05 % NBT stock solution

0.05 % BCIP stock solution

(v/v) in carbonate buffer

---

### 2.3.8.7 'Stripping' of nitrocellulose membranes

To reuse membranes, bound antibody complexes were removed from the membranes. This was achieved by 10 min incubation in stripping solution at room temperature. After thorough washing in 1×TBST, the membrane could be reused for immunodetection.

<b>Stripping solution</b>
---------------------------

---

100 mM Glycine

pH adjusted to 2.5

---

### 2.3.9 In-gel tryptic digest and mass spectrometric analysis

After separation of proteins with SDS-PAGE (2.3.4) and subsequent Coomassie staining (2.3.5), bands of interest were excised from the PAA-gel and placed in a reaction tube washed twice with 0.1 % (w/v) trifluoroacetic acid/60 % (v/v) acetonitrile. Samples were prepared and tryptic digest performed according to Ströher and Dietz (2008). The mass spectra were obtained with a Biflex III matrix assisted laser desorption/ionisation-time of flight (MALDI-TOF)-MS (Bruker, Bremen, Germany).

The peptide mass fingerprints were annotated via MASCOT software (Matrix Science, London, UK) and subsequent search was performed in the National Center for Biotechnology Information (NCBI) protein database (<http://www.ncbi.nlm.nih.gov>).

### **2.3.10 Oxidation and overoxidation of 2-Cys Prx**

Different oxidation states of 2-Cys Prx were adjusted by incubation of the protein with DTT and H<sub>2</sub>O<sub>2</sub>, respectively. For oxidation, 2-Cys Prx was first incubated with 50 mM DTT for one hour followed by overnight dialysis against 40 mM K-P<sub>i</sub> buffer, pH 7.0 supplemented with 50 μM H<sub>2</sub>O<sub>2</sub>. Thereafter, the protein was dialysed twice against 40 mM K-P<sub>i</sub> buffer, pH 7.0 without H<sub>2</sub>O<sub>2</sub> added. For overoxidation, the protein was first treated for five minutes with 30 mM DTT followed by a 1 h incubation with 100 mM H<sub>2</sub>O<sub>2</sub>. The protein was dialysed against 40 mM K-P<sub>i</sub> buffer, pH 7.0, with two buffer changes. SDS-PAGE under reducing and non-reducing conditions was performed in order to check the oxidation state of the protein.

## **2.4 Biochemical methods**

### **2.4.1 Thioredoxin dependent peroxiredoxin activity assay**

H<sub>2</sub>O<sub>2</sub> detoxification capacity of peroxiredoxins can be measured in a coupled assay using *E. coli* thioredoxin (TrxA) and thioredoxin reductase (TR) as regeneration system. Reduction of H<sub>2</sub>O<sub>2</sub> was determined via the decrease of A<sub>340</sub> due to NADPH oxidation. The assay typically contained 50 μM H<sub>2</sub>O<sub>2</sub>, 1 mM EDTA, 3.2 μM Prx, 8.3 μM TrxA, and 3.2 μM TR in 100 mM K-P<sub>i</sub> buffer (pH 7.0). The slope between 12 s and 42 s after addition of H<sub>2</sub>O<sub>2</sub> allowed for calculation of the initial rate of NADPH oxidation after correction for background oxidation of NADPH measured in coupled assay without peroxiredoxin (König et al., 2002).

### **2.4.2 Peroxiredoxin activity assay with xylenol orange assay**

Detoxification capacity of peroxiredoxins towards H<sub>2</sub>O<sub>2</sub> and alkyl hydroperoxides was determined by employing the xylenol orange reagent (see Tab. 2.15). This assay is based on the complexation of the dye xylenol orange with the peroxide substrate, which can be measured spectrophotometrically at 560 nm. Dependent on the kind of substrate the incubation time of the reaction with xylenol orange reagent was either exactly 5 or

10 min (see Tab. 2.14). The activity of Prx was determined by following the decrease of  $A_{560}$  in dependence on reaction time (time points of 20 s, 40 s, 60 s, and 80 s). The value was corrected for background reduction of the substrate in the absence of the peroxiredoxin. The assay typically contained 0.5  $\mu\text{M}$  Prx, 10 mM DTT, and 400  $\mu\text{M}$  peroxide in 40 mM K- $\text{P}_i$  buffer (pH 7.0). The working reagent was routinely calibrated against solutions of  $\text{H}_2\text{O}_2$  with known concentrations.

**Tab. 2.14: Incubation times of the assay dependent on the peroxide substrate.**

Incubation time	Peroxide substrate
5 min	Hydrogen peroxide tertiary Butylhydroperoxide
10 min	Cumene hydroperoxide

**Tab. 2.15: Components of xylenol orange reagent.** The components of the working reagent containing the dye xylenol orange were added in the depicted order.

Component	Percentage
dd $\text{H}_2\text{O}$	60
1 M Sorbitol	10
250 mM $\text{H}_2\text{SO}_4$	10
2.5 mM $\text{Fe}(\text{NH}_4)(\text{SO}_4)_2$	10
1.25 mM Xylenol orange	10

### 2.4.3 DNA cleavage assay

DNA protective function of peroxiredoxins in presence of reactive oxygen species (ROS) was determined by the DNA cleavage assay modified from Bernier-Villamor et al. (2004). Incubation of 3  $\mu\text{M}$   $\text{FeCl}_3$  with 10 mM DTT (metal catalysed oxidation (MCO) solution) for 3 h at 37 °C led to the generation of ROS via Fenton reaction. 2  $\mu\text{g}$  plasmid DNA (empty pCR<sup>®</sup>T7/NT-Topo<sup>®</sup> vector) was incubated with MCO solution in presence or absence of Prx (generally 6  $\mu\text{g}$ ) at 37 °C for 5 h. Samples were supplemented with 6 $\times$ DNA loading buffer, loaded on a 1% (w/v) agarose gel supplemented with 0.5  $\mu\text{g ml}^{-1}$  ethidium bromide, and separated for 30 min at 100 V (see 2.2.4).

## 2.5 Surface plasmon resonance

In order to examine immobilisation of His-tagged protein on Ni-NTA surface, the binding of the protein of interest was analysed via surface plasmon resonance (SPR) with a BIAcore 3000 instrument (BIAcore AB, Uppsala, Sweden). Prior to the immobilisation procedure the purified protein (compare 2.3.1.2) was dialysed over night against running buffer. In contrast to the manufacturer's manual, it contained neither EDTA nor Tween 20 as these components disturbed the immobilisation of the protein on the 'Sensor Chip NTA' (BIAcore BA, Uppsala, Sweden). Equilibration and activation of the sensor chip and priming of the system were performed as recommended by the manufacturer. After obtaining a stable baseline of the buffer-washed system, the attachment of the 6×His-tagged protein to the chip was achieved by giving 60 s pulses with a protein concentration of 200 nM at a flow rate of 20  $\mu\text{l min}^{-1}$ . Long-time immobilisation was analysed by washing the system with running buffer for about 16 h at a reduced flow rate of 5  $\mu\text{l min}^{-1}$ . Regeneration and storage of the sensor chip was performed according to the manual.

Running buffer
10 mM HEPES
150 mM NaCl
pH adjusted to 7.4

## 2.6 Labelling of protein cysteinyl variants with gold colloids

In order to achieve a specific labelling with gold colloids of cysteine residues that were introduced via site directed mutagenesis (see 2.2.3.4), different buffer conditions and pH values were adjusted and analysed. During continuous stirring, a solution of 0.1  $\mu\text{g } \mu\text{l}^{-1}$  protein was added stepwise to gold colloid containing solution (0.01 % AuCl<sub>3</sub>, Kisker-Biotech, Steinfurt, Germany) and incubated for 15 min at room temperature. Centrifugation (1 h, 4 °C) was performed with centrifugational speed depending on colloid size, i.e. either 6,000xg in case of 40 nm colloids or 64,000xg for colloids of 4 nm size. The supernatant containing unbound protein was discarded and

the sediment resuspended in buffer A and loaded on a discontinuous gradient of identical volumes of 30 %, 20 %, and 10 % (v/v) glycerol in buffer A for further purification. A centrifugation step (1 h, 4 °C) followed at 8,000xg and 125,000xg for 40 nm and 4 nm gold colloids, respectively.

<b>Buffer A</b>
0.1 % (w/v) BSA
0.1 % (w/v) NaN <sub>3</sub>
Solved in 1×TBS, pH 8.2

Subsequently, fractionation of the gradient was performed and the different fractions were analysed via dot blot analysis (2.3.8.2) applying either chemiluminescence (2.3.8.5) or NBT/BCIP (2.3.8.6) detection with gold bound proteins being expected in the lowest fraction of the gradient.

### 3. Results and Discussion

#### **3.1 Establishment of *Arabidopsis thaliana* 2-cysteine peroxiredoxin A as a model protein for time-resolved dynamical x-ray imaging – modifications and prerequisites to enable visualisation of conformational changes**

2-Cysteine peroxiredoxin A (2-Cys Prx) is a protein that undergoes conformational changes at different levels. As described in the introduction, 2-Cys Prx is able to acquire different aggregation forms dependent on its redox-state, with the oligomerised form being favoured under reducing and overoxidising conditions (König et al., 2002; Schröder et al., 2000), and formation of dimers if oxidised. Furthermore during its catalytic cycle, intermolecular conformational changes occur that regulate the accessibility of the cysteine residues to enable catalytic activity (Wood et al., 2003 a). Also other chemical features of the protein environment like e.g. high or low ionic strength as well as low pH promote formation of oligomers (König et al., 2002; Kitano et al., 1999; Kristensen et al., 1999). These strong alterations of quaternary structure, which additionally are easy to induce by modification of the surrounding medium, make 2-Cys Prx a promising model system when it comes to the establishment of a technique aiming at the time-resolved imaging of molecule dynamics by utilisation of x-rays.

In general, dynamical x-ray imaging may allow for real time detection of single molecule dynamics if selectively labelled with nanoparticles like gold colloids or crystals. The utilised technique is called ‘Diffracted X-Ray Tracking’ (DXT) (Sasaki et al., 2000). It is based on site specifically bound gold crystals, that generate a characteristic diffraction pattern due to Laue diffraction when irradiated with white x-rays (Friedrich et al., 1912; Sasaki et al., 2000). If conformational alterations of an immobilised protein are induced e.g. by changing conditions of the surrounding medium, this can subsequently be detected by changes in x-ray diffraction patterns upon irradiation due to the changing orientation of the introduced nanocrystals (Sasaki et al., 2004) (compare Fig. 3.1).

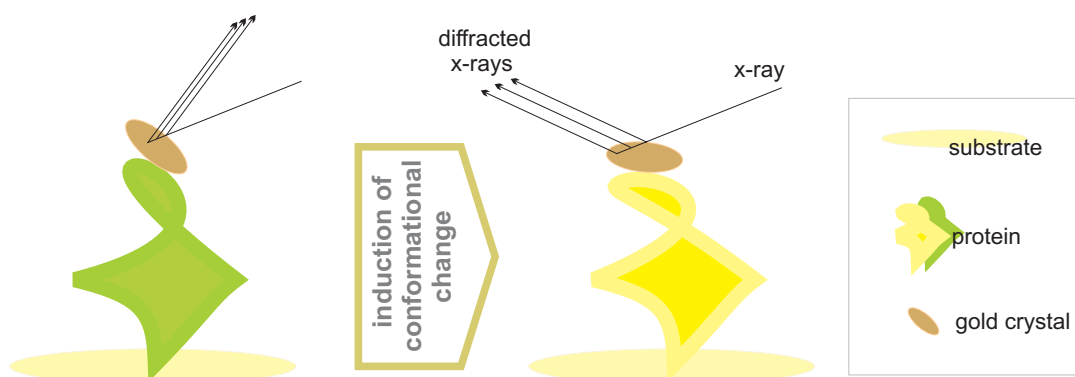


**Fig. 3.1: Schematic depiction of dynamical x-ray imaging, based on the technique of ‘Diffracted X-Ray Tracking’ (DXT).** The immobilised protein labelled with a gold nanocrystal is subjected to conditions altering its conformational state (the resulting yellow conformation). This in turn leads to a new orientation of the crystal and consequently results in a different diffraction pattern (indicated by black arrows) following x-ray irradiation compared to control conditions (green protein).

Up to now, this dynamical x-ray imaging method is established in context of documentation of Brownian motion in different systems (Sasaki et al., 2000; Okumura et al., 2004) as well as for conformational changes occurring in actin filaments upon addition of  $\text{CaCl}_2$  and folding and unfolding of an immunoglobulin-fold protein, namely  $\beta 2$ -microglobulin (Sasaki et al., 2001; Sasaki et al., 2006). As conformational dynamics of redox-active proteins have not been visualised via this technique before, its establishment was the aim of the project D9 ‘Dynamical Real Time Observation of Protein Single Molecules by Means of X-Ray’ within the SFB 613. It was implemented in cooperation with the department of ‘Molekül- und Oberflächenphysik’ of the Faculty of Physics. In this context the 2-Cys Prx A should be tested as model protein for the described system and was part of the presented work.

Several prerequisites must be met to achieve the goal of visualising redox-dependent conformational changes via this technique. These points which will be addressed and discussed in the following sections are: (i) design and generation of functional protein variants enabling the specific labelling with gold nanocrystals, (ii) directed immobilisation of the protein on an adequate substrate, (iii) specific labelling with gold nanocrystals, and (iv) characterisation of x-ray induced damage on protein conformation and function.

### **3.1.1 Design and generation of functional 2-Cys Prx cysteinyl variants**

A first prerequisite to enable the technique of dynamical x-ray imaging is the modification of the protein of interest in order to realise two features. Besides the generation of specific attachment regions within its sequence to allow for the stable labelling with nanocrystals, it is necessary to immobilise the polypeptide on an adequate surface.

To achieve the specific labelling of 2-Cys Prx proteins with gold crystals, the sulphur-containing amino acid cysteine was introduced into the amino acid sequence at selected additional positions, serving as a potential anchor of the crystals. Sulfhydryl groups can mediate covalent links to gold (Nath et al., 2006; Wang and Du, 2000) due to an exothermic reaction of about 165-190 kJ mol<sup>-1</sup> released energy (Fick, 2005; Dubois et al., 1987 and 1990). This covalent binding was expected to realise a stable binding between the gold nanocrystal and the target protein.

For the immobilisation on the support surface, the protein variants were expressed as His-tagged fusion proteins by cloning the mutagenised sequences in vectors which N-terminally contain a sequence encoding a 6×histidine tag. On the one hand, this allows for purification of the protein according to a routinely applied protocol (2.3.1.2), and – even more important – is expected to facilitate the binding of the protein on a Ni-NTA substrate as described in section 3.1.2.

#### **3.1.1.1 Generation of different 2-Cys Prx cysteinyl variants**

The positions for introducing the cysteinyl residues were selected taking two important aspects into consideration, the localisation on the protein surface and the possible impact on the catalytic activity. Therefore, exposed amino acids had to be identified, which exhibit a low degree of conservation, as the introduced cysteine had to be on the one hand accessible for the colloid and on the other hand functional disturbances had to be avoided.

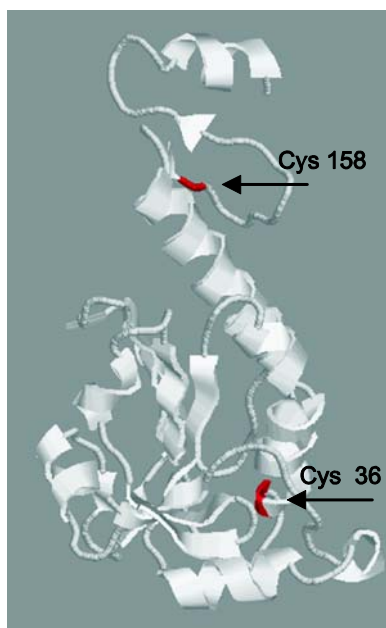


**Fig. 3.2: 3D-structure of 2-Cys Prx A from *A. thaliana*.** In this ribbon structure presentation the two highly conserved cysteines, namely the catalytic (Cys158) and the resolving one (Cys36) are marked in red. The model was generated with RasMol software (basis: 1qmvG, sequence identity: 63.5 %).

A first step for this realisation was the modelling of a three dimensional structure of 2-Cys Prx A, using the SWISS-MODEL server ([www.swissmodel.expasy.org](http://www.swissmodel.expasy.org)). A model of 2-Cys Prx A (Fig. 3.2) was generated based on the structure available for a human 2-cysteine peroxiredoxin in the RCSB Protein Databank (<http://www.rcsb.org/pdb/home/home.do>; pdb-no. 1qmvG) i.e. the monomeric thioredoxin peroxidase B from red blood cells (Schröder et al., 2000). Subsequently, the visualisation tool RasMol (RasMol Version 2.7.3) was used to identify amino acids being localised on the protein surface. These amino acids were analysed with respect to their degree of conservation to minimise the possible influence on protein functionality. As 2-Cys Prx is a ubiquitous protein, members throughout different kingdoms were chosen for this analysis. The alignment of amino acid sequences originating from *Crithidia fasciculata* (Alphey et al., 2000), *Homo sapiens* (Declercq et al., 2001), *Rattus norvegicus* (Hirotzu et al., 1999), *Helicobacter pylori* (Papinutto et al., 2005), and *Salmonella typhimurium* (Parsonage et al., 2005) gave indications for appropriate candidates for exchange (Fig. 3.3).

<i>R. norvegicus</i>	MSSGNAKIGHPPSPFKATAVMPDQGF <sup>KD</sup> -ISLSDYKG-KYVVFFYPPLDFTFV <sup>CP</sup> -TEII 57
<i>C. fasciculata</i>	MSCGAAKLNHPAPEFDDMALMPNGTF <sup>KK</sup> -VSLSSYKG-KYVVLFYPMDFTFV <sup>CP</sup> -TEII 57
<i>A. thaliana</i>	-----AEAVF-DQEF <sup>Q</sup> VKLSDYIGKKYVILFFYPPLDFTFV <sup>CP</sup> -TEIT 41
<i>H. pylori</i>	-----MVVTKLAPDFKAPAVLGNNEVD <sup>HF</sup> FELSKNLGKNGVILFFWPKDFTFV <sup>CP</sup> -TEII 54
<i>S. typhimurium</i>	-----SLINTKIKPFKNQAFK-NGEF <sup>IE</sup> -VTEKDTEG-RWSVFFYPADFTFVSP-TELG 51
<i>H. sapiens</i>	-----APIKVGDAIPAVEVFEGEP <sup>GN</sup> KVNLAELFKGKGVLFVGPVGAFTPG <sup>CS</sup> SKTHLP 53
	. . . . . : * * * * . . . :
<i>R. norvegicus</i>	AFSDRAEEFKKLNQVIG-ASVDSHFSHLAWIN <sup>TPKKQ</sup> GGLGPMNIPLVSDPKRTIAQDY 116
<i>C. fasciculata</i>	QFSDDAKRFAEINTEVIS-CSCDSEYSHLQWTS <sup>YDRKK</sup> GGLGPMIAPMLADKTKAIARAY 116
<i>A. thaliana</i>	AFSDRHSEFEKLNTEVLG-VSVDVFSHLAWVQ <sup>DRKS</sup> GGLGDLNPLISDVTKSISKSF 100
<i>H. pylori</i>	AFDKRVKDFHEKGFNVIG-VSIDSEQVHFAWKNT <sup>TPVEK</sup> GGIGQVSFPMVADITKISISRDY 113
<i>S. typhimurium</i>	DVADHYEELQKLGVDVYS-VSTDTHTFKAWHSS <sup>SE</sup> ---TIAKIKYAMIGDPTGALTRNF 107
<i>H. sapiens</i>	GFVEQAEALKAKGVQVVA <sup>CLSV</sup> NDAFVTGEWGRA <sup>HK</sup> ---AEGKVRLLADPTGAFGKET 108
	. . . . . : * * * * . . . :
<i>R. norvegicus</i>	GVLK <sup>AD</sup> EGISFRGLFIIDDK-GILRQITINDLPVGRSVDEILRLVQAFQFTDKHG-EV <sup>CP</sup> 174
<i>C. fasciculata</i>	GVLDE <sup>DS</sup> GVAYRQVFIIDPN-GKLRQIIINDMPIGRNVEEVIRLVEALQFVEEHG-EV <sup>CP</sup> 174
<i>A. thaliana</i>	GVL <sup>TD</sup> QGIALRGLFIIDKE-GVIQHSTINNLGIGRSVDETMRTLQALQYIQENPDEV <sup>CP</sup> 159
<i>H. pylori</i>	DVLF <sup>EA</sup> -IALRGAFLIDKN-MKVRHAVINDLPLGRNADEMLRMVDALLHFEEHG-EV <sup>CP</sup> 170
<i>S. typhimurium</i>	DNMR <sup>ED</sup> DEGLADRATFVVDPPQ-GIIQAIIEVTAEGIGRDASDLLRKIKAAQYVA <sup>AHP</sup> GEV <sup>CP</sup> 166
<i>H. sapiens</i>	DLL <sup>LD</sup> DSLVSIFGNRRLRKRFMSVMVQDGI <sup>VKAL</sup> NVEPDGTGLTCSLAPNIISQL----- 161
	. . . . . : * * * * . . . :
<i>R. norvegicus</i>	AGWKPGSDTIKPDV <sup>NKS</sup> KEYFSKQK--- 199
<i>C. fasciculata</i>	ANWKKG-----DA <sup>KK</sup> KEGH----- 188
<i>A. thaliana</i>	AGWKPGEKSMKPD <sup>IK</sup> SKEYFSAI---- 183
<i>H. pylori</i>	AGWRKGDKGMKATH <sup>Q</sup> GVAEYLKENSIKL 198
<i>S. typhimurium</i>	AKWKEGEATLAPSL <sup>DL</sup> VGKI----- 186
<i>H. sapiens</i>	-----

**Fig. 3.3: Alignment of 2-Cys Prx amino acid sequences from different organisms.**

Amino acids of interest are highlighted in different colours (yellow = Lys11; orange = His105; blue = Lys174; green = triple variant indicated by the green box with Asp75, Lys77, and Ser78; the different numbers refer to positions within the *A. thaliana* sequence without signal peptide). Red circles mark those exposed amino acids that were chosen to be exchanged for cysteines in 2-Cys Prx A from *A. thaliana*. Additionally, the highly conserved cysteines are coloured in red and indicated by black arrows.

Based on this analysis of amino acid localisation within the protein structure and degree of conservation, different 2-Cys Prx cysteinyl variants were generated. Three of these, namely Lys25, His119, and Lys188 already existed at the beginning of this work, generated within the diploma thesis of Andreas Goergens (2005). According to bioinformatical prediction, these constructs still contained a fragment of 14 amino acids of the 2-Cys Prx signal peptide which is responsible for chloroplast localisation. Since these 14 additional amino acids might impair proper folding, the variants were re-cloned as shortened variants within this work. The resulting variants will be referred to as Lys11, His105, and Lys174 according to the actual locations of the introduced cysteines within the amino acid sequence (compare Fig. 3.4 A).

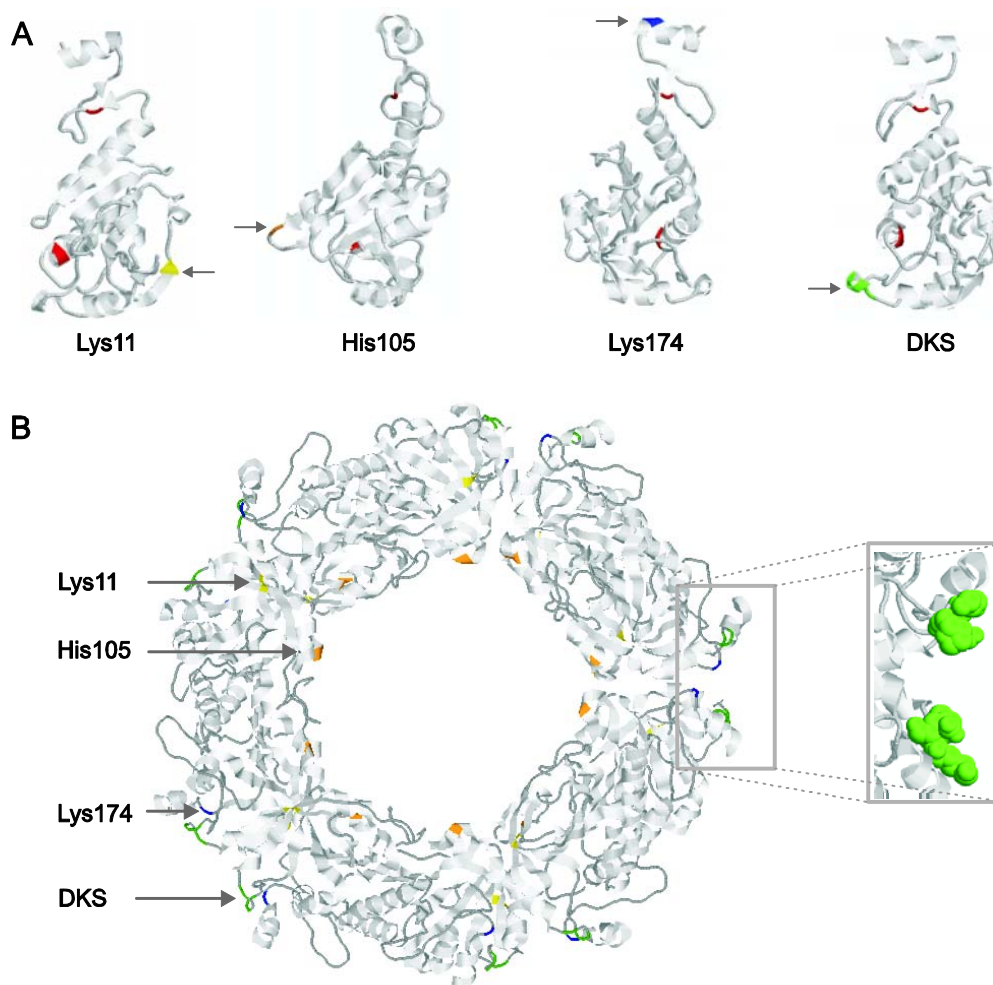


**Fig. 3.4: 2-Cys Prx cysteinyl variants.** Introduced cysteines are highlighted in different colours which code for the cysteinyl variants according to location and nature of exchanged amino acid in *A. thaliana* (yellow = Lys11, orange = His105, blue = Lys174, green = DKS). A) Monomeric form of *A. thaliana* (structure generated with RasMol software; the basis was the reference structure 1qmvG) with catalytic and resolving cysteine being depicted in red. B) Decameric conformation of *H. sapiens* 2-Cys Prx (thioredoxin peroxidase B from red blood cells; sequence identity with *A. thaliana* 2-Cys Prx is 63 % and the coloured amino acids correspond to the exchanged ones in the Arabidopsis sequence; basis: 1QMV). The enlarged section depicts the orientation of the introduced cysteines of the DKS variant.

Furthermore the triple cysteinyl variant DKS was designed (named according to the three exchanged amino acids D=Asp75, K=Lys77, and S=Ser78) in order to obtain improved properties: (i) with three neighbouring cysteinyl residues serving as anchor for a gold colloid (Fig. 3.4 B), a higher stability of the binding event is expected, (ii) as the 2-Cys Prx exists in different conformational states and not exclusively as a monomer (Wood et al., 2003 b; König et al., 2003; König et al., 2002), it is of utmost importance that the exchanged amino acids are accessible in either structural form. This

prerequisite of being exposed in the dimer and decamer, respectively, was not realised in all single variants (compare Fig. 3.4), as His105 for instance is located in the inner ring of the donut shaped decamer and Lys11 is found in the contact surface of two monomers (Fig. 3.4 B). As can be seen in Fig. 3.4 A and B, DKS realises both aspects and therefore is expected to be the most promising candidate for optimal nanocrystal attachment and realisation of the dynamical imaging of conformational changes via DXT.

For control purposes, a cysteine free variant was utilised, that contained the amino acid serine instead of the catalytic and resolving cysteine at the corresponding positions. It served for instance as a control for the establishment of specific labelling conditions of the cysteinyl residues with gold colloids as described in section 3.1.3.

### 3.1.1.2 Generation of 2-Cys Prx cysteinyl variants – optimisation of expression and purification

For heterologous expression in *E. coli* and purification of 2-Cys Prx A cysteinyl variants, different vector systems were used to optimise the final protein amount; namely the pEXP5-NT/TOPO<sup>®</sup> vector (Invitrogen, Karlsruhe, Germany) as well as the pQE30 vector (Qiagen, Hilden, Germany).

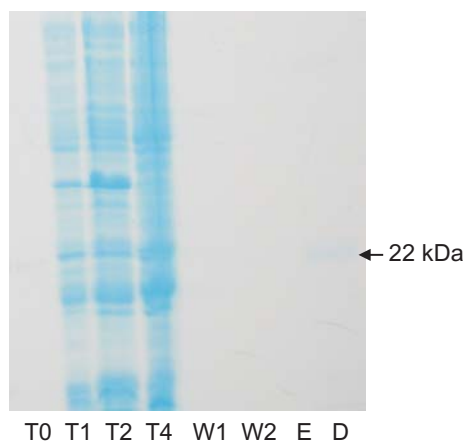


**Fig. 3.5: Documentation of expression and purification of the 2-Cys Prx variant DKS.** The samples for reducing SDS-PAGE with subsequent Coomassie staining were taken during expression (T0, T1, T2, T4 corresponding to the time points directly, 1 h, 2 h, and 4 h after induction with IPTG, respectively), as well as of washing buffer 1 (W1), washing buffer 2 (W2), directly after elution (E), and of the dialysed protein (D). Either 5  $\mu$ l of resuspended bacteria of expression samples or 20  $\mu$ l of washing and elution fractions were loaded.

Variants without signal peptide, cloned into the pEXP5-NT/TOPO<sup>®</sup> vector, were expressed and purified according to the routinely applied protocol (2.3.1.1 and 2.3.1.2) as depicted exemplarily for the DKS-variant in Fig. 3.5. After gel electrophoresis, only a faint band with the size of 22 kDa – correlating to the molecular mass of His-tagged 2-Cys Prx A without signal peptide – can be detected in the lane of dialysed protein (Fig. 3.5). As shown exemplarily for DKS, the protein amount of neither cysteinyl variant was sufficient for subsequent application to investigate different functional features of the proteins (compare section 3.1.1.3), and therefore cloning into pQE30 vector (Quiagen, Hilden, Germany) was performed. Again due to low protein amounts, further optimisations had to be carried out. This concerned on the one hand the amount of expressed recombinant protein as this did not increase very strongly after induction with IPTG (Fig. 3.5). On the other hand, alterations of the purification protocol were expected to improve total recombinant protein yield.

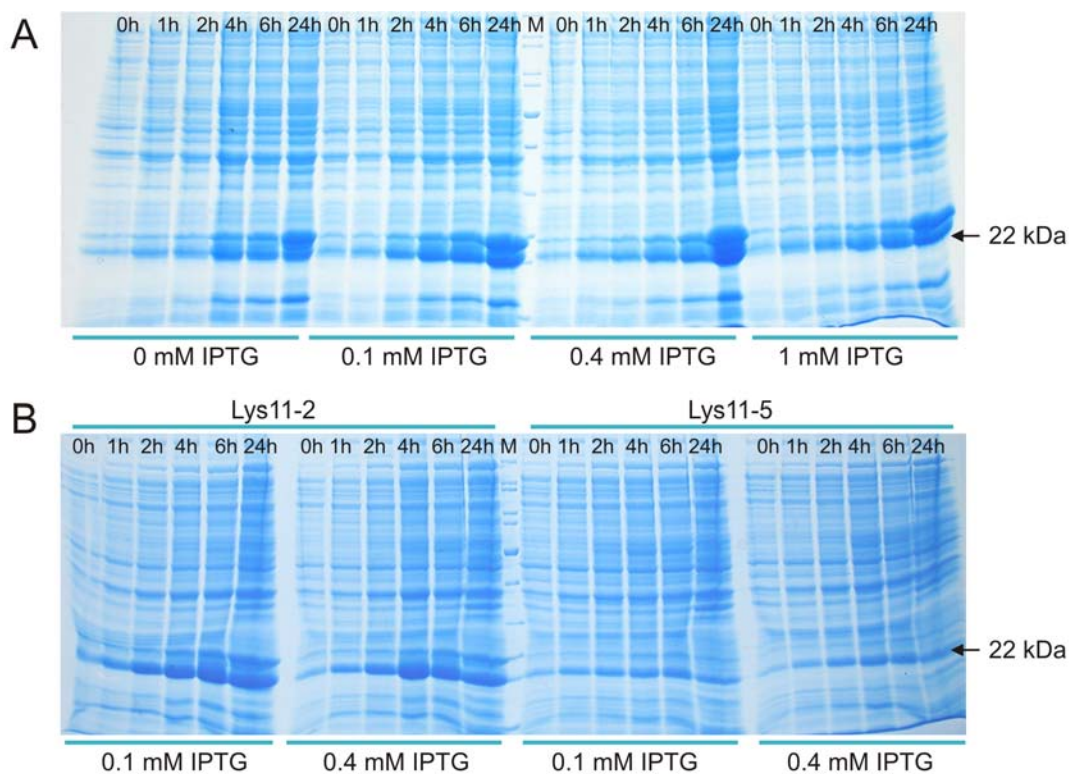


**Fig. 3.6: Exemplary depiction of time- and IPTG-dependent protein expression as carried out for yield optimisation.** For each lane of reducing SDS-PAGE with subsequent Coomassie staining 5  $\mu$ l resuspended bacteria sample was loaded alongside with protein marker ‘PageRuler<sup>™</sup> Unstained Protein Ladder’ (M). To investigate time-dependency of expression, samples were taken directly (0 h), 1 h, 2 h, 4 h, 6 h, and 24 h after induction with IPTG. A) Exemplary display of 2-Cys Prx expression after application of different concentrations of IPTG. B) Differential expression of 2-Cys Prx variant Lys11 is shown exemplarily for the BL21 strains Lys11-2 and Lys11-5.

For optimisation of expressed protein amount, not only different BL21 strains of the constructs were tested but additionally various expression times, and IPTG concentrations. Expression patterns were quite different in dependence of IPTG concentration as well as for utilised strains, as it can be seen in Fig. 3.6. Besides differential expression of single positive BL21-strains of the same construct (Fig. 3.6 B), it could also be observed, that the routinely applied final concentration of IPTG (0.4 mM) was not optimal for most of the variants. Therefore, expression parameters were individually defined for the different constructs, and consequently the amount of expressed protein could be improved significantly.

Furthermore, conditions for protein purification were altered in respect of (i) increasing protein yield by extended incubation of protein lysate with Ni-NTA substrate compared to the original protocol and (ii) concerning protein purity due to modification of buffer conditions. Whereas purification was carried out under reducing conditions to avoid co-purification of bound proteins due to disulfide bridge formation, an increase of sodium chloride (800 mM) and glycerol (20 %) as well as the addition of detergent such as Tween 20 (0.5 %) were used to minimise unspecific binding of *E. coli* proteins to the purification matrix due to ionic or hydrophobic interactions. All components were applied in the concentration range as recommended by the supplier (Qiagen Expressionist).

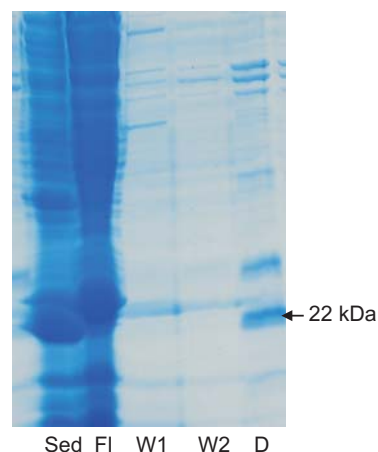


**Fig. 3.7: Documentation of His105 purification according to optimised protocol.** For reducing SDS-PAGE with subsequent Coomassie staining, 5  $\mu$ l of resuspended bacteria sediment (Sed) and ‘flow through’ of the column (Fl) as well as 20  $\mu$ l of washing buffers 1 and 2 (WP1, WP2) and dialysed protein (D) were applied.

As shown in Fig. 3.7, most 2-Cys Prx was found in the sediment after centrifugation of protein lysate. This indicates a partitioning of 2-Cys Prx in inclusion bodies, preventing

a native purification. Although washing with both buffers was carried out until  $OD_{280}$  reached zero, the dialysed protein still contained different other proteins. Further optimisation concerning the washing procedure could not diminish this problem.

As additional proteins could be found in every 2-Cys Prx variant (Fig. 3.8 A), an immunodetection with 2-Cys Prx specific antibody was performed and allowed for verification of the presence of variants in the dialysed protein fractions (Fig. 3.8 B). It can be concluded, that although the dialysed protein was still impure due to the presence of *E. coli* proteins, the yield of 2-Cys Prx variants could be increased, enabling subsequent functional investigations (compare section 3.1.1.3).

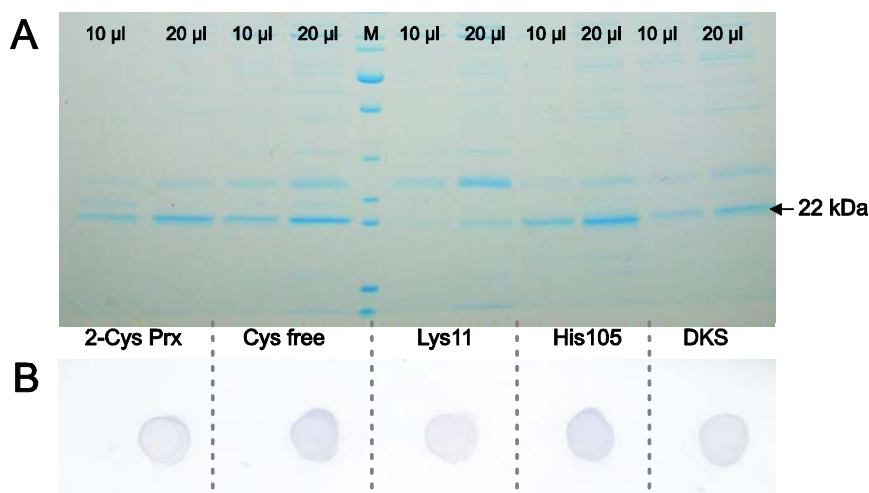


**Fig. 3.8: Dialysed protein fractions after purification containing 2-Cys Prx variant proteins.** A) Coomassie staining following reducing SDS-PAGE with 10  $\mu$ l and 20  $\mu$ l of dialysed protein loaded per lane showed additional bands besides the band at 22 kDa. M = protein marker ‘PageRuler™ Unstained Protein Ladder’ B) Dot-blot with subsequent 2-Cys Prx specific immunodetection using NBT/BCIP staining, for each variant 10  $\mu$ l of purified protein were spotted.

### 3.1.1.3 2-Cys Prx cysteinyl variants show functionality in spite of exchanged amino acids

A very important aspect in case of proteins generated via site directed mutagenesis is the conservation of functionality as the exchange of amino acids may have an influence for instance on folding. In the case of the 2-Cys Prx cysteinyl variants different functional features have been investigated so far. As part of the diploma thesis of Andreas Goergens (2005), catalytic activity has been shown to be present in all examined variants. Additionally, in band-shift experiments electrophoretic mobility of

the variants was tested under different conditions such as an oxidising or reducing environment, revealing a similar behaviour to wild type 2-Cys Prx (Goergens, 2005). Investigation of the band shift behaviour under the given conditions is especially helpful as it allows for characterisation of the variants in comparison to various former studies dealing with 2-Cys Prx conformational changes (König et al., 2003; Gourlay et al., 2003; Wood et al., 2003 b).

A functional feature being described for peroxiredoxins and still unexplored for these variants is the ability of protecting plasmid DNA in a metal catalysed oxidation (MCO) system against ROS-mediated cleavage as described in different studies, e.g. for the wild type 2-Cys Prx from *Pisum sativum* and *Arabidopsis thaliana* (Bernier-Villamor et al., 2003; Laxa et al., 2007). Therefore this missing functional aspect of characterisation of 2-Cys Prx variants was investigated within this work.

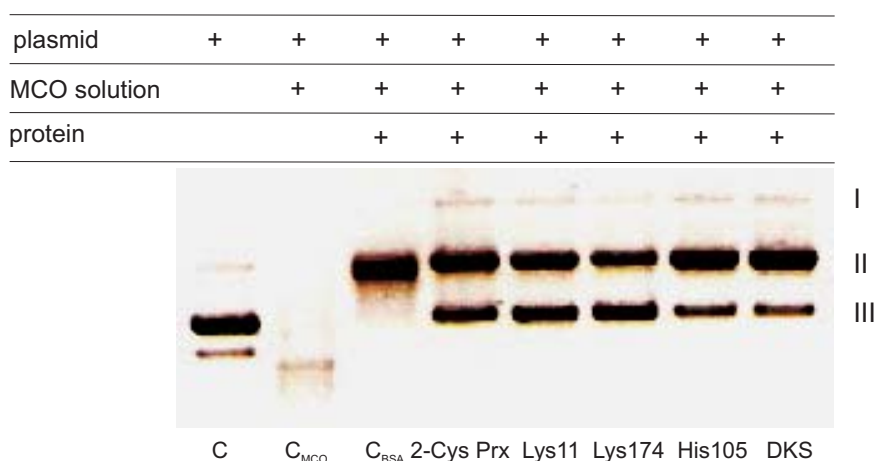


**Fig. 3.9: DNA protective function of 2-Cys Prx wild type protein and the different variants.** I = linear form of plasmid DNA, II = open circular form, III = supercoiled form. C indicates control containing plasmid DNA without MCO solution.  $C_{MCO}$  shows maximal damage of plasmid DNA in absence of any protein and  $C_{BSA}$  demonstrates an unspecific protection effect in presence of bovine serum albumin (BSA). All variants exhibit a similar protective function as it is the case for wild type 2-Cys Prx. The experiment was conducted three times with similar results.

All variants – independent of the kind of amino acid exchange – exhibited full functionality in DNA protection against ROS-mediated damage (Fig. 3.9). The nicking of supercoiled plasmid DNA, resulting in an increase of open circular form is consistent with observations by Laxa et al. (2007), showing that in absence of a regenerator for 2-Cys Prx A the protein did not exhibit full protective capacity. As the variants show the same behaviour upon MCO-solution treatment, it can be concluded that the

exchange of amino acids does not impair the DNA protective function of the proteins. The results confirm that the variants are functional and can be employed for further experiments in context of establishing the dynamical x-ray imaging.

### **3.1.2 His-tagging of 2-Cys Prx enables long-term immobilisation on Ni-NTA surface**

As described before, another important prerequisite to realise dynamical observations of protein conformation of single molecules via DXT is the stable immobilisation of the protein on an adequate substrate. This allows for the detection and the assignment of different diffraction patterns in dependence of the protein conformation due to the stable fixation of the protein-crystal complex (compare Fig. 3.1).

Within this project, an immobilisation of 2-Cys Prx variants was expected to be realised via binding of the N-terminally fused His-tag of the protein to a Ni-NTA surface (Collins et al., 2003; Nieba et al., 1997). This non-covalent binding is not only routinely applied in protein purification but can furthermore be used for immobilisation of proteins for different purposes. It can be analysed for instance via surface plasmon resonance (SPR) using the BIAcore technique (BIAcore, Uppsala, Sweden). The SPR technique is based on the measurement of the refractive index near a sensor chip surface, leading to an increase of relative response units in case of binding events that take place on this chip surface. SPR is not only applied for immobilisation analyses as it is the case in the present work, but it is furthermore used for interaction studies (Nakamura et al., 2000). According to the supplier's manual, one response unit corresponds to about 1 pg protein mm<sup>-2</sup>.

As displayed in Fig. 3.10 repeated injection of the 2-Cys Prx variant Lys174, which was chosen for exemplary investigation of His-tagged protein immobilisation on a Ni-NTA chip, led to a stepwise increase in response units, revealing a successive loading of the Ni-NTA chip surface with every new addition of protein. The final response level of about 4,000 RU above background revealed a successful binding of the protein, as a minimum response of 1,000 RU already indicate a stable interaction (personal communication Dr. Uwe Bierfreund, BIAcore company).

Furthermore it was of great interest to investigate the possibility of long-time immobilisation of the protein in order to ensure a stable binding necessary for DXT measurement which requires an exchange of the protein environment to perform dynamical x-ray imaging.

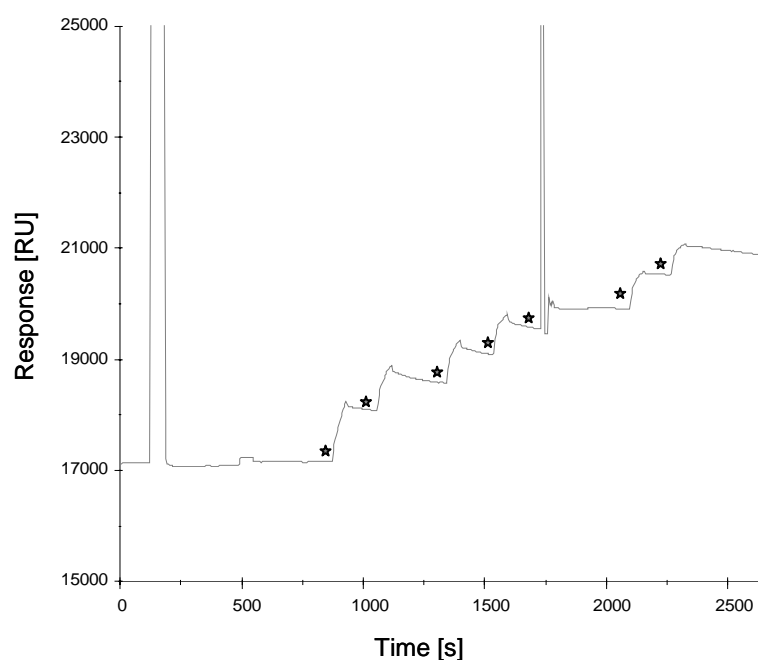


**Fig. 3.10: Loading of Ni-NTA sensor chip with His-tagged 2-Cys Prx variant Lys174.** SPR analysis of binding of His-tagged Lys174 showed successive loading with protein. Every injection of 20  $\mu$ l of 0.2  $\mu$ M protein solution is indicated by a grey star and led to an increase in relative response units (RU), resembling a successive increase of binding events on the chip surface. The measurements were performed with the kind support of Dr. Iris Finkemeier.

During long-time immobilisation, the sensor chip with immobilised protein was rinsed with buffer for more than 16 hours as shown in Fig. 3.11. Despite of the constant buffer flow, the remaining response still comprised 2,500 RU above background in total at the end of the experiment – indicating a stable binding of the immobilised protein. The decrease from maximal response of 4,000 RU to about 2,500 RU may be caused by two mechanisms: (i) loosely and non-specifically attached protein may be washed from the surface while protein being bound via His-tag remained on the chip, or (ii) this decrease may be due to a dilution effect of 2-Cys Prx which is accompanied by a conformational change, as shown by Barranco-Medina et al. (2008 a). That work revealed the formation of decameric form in case of high concentrations of 2-Cys Prx protein, which is true for the conditions in the flow cell of the sensor chip. Therefore it can be expected, that the decamerisation with His-tag bound proteins caused an additional increase in signal. The following constant buffer flow will decrease the concentration of 2-Cys Prx within the flow cell and may consequently result in the dissociation of the decameric conformation

in favour of the dimeric form and therefore a decrease of signal due to the loss of disassembled proteins might have been detected.

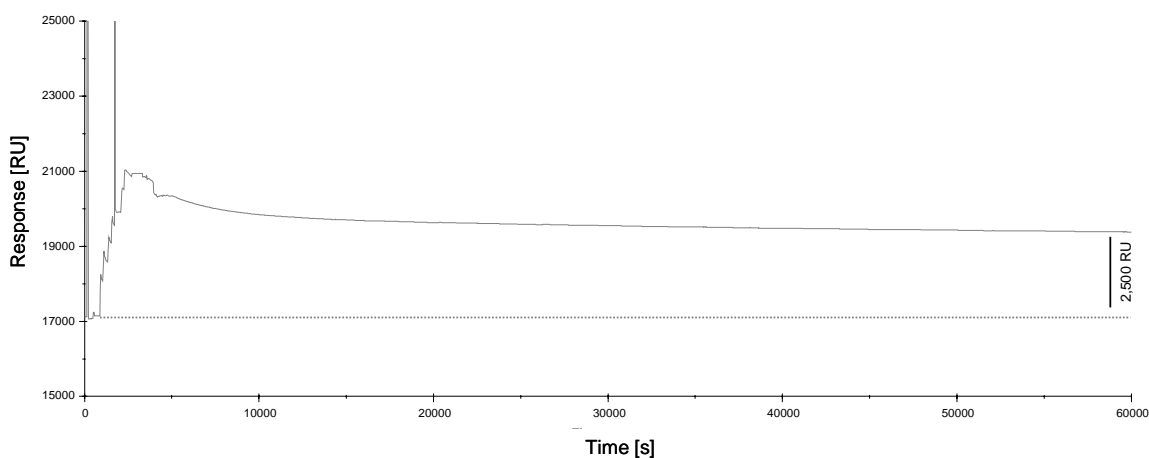


**Fig. 3.11: Long-time immobilisation of His-tagged 2-Cys Prx variant Lys174 on a Ni-NTA sensor chip.** SPR analysis of Lys174 binding via His-tag displayed a stable immobilisation of the protein even after about 16 h, with the flow cell being rinsed with  $5 \mu\text{l min}^{-1}$  buffer. The measurements were performed with the kind support of Dr. Iris Finkemeier.

Although the SPR signal (Fig. 3.11) decreased after maximal loading of the chip due to either or both described mechanisms, it was observed that after about seven hours of rinsing the flow cell with buffer, the signal remained stable. This stable response of about 2,500 RU above background indicates successful binding events and stable association of the protein. The results proved that His-tag/Ni-NTA represents a suitable system to realise the necessary substrate fixation of 2-Cys Prx variants.

### 3.1.3 Binding of gold colloids to 2-Cys Prx cysteinyl variants

2-Cys Prx variants were generated in order to allow for specific labelling of introduced cysteinyl residues with gold colloids. For investigation and optimisation of labelling events especially with respect to binding specificity, different gold colloids and detection methods were compared. Furthermore, various buffer conditions were tested to restrict binding of the gold colloids to the introduced cysteinyl residues. The efficiency of the labelling reaction was followed by purification of the gold colloid-protein complexes with subsequent immunodetection as exemplarily displayed in Fig. 3.12.

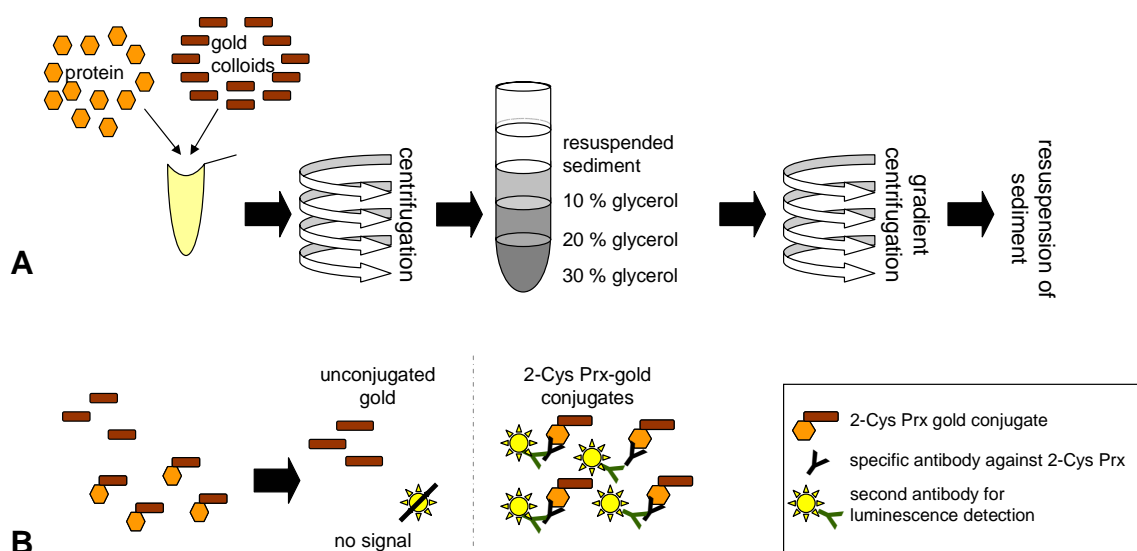


**Fig. 3.12: Schematic presentation of protein-gold conjugates detection by gradient centrifugation and immunodetection.** A) Different buffer conditions were tested during labelling approaches in order to optimise the protein thiol-gold coupling. The first centrifugation step separated the colloids with bound protein from the unbound protein in solution. Gradient centrifugation was performed in order to further purify the colloid-protein conjugates. B) Positive labelling events were detected by dot-blot analysis of protein samples immobilised on a membrane. Membrane areas with 2-Cys Prx-gold conjugates bound the 2-Cys Prx antibodies which subsequently allowed enzyme-linked immunodetection. After application of substrate the light emission was semiquantified via exposure of an x-ray film. Gold colloids without bound protein gave no signal.

### 3.1.3.1 Conjugation of 15 nm gold crystals to 2-Cys Prx variant Lys174

First labelling approaches were realised with gold crystals of approximately the size of 15 nm, prepared by the group of Prof. Dr. Heinzmann within the department of 'Molekül- und Oberflächenphysik'. Positive conjugation events after labelling according to Fig. 3.12 A were visualised via immunodetection with 15 nm gold labelled antibodies (Fig. 3.13 A). Subsequent Transmission Electron Microscopy (TEM) allowed for detection of single binding events, as indicated in Fig. 3.13 B with two gold colloids being located in a distinct distance to each other.

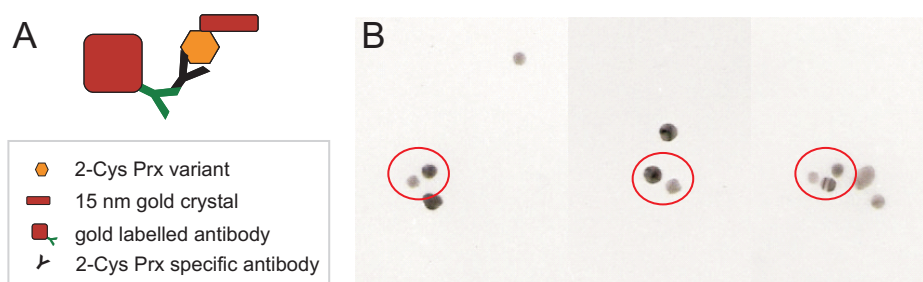


**Fig. 3.13: Labelling of 2-Cys Prx variant Lys174 with 15 nm gold crystals.** A) Schematic depiction of antibody labelled protein-gold conjugates. B) Protein-gold conjugates are identified by combination of two gold particles as highlighted by the red circle. TEM detection was conducted by Dr. Uwe Kahrmann.

The close proximity of two different gold particles (highlighted in Fig. 13.3 B) is indicative for successful labelling with 15 nm crystals of the 2-Cys Prx variant Lys174. Unfortunately the concentration of gold crystals in the provided solution was not sufficient to investigate binding of gold crystals to other variants. This necessitated the application of other particles to investigate the gold labelling of the other variants and especially to perform control experiments to test for the specificity of these labelling events, as described in the following.

### 3.1.3.2 Gold-labelling of different 2-Cys Prx variants with 5 nm gold colloids

Due to the low concentrations of 15 nm gold crystals, further labelling reactions were performed with commercially available 5 nm gold colloids (Kisker-Biotech, Steinfurt, Germany) according to the supplier's manual. TEM detection of gold labelling of different 2-Cys Prx variants exhibited protein-gold conjugations in every sample (Fig. 3.14). Despite a localisation of several of these conjugates with other colloids in their direct environment, the corresponding combination of two crystals resembling a conjugate (Fig. 3.14, red circles) was unlikely a coincidental arrangement. This can be assumed, as there were also several of these arrangements occurring separately. However these labelling reactions revealed a binding not only in 2-Cys Prx variants containing additional exposed cysteines, but also in case of the Cys free variant (Fig. 3.14). The latter contains no cysteines, they are exchanged for serines. Consequently it was concluded that binding of the colloids is not or not exclusively brought about by a specific interaction between the thiol group of the protein and the gold surface. The result revealed the problem of unspecific binding of the colloid to the protein surface due to ionic and especially hydrophobic interactions, which is an already well described phenomenon (Furuya et al., 2006; Tang et al., 2004). Since such type of

binding is unlikely to be restricted to a certain region such as the exposed cysteine(s) and also may occur at several sites simultaneously the result was unsatisfactory as basis for subsequent x-ray diffraction analysis.

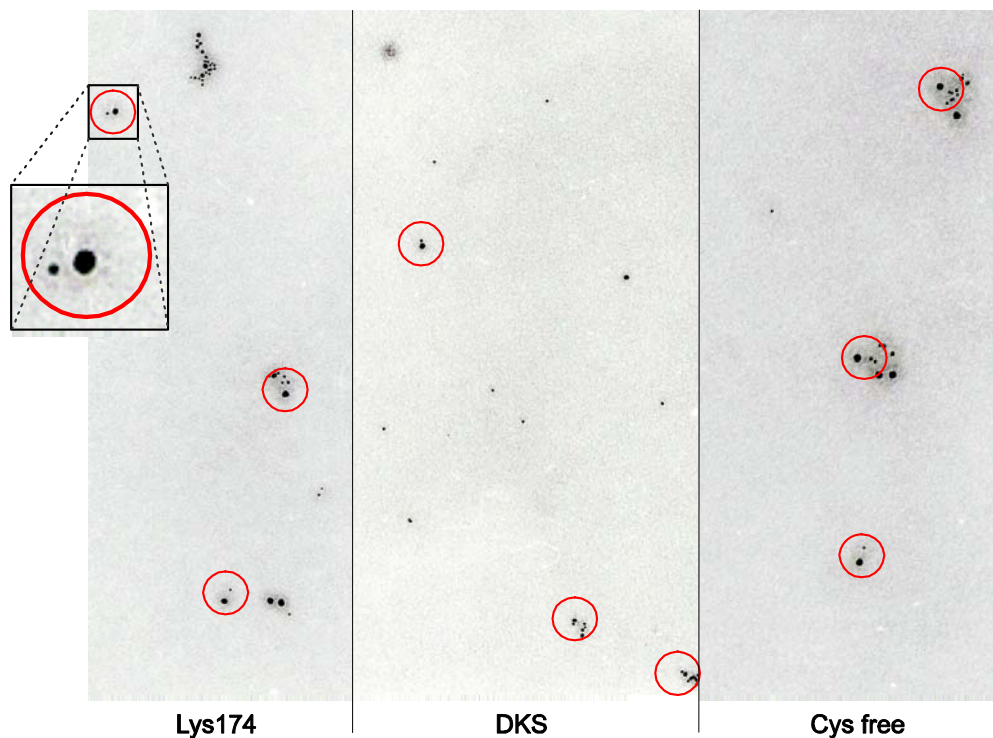


**Fig. 3.14: Conjugation of 5 nm gold colloids to different 2-Cys Prx variants.** Positive labelling events with two differentially sized gold colloids are highlighted with a red circle and were found for all investigated 2-Cys Prx variants. This included also cysteine free (Cys free) 2-Cys Prx. TEM detection was conducted by Dr. Uwe Kahrman.

The strongest interference with the covalent binding between sulphur and gold is assumed to be due to hydrophobic interactions. Many amino acids on the surface of 2-Cys Prx are hydrophobic ones like alanine, phenylalanine, valine, leucine, proline, and isoleucine, resulting in big hydrophobic areas on the protein surface (Fig. 3.15). Consequently, the labelling procedure necessitated an optimisation in respect to conditions like the applied buffer and pH, as these factors strongly influence the binding events taking place.

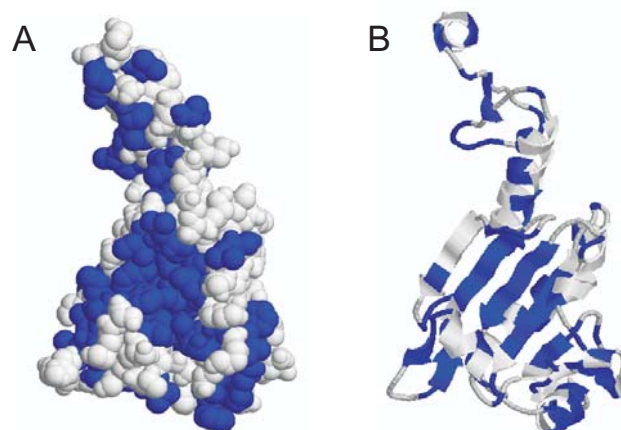


**Fig. 3.15: Depiction of hydrophobic amino acids on the protein surface of 2-Cys Prx.** Hydrophobic regions within the 3D-structure of 2-Cys Prx from *A. thaliana* (compare with Fig. 3.2) being highlighted in blue on (A) the molecular surface in the space filling structure and (B) in ribbon structure. Modelling was performed with RasMol software.

### 3.1.3.3 Gold labelling of 2-Cys Prx variants – optimisation of conditions improves binding specificity

To optimise the binding conditions and to reduce protein and gold crystal requirement, the labelling reaction was varied with respect to sample volume, pH, and ions (compare Fig. 3.12 A).

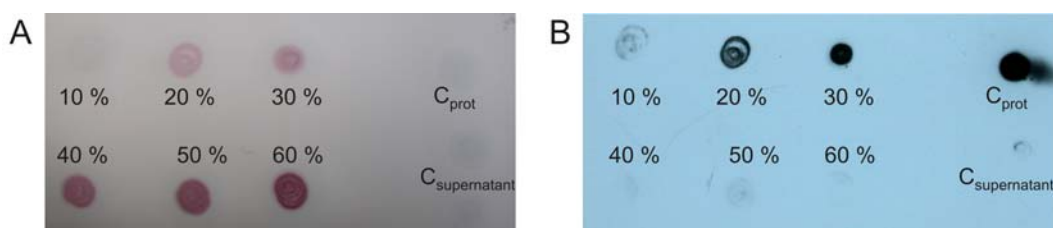


**Fig. 3.16: Optimisation of gold colloid amount in the labelling reaction.** 2-Cys Prx variant protein was used for labelling with different concentrations (10 % to 60 %) of 40 nm gold colloids. For analysis, 10  $\mu$ l of resuspended sediment obtained by gradient centrifugation were spotted on a nitrocellulose membrane. As control the identical volumes of unlabelled protein ( $C_{\text{prot}}$ ) and of the supernatant after centrifugation of the labelling reaction containing 30 % gold colloids ( $C_{\text{supernatant}}$ ) were also spotted onto the membrane. Similar results were obtained in two experiments with different detection method. The intensity of purple staining of the dots (A) was correlated with the increasing colloid concentrations and also the chemiluminescent detection of the spotted labelled samples (B) showed the dependence of positive conjugation events on colloid amount.

The sample volume was decreased to reduce the required protein amount and the purification procedure for protein-gold conjugates as well as the amount of applied gold colloids. Optimal conditions were identified by variations of the standard protocol. Investigation of positive conjugation events in dependence of gold colloid amounts by immunodetection via chemiluminescence (compare Fig. 3.12 B) showed that the labelling efficiency highly depended on colloid concentration in the sample (Fig. 3.16). For optimisation of the labelling conditions in respect to buffer and pH, a gold colloid amount of 30 % was chosen, as the yield of positive conjugation events increased with concentrations up to 30 % and afterwards decreased rapidly (Fig. 3.16 B).

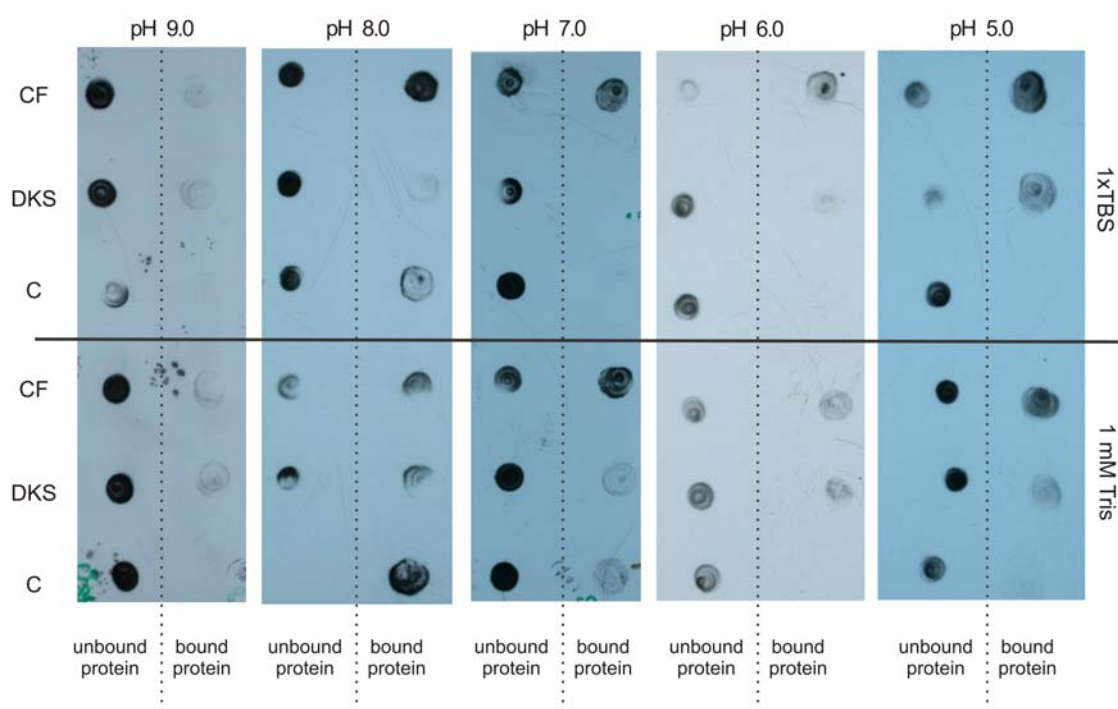


**Fig. 3.17: pH dependent gold labelling of 2-Cys Prx variants DKS and Cys free.** For optimisation of labelling specificity the buffer systems 1 mM Tris and 1×TBS, respectively, were analysed after adjustment to different pH values. To investigate gold-bound protein, 10 µl of resuspended sediment were spotted on the membrane, whereas for detection of unbound protein, 10 µl of supernatant after centrifugation of the labelling reaction were immobilised on the membrane. As technical control (C), the corresponding fractions of a labelling reaction containing Cys free variant but no gold colloids were used to verify the specific assignment of signals to the protein-gold conjugates. Immunodetection via chemiluminescence was performed using 2-Cys Prx specific antibody.

As shown in section 3.1.3.2, routinely applied 2 mM borate (pH 9.0) is no ideal condition to achieve a specific conjugation of gold colloids to the cysteines, as protein-

gold conjugates could also be detected in case of the cysteine free variant (Fig. 3.14). Although cysteine-specific labelling is described by Ackerson et al. (2006) under these conditions, the buffer environment for the gold conjugation to 2-Cys Prx had to be adjusted. As alternatives, two other buffer systems were tested in the reaction. Besides application of 1 mM Tris – as this buffer condition is reported to allow for a successful binding of yeast cytochrome c to a gold electrode by specific cysteine-gold binding (Bonanni et al., 2003) also 1×TBS was applied, as the included sodium chloride was expected to counteract unspecific binding. To differentiate between specific and unspecific binding, two variants were investigated in parallel, namely the DKS variant which is expected to allow for the most stable binding of gold colloids among 2-Cys Prx variants (compare section 3.1.1.1) and the Cys-free variant to exhibit the unspecific labelling events as it does not contain any cysteines. For subsequent immuno blot analysis of the labelling reactions, samples of the resuspended sediment as well as the supernatant obtained after gradient centrifugation were taken to quantify the amounts of bound and unbound protein, respectively. A parallel approach containing Cys free variant but no gold colloids served as a technical control.

For every employed condition, the signals for the bound protein of Cys free variant were either of the same intensity or even stronger than in the DKS variant although same amounts of protein were applied (Fig. 3.17). The result was moreover reflected in an inverse manner by the signals for unbound protein in the supernatant samples, exhibiting the same or an even stronger intensity in the DKS compared to Cys free variant for unbound protein (Fig. 3.17). It was concluded that the application neither of 1 mM Tris nor of 1×TBS improves the binding specificity irrespective of the pH in the range between 5 and 9 (Fig. 3.17). This again indicated that the coupling of protein and gold colloid was due to unspecific interactions. Consequently other variations of experimental conditions were carried out to achieve a reduction of unspecific interactions. As there was shown to be a strong interaction of gold particles with the amino acid aspartic acid at physiological pH (Joshi et al., 2004), the polyamine spermine was added to 1 mM Tris (pH 7.0) or 1×TBS (pH 7.0) to create an alkaline environment. But also this labelling condition, that was again either Tris- or TBS-based, showed no improvement of specificity (Fig. 3.18).

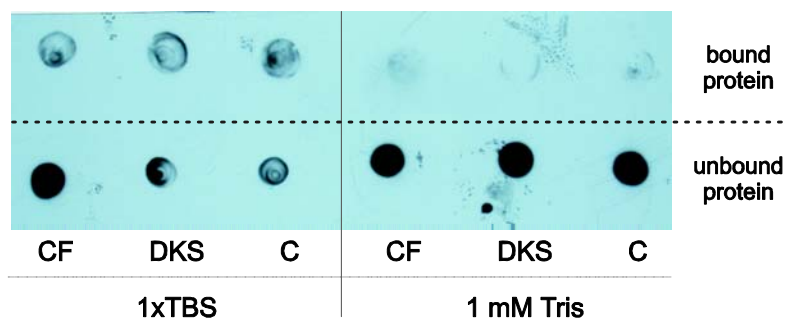


**Fig. 3.18: Lack of binding specificity of 2-Cys Prx labelling to gold on the presence of spermine.** To investigate gold-bound protein, 10  $\mu$ l of resuspended sediment were spotted on the membrane, whereas for detection of unbound protein, 10  $\mu$ l of supernatant after centrifugation of the labelling reaction were immobilised on the membrane. As technical control (C), the corresponding fractions of a labelling approach containing Cys free variant but no gold colloids were loaded to verify the assignment of signals to the protein-gold conjugation. Immunodetection via chemiluminescence was performed using 2-Cys Prx specific antibody.

To counteract hydrophobic interactions, glycerol was added, as it is well established for protein purification to suppress these kinds of binding reactions. Therefore different amounts of glycerol were added to the gold labelling reaction as supplement to both buffer conditions. In combination with 1 mM Tris buffer (pH 7.0) there was no effect of this addition. In contrast, a clear effect was observed for the employed combination of glycerol and 1 $\times$ TBS buffer (pH 7.0, Fig. 3.19 A and B). In these labelling reactions the signal intensities for the DKS variant increased, whereas the Cys free variant showed a much weaker signal, indicating an enhancement of thiol-gold affinity upon these conditions. The positive effect was already visible with 20 % glycerol added to 1 $\times$ TBS, but was not enhanced with increasing glycerol amount (Fig. 3.19 A) to 25 or 30 %. It can be hypothesised that the observed difference in specific thiol-gold coupling between the two utilised buffers upon glycerol addition was due to the presence of sodium chloride leading to an additional suppression of ionic interactions. Therefore further labelling approaches were performed with TBS containing different amounts of sodium chloride in presence of 20 % glycerol (Fig. 3.19 B). This modification of the labelling approaches did not allow for an improvement of specificity; it even caused a decrease of directed thiol-gold labelling events as visible from the relation of signal intensities in Cys free and DKS variant (Fig. 3.19 B).

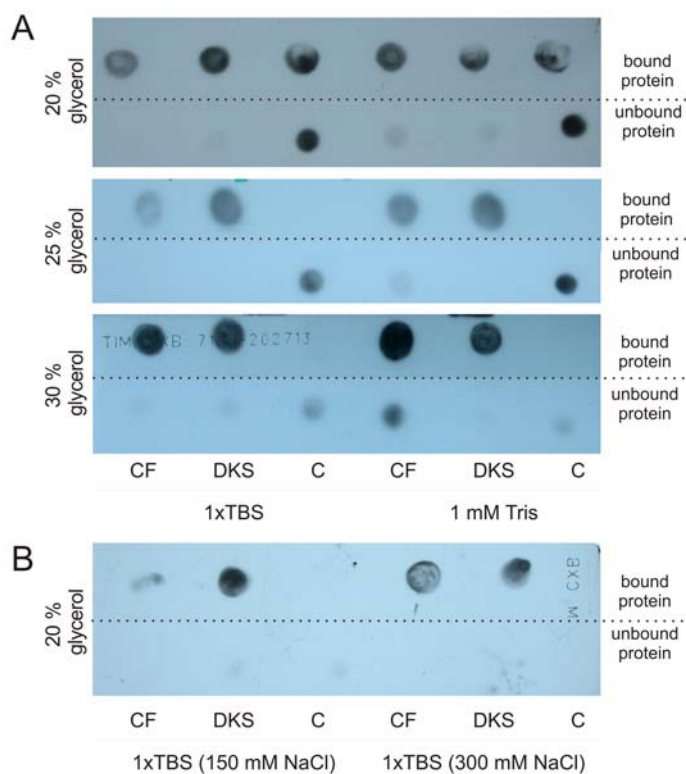


**Fig. 3.19: Increase of specific thiol-gold labelling upon addition of glycerol.** To investigate gold-bound protein, 10  $\mu$ l resuspended sediment was spotted on the membrane, whereas for detection of unbound protein, 10  $\mu$ l supernatant after centrifugation of the labelling approach was immobilised on the membrane. As technical control (C), the corresponding fractions of a labelling reaction containing Cys free variant but no gold colloids were utilised to verify the specific assignment of the fractions to the protein-gold conjugation. Immunodetection via chemiluminescence was performed using 2-Cys Prx specific antibody. A) Different amounts of glycerol were added to 1 mM Tris and 1 $\times$ TBS. B) Effect of additional NaCl was investigated.

Apparently the combination of sodium chloride and glycerol in a Tris-buffered environment was responsible for the decrease of gold colloid binding to the Cys free variant. The decrease in binding to the Cys-free variant was paralleled by an increased binding to the DKS variant with exposed cysteines. It was concluded, that these conditions mediate a strong suppression of unspecific interactions in favour of a thiol-gold conjugation specificity. Under these conditions, specificity is expected to be sufficient for DXT measurements as hydrophobic and ionic interactions were almost completely abolished (Fig. 3.19 A and B).

### **3.1.4 Characterisation of x-ray induced damage to 2-Cys Prx conformation and function**

The characterisation of damaging effects on protein function and aggregation behaviour that occur as a consequence of x-ray irradiation is of significant interest when it comes to the establishment of 2-Cys Prx as a model protein for dynamical imaging of conformational changes via DXT. This knowledge is needed to avoid a false assignment of x-ray mediated detrimental effects to redox-related conformational alterations. For this reason different x-ray parameters were investigated in order to characterise the impact of irradiation on 2-Cys Prx functional features. Additionally, such investigations are of general interest as up to now x-ray related damage to proteins was mostly investigated in context of structural studies that are implemented in crystallographic analyses (Ravelli and McSweeney, 2000; Leiros et al., 2001). A number of studies revealed specific sites within proteins as being predominantly impaired by x-ray irradiation. Besides the breakage of disulfide bonds also decarboxylation of aspartate and glutamate residues and the loss of hydroxyl groups from tyrosines were reported (Weik et al., 2000; Burmeister, 2000; Carugo and Djinovic Carugo, 2005). In contrast to various studies dealing with damage on structural level, the consequences for protein functionality of x-ray irradiation are still poorly understood. Therefore x-ray treated 2-Cys Prx was investigated on the one hand in respect of electrophoretic separation patterns, as it is a well known feature of this protein to adopt different aggregation forms dependent on oxidation state of the protein and suspension conditions (König et al., 2002; Wood et al., 2002). On the other hand different biochemical features allow for characterisation of functionality, as there are the DNA-protective function and the detoxification activity towards various peroxides (Bernier-Villamor et al., 2003; König et al., 2003). In the following sections, both structural and functional aspects will be investigated and discussed in order to give detailed insights into x-ray mediated damage of 2-Cys Prx as a redox-active protein.

#### **3.1.4.1 Short term irradiation had no impact on 2-Cys Prx amount and functionality**

First insight into effects of x-ray irradiation on both functional and structural characteristics was expected to be derived from the exposure of a 2-Cys Prx solution to an x-ray lab source emitting  $5\text{-}6 \times 10^8$  photons  $\text{s}^{-1}$  for a time period of three hours. The treatment added up to an overall dose of about 540 Gy. Afterwards protein amount of

monomeric 2-Cys Prx was investigated via reducing SDS-PAGE with subsequent silver staining (Fig. 3.20 A). No protein loss or alterations in separation behaviour were observed in comparison to the controls either kept on ice or at room temperature. The latter control was conducted to exclude temperature effects to be responsible for possible alterations in the irradiated samples, as these experiments had to be likewise performed at room temperature. The remaining question for functionality was examined via application of DNA cleavage assay.

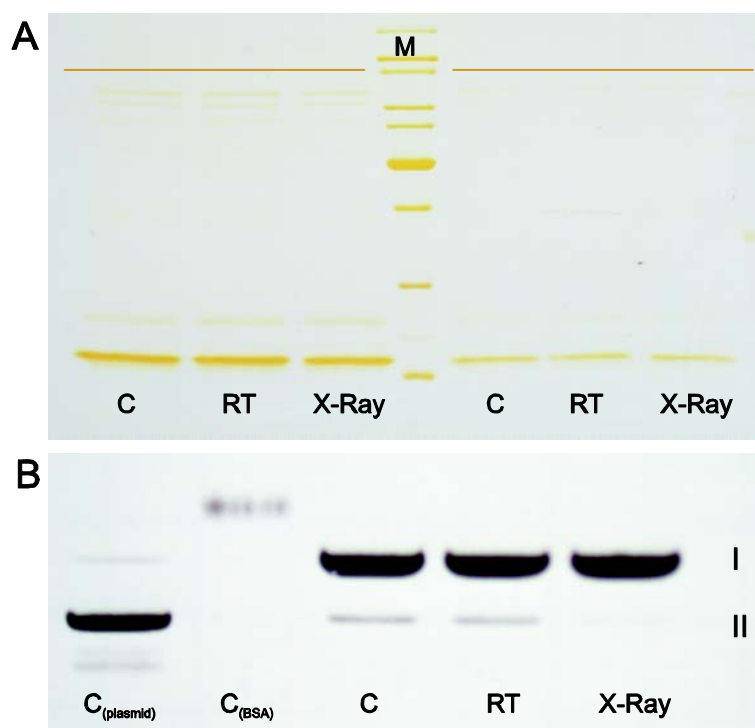


**Fig. 3.20: Short term irradiation of 2-Cys Prx.** Each experiment was performed twice with similar results (C = control on ice, RT = control at room temperature, X-Ray = x-ray exposed samples). A) Amount of monomeric 2-Cys Prx after different treatments visualised by separation in a reducing SDS-PAGE with subsequent silver staining. 13  $\mu\text{g}$  protein was loaded on the left side, 6.5  $\mu\text{g}$  on the right side of the PAA-gel. B) Protection of DNA in a metal-catalysed oxidation system (MCO).  $C_{(\text{plasmid})}$  = plasmid;  $C_{(\text{BSA})}$  = plasmid + MCO solution + BSA, revealing maximal cleavage; C, RT, X-Ray = plasmid + MCO solution + 6  $\mu\text{g}$  differentially treated 2-Cys Prx. I = supercoiled plasmid DNA, II = open circular form.

Severe damage was visible in control samples with BSA indicating maximal cleavage within this system. In a converse manner irradiated 2-Cys Prx samples as well as the untreated control protein exhibited a similar extent of DNA protective function as the amounts of supercoiled and open circular form were not altered. The comparison of this functional feature exhibited no damaging effect of the x-ray treatment (Fig. 3.20 B).

However, ROS-mediated nicking of plasmid DNA occurred in all differentially treated 2-Cys Prx samples, leading to an increase of relaxed form on expense of supercoiled plasmid (Fig. 3.20 B). This is consistent with former experiments investigating functionality of 2-Cys Prx cysteinyl variants (compare section 3.1.1.3) and results from Laxa et al. (2007) also showing slight ROS-mediated damage in absence of regenerating proteins.

Consequently it can be concluded, that the exposure to an overall radiation dose of about 540 Gy neither affects the structural nor functional integrity of 2-Cys Prx protein. As studies dealing with x-ray damage of proteins are usually incorporated in crystallographic analyses and the x-ray sources utilised for these single crystal diffraction studies are becoming increasingly powerful. The deposited energy from such sources is very high and therefore several orders of magnitude stronger than that used in the short-time experiments conducted within this work. In contrast, exposure of protein samples to similar irradiation intensities as applied in this work is found for gamma irradiation studies. As both, x- and gamma rays are ionising forms of radiation with similar characteristics and impacts on solutions and living matter (Janatpour et al., 2005; Kempner et al., 2001) the resulting effects in respect of structure and function can be compared. Gamma radiation experiments with bovine RNase A for instance showed an impairment of cysteine residues (Ferreri et al., 2004) as well as an inhibition of enzymatic activity to residual 67 % after exposure to only 33 Gy (Torreggiani et al., 2006). An increase of radiation intensity to 501 Gy even lead to an inactivation of RNase A by 50 % (Torreggiani et al., 2006). In this study, the exposure to 540 Gy had no significant effects on structural and functional integrity of 2-Cys Prx, indicating a high robustness of this protein to x-ray treatment. This underlines on the one hand the general findings of peroxiredoxins being stable peroxidases as they are independent of sensitive co-factors (Dietz, 2003 a) and show residual catalytic activity even under harsh environmental conditions (Dietz et al., 2006) with inactivation only occurring at non-physiological conditions (König et al., 2002). On the other hand, these findings also support the assumption of 2-Cys Prx being an ideal candidate for DXT analyses as besides the already discussed features it exhibits a considerable stability towards irradiation.

### 3.1.4.2 Long time irradiation revealed partial modification of 2-Cys Prx aggregation pattern

As short term irradiation experiments showed neither structural nor functional impairments of 2-Cys Prx, irradiation effects were expected to be enhanced by elongation of exposure time to 16 h. With the utilised x-ray lab source delivering  $5\text{-}6 \times 10^8$  photons  $\text{s}^{-1}$ , this corresponds to an overall radiation dose of about 2,900 Gy. The investigation of electrophoretic separation behaviour via reducing SDS-PAGE exhibited differences between irradiated and control samples (Fig. 3.21).

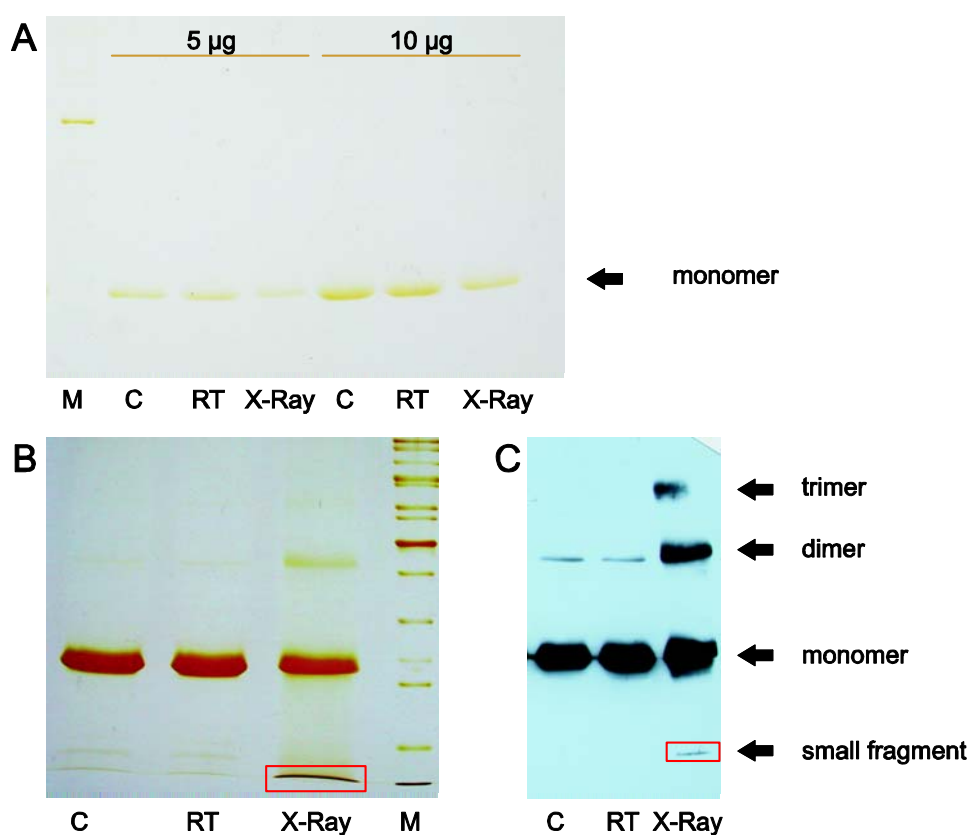


**Fig. 3.21: Changes in aggregation pattern of 2-Cys Prx after long term irradiation.** (C = control on ice, RT = control at room temperature, X-Ray = x-ray exposed samples). Each experiment was performed at least three times with similar results. A) Loss of monomeric form as consequence of x-ray treatment visualised via silver staining following reducing SDS-PAGE. Different protein amounts (5 µg and 10 µg) were analysed. B) Loading of higher protein amount (40 µg) combined with a longer development time during silver staining showed augmented formation of dimers with a size of about 44 kDa and smaller fragments with a size of less than 10 kDa as indicated by the red boxes. C) Western blot analysis of 2-Cys Prx revealed formation of aggregates with higher molecular mass and the presence of a small fragment (red box).

On the one hand the extension of exposure time resulted in a clearly visible loss of monomeric 2-Cys Prx in irradiated samples (Fig. 3.21 A) which was accompanied by an augmented formation of aggregated forms. These were visible after SDS-PAGE that was performed with increased protein amounts in combination with a prolonged development time during silver staining and correlated with a concomitant increase in 2-Cys Prx dimers with a molecular mass of about 44 kDa (Fig. 3.21 B). A further increase in sensitivity of detection method revealed the formation of aggregates with even higher molecular masses as detected by Western blot analysis (Fig. 3.21 C). These aggregates according to their size of about 70 kDa might represent trimers. Furthermore, the occurrence of smaller fragments with the size of less than 10 kDa was seen both in silver stained SDS-PAGE (Fig. 3.21 B) and Western blot analysis (Fig. 3.21 C). The mechanism of formation of dimers and higher molecular mass aggregates during long term irradiation is not easily to determine and will be discussed in the following. Two main mechanisms may contribute to the described alteration of aggregation pattern. On the one hand it was reported for cysteines to be very sensitive towards radiation induced damage both in a solid crystalline state (Leiros et al., 2006; Weik et al., 2000) and in aqueous environment (Ferreri et al., 2004; Saha et al., 1995), which either means the implementation in crystallographic studies or gamma irradiation experiments. Additionally, for low radiation doses of about 33 Gy modifications of cysteine residues were detected in an aqueous system (Ferreri et al., 2004). As 2-Cys Prx with its two highly conserved cysteines is well known to form homodimers via disulfide bonds during its catalytic cycle (Horling et al., 2002; König et al., 2003; Wood et al., 2003 b), it may be assumed that these reactive cysteinyl residues are involved in dimerisation upon irradiation, for example by overoxidation or radical-mediated cross-linking. This involvement might be rather due to a more complex mechanism and not caused by simple oxidative formation of dimers by dithiol-disulfide transition of the protein, as the dimers were stable during reducing SDS-PAGE (Fig. 3.21). To investigate this hypothesis of x-ray induced overoxidation, the separation pattern after modification of cysteine residues via incubation with hydrogen peroxide, leading primarily to an oxidation and at higher concentrations and during prolonged exposure to overoxidation by formation of sulfinic acid derivative (Jang et al., 2006), was compared to the aggregation forms arising upon x-ray exposure (Fig. 3.22).

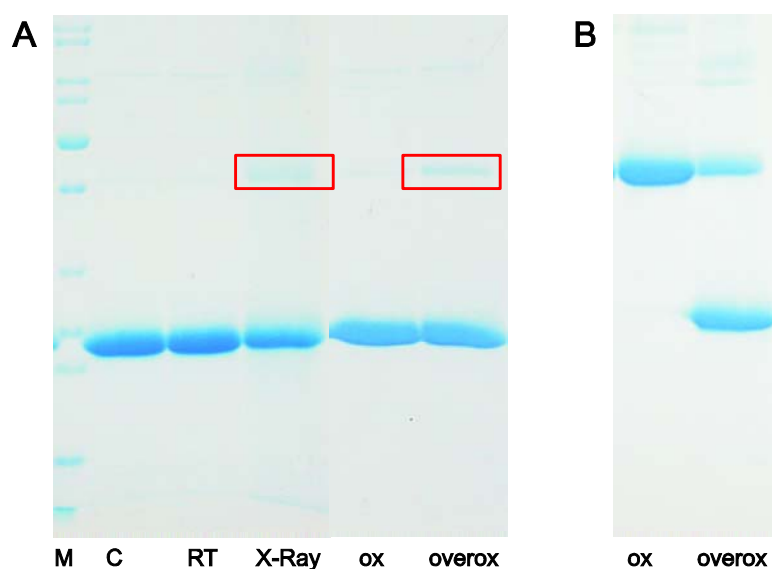


**Fig. 3.22: SDS-PAGE separation with subsequent Coomassie staining of the differentially treated 2-Cys Prx samples.** 6  $\mu\text{g}$  of protein including 2-Cys Prx adjusted to the different oxidation states (ox = oxidised, overox = overoxidised) were loaded per lane. Each experiment was performed at least twice. A) SDS-PAGE under reducing conditions (C = control on ice, RT = control at room temperature, X-Ray = x-ray exposed samples). Red boxes indicate similar dimerisation in x-ray treated and partially overoxidised sample, respectively. B) Oxidised and overoxidised 2-Cys Prx under non-reducing conditions for confirmation of differential oxidation states of the protein.

As visible after separation by reducing SDS-PAGE (Fig. 3.22 A), there was a strong similarity in separation pattern between partially overoxidised and irradiated sample. In addition to the monomeric form both these protein samples exhibited a significant band with the size of about 44 kDa correlating to 2-Cys Prx dimers. In order to confirm the oxidation states of both oxidised and overoxidised form (compare section 1.3.3. of introduction) SDS-PAGE was performed under non-reducing conditions (Fig. 3.22 B). Again a strong similarity in banding pattern indicates the involvement of cysteines in the development of the observed dimerisation products. The utilisation of x-rays within single crystal diffraction analyses is known to cause a preferential deposition of photoelectrons within disulfide bonds leading primarily to an elongation and finally to the breakage of these structures after formation of thiol-radicals (Weik et al., 2000 and 2002). As the protein redox and separation behaviour in the irradiated solution matched that in oxidising conditions, the described mechanism could be hypothesised to be responsible for dimerisation due to a corresponding cross-linking reaction in the samples (Fig. 3.21). Consequently, the resulting reactive thiol-radicals are expected to

be responsible for the formation of the covalently bound dimers due to subsequent reaction as a result of their extremely high reactivity.

In this context, MALDI-TOF analyses following tryptic digestion of the different 2-Cys Prx aggregation forms that were excised from PAA-gel after reducing SDS-PAGE with subsequent Coomassie staining were expected to verify the modification of cysteinyl residues, as sulfenic or sulfinic acid derivatives (Shetty et al., 2007). Unfortunately, the cysteine containing protein fragments were not detected within this analysis, neither in the irradiated monomeric or dimeric band nor in the untreated monomeric protein control. Furthermore, the calculation of mass changes of cysteine-containing fragments due to oxidation or overoxidation did not lead to identification of the corresponding fragments within the detected peptide fragments (data not shown).

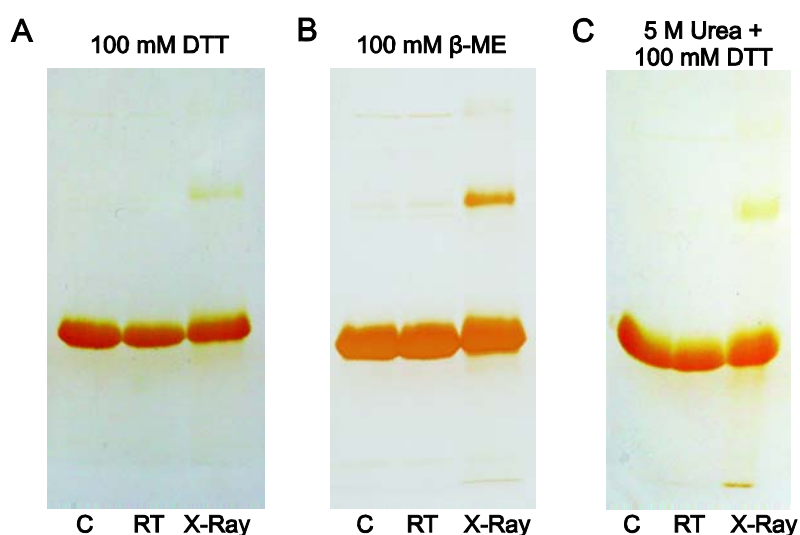


**Fig. 3.23: Aggregation pattern of 2-Cys Prx after treatment with different reducing agents.** SDS-PAGE of 12  $\mu$ g protein was performed with subsequent silver staining. C = control on ice, RT = control at room temperature, X-Ray = x-ray exposed samples. Each experiment was performed at least twice with similar results. Samples were reduced by incubation with 100 mM DTT (A, C) as routinely applied or 100 mM  $\beta$ -mercaptoethanol ( $\beta$ -ME) (B), further denaturation was stimulated by supplementation with 5 M urea (C) prior to SDS-PAGE.

Consequently further investigations to verify the chemical nature of the dimers were conducted. To analyse the nature of the bonds responsible for dimer formation, samples were treated with different reducing or denaturing agents. Besides reduction being routinely performed with DTT (Fig. 3.23 C), additionally  $\beta$ -mercaptoethanol was applied (Fig. 3.23 B) as it is described for certain cysteine residues that they are better

accessible to this smaller reductant (Peskin et al., 2007). Furthermore, irradiated samples were incubated with urea in presence of DTT and SDS aiming at weakening of hydrogen bonds (Bennion and Daggett, 2004) to investigate their involvement in dimer formation. The latter treatment was of special interest as it could be shown for PrxIIF from *Pisum sativum*, that the formation of hexameric complexes requires similar conditions to achieve their disassembly (Barranco-Medina et al., 2008 b). However, none of the described treatments enabled a monomerisation of the dimeric structure formed in irradiated protein samples (Fig. 3.23). This largely excluded a role of both hydrogen bonds and disulfide bridges in the generation of these structures and consequently indicates a covalent binding due to cross-linking reactions of the monomers most likely via radical intermediates.

Whereas in case of dimers, an involvement of cysteines in these covalent bonding might be possible due to the already described mechanism, trimer formation (Fig. 3.21 C) is unlikely to be due to these reactive amino acids. First of all, the presence of just two cysteines as well as their localisation within the 2-Cys Prx molecule limits the sites for binding and – even more important – up to now, there are no reports for chemical conditions *in vivo* or *in vitro* that give rise to the oligomerisation form of trimers (Wood et al., 2002). They could only be observed in cross-linking studies and therefore appear of artificial nature, not originating from cysteine residues (Chauhan and Mande, 2001). Consequently, other amino acids have to be responsible for the establishment of covalent binding upon x-ray irradiation as it cannot be traced back to thiol-oxidation or -overoxidation of 2-Cys Prx. In general, the establishment of covalent bonds due to protein-protein cross-linking reactions upon irradiation is a common observation (Hawkins and Davies, 2001; Stadtman, 1995). In case of gamma irradiated bovine RNase A for instance, charged amino acid residues like lysyl, glutamyl, and asparagyl residues were responsible for the formation of covalent associations (Torreggiani et al., 2006). It is furthermore established that tyrosine residues are very sensitive towards radiation mediated damage, as reported from studies applying x-rays on solid phase protein crystals and also by utilising gamma radiation in aqueous solutions (Burmeister, 2000; Ravelli and McSweeney, 2000; Matsui et al., 2002; Ferreri et al., 2004; Torreggiani et al., 2006). Thereby, irradiation does not only lead to the formation of tyrosyl radicals but it can consequently entail the generation of dityrosines (Torreggiani et al., 2006; Stuart-Audette et al., 2003; Audette et al., 2000). On the surface of 2-Cys Prx A, different tyrosines are located at exposed positions as depicted in

Fig. 3.24 A. In contrast to only two cysteines there are in total six tyrosine residues (Fig. 3.24 B) within the amino acid sequence of this protein. Thus the probability for generation of tyrosine radicals seems considerably higher than the formation of thiol radicals.

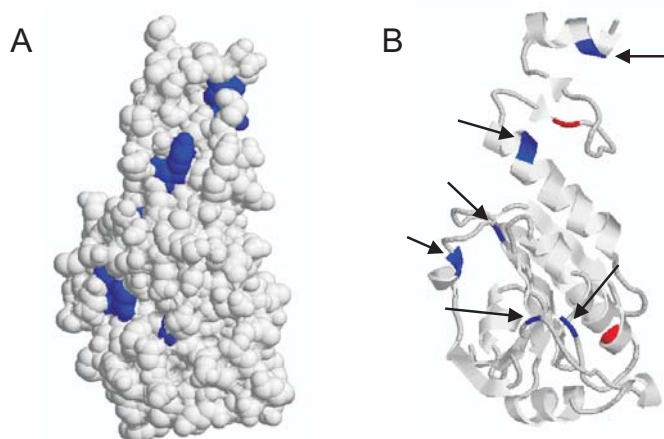


**Fig. 3.24: Schematic depiction of tyrosine residues on protein surface of 2-Cys Prx.**

Tyrosine residues within the 3D-structure of 2-Cys Prx from *A. thaliana* (compare Fig. 3.4) are highlighted in blue on the molecular surface (A) and in ribbon structure (B, see black arrows). Cysteine residues are additionally coloured in red in ribbon structure. Modelling was performed with RasMol software.

From human and mammalian systems, tyrosine residues are well known to be primary targets of oxidative modifications occurring as a consequence of oxidative stress. These modifications often mark the affected proteins for degradation (Stadtman and Levine, 2003; Giulivi et al., 2003). In aqueous solutions, ionising radiation was shown to generate water radicals (Southworth-Davies and Garman, 2007; Murray and Garman, 2002; Filali-Mouhim et al., 1997). Besides the direct effect of photoelectrons the radicals may damage proteins indirectly. These oxidising conditions may foster the generation of tyrosyl radicals and subsequent formation of dityrosines. Therefore, the development of protein-protein cross-linking events occurring during irradiation of 2-Cys Prx could also be due to the damage of tyrosines by long term irradiation. According to the just described mechanism, the highly oxidising environment generated by irradiation mediated water radicals may resemble the conditions during overoxidation treatment of 2-Cys Prx. The similarity of dimerisation products in overoxidised and irradiated protein (Fig. 3.22 A, red boxes) supports the hypothesis that other amino acids such as tyrosines rather than cysteines are involved. However, an involvement of cysteine residues in damage development cannot be excluded. In order

to further characterise the mechanism of damage occurring in case of long term x-ray treatment, investigations on functional level were performed as described in the following (section 3.1.4.3).

Besides the formation of different aggregates upon irradiation, also a fragmentation of 2-Cys Prx was observed in reducing SDS-PAGE (Fig. 3.21). Protein fragmentation upon ionising radiation is a well described effect, especially in aqueous system (Torreggiani et al., 2006; Le Maire et al., 1990; Audette et al., 2000). In many cases, the occurring fragmentation was due to a specific effect, leading to cleavage of protein backbones at defined sites (Torreggiani et al., 2006). Therefore it was important to analyse fragmentation mechanisms in case of 2-Cys Prx irradiation.

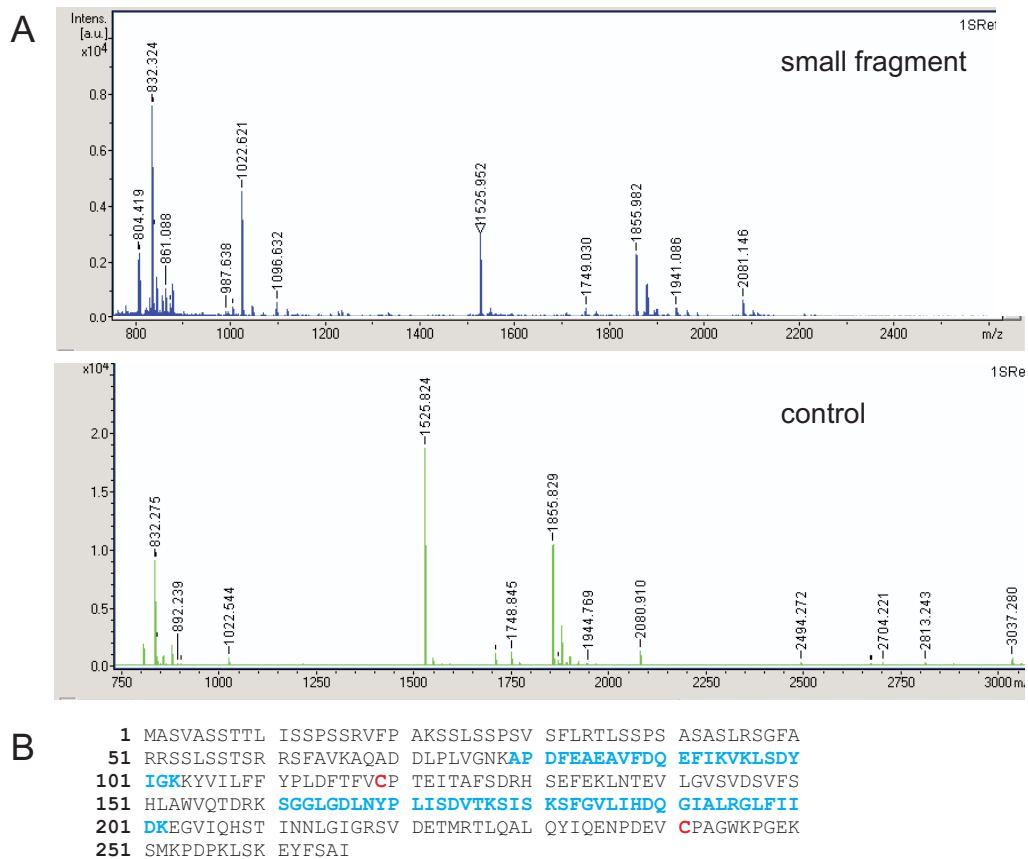


**Fig. 3.25: Mass spectrometric analysis of the small protein fragment formed upon irradiation of 2-Cys Prx.** A) Comparable analysis of mass spectra obtained for the small fragment (blue) and untreated 2-Cys Prx (green) separated as monomer in reducing SDS-PAGE revealed no significant differences. B) The assigned fragments are depicted in blue in amino acid sequence of 2-Cys Prx (including signal peptide) with cysteine residues highlighted in red.

To achieve this goal, a sample of the fragment correlating to about 10 kDa within reducing SDS-PAGE (Fig. 3.21 A and B) was analysed by MALDI-TOF mass spectrometry after tryptic digestion. The obtained mass spectra of the small fragment and untreated 2-Cys Prx did not differ considerably. Additionally, the identified 2-Cys Prx fragments could not be assigned to certain parts within the whole protein structure, e.g. correlating to significantly exposed or sensitive regions, but were spread among the primary sequence (Fig. 3.25). Furthermore, the appearing of a single band in contrast to two bands as it could be expected in case of one distinct cleavage site indicated an undirected fragmentation of the irradiated protein with the resulting localisation within the running front. Therefore it is concluded that fragmentation during irradiation of 2-Cys Prx occurred due to a random mechanism. As the major quantity of irradiated protein seemed to remain unaffected, the mechanism for the fragmentation of just a small amount of 2-Cys Prx is assumed to be the result of overexposure. As the distribution of deposited energy within the content of the glass vessel during irradiation is not homogenous (Fig. 3.26), it is expected that there are proteins absorbing a higher quantity of energy. Although diffusion is taking place within the vessel, it is unlikely to allow for complete mixing of the sample. Consequently, the absorbed dose per protein may vary considerable and the 2-Cys Prx molecules remaining in the focus of irradiation for the longest time (compare Fig. 3.26) will experience a significantly higher dose than calculated as the average of the whole sample. The locally increased dose will stimulate the damaging effects with protein fragmentation.

The damaging impact of irradiation on 2-Cys Prx showed a clear dose dependency, as the overall dose of 540 Gy did not impair the separation behaviour in contrast to long term irradiation with a total of 2,900 Gy. Also in crystallographic studies, the damage to protein structures increased with increasing x-ray doses (Shimizu et al., 2007).

Further investigations in relation to the dose dependency of irradiation effects were conducted with a special focus on the mechanisms of damage development. In this context the DNA protective function and the catalytic activity of 2-Cys Prx were investigated by means of DNA cleavage assay and measurement of hydrogen peroxide turnover, respectively.

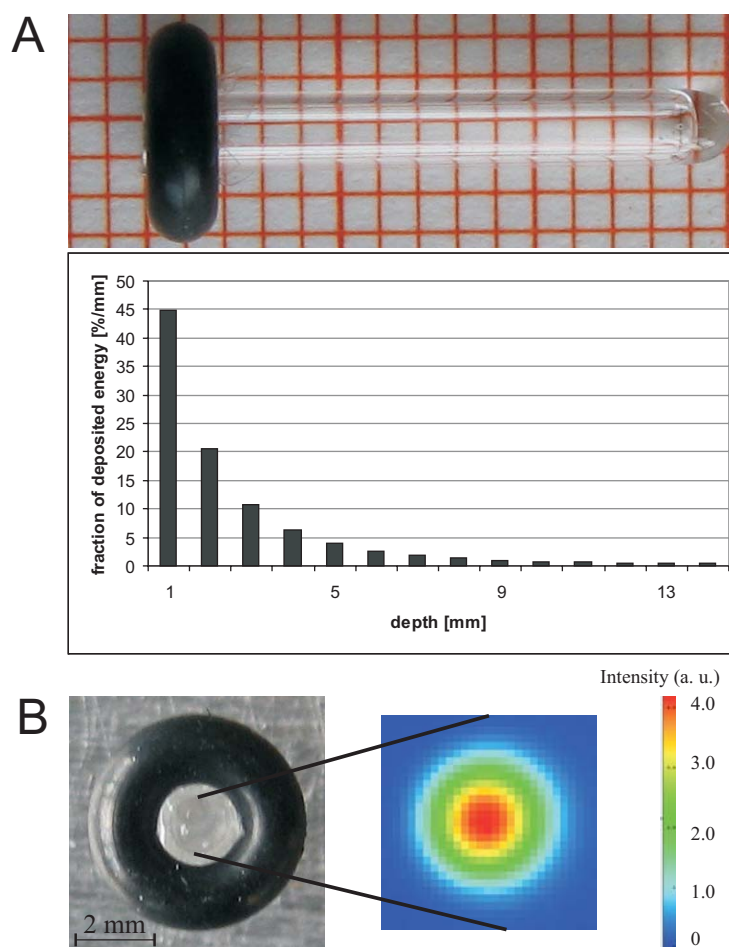


**Fig. 3.26: Irradiation of the 2-Cys Prx solution in the utilised glass vessel.** A) The difference between two spectra at different depth (distance: 1 mm), calculated by convolving the spectral absorbance of water with the estimated x-ray spectrum, weighted with the photon energy and normalised to the incident beam energy, resulted in the fraction of the deposited energy per mm (bottom). Fractions of deposited energy are displayed correlating to side view of the vessel (top). B) Front side view of the glass vessel (left) is depicted with x-ray beam profile (right) being displayed true to scale. Different colours indicate different x-ray intensities. Irradiation and calculation were performed by Jawad Slieh and Dr. Armin Brechling from the Department of ‘Molekül- und Oberflächenphysik’ of Bielefeld University.

### 3.1.4.3 Inhibition of 2-Cys Prx functions upon long term irradiation

The extended exposure to the x-ray lab source emitting  $5\text{-}6 \times 10^8$  photons  $\text{s}^{-1}$  resulted in altered structural features of 2-Cys Prx (compare section 3.1.4.2). Therefore the irradiation was also expected to affect functionality of the protein. Firstly, catalytic activity was investigated via measurement of hydrogen peroxide turnover within a thioredoxin (Trx) and thioredoxin reductase (TR) dependent regeneration system. The detoxification capacity in this spectrophotometry-based assay can be monitored via

NADPH oxidation as measured at 340 nm (Fig. 3.27 A). Fig. 3.27 B exemplarily depicts the oxidation rate for the blank reaction containing no protein as well as for one set of measurements with three samples, namely irradiated protein as well as controls on ice and at room temperature.

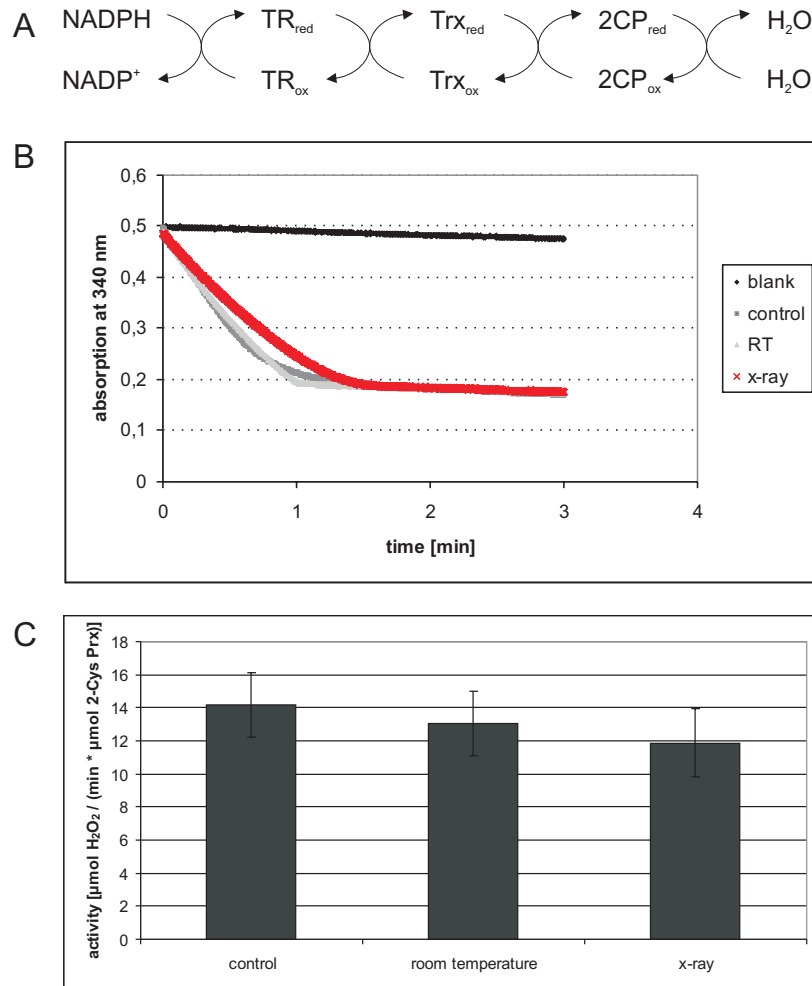


**Fig. 3.27: Hydrogen peroxide detoxification activity of 2-Cys Prx after long term irradiation.** A) Electron flow in the reconstituted assay containing 2-Cys Prx (2CP), *E. coli* Trx and *E. coli* TR as regeneration system (red = reduced, ox = oxidised). B) Kinetics of  $\text{H}_2\text{O}_2$  detoxification as measured by time dependent absorption changes of NADPH. Activity of differentially treated 2-Cys Prx was measured by monitoring NADPH oxidation as decrease of  $\text{Abs}_{340}$  (control, RT, x-ray) and sample without 2-Cys Prx in the sample (blank), as depicted exemplarily for one set of measurements. C) Measurement of catalytic activities of differentially treated 2-Cys Prx after long term irradiation. Activities are corrected for autoxidation of NADPH and depicted as mean values with standard deviations, differences between the single conditions were significant according to Student's T-test with at least  $P < 0.1$  as indicated by the different letters (n = 15-38).

As seen in Fig. 3.27 C the long term irradiation of 16 h with an irradiation deposition of about 2,900 Gy, did not only have an impact on the aggregation state of 2-Cys Prx (compare section 3.1.4.2) but also significantly affected the hydrogen peroxide detoxification capacity. Whereas control samples on ice exhibited an average activity of  $14.2 \pm 2.0 \mu\text{mol H}_2\text{O}_2/(\text{min } \mu\text{mol 2-Cys Prx})$ , which resembles the hydrogen peroxide detoxification capacities described for barley and *A. thaliana* (König et al., 2003; Horling et al., 2003), the room temperature incubation already resulted in a significant decrease of NADPH consumption to  $13.1 \pm 1.9 \mu\text{mol H}_2\text{O}_2/(\text{min } \mu\text{mol 2-Cys Prx})$  (Student's T-Test  $P < 0.05$ ). However, the irradiation of 2-Cys Prx sample for 16 h caused a further decrease of detoxification capacity to a considerably larger extent with a remaining activity of  $11.9 \pm 2.1 \mu\text{mol H}_2\text{O}_2/(\text{min } \mu\text{mol 2-Cys Prx})$  (Student's T-Test with  $P < 0.005$  for Control (on ice) and X-Ray). As hydrogen peroxide detoxification capacity is directly linked to functionality of the cysteine residues, the impairment of catalytic activity as a result of x-ray treatment may indicate an involvement of these amino acids in the observed damage development. To investigate this hypothesis, again functionality of partially overoxidised 2-Cys Prx was analysed in respect of catalytic activity as this treatment specifically leads to a modification of cysteine residues.

The measurement of  $\text{H}_2\text{O}_2$  turnover by partially overoxidised protein exhibited a similar decrease of 2-Cys Prx activity as observed upon irradiation (Fig. 3.28). Whereas untreated ( $13.4 \pm 0.2 \mu\text{M H}_2\text{O}_2/(\text{min} \cdot \mu\text{M 2-Cys Prx})$ ) and, prior to the measurement, oxidised protein as additional control ( $14.5 \pm 0.2 \mu\text{M H}_2\text{O}_2/(\text{min} \cdot \mu\text{M 2-Cys Prx})$ ) showed activities similar to previously described assays (cf. Fig. 3.27 C; König et al., 2003; Horling et al., 2003), a treatment aiming at the overoxidation of 2-Cys Prx protein reduced the catalytic activity to  $8.5 \pm 0.3 \mu\text{M H}_2\text{O}_2/(\text{min} \cdot \mu\text{M 2-Cys Prx})$ . Samples exposed to conditions favouring the formation of sulfinic acid derivatives had similar activities as seen after irradiation, supporting the tentative assumption of impairment of the cysteinyl residues. Naturally, the x-ray mediated impairment of any other amino acid with significance for catalytic activity could have the same impact on functionality. However, the just described impact of overoxidation on peroxidase function (Fig. 3.28) as well as the assignment of cysteines as primary targets upon radiation-mediated enzyme-inactivation in aqueous systems (Saha et al., 1995) strongly point towards an involvement of exactly these highly reactive residues.

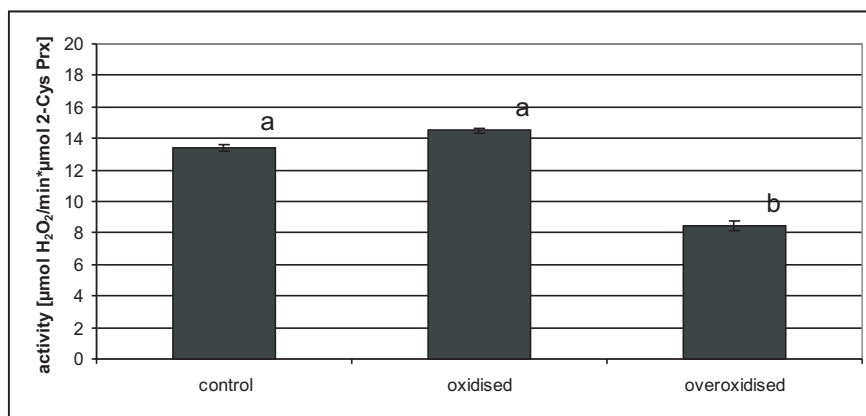


**Fig. 3.28: Hydrogen peroxide reducing activity of initially oxidised and partly overoxidised 2-Cys Prx.** Trx/TR dependent activities were corrected for NADPH autoxidation and are given as mean values with standard deviations of at least five measurements. Different letters indicate significance of difference according to Student's T-test with  $P < 0,001$ .

Furthermore, DNA protective function of 2-Cys Prx was investigated in dependence on the different treatments. Interestingly, the x-ray mediated damage was considerably higher for this functional feature than for the catalytic activity (Fig. 3.29 A).

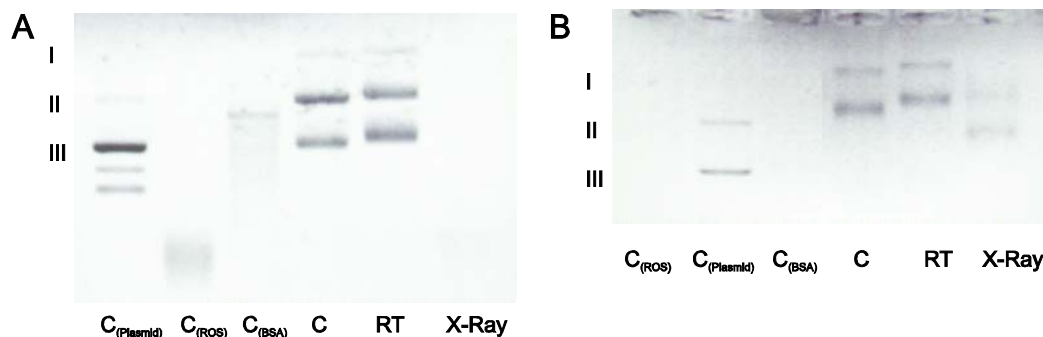


**Fig. 3.29: DNA cleavage assay of differentially treated 2-Cys Prx.** Each sample contained 2 µg of plasmid DNA ( $C_{(Plasmid)}$  = plasmid;  $C_{(ROS)}$  = plasmid + MCO solution;  $C_{(BSA)}$  = plasmid + MCO solution + BSA, corresponding to maximal cleavage). III = supercoiled plasmid DNA, II = open circular form, I = linearised plasmid. Experiments were performed at least three times with similar results. A) DNA protective function of 6 µg 2-Cys Prx in the metal-catalysed oxidation (MCO) system was strongly impaired after 16 h of x-ray (X-Ray) treatment compared to the control conditions (C = control on ice, RT = control at room temperature). B) DNA protective function of differentially treated 2-Cys Prx in presence of thioredoxin A, thioredoxin reductase, and NADPH as regeneration system.

Whereas samples of both control conditions, i.e. samples kept on ice or at room temperature, revealed full 2-Cys Prx protective function from ROS-mediated cleavage

of plasmid DNA (compare Laxa et al., 2007), x-ray irradiation lead to an almost complete loss of protection (Fig. 3.29 A) indistinguishable from the controls with either no protein or in the presence of BSA, and therefore demonstrating maximal damage. To identify the cause for the strong discrepancy in irradiation effects on both functional properties with the significantly higher impact on DNA protective function, the DNA cleavage assay was modified. The basic difference of both assays monitoring detoxification of either one specific reactive species (hydrogen peroxide) or ROS in general (generated in MCO solution) is the presence or absence of Trx/TR system providing regeneration of 2-Cys Prx (Yamamoto et al., 1999; König et al., 2002 and 2003; Horling et al., 2003). Therefore DNA cleavage assay was performed upon addition of all components of this regeneration system (Fig. 3.29 B).

Upon supplementation of the different DNA cleavage approaches with the components of the Trx/TR system, the plasmid protective function mediated by 16 h irradiated 2-Cys Prx could be rescued to a certain extent as visible in Fig. 3.29 B. Although the addition of these proteins resulted in an uncontrolled alteration in electrophoretic mobility of plasmid DNA, the bands of supercoiled and open circular form were detectable in every sample. Unfortunately, the extent of impairment on irradiated protein is not easy to determine. However, this leads to the hypothesis that the discrepancy in the degree of damage between both functional features was due to the absence of an efficient regeneration system for re-reduction of 2-Cys Prx which is needed to maintain its ROS detoxification capacity (Yamamoto et al., 1999; König et al., 2002 and 2003; Horling et al., 2003). Thus the difference is not or only partly a consequence of different sites of x-ray mediated damage as one could have assumed after the first experiments.

The analysis of radiation mediated damage in respect of functional properties of 2-Cys Prx revealed an involvement of cysteines in damage development at least for these biochemical attributes. Not only the observed loss of DNA protective function and the partly re-established ability to act as DNA protectant by addition of Trx, TR, and NADPH indicated these residues as targets. Also the decrease of catalytic activity to approximately 85 % hints to their participation – especially in the light of a similarly inhibited catalytic activity in partially overoxidised protein. Although the structural impairments of 2-Cys Prx may be predominantly linked to tyrosine modifications (compare section 3.1.4.2), functional alterations can tentatively be assigned to cysteine residues.

Furthermore, it can be concluded that additional to the structural alterations of 2-Cys Prx in dependence of irradiation (compare section 3.1.4.2) also the effects on functionality of 2-Cys Prx were changed in a dose dependent manner. As an overall radiation dose of about 540 Gy had no impact on 2-Cys Prx function as visualised via DNA protection in the cleavage assay (Fig. 3.20 B), an increase of dose to about 2,900 Gy was paralleled by evolving impacts on functionality. This dose dependency is not only known in context of crystallographic x-ray applications (Shimizu et al., 2007), but also clearly visible in studies applying gamma-irradiation in aqueous systems (Torreggiani et al., 2006). In comparison to a study with bovine RNase A, the x-ray impact on 2-Cys Prx functionality was comparably low with a decrease in catalytic activity by merely 15 % upon irradiation with 2,900 Gy. In contrast, RNase A activity already decreased by 33 % after applying doses of 33 Gy (Torreggiani et al., 2006). Consequently the investigation of functional impairment as a result of long term x-ray treatment again revealed a high stability and robustness of 2-Cys Prx, a feature that was assigned to this type of peroxidase before (Dietz, 2003 a; Dietz et al., 2006; König et al., 2002).

#### **3.1.4.4 Augmented x-ray damage on structural and functional features of 2-Cys Prx in presence of gold colloids**

As the dynamical imaging of conformational changes via DXT requires the labelling of the protein molecules with x-ray-defracting nanocrystals, it was necessary to investigate the effect of gold during long term x-ray irradiation. This is of particular importance, as metals are known to absorb photoelectrons upon x-ray treatment and subsequently to release low-energy electrons (Carter et al., 2007). These electrons have the tendency to directly deposit their energy, a process which in aqueous solutions leads to a high rate of interactions with water molecules and thereby generates so-called water radicals (Turner et al., 1983; Carter et al., 2007). This process may consequently cause additional damaging effects during irradiation of biological matter as for instance on proteins (Zheng et al., 2008). The effects are even more pronounced in nanocrystals which have a comparably large surface-to-volume ratio (Carter et al., 2007). As the dynamical imaging of conformational changes via DXT is based on labelling of the target proteins with gold nanocrystals, it was of special interest to investigate the potentially additional impact of x-ray irradiation in presence of gold nanocrystals on

2-Cys Prx protein structure and function. Therefore irradiation experiments were conducted upon supplementation of the protein solution with 40 nm gold colloids. To get first insights into damage development in presence of gold colloids, identical amounts of differentially treated 2-Cys Prx were analysed by reducing SDS-PAGE. Corresponding to the analyses described above to generally characterise long term irradiation mediated damage (compare section 3.1.4.2 and 3.1.4.3), initially the amount of monomeric 2-Cys Prx was investigated in dependence of the different treatments. As visible from Fig. 3.30 A, part of the monomeric form was lost in x-ray treated samples both in presence and absence of gold colloids in comparison to the controls on ice and at room temperature. Upon addition of the nanoparticles, the loss of monomeric 2-Cys Prx seemed to be slightly more pronounced, an effect which was especially obvious in samples with 10  $\mu\text{g}$  of loaded protein (Fig. 3.30 A).

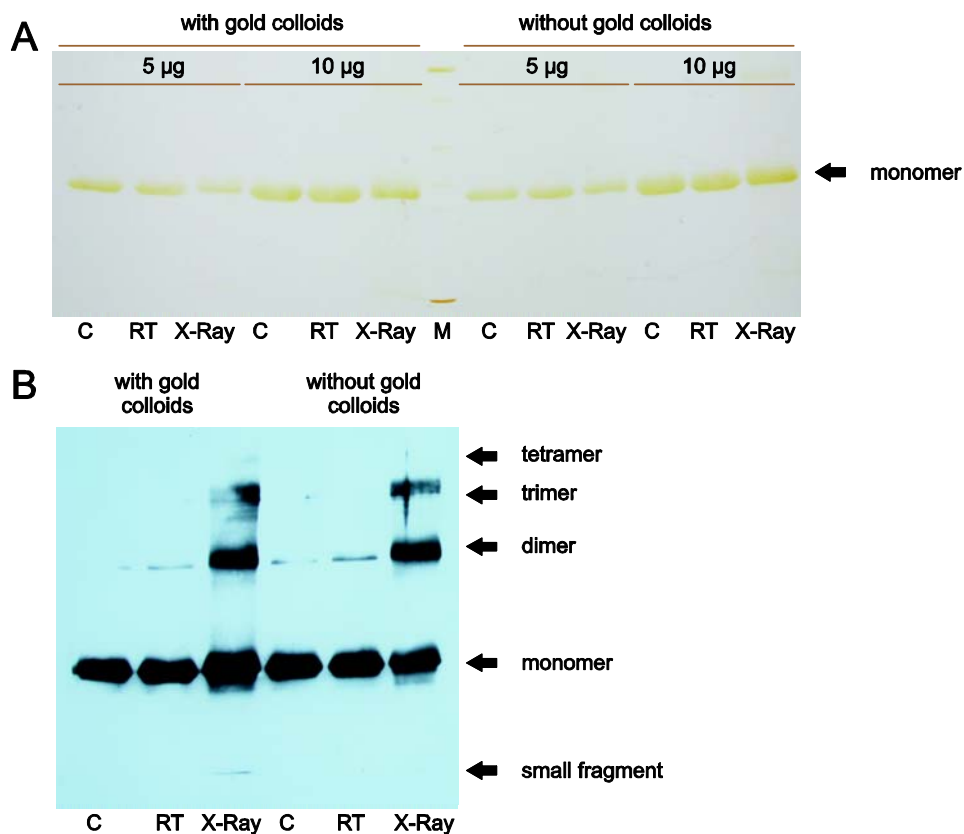


**Fig. 3.30: Changes in separation behaviour of 2-Cys Prx after long term irradiation with and without gold particles.** (C = control on ice, RT = control at room temperature, X-Ray = x-ray exposed samples). Each experiment was performed at least twice with similar results. A) Loss of monomeric form as consequence of x-ray treatment visualised via silver staining following reducing SDS-PAGE. Different protein amounts (5  $\mu\text{g}$  and 10  $\mu\text{g}$ ) were analysed. B) Western blot analysis of 2  $\mu\text{g}$  2-Cys Prx

employing 2-Cys Prx specific antibody revealed formation of aggregates with higher molecular mass as well as the appearance of a small fragment.

A further observation of structural alterations upon irradiation with an overall radiation dose of 2,900 Gy was the formation of higher molecular mass aggregates on expense of monomeric 2-Cys Prx which again were not reducible with the added 100 mM DTT. Via Western blot analysis with 2-Cys Prx specific antibody it has been shown above that besides the formation of dimers also trimers were generated (Fig. 3.30 B, compare also Fig. 3.21 C). Samples containing gold colloids additionally aggregated as complex with a molecular mass of about 90 kDa which according to their size were tentatively assigned to tetramers (Fig. 3.30 B). This effect again revealed an enhanced x-ray mediated damage in presence of gold colloids. Simultaneously a clearly detectable fragmentation of 2-Cys Prx in presence of gold colloids was detectable, leading to the same conclusion. In addition to the evidence for enhanced nanogold-mediated damage, the characterisation of these structural alterations may give further insights into the underlying mechanisms. As already discussed within section 3.1.4.2, the generation of 2-Cys Prx aggregates which can be assigned to trimers is unlikely to be due to an exclusive impact on cysteine residues (Wood et al., 2002; Chauhan and Mande, 2001), as the interaction of just two of these reactive residues would not be sufficient to form these kinds of structures, albeit one could postulate the occurrence of concatemer-like assemblies even with two Cys residues per subunit. The latter is unlikely since the obligate 2-Cys Prx dimer with complementary interfaces structurally impedes this type of interaction. Furthermore it might be assumed, that tyrosines which also are primary targets for radiation-induced damage (Ferreri et al., 2004; Matsui et al., 2002) could be involved in tri-, tetra- or oligomerisation. Tyrosyl residues are well-known to be prone to radicalisation subsequently leading to the formation of dityrosines (Torreggiani et al., 2006; Stuart-Audette et al., 2003). Structures like tetramers are described for the two human 2-Cys Prx isoforms Prx1 and Prx2 that contain one or two additional cysteine residues, respectively (Lee et al., 2007). Only these additional ones allow for the formation of tetramers. Consequently, the mechanism of aggregate formation might be the result of tyrosine modification instead of an involvement of cysteines.

Also on the functional level, evidence could be adduced for a slightly more pronounced damage after supplementation with gold colloids. As seen from Fig. 3.31, the presence of gold particles in the samples further decreased the hydrogen peroxide detoxification capacity during long term irradiation to  $10.0 \pm 2.0 \mu\text{mol H}_2\text{O}_2/(\text{min } \mu\text{mol 2-Cys Prx})$

from  $11.9 \pm 2.1 \mu\text{mol H}_2\text{O}_2/(\text{min } \mu\text{mol 2-Cys Prx})$  in the absence of gold nanoparticles. This corresponds to an activity decrease from 15 % to 27 % (Fig. 3.31 C). To exclude a disturbing effect of gold colloids on the NADPH-dependent activity assay, similar measurements of controls that had been kept on ice or at room temperature were conducted in presence and absence of gold colloids. These determinations exhibited no significant differences (Fig. 3.31 B). Consequently, the observed additional damaging effects in irradiated samples must have been triggered by the added gold colloids.

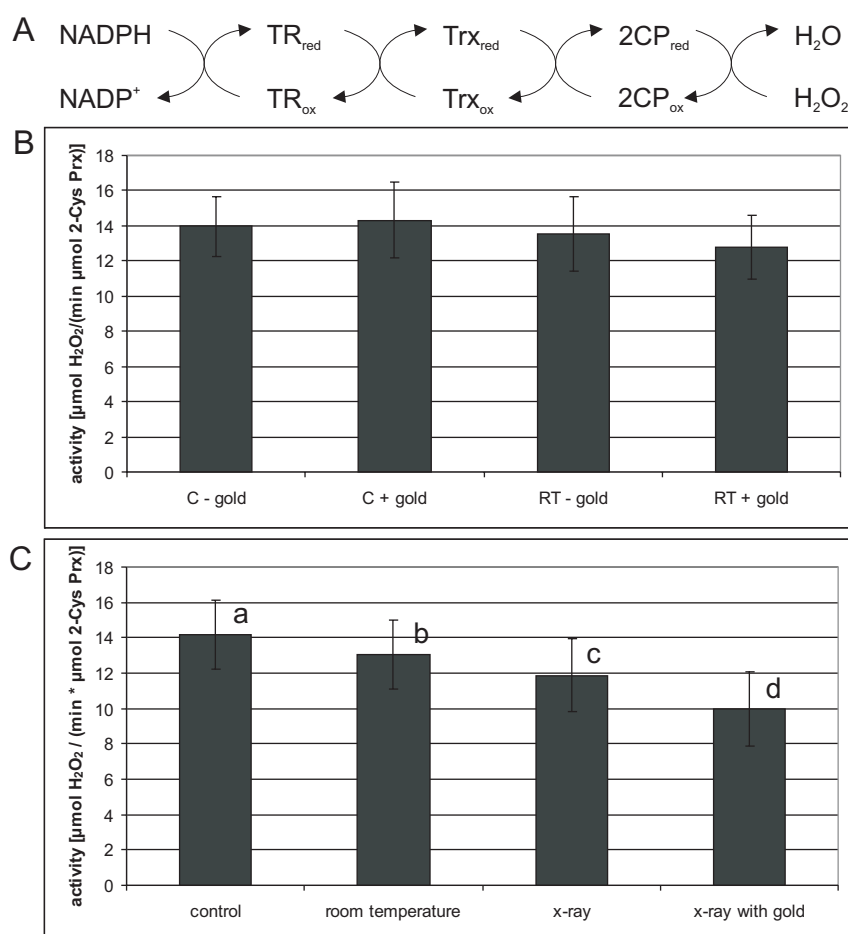


**Fig. 3.31: Hydrogen peroxide reducing activity of 2-Cys Prx after long term irradiation in dependence of supplementation with gold colloids.** (C = control on ice, RT = control at room temperature) (A) Electron flow in the reconstituted assay containing 2-Cys Prx (2CP), *E.coli* Trx and *E.coli* TR. The NADPH oxidation activity was monitored as decrease of Abs<sub>340</sub> and corrected for NADPH autooxidation without 2-Cys Prx in the assay. (B) Detoxification capacities of control samples with and without gold colloids in the assay. Results are given as mean values with standard deviation (n = 8-38). (C) Detoxification capacity of 2-Cys Prx after long term treatment. 2-Cys Prx was irradiated in presence and absence of gold colloids. Results from samples with and without gold colloids were pooled for both control conditions (without x-ray

irradiation), as no significant difference could be detected (compare B of this figure).

Letters indicate significant differences according to Student's T-test with  $P < 0.1$ .

Additionally, the consequences of gold colloid supplementation were analysed in respect of the function of 2-Cys Prx as DNA protectant. As the impact of irradiation on DNA protective function in absence of a regenerating system was severe (compare Fig. 3.29) and this assay does not allow for a quantitative analysis, the additional effect of gold colloids can just be estimated roughly. Irradiation of 2-Cys Prx in absence of gold particles already led to considerable impairment of its DNA protective function, however specific long length DNA fragments were still preserved (Fig. 3.32, X-Ray without gold colloids).

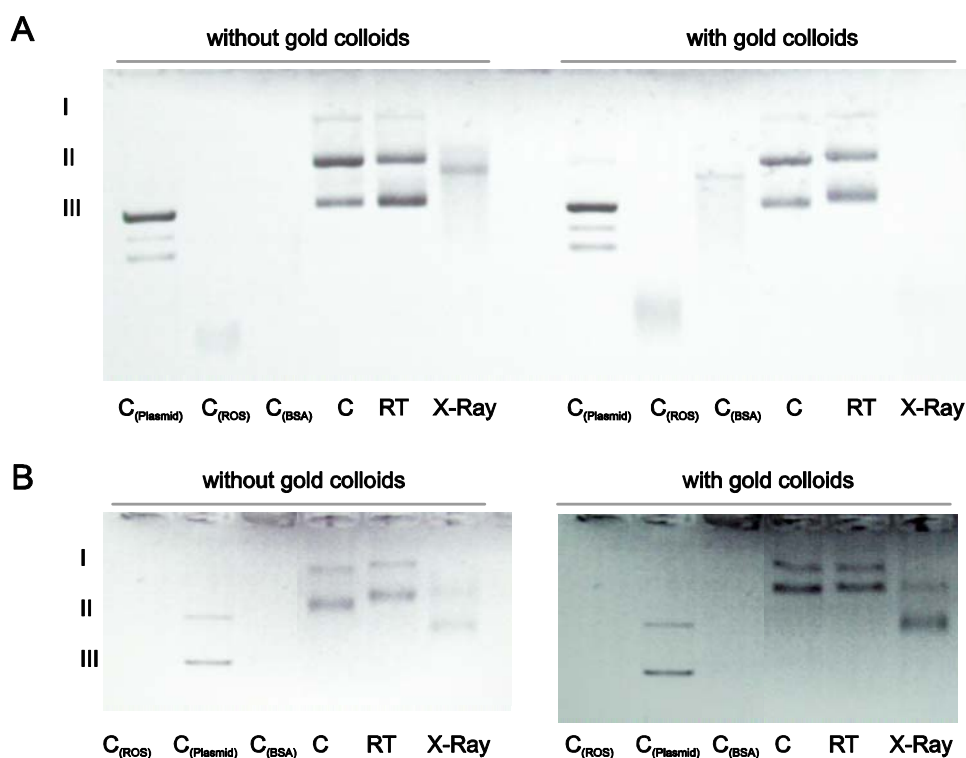


**Fig. 3.32: DNA cleavage protection by differentially treated 2-Cys Prx in dependence of gold colloid supplementation.** Each sample contained 2  $\mu$ g of plasmid DNA ( $C_{(Plasmid)}$  = plasmid;  $C_{(ROS)}$  = plasmid + MCO solution;  $C_{(BSA)}$  = plasmid + MCO solution + BSA, corresponding to maximal cleavage). III = supercoiled plasmid DNA, II = open circular form, I = linearised plasmid. Experiments were performed at least twice times with similar results. A) DNA protective function of 6  $\mu$ g 2-Cys Prx in the metal-catalysed oxidation (MCO) system was strongly impaired after 16 h of x-ray (X-Ray) treatment compared to the control conditions (C = control on ice, RT = control at room temperature). The observed effect was more pronounced upon supplementation of the sample with gold particles. B) DNA protective function of differentially treated 2-Cys Prx in presence of thioredoxin A, thioredoxin reductase, and NADPH as regeneration system.

2-Cys Prx irradiated in the presence of gold nanoparticles exhibited no apparent residual protective function resulting in a complete decomposition of the plasmid DNA to small products unresolved in the agarose gel (Fig. 3.32 X-Ray with gold particles). By addition of Trx/TR system for regeneration of 2-Cys Prx, the function as DNA protectant in presence of gold particles could be re-established in both treatments (Fig. 3.32 B).

Besides its already described role in enhancing radical formation in an aqueous environment gold may also alter the irradiation dose absorbed by the protein, as atoms exhibit different absorption behaviours of photoelectrons due to their atomic number (Debnath et al., 2004). A comparative calculation of deposited energy in the different fractions of the irradiated samples revealed just a minor difference between both treatments, i.e. with and without 0.01 % gold colloids (Fig. 3.33).

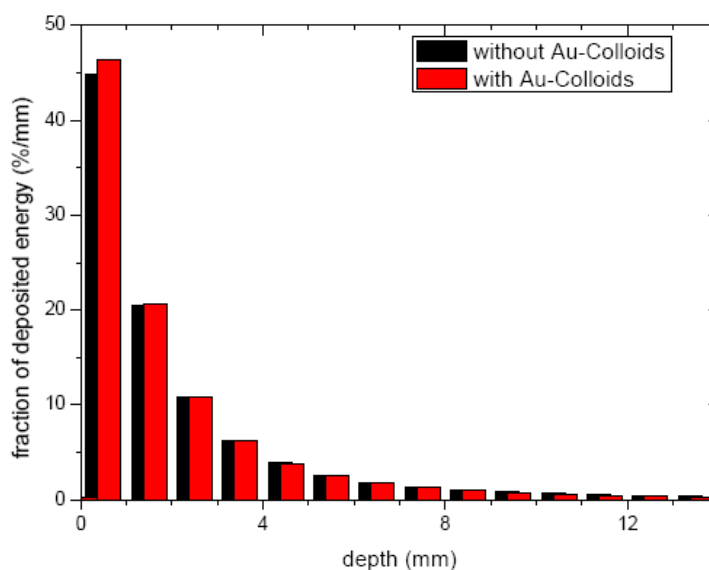


**Fig. 3.33: Deposited energy in different fractions of a protein sample without and with gold colloids.** The difference between the two spectra at different depth (for 1 mm sections), calculated by convolving the spectral absorbance of water with the estimated x-ray spectrum, weighted with the photon energy and normalised to the incident beam energy, resulted in the fraction of the deposited energy per mm (depicted in black). Correspondingly the calculation was performed for gold colloid-containing solution (depicted in red). The calculations were conducted by Dr. Armin Brechling from the department of ‘Molekül- und Oberflächenphysik’ from Bielefeld University.

As seen from Fig. 3.33, the presence of gold colloids only slightly increased the absorption within the first two 1 mm-sections by less than 2 %, while the energy dose was the same in the third 1 mm-sections. Thus, the influence of gold colloids on

absorbed radiation dose is not critical. It is concluded, that this effect does not falsify the assignment of radiation-mediated effects in presence of gold colloids.

The previous experiments addressed the question whether the 2-Cys Prx might be suitable to dynamically image conformational changes via DXT. The rather high stability suggests that 2-Cys Prx represents a good candidate protein despite the slight damaging impact in all investigated biochemical properties of this protein. Functionality was maintained to a significant extent upon x-ray irradiation as shown by activity measurements and also on structural level, and also the effects observed without gold were only slightly more pronounced in its presence. The described impairment of 2-Cys Prx was small in comparison to other studies dealing with structural and functional damage to proteins mediated by ionising radiation in aqueous systems (Torreggiani et al, 2006; compare sections 3.1.4.1 and 3.1.4.3).

Furthermore the approach utilising gold colloids in the samples may also have the advantage to classify the damage arising within 2-Cys Prx solution. As described for both, solid and aqueous phase, there are two kinds of effects occurring as the result of irradiation, namely direct effects and indirect ones (Bonifacic and Asmus, 1976; Carugo and Djinovic Carugo, 2005). Whereas direct effects are caused by immediate energy deposition into the protein, the indirect effects deploy their detrimental impacts via the generation of radicals by ionising solvent molecules, which in case of an aqueous environment are water radicals (Southworth-Davies and Garman, 2007). The generation of water radicals furthermore leads to the damage expansion, as diffusion is much more pronounced in an aqueous system in comparison to solid phase system that is analysed in crystallographic approaches (Kempner, 2001). As the supplementation of the samples with gold colloids is primarily expected to enhance the water radical generation (Carter et al., 2007), gold colloids are expected to stimulate secondary effects. The slight increase of irradiation mediated effects visible on structural and functional level (Fig. 3.30, Fig. 3.31, Fig. 3.32), led to the hypothesis that these effects arose most likely due to secondary effects. As to finally clarify these assumptions there is the necessity to perform further experiments. In this context additional analyses were conducted utilising scavenging molecules that were known to reduce secondary effects in different applications and systems (Southworth-Davies and Garman, 2007; Cigarrán et al., 2004), as described in the following section in more detail.

### **3.1.4.5 Long term irradiation in presence of scavengers exhibited a decrease of irradiation induced damage especially on structural level**

As described before, effects of radiation-induced damage may occur due to different mechanisms, as there are direct and indirect influences. These are characterised according to the energy deposition either into the target structure itself (in this case the protein 2-Cys Prx) or into solvent molecules, resulting in solvent molecule ionisation and the formation of “water”-radicals (Le Maire et al., 1990; Carugo and Djinovic Carugo, 2005). Consequently the addition of molecules that are able to scavenge and quench these radicals reduces the damage development occurring as a consequence of indirect damaging effects (Cigarrán et al., 2004; O’Neill et al., 2002). To explore this interrelationship three different scavengers were applied with the aim to dissect direct and indirect irradiation effects upon ionising irradiation and to possibly reduce structural and functional impairment.

Dimethyl sulfoxide (DMSO) quenches hydroxyl radicals (OH<sup>•</sup>). To maximise the scavenging effect during x-ray irradiation the rather high concentration of 1 M DMSO was utilised to counteract indirect damaging effects by OH<sup>•</sup> based mostly on the radiolysis of water (Littlefield et al., 1989; Cigarrán et al., 2004). Furthermore glycerol was applied which is described to prevent from secondary effects during protein crystallographic analyses (O’Neill et al., 2002), using same concentrations as in case of DMSO. As a third scavenger, ascorbate was utilised as is known to exhibit protective effects during crystallographic approaches (Southworth-Davies and Garman, 2007; Murray and Garman, 2002). Also in aqueous solutions at ambient temperature ascorbate provides protection against superoxide anions, hydrogen peroxide and OH<sup>•</sup>. In addition ascorbate was shown to ‘repair’ damaged tyrosine residues (Wardman et al., 1989) and to reduce S-nitrosylated thiols. Since part of the structural alterations of 2-Cys Prx upon irradiation were hypothesised to be caused by damaging impacts on tyrosine residues (compare sections 3.1.4.2 and 3.1.4.4) the ascorbate was of particular interest within these analyses.

A standard irradiation experiment was performed without and with scavengers and the separation pattern of 2-Cys Prx was determined as a first analysis of damaging impact on structural properties of 2-Cys Prx. In contrast to the irradiation experiments without scavengers (Fig. 3.21 and Fig. 3.30), their addition caused neither a protein fragmentation nor a loss of monomeric 2-Cys Prx. This was seen for both, SDS-PAGE with subsequent silver staining (Fig. 3.34 A, B, and C) and Western blot analysis

(Fig. 3.34 D, E, and F). The faint signal of monomeric band in x-ray irradiated sample supplemented with glycerol (Fig. 3.34 E) was not due to a loss of monomeric form of 2-Cys Prx but due to a detection artefact, as the outline of the band was visible and a strong signal was detectable in Ponceau S staining directly after blotting (data not shown) as well as in silver stained PAA-gel.

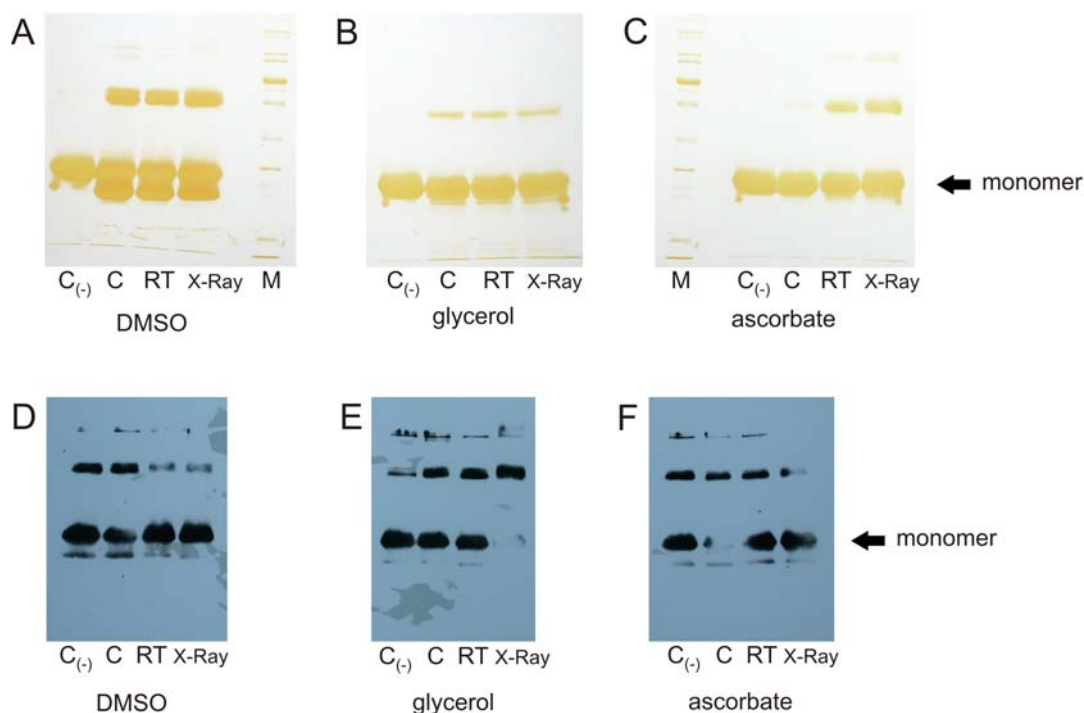


**Fig. 3.34: Analysis of aggregation pattern of 2-Cys Prx after long term irradiation in presence of different scavengers.** As scavengers 1 M DMSO, 1 M glycerol, and 0.5 M ascorbate were applied. (C<sub>(-)</sub>= control on ice without added scavenger, C = control on ice, RT = control at room temperature, X-Ray = x-ray exposed samples). Each experiment was performed twice with similar results. A, B, C) Reducing SDS-PAGE with subsequent silver staining. 10  $\mu$ g of protein were analysed. D, E, F) Western blot analysis with 2-Cys Prx specific antibody, with 2  $\mu$ g of protein loaded per lane.

Interestingly, the addition of scavengers altered the aggregation pattern in comparison to control without these substances (Fig. 3.34 A, B, and C). However, there were no visible differences in aggregation pattern upon scavenger supplementation between irradiated samples and both controls on ice and at room temperature, which could be observed in both silver stained PAA-gels and Western blots (Fig. 3.34). Obviously the scavengers provided radioprotective function on the structural level, as none of the observed impairments of long term irradiation (small fragment, trimer and tetramer formation; Fig. 3.21 and Fig. 3.30) could be detected in their presence. The only draw-

back in their application was the partial influence on separation behaviour of 2-Cys Prx which may have overlaid radiation-mediated effects to some extent. However, no increase in any of the higher mass aggregation forms could be detected. Therefore, it is concluded that all three applied scavengers protected 2-Cys Prx from irradiation-mediated damage of structural properties.

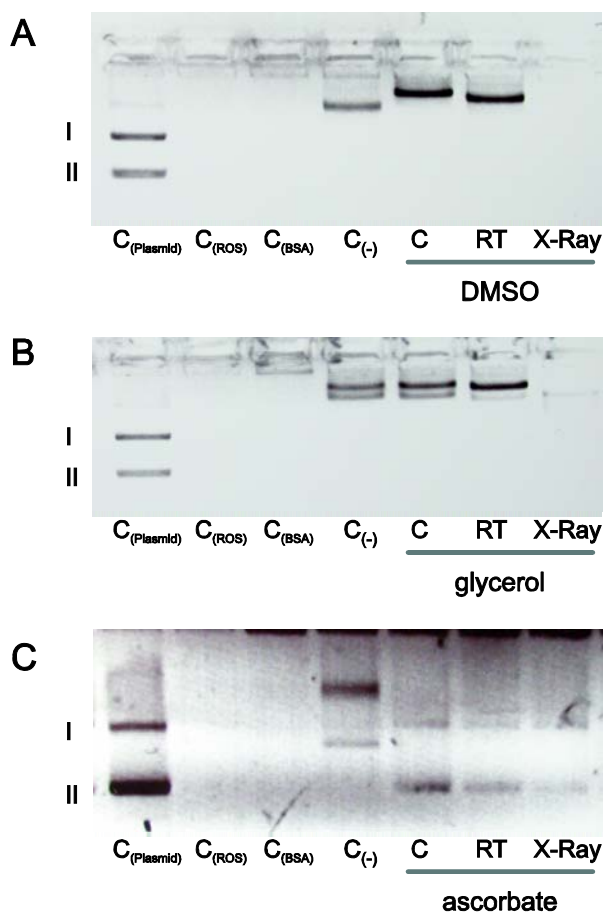


**Fig. 3.35: DNA cleavage assay of differentially treated 2-Cys Prx upon supplementation with different scavengers.** Each sample contained 2  $\mu\text{g}$  of plasmid DNA ( $C_{(\text{Plasmid})}$  = plasmid;  $C_{(\text{ROS})}$  = plasmid + MCO solution;  $C_{(\text{BSA})}$  = plasmid + MCO solution + BSA;  $C_{(\text{ROS})}$  and  $C_{(\text{BSA})}$  are corresponding to maximal cleavage). II = supercoiled plasmid DNA, I = open circular form. Experiments were performed two times with similar results. DNA protective function of 6  $\mu\text{g}$  2-Cys Prx in the metal-catalysed oxidation system was strongly impaired after 16 h of x-ray (X-Ray) treatment compared to the control conditions ( $C_{(-)}$ ) = control on ice without added scavenger, C = control on ice, RT = control at room temperature). A) Addition of 1 M DMSO as scavenger. B) Supplementation with 1 M glycerol. C) 0.5 M ascorbate was applied as scavenger.

The protective effect of scavengers was also investigated on the functional level of DNA protection in the cleavage assay. Although there was an uncontrolled shift of

plasmid DNA similar to the samples containing Trx A and TR (Fig. 3.29), differences between x-ray treatment in the presence of DMSO and glycerol and the controls on ice and at room temperature were apparent (Fig. 3.35). Obviously, there was no re-establishment of DNA protective function upon addition of 1 M DMSO and 1 M glycerol (Fig. 3.35 A and B) as severe damage of plasmid DNA occurred despite their presence. Only in case of supplementation with 0.5 M ascorbate, the DNA protective function was re-established (Fig. 3.35 C). However, ascorbate could also be shown to provide for reduction of 1-Cys Prx (Monteiro et al., 2007). Additionally the impact of regenerating system for the re-establishment of DNA protective function was already shown for the Trx system (Fig. 3.29 B). Consequently it cannot be ruled out, that the observed re-establishment of DNA-protective function might be due to secondary effects which may interfere with the assignment of the results to function of ascorbate as scavenger.

It can be hypothesised that the addition of scavengers led at least to some protection of 2-Cys Prx from irradiation-induced damage on the structural level since the migration behaviour upon long term irradiation was indistinguishable from the controls. Interestingly in context of mixed function oxidation assay with DNA the protective activity could not be preserved. Additionally, these results allow for the classification of the damaging mechanism, as the already described x-ray inflicted damage can be subdivided into direct and indirect mechanisms (Bonifacic and Asmus, 1976; Carugo and Djinovic Carugo, 2005). The latter can be counteracted by the supplementation with substances that have the ability to quench the responsible water radicals (Cigarrán et al., 2004; O'Neill et al., 2002). The supplementation with DMSO, glycerol, or ascorbate suppressed the structural impairments caused by x-ray treatment as visualised by SDS-PAGE. These findings allow to assign the effects to the category of secondary damages. This assignment is in line with the results from gold-colloid supplementation (compare section 3.1.4.4). The addition of gold-colloids supporting the formation of water-radicals caused an enhancement of all those structural impairments that were prevented during addition with scavengers, namely protein fragmentation, loss of monomeric 2-Cys Prx and formation of protein aggregates (Fig. 3.30). Consequently, indirect damaging effects by water-radicals seem to involve tyrosine residues, as these were hypothesised to be responsible for structural alterations above based on the oligomerisation effects (compare section 3.1.4.2). As the functional impairments could not be rescued by the utilised scavengers, they can be tentatively assigned to direct

impacts of irradiation. These biochemical features and the reaction mechanism during detoxification are linked to redox state of cysteine residues (Dietz, 2003 a; Jang et al., 2006; compare section 3.1.4.3); therefore this reactive amino acid seems to be prone to direct effects of the x-ray treatment.

In context of dynamical imaging of conformational changes via DXT this characterisation of long term irradiation in presence of scavenging molecules proved again the suitability of 2-Cys Prx for these kinds of investigations. As the irradiation effects were already shown to be comparably low, the additional supplementation with scavengers was even able to minimise the observed impairments.

#### **3.1.4.6 Conclusion on damage development during x-ray treatment of 2-Cys Prx**

This section summarises the radiation-mediated effects on 2-Cys Prx A as addressed in the previously described experiments. (i) A dose dependent damage development was observed. The overall radiation dose of 540 Gy exhibited no structural or functional impairments, whereas long term treatment with 2,900 Gy revealed different effects on both levels. (ii) Random fragmentation and generation of higher molecular mass aggregates on expense of monomeric form of 2-Cys Prx characterise structural changes. The latter were tentatively assigned to an involvement of tyrosine residues. (iii) On functional level, the decrease in catalytic activity as well as the loss of DNA protective capacity appears to result from an irradiation effect on the cysteinyl residues. Consequently it has to be noted, that irradiation of 2-Cys Prx revealed two distinct sites of damage. (iv) The classification of the observed effects was attempted by employing different scavengers. DMSO, glycerol, and ascorbate reduced the damaging effects on 2-Cys Prx structure. In contrast functional features were still impaired when irradiated in the presence of DMSO and glycerol. Interestingly, ascorbate mediated protection in the DNA cleavage assay. Therefore, fragmentation, loss of monomeric form of 2-Cys Prx as well as the generation of higher molecular mass aggregates could be assigned to indirect damage which occurred as consequence of water radical release during x-ray irradiation. It can be hypothesised that tyrosine residues are major targets of these reactive species.

### **3.1.5 Establishment of 2-Cys Prx as a model protein for dynamical x-ray imaging: concluding remarks**

Dynamical x-ray imaging has been suggested to be a promising method to detect conformational changes in proteins and is therefore very important when it comes to the understanding of functional dependencies related to small dynamical structural changes of proteins. Different prerequisites must be fulfilled if a protein shall serve as a model molecule for this method, i.e. availability of recombinant protein, construction of bifunctional attachment sites for immobilisation on the solid support and fixation of the x-ray diffracting nanocrystal and a sufficient robustness against x-ray irradiation. In this context it could be shown, that there are different locations of exposed and non-conserved amino acids in the 2-Cys Prx protein that allow for an exchange towards a cysteine residue to establish a binding site for goldcrystals without loss of activity. Even the generation of a 2-Cys Prx variant with three exchanged amino acids did not lead to an impairment of function as shown by means of DNA cleavage assay. The expressed and purified protein variants were furthermore shown to allow for a stable immobilisation on a Ni-NTA surface due to the N-terminally fused His-tag. According to the nature of 2-Cys Prx surface it was difficult to achieve a specific labelling of cysteinyl residues. Nevertheless, the specificity of binding events could be considerably increased via the addition of additives which resulted in the reduction of unspecific hydrophobic interactions. As a last and the probably most important aspect, irradiation impacts on different biochemical properties of 2-Cys Prx were characterised. In this context, this protein exhibited a remarkably high stability upon x-ray treatment and thereby underlined its suitability as candidate for the application in dynamical imaging via DXT. Additionally, it could be shown that the supplementation of different scavengers offers the possibility to further minimise the radiation-mediated damage.

It finally can be concluded that the subject of the present work, namely the establishment of 2-Cys Prx as a model-protein for time-resolved x-ray imaging could be completed, since each step defined as prerequisite was optimised successfully. Of course it will be of interest to see the visualisation of redox dependent conformational changes via DXT realised as the subject of a following project.

### 3.2. Biochemical characterisation of cytosolic PrxII B and PrxII C and their differentiation

*A. thaliana* contains three isoforms of type II Prx localised in the cytosol, namely PrxII B, PrxII C, and PrxII D (Dietz, 2003 a). These proteins reveal extremely high degrees of identity ranging from 93 % between PrxII B and PrxII D to 98 % between PrxII C and PrxII D. Identities are much lower to type II Prx targeted to other compartments (Fig. 3.36). As a differential regulation was already observed on transcript level between PrxII B versus PrxII C and PrxII D upon a diversity of treatments (Horling et al., 2002 and 2003), a comparative analysis of catalytic properties of PrxII B and PrxII C was performed to differentiate these proteins on the functional level.

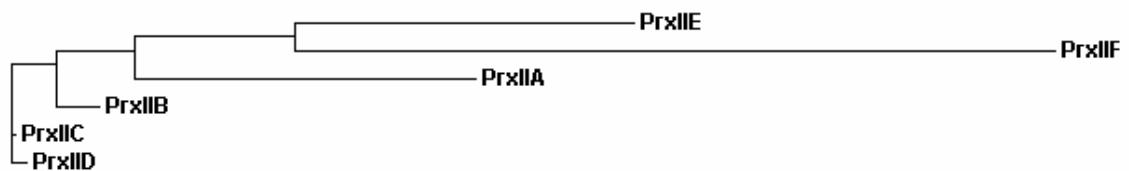


**Fig. 3.36: Phylogenetic tree of different type II Prx from *A. thaliana*.** The tree was generated with the programme ClustalW. The length of the branches correlates with the number of amino acid exchanges (<http://www.ebi.ac.uk/Tools/clustalw2/index.html>).

#### 3.2.1. Peroxide detoxification by PrxII B and PrxII C

As oxidative stress exerts detrimental effects on various macromolecules of the cell (Chang et al., 2004), it is important for each cell to express enzymes to detoxify the different ROS types. One particular assay to investigate the ROS detoxification capacity of an antioxidant protein of interest is the DNA cleavage assay. Different amounts of heterologously expressed PrxII B and PrxII C protein were incubated with plasmid DNA in a ROS generating environment (MCO-solution). Both Prx exhibited ROS detoxification capacity, and even a decrease of protein amount to 1  $\mu$ g did not fully abolish the function as DNA protectant (Fig. 3.37), since there was a slight impairment of DNA protective capacity with reduction of protein amount to 20 %. This is deduced from the increased ratio of supercoiled to coiled DNA form which indicates nicking of the supercoiled plasmid.

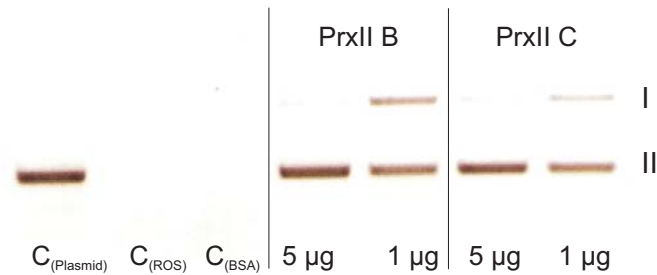


**Fig. 3.37: DNA protective function of PrxII B and PrxII C analysed via DNA cleavage assay.** DNA protection in a metal-catalysed oxidation system (MCO).  $C_{(\text{Plasmid})}$  = plasmid;  $C_{(\text{ROS})}$  = plasmid + MCO solution;  $C_{(\text{BSA})}$  = plasmid + MCO solution + BSA, revealing maximal cleavage; I = supercoiled plasmid DNA, II = open circular form. The experiment was performed three times with similar results.

In comparison the ROS detoxification capacity of the two cytosolic type II Prx considerably exceeded that of 2-Cys Prx, as full protection was achieved by PrxII B and PrxII C whereas 2-Cys Prx of *A. thaliana* could not completely prevent ROS-mediated nicking of plasmid DNA in absence of efficient regenerators (Laxa et al., 2007; compare also findings within this work e. g. Fig. 3.9). The ability of PrxII B to prevent plasmid DNA from ROS-mediated cleavage was also reported by Bréhélin and co-workers (2003). Also in comparison with chloroplastidic PrxII E the cytosolic isoforms revealed a considerably higher detoxification capacity (Bréhélin et al., 2003). This strong detoxification capacity indicated a very high peroxidase activity of both investigated cytosolic type II Prx isoforms.

### 3.2.2. Determination of crucial catalytic parameters of PrxII B and PrxII C – maximum velocity ( $v_{\text{max}}$ ) and the Michaelis-Menten constant ( $K_M$ )

The basic biochemical characteristics of enzyme activity are the maximal velocity  $v_{\text{max}}$  reached at high substrate concentrations and the Michaelis-Menten constant ( $K_M$ ) defined as the substrate concentration enabling half-maximal enzyme activity.  $\text{H}_2\text{O}_2$  detoxification activity was measured in the concentrations range between 20  $\mu\text{M}$  and 700  $\mu\text{M}$ . Rising  $\text{H}_2\text{O}_2$  concentrations resulted in a hyperbolic increase of enzyme activity in both PrxII B (Fig. 3.38 A) and PrxII C (Fig. 3.38 B). In general, PrxII C revealed higher activities than PrxII B. This was visible on the one hand by a faster increase of  $\text{H}_2\text{O}_2$  conversion rate with lower peroxide concentrations and on the other hand by the higher turnover throughout all tested concentrations.

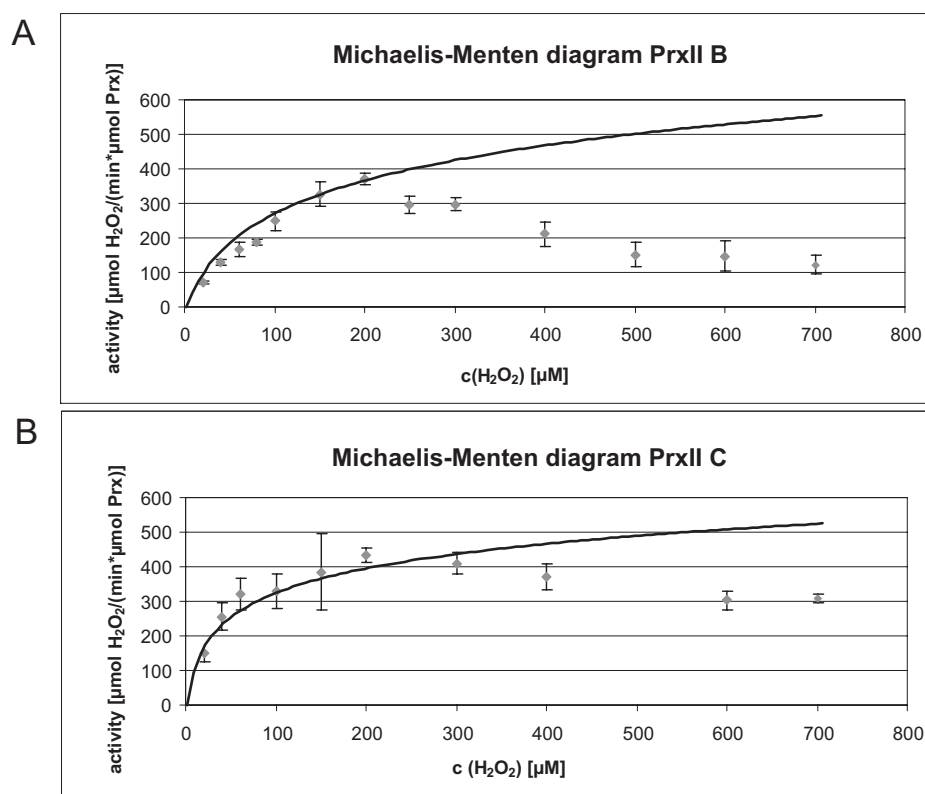


**Fig. 3.38: Michaelis-Menten diagrams of cytosolic PrxII B and PrxII C.** Catalytic activity on the y-axis is depicted in dependence of  $\text{H}_2\text{O}_2$  concentration in a range of 20  $\mu\text{M}$  to 700  $\mu\text{M}$  on the x-axis. Activities are given as mean value with standard deviation ( $n \geq 6$ ). Regression curves mimic tendencies for uninhibited reaction estimated from activities for 20  $\mu\text{M}$  to 200  $\mu\text{M}$  substrate concentration. A) PrxII B, B) PrxII C.

Interestingly, the increase of substrate concentration above 200  $\mu\text{M}$   $\text{H}_2\text{O}_2$  caused a decrease of reaction rate in both series of measurements (Fig. 3.38). The loss of catalytic activity was considerably more pronounced for PrxII B with only 33 % ( $122 \pm 26 \mu\text{mol H}_2\text{O}_2/(\text{min} \cdot \mu\text{mol Prx})$ ) residual activity at 700  $\mu\text{M}$   $\text{H}_2\text{O}_2$  in comparison to the highest activity measured at 200  $\mu\text{M}$   $\text{H}_2\text{O}_2$  ( $371 \pm 17 \mu\text{mol H}_2\text{O}_2/(\text{min} \cdot \mu\text{mol Prx})$ ). In contrast, peroxide turnover of PrxII C still represented 71.3 % ( $309 \pm 12 \mu\text{mol H}_2\text{O}_2/(\text{min} \cdot \mu\text{mol Prx})$ ) compared to  $434 \pm 22 \mu\text{mol H}_2\text{O}_2/(\text{min} \cdot \mu\text{mol Prx})$  measured with a substrate concentration of 200  $\mu\text{M}$  (Fig. 3.38 B). The underlying mechanism for this inhibition of peroxidase activity may be found in overoxidation of both proteins, as this is a common observation for Prx under highly oxidising conditions (Jacob et al., 2004; Chevallet et al., 2003; Lehtonen et al., 2005; Wagner et al., 2002). Although this modification is mostly observed for 2-Cys Prx (Jara et al., 2007; Jönsson and Lowther, 2007; Jang et al., 2006), it was also described for the atypical 2-Cys Prx (synonym for type II Prx) Ahp 1 from the yeast *Saccharomyces cerevisiae* (Trivelli et al., 2003). On functional level, the formation of sulfinic acid derivatives leads to a decrease

of catalytic activity (Georgiou and Masip, 2003; Trivelli et al., 2003). This inactivation is discussed to represent a regulatory mechanism rather than a limitation of catalytic cycle, as these proteins may act as ‘floodgates’ modulating cellular responses during elevated endogenous production of  $H_2O_2$  (Wood et al., 2003 a). The subsequent inactivation of catalytic activity allows for  $H_2O_2$  accumulation sufficient to modulate cell signalling (Georgiou and Masip, 2003). Likewise, both cytosolic type II Prx may not only be involved in antioxidant defence but may also participate in signalling pathways by sensing and modulation of  $H_2O_2$ -dependent cellular responses. The observed differences between PrxII B and C in the extent of inactivation in combination with differential expression of both genes may provide a mechanistic framework for the cell to fine-tune  $H_2O_2$  signal transduction by differential expression of these enzymes.

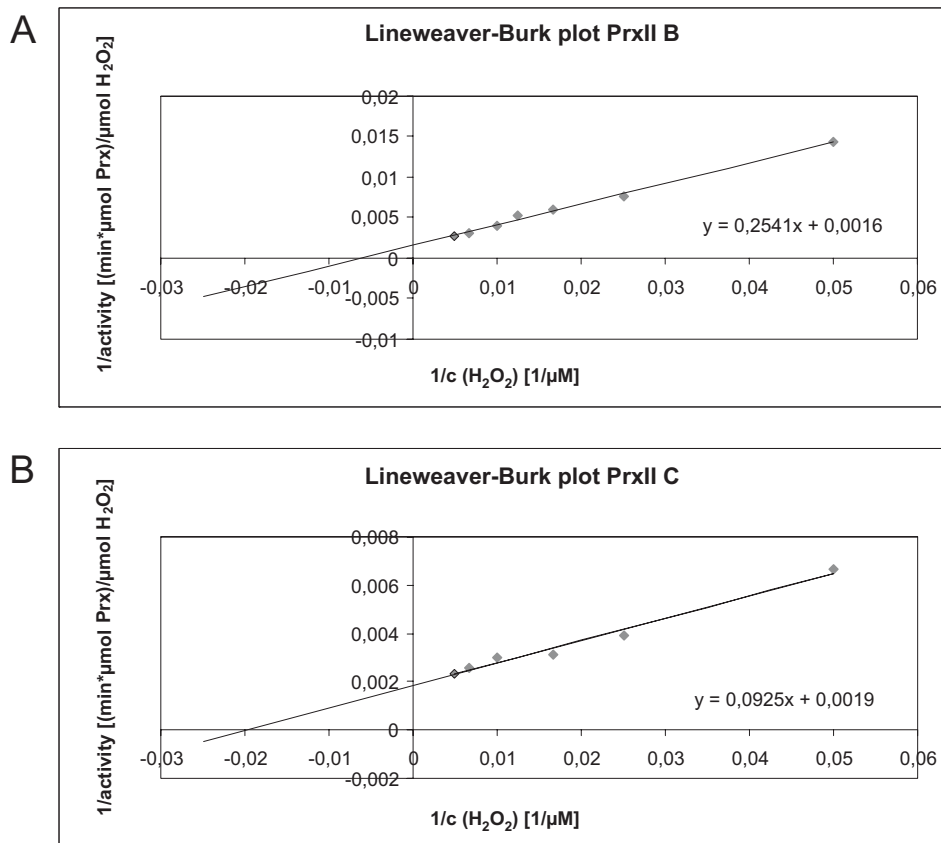


**Fig. 3.39: Lineweaver-Burk plots of cytosolic PrxII B and PrxII C activity data.**

The reciprocal Prx activities on the y-axis are plotted against the reciprocal  $H_2O_2$  concentration on the x-axis. The data are the same as those depicted in Fig. 3.38.  $v_{\max}$  and  $K_M$  are estimated from the reciprocals of the y- and x- intercept, respectively. For both series of measurements values between 20  $\mu\text{M}$  and 200  $\mu\text{M}$  are represented with  $n \geq 6$ . A) PrxII B, B) PrxII C.

Additional to the  $V_0$ -versus-[S]-diagram (Fig. 3.38), the obtained data were visualised by means of Lineweaver-Burk plots providing an easier method of estimating  $v_{\max}$  and

$K_M$ . In this double reciprocal plot  $v_{max}$  and  $K_M$  are depicted by the y- and x-intercept, respectively. For PrxII B  $v_{max}$  was calculated with  $625 \mu\text{mol H}_2\text{O}_2/(\text{min} \cdot \mu\text{mol Prx})$  and the  $K_M$  amounted to  $159 \mu\text{M H}_2\text{O}_2$ , whereas in case of PrxII C  $v_{max}$  and  $K_M$  were estimated to be  $525 \mu\text{mol H}_2\text{O}_2/(\text{min} \cdot \mu\text{mol Prx})$  and  $49 \mu\text{M H}_2\text{O}_2$  as revealed by Lineweaver-Burk plot (Fig. 3.39).

As the linear regression analysis of the Lineweaver-Burk plot data unevenly weights the different data points with emphasis on the lower concentrations,  $v_{max}$  and  $K_M$  were additionally estimated by means of Eadie-Hofstee diagrams. In this graphical representation of enzyme kinetics, the reaction velocity is plotted as a function of the ratio calculated from velocity and substrate concentration. Consequently, it is more robust against error-prone data. In this plot  $v_{max}$  and  $K_M$  are represented by the y-intercept and the negative slope of the graph, respectively (Fig. 3.40).

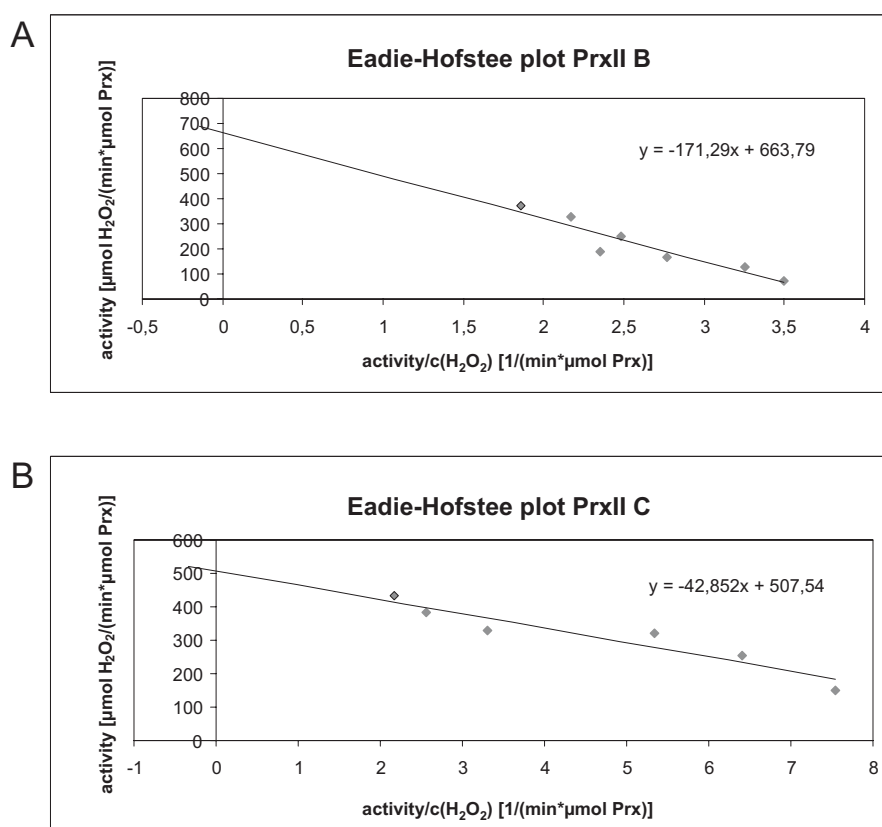


**Fig. 3.40: Eadie-Hofstee plots of cytosolic PrxII B and PrxII C.** This type of plot depicts the enzymatic activities as a function of the ratio of activity and substrate concentration.  $V_{max}$  and  $K_M$  is derived from the y-intercept and the negative slope of the graph, respectively. For both series of measurements values between  $20 \mu\text{M}$  and  $200 \mu\text{M}$  are represented with  $n \geq 6$ . A) PrxII B, B) PrxII C.

As seen from Fig. 3.40, PrxII B and PrxII C revealed similar  $v_{max}$  and  $K_M$  values with  $664 \mu\text{mol H}_2\text{O}_2/(\text{min} \cdot \mu\text{mol Prx})$  and  $171 \mu\text{M H}_2\text{O}_2$ , respectively, for the former and

508  $\mu\text{mol H}_2\text{O}_2/(\text{min} \cdot \mu\text{mol Prx})$  and 43  $\mu\text{M H}_2\text{O}_2$  for the latter. It should be noted that both Prx exhibited maximal velocities that are considerably higher than those reported by Horling et al. (2003) with  $150 \pm 12 \mu\text{mol H}_2\text{O}_2/(\text{min} \cdot \mu\text{mol Prx})$  in case of PrxII B and  $156 \pm 5 \mu\text{mol H}_2\text{O}_2/(\text{min} \cdot \mu\text{mol Prx})$  for PrxII C. The estimated  $v_{\text{max}}$ -values of the present study are three to more than four times higher. As a consequence of inhibition at high  $\text{H}_2\text{O}_2$  concentration of the estimated  $v_{\text{max}}$ -values were not reached. The highest activities measured at 200  $\mu\text{M H}_2\text{O}_2$  were still two times (PrxII B,  $371 \pm 17 \mu\text{mol H}_2\text{O}_2/(\text{min} \cdot \mu\text{mol Prx})$ ) or almost three times higher (PrxII C,  $434 \pm 22 \mu\text{mol H}_2\text{O}_2/(\text{min} \cdot \mu\text{mol Prx})$ ). With the just described velocities PrxII B and PrxII C reveal by far the highest activities among *A. thaliana* Prx (Horling et al., 2002 and 2003; Finkemeier et al., 2005; Lamkemeyer et al., 2006). Even in comparison with different Prx from other plant species, the measured activities and therefore the antioxidative potential of both cytosolic type II Prx are remarkable, as they are at least twice (Rouhier et al., 2004) or even around ten-fold higher (König et al., 2002 and 2003; Dietz et al., 2006; Kiba et al., 2005).

The estimated  $K_M$  values of PrxII B and PrxII C differ considerably, as the estimated  $K_M$  for PrxII B is with 159  $\mu\text{M H}_2\text{O}_2$  about three times as high as the one predicted for PrxII C (49  $\mu\text{M H}_2\text{O}_2$ ; both values according to Lineweaver-Burk plot, Fig. 3.39). This revealed a clearly stronger affinity of PrxII C to this substrate than of PrxII B, again showing a difference in biochemical properties of these isoforms. For PrxII E a considerably lower  $K_M$  of 21.7  $\mu\text{M H}_2\text{O}_2$  was measured in presence of Grx system as regeneration system (Gama et al., 2008). In comparison, catalase (CAT) as one of the main  $\text{H}_2\text{O}_2$  detoxifying enzymes exhibits much higher  $K_M$ , for instance in *Beta vulgaris* a  $K_M$  of 50 mM  $\text{H}_2\text{O}_2$  was described (Dincer and Aydemir, 2001), which is about  $3 \cdot 10^3$  times and  $10^4$  times higher than the one measured for PrxII B or PrxII C, respectively. Cytosolic ascorbate peroxidases (APX) from different organisms which play an important role in  $\text{H}_2\text{O}_2$  metabolism, revealed  $K_M$  values of 20  $\mu\text{M H}_2\text{O}_2$  (*Glycine max*, Dalton et al., 1996), 24  $\mu\text{M H}_2\text{O}_2$  (*Brassica rapa*, Ishikawa et al., 1996), and 35  $\mu\text{M H}_2\text{O}_2$  (*Zea mays*, Koshiba, 1993). Two isoforms from rice seedlings, namely APX1 and APX2, exhibited  $K_M$  values of 33  $\mu\text{M H}_2\text{O}_2$  and 76  $\mu\text{M}$ , respectively (Sharma and Dubey, 2004). For a glyoxisomal APX and a mitochondrial one the  $K_M$ -values were determined with 60  $\mu\text{M H}_2\text{O}_2$  (*Ricinus communis*, Karyotou and Donaldson, 2005) and 80  $\mu\text{M H}_2\text{O}_2$  (*Solanum tuberosum*, De Leonardis et al., 2000), respectively. Thus, the  $K_M$ -values of PrxII B and PrxII C are up to two-fold higher than that of mitochondrial

APX (De Leonardis et al., 2000). This may suggest a preferred function in decomposing ROS during oxidative stress and not at sites of constant generation of ROS.

Interestingly despite their high amino acid sequence similarity, PrxII B and PrxII C revealed differences of their biochemical properties, namely  $v_{\max}$  and especially  $K_M$ . Also the inhibition of activity, which occurred most likely due to overoxidation of the proteins, was different for both Prx.

### 3.2.3 Substrate specificity of PrxII B and PrxII C

Prx reduce a wide variety of peroxide substrates. PrxII C is known to reveal specificity towards smaller peroxides like  $H_2O_2$  and tertiary butylhydroperoxide (t-BOOH) (Jacob, 2005). With higher structural complexity of the peroxide substrates the activity decreases e.g. for cumene hydroperoxide (COOH) and the role in detoxification of lipid peroxides might be negligible *in vivo* (Jacob, 2005). Within this work a comparative analysis of substrate specificity of both type II Prx was performed. Thereby, each substrate was measured with two different concentrations to investigate the inhibitory effect observed for  $H_2O_2$  also for the other peroxides.

PrxII C exhibited the already described specificity towards the smaller peroxides  $H_2O_2$  ( $330 \pm 49 \mu\text{mol } H_2O_2 / (\text{min} \cdot \mu\text{mol Prx})$  at a substrate concentration of  $100 \mu\text{M}$ ) and t-BOOH ( $320 \pm 29 \mu\text{mol t-BOOH} / (\text{min} \cdot \mu\text{mol Prx})$  at  $100 \mu\text{M t-BOOH}$ ) (Fig. 3.41 B). For PrxII C a significant difference between these reaction velocities could not be detected at  $100 \mu\text{M}$  concentration. The turnover of COOH was considerably lower ( $48 \pm 18 \mu\text{mol COOH} / (\text{min} \cdot \mu\text{mol Prx})$  at  $100 \mu\text{M COOH}$ ) (Fig. 3.41 B). Interestingly, the inhibition of peroxidase activity that was observed for  $H_2O_2$  (compare Fig. 3.38) was more pronounced for t-BOOH with just 48.8 % remaining activity at  $400 \mu\text{M}$  substrate concentration in comparison to  $100 \mu\text{M}$ . In contrast, in the presence of  $400 \mu\text{M COOH}$  the residual activity was about 84 %, however on the generally low activity level. Also PrxII B exhibited a strong preference for detoxification of smaller peroxides with  $248 \pm 27 \mu\text{mol } H_2O_2 / (\text{min} \cdot \mu\text{mol Prx})$  at  $100 \mu\text{M } H_2O_2$  and  $165 \pm 69 \mu\text{mol t-BOOH} / (\text{min} \cdot \mu\text{mol Prx})$  at  $100 \mu\text{M t-BOOH}$  (Fig. 3.41 A). Thus these two peroxide substrates revealed a distinct substrate specificity of the two type II Prx. PrxIIB favours the small  $H_2O_2$  whereas detoxification mediated by PrxII C was nearly at the same level for both,  $H_2O_2$  and t-BOOH (Fig. 3.41 B). PrxII B failed to detoxify COOH, while PrxII C retained a significant detoxification activity towards COOH (Fig. 3.41 A).

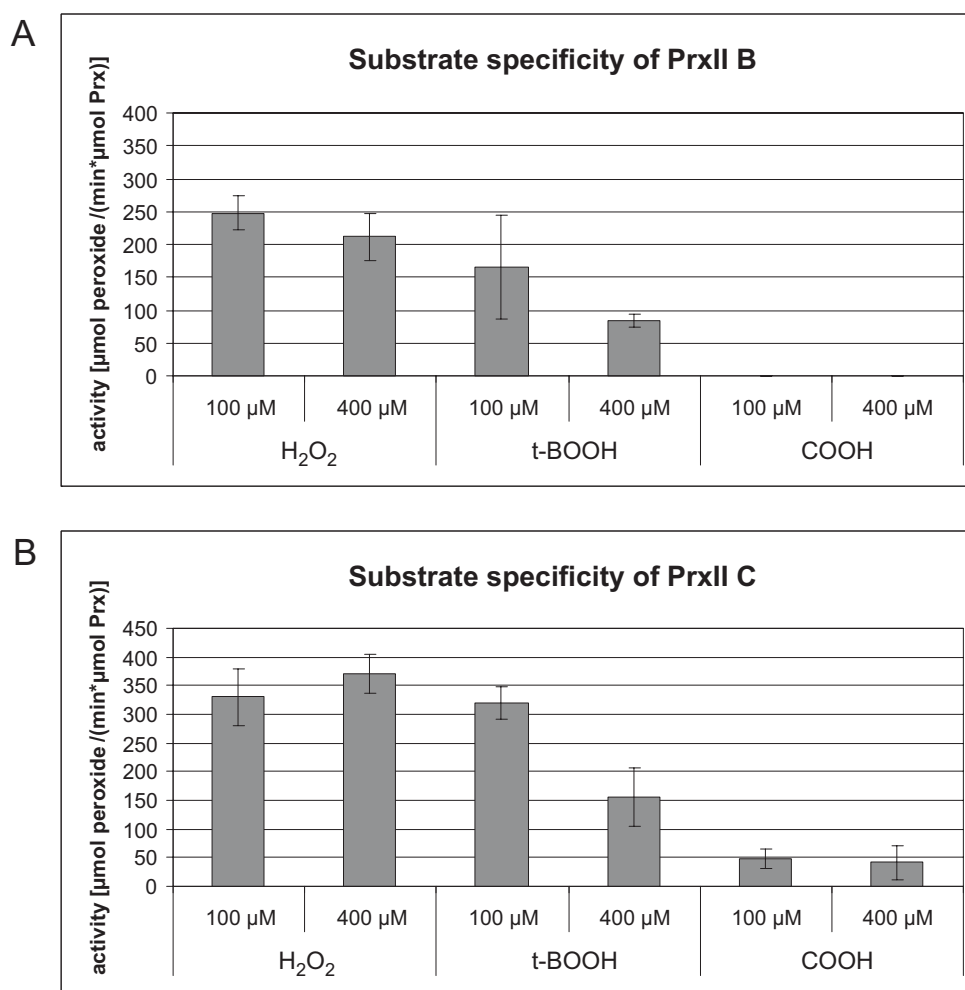


**Fig. 3.41: Determination of substrate specificity of cytosolic PrxII B and PrxII C.** Catalytic activity is depicted in dependence of different substrates ( $\text{H}_2\text{O}_2$  = hydrogen peroxide; t-BOOH = tertiary butylhydroperoxide; COOH = cumene hydroperoxide) for two concentrations each, i.e. 100  $\mu\text{M}$  and 400  $\mu\text{M}$ . Each data point is the mean value of at least  $n = 5$  measurements. A) PrxII B, B) PrxII C.

A reason for these functional differences may be found in structural arrangements of these proteins as visible from amino acid alignment (Fig. 3.42 A) and modelled 3D-structure of PrxII C (Fig. 3.24 B). Of special interest are those amino acids being localised in close proximity to cysteines as they could influence interaction behaviour during the catalytic cycle.

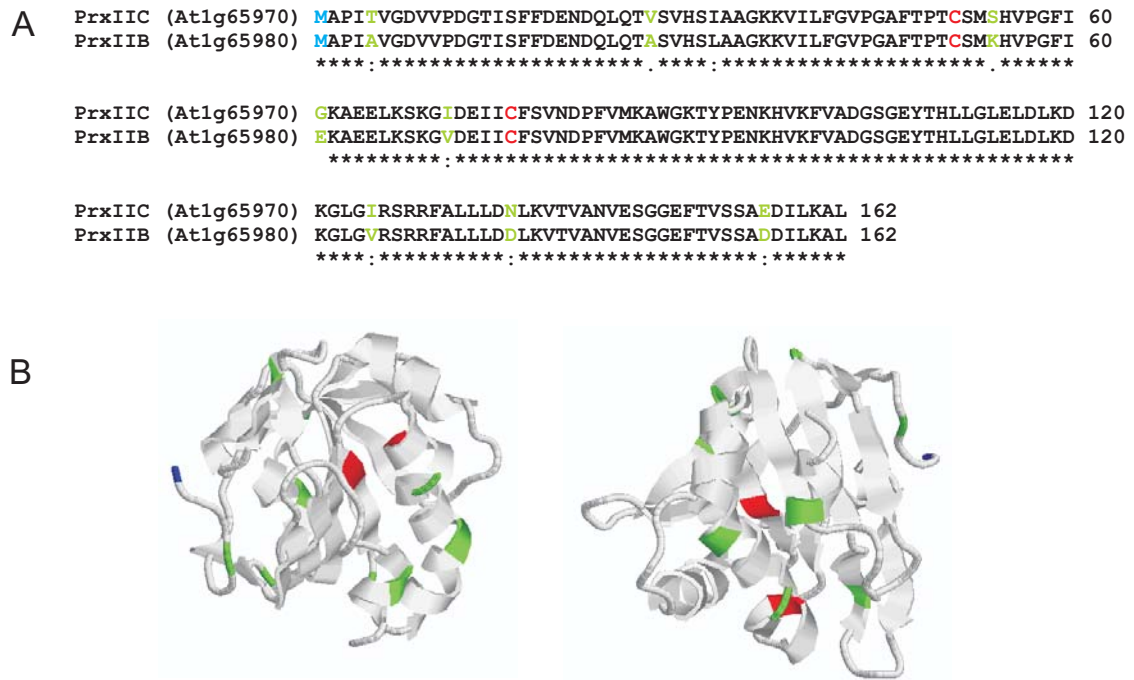


**Fig. 3.42: Structural comparison of PrxII B and PrxII C.** A) Alignment of PrxII B and C amino acid sequences with cysteines highlighted in red. Differing amino acids are coloured in green. The alignment was generated with the programme ClustalW (<http://www.ebi.ac.uk/Tools/clustalw2/index.html>). B) In this ribbon structure presentation of PrxII C (shown in two different orientations) cysteines are highlighted in red and positions of amino acids differing from PrxII B are coloured green. The N-terminus is depicted in blue. The model was generated using RasMol software (basis: 1tp9B, sequence identity: 79 %).

Additionally, the investigation of peroxide turnover in dependence of two different concentrations again showed the inactivation of peroxidase function with  $H_2O_2$ . But also increased concentrations of t-BOOH led to the inhibition of this enzyme, resulting in residual activity of 51 % which equalled the decrease observed for PrxII C (48.8 %). It has to be taken into consideration that the loss of activity may be even more pronounced, as 100  $\mu$ M is unlikely to saturate the enzyme, this may be achieved far above 100  $\mu$ M. This may also account for the fact that  $H_2O_2$  detoxification velocity did not decrease with increasing concentrations.

In comparison to other Prx from *A. thaliana* the cytosolic isoforms exhibit a more restricted substrate spectrum. Mitochondrial PrxII F for instance showed a broad substrate range that besides the smaller peroxides also included COOH as well as linoleic acid hydroperoxide and phosphatidylcholine dilinoleoyl hydroperoxide. However, PrxII F also preferred  $H_2O_2$  (Finkemeier et al., 2005). The reported reaction rates for  $H_2O_2$  and t-BOOH are considerably lower than the ones observed for PrxII B

and PrxII C. Similar to PrxII F the chloroplastidic 2-Cys Prx also revealed a very broad range of peroxide turnover (König et al., 2003). Other chloroplastidic Prx like Prx Q hardly convert linoleic acid hydroperoxide and phosphatidylcholine dilinoleoyl hydroperoxide, but prefer smaller peroxides (Lamkemeyer et al., 2006). In contrast to the just described versatility of converted substrates, a very distinct preference in turnover was also observed for PrxII E. This chloroplastidic Prx was also found to detoxify merely  $\text{H}_2\text{O}_2$  and t-BOOH but did not reduce COOH (Gama et al., 2008) resembling the spectrum of cytosolic type II Prx and especially PrxII B. Due to their very distinct substrate spectra cytosolic type II Prx function *in vivo* may tentatively be assigned to the reduction of  $\text{H}_2\text{O}_2$ , whereas a role in lipid peroxide turnover may be negligible or excluded.

#### 3.2.4. Search for *in vivo* regenerators of PrxII B and PrxII C

Although different biochemical parameters of PrxII B and PrxII C were determined using DTT as artificial electron donor, it is of special interest to identify possible *in vivo* regenerators for these proteins. For type II Prx both, Grx and Trx were described to provide regeneration during the catalytic cycle, as for instance shown for mitochondrial PrxII F (Finkemeier et al., 2005). Furthermore, a homologous cytosolic type II Prx from *Populus tremula* was reduced by both systems (Rouhier et al., 2001). Therefore, these systems were investigated in respect to their possible regenerating function for PrxII B and C.

PrxII B and C could be regenerated by Trx/TR and Grx/GSH/GR system, although the addition of latter achieved a considerably higher activity (Fig. 3.43). Interestingly, every tested condition in the present work revealed a higher activity of PrxII C compared to PrxII B (e. g. Fig. 3.38), which was not seen with the Trx/TR system (Fig. 3.43). Although activities were quite low with  $3.2 \pm 0.3 \mu\text{mol H}_2\text{O}_2 / (\text{min} * \mu\text{mol Prx})$  for PrxII B and  $1.9 \pm 0.6 \mu\text{mol H}_2\text{O}_2 / (\text{min} * \mu\text{mol Prx})$  for PrxII C, a significant difference to the Prx-free control sample was calculated according to Student's T-Test ( $p < 0.01$ ). In contrast, Grx-dependent activities were higher for PrxII C than for PrxII B. This was the case for Grx CxxC4 (At5g20500), a cytosolic Grx and homologue of a poplar Grx that was shown to regenerate poplar type II Prx (Rouhier et al., 2001) which itself is a homologue of the At-PrxII B and C. This Grx could already be shown to regenerate PrxII C (Jacob, 2005) and the obtained reaction rates were in the same range as measured within this work ( $28.0 \pm 4.8 \mu\text{mol H}_2\text{O}_2 / (\text{min} * \mu\text{mol Prx})$  at  $100 \mu\text{M H}_2\text{O}_2$ ).

Also PrxII B could be reduced by this Grx, although with merely one third compared to PrxII C (Fig. 3.43). Grx CxxC5, Grx CxxC10, and Grx CxxS12 did not support any peroxidase activity of PrxII B and C (Fig. 3.43), nor did GR and/or GSH (data not shown). Among the tested Grxs was another cytosolic member of the protein family, namely Grx CxxC10 (At5g11930). In contrast, Grx CxxC5 (At4g28730) and Grx CxxS12 (At2g20270) are targeted to the chloroplast (Ströher, 2008). Despite their localisation, they were tested as Grx CxxC5 displays unique catalytic features among the chloroplastidic Grx (Ströher, 2008) whereas Grx CxxS12 was employed due to its characteristic as monothiol Grx and its regeneration capacity for chloroplastidic PrxII E (Gama et al., 2008).

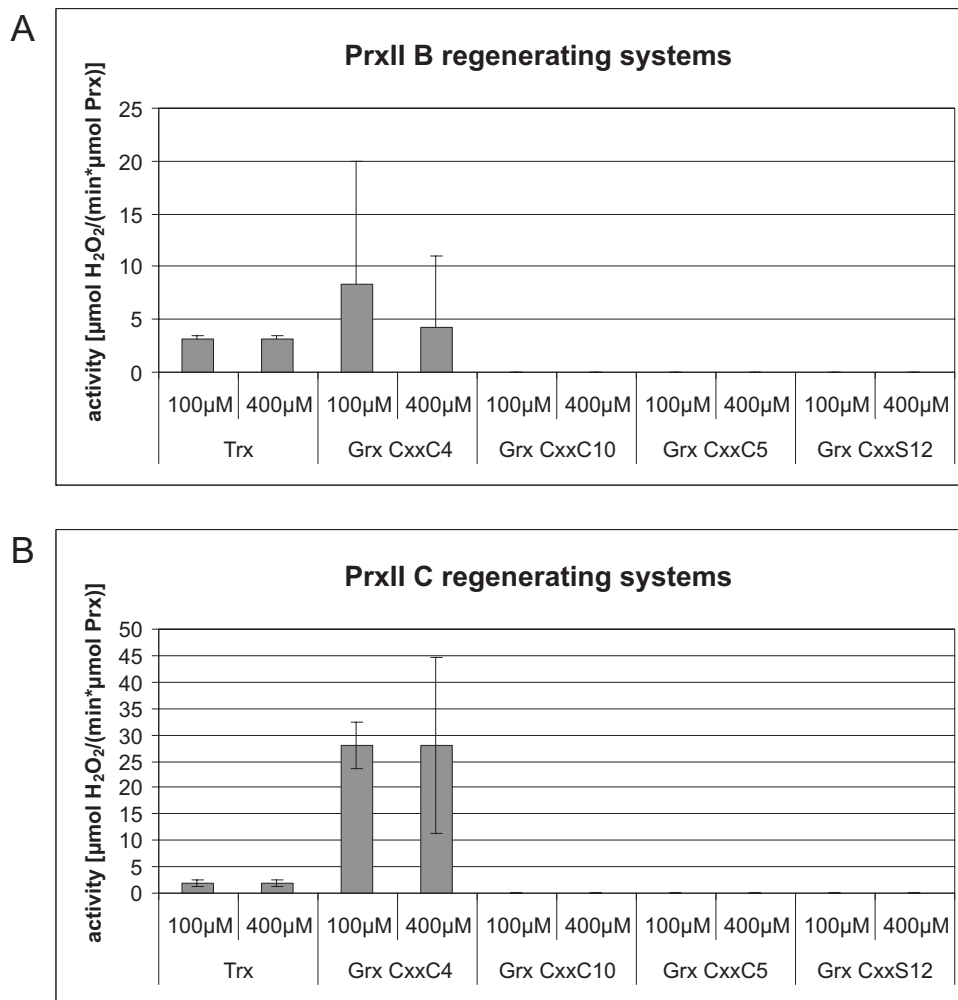


**Fig. 3.43: Investigation of different regenerating systems for reduction of PrxII B and PrxII C during  $\text{H}_2\text{O}_2$  detoxification.** Catalytic activity is depicted in dependence of different regenerating systems. Besides the regeneration by *E. coli* Trx/TR system, also different Grxs were added (in combination with GSH and 6  $\mu\text{g/ml}$  yeast GR), namely Grx CxxC4, Grx CxxC5, Grx CxxC10, and Grx CxxS12. A) PrxII B, B) PrxII C.

Compared to the activities obtained by application of DTT as artificial electron donor, the activities in the presence of either Trx/TR or Grx/GSH/GR were quite low. However when ranked with activities obtained for other Prx these reaction rates were in exactly the same range (Horling et al., 2003; Finkemeier et al., 2005; Lamkemeyer et al., 2006). Finally it has to be noted, that again clear differences between cytosolic PrxII B and PrxII C could be obtained concerning H<sub>2</sub>O<sub>2</sub> detoxification rates in the presence of different regenerating systems. In context with the different biochemical parameters such as  $v_{\max}$  and  $K_M$ , as well as the differential substrate specificity it has to be hypothesised that PrxIIB and C play distinct functional roles within the plant cell despite their very high degree of identity in their amino acid sequence (94 %).

### **3.2.5. Differential regulation of PrxII B and PrxII C transcript levels**

Transcript quantification has revealed differential regulation patterns upon selected treatments as summarised in more detail in the introductory parts (compare section 1.3.2.) (Horling et al., 2002 and 2003). To update the knowledge on transcript regulation, a bioinformatic analysis was performed to gain more insight into transcriptional regulation of these Prx. An *in silico* analysis of publicly available expression data with focus on the tissue- or organ-specific expression, as well as induction and repression of transcripts upon certain stress conditions was expected to provide hints towards PrxII B and C functions in the plant.

The investigation of transcript patterns from Affymetrix chip array data sets with the ‘Genevestigator Database and Toolbox’ (Zimmermann et al., 2004; <http://www.genevestigator.ethz.ch>) and visualisation by ‘Meta Profile Analysis’ enabled a comprehensive overview on regulation in different tissues and states. In this context it has to be noted that the extremely high sequence identity of PrxII C and PrxII D impedes a separate analysis of both transcripts by Genevestigator analysis.

First of all, the development-dependent expression of PrxII B and PrxII C/D was investigated. In general, PrxII C/D revealed a severalfold lower transcript level than PrxII B (Fig. 3.44). Especially in germinated young seedlings as well as in flowering plants, the expression of PrxII B was further pronounced, a regulation which was not seen for PrxII C/D. During plant development PrxII C/D exhibited a continuous decrease in overall transcript until reaching the flowering state. This could also be detected on the protein level by Western blot analysis with an antibody raised against PrxII C (Lahrmann, 2007). In the next step the organ specific distribution was tested.

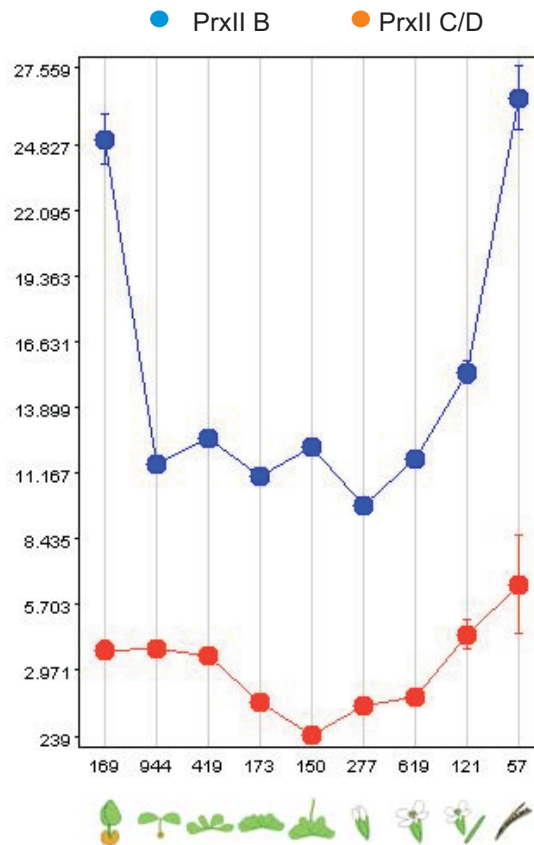


**Fig. 3.44: Transcript abundance of PrxII B and PrxII C/D depicted in dependence of developmental state of *A. thaliana*.** Relative transcript levels are presented as means  $\pm$  standard deviation. The evaluated number of chips is given directly below the diagram. This figure was extracted from Geneinvestigator Database (<http://www.geneinvestigator.ethz.ch>). The high sequence identity between PrxII C and PrxII D precludes separate analysis of both transcripts.

PrxII B revealed a quite high transcript level in almost all analysed plant organs with particularly strong expression in seeds (Fig. 3.45). In contrast, PrxII C/D exhibited a generally low steady-state level. PrxII C/D expression was slightly induced in roots, seeds and flowers, with a high preference for stamen. In two arrays a strongly pronounced expression could be assigned to pollen tissue. A corresponding localisation of PrxII C/D was also shown on protein level by means of plants modified with promoter-GUS constructs (Bréhélin et al., 2003). Apparently the expression patterns for specific plant tissues and organs differ considerably for PrxII B and PrxII C/D.

Prx are directly involved in cellular defence mechanisms. Therefore stress induction is a feature of special interest. An *in silico* analysis via Geneinvestigator Database also allows for the comparison of transcripts in dependence of a multitude of exogenous stimuli.

The compilation of transcript regulations depicted in Fig. 3.46 aimed at defining the differential stress induction/or repression of PrxII B and PrxII C/D.

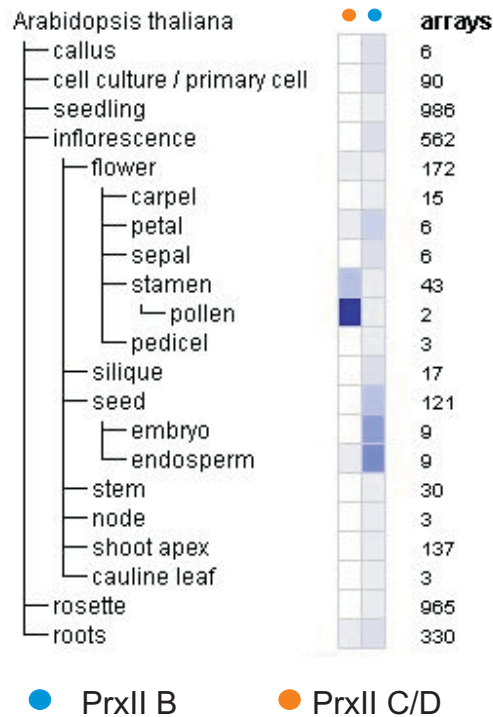


**Fig. 3.45: Transcript abundance of PrxII B and PrxII C/D in different organs of *A. thaliana*.** Relative transcript levels are depicted as heat map with the degree of expression resembled by the intensity of blue colouration. The evaluated number of Affimetrix chips is given directly next to the diagram. This figure was extracted from Genevestigator Database (<http://www.genevestigator.ethz.ch>). The especially high sequence identity of PrxII C and PrxII D precludes separate analysis of both transcripts.

This set of different stress treatments revealed regulations for PrxII C/D that were considerably stronger than the ones observed for PrxII B (Fig. 3.46). Not only the number of treatments resulting in an up- or down-regulation was more pronounced for PrxII C/D transcript, but also the magnitude of these modulations was higher than in case of PrxII B. This is especially interesting as the steady state level of this transcript is remarkably low (compare Fig. 3.44, Fig. 3.45). The high amplitudes of transcript levels reflect a high regulatory potential. The stress dependent responses of both cytosolic type II Prx resembled that observed by RT-PCR-based transcript analyses (Horling et al., 2002 and 2003) and furthermore add to the biochemical findings that also allowed for the differentiation between PrxII B and PrxII C.

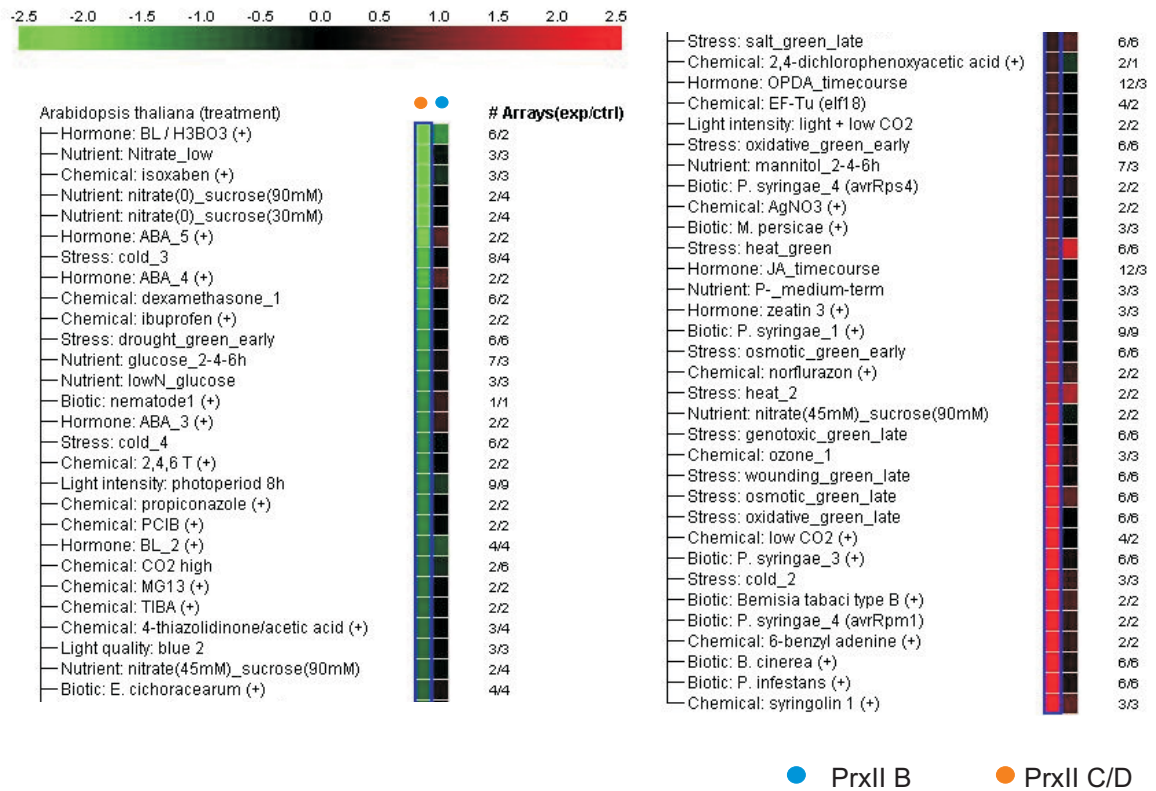


**Fig. 3.46: Transcript abundance of PrxII B and PrxII C/D upon different exogenous stimuli.** Relative transcript regulations are depicted as heat map represented by green (down-regulation) and red (up-regulation) squares. The colour intensity reveals the degree of regulation. The evaluated number of Affimetrix chips is given directly next to the diagram. This figure was extracted from Geneinvestigator Database (<http://www.geneinvestigator.ethz.ch>). The high sequence identity precludes separate analysis of PrxII C and PrxII D transcripts.

Besides the comparison of expression patterns in respect of developmental regulations, organ specificity, and stress induction, *in silico* analyses additionally allow for the determination of co-expression patterns. These can eventually hint at interaction partners of a protein of interest. As besides Grx and Trx, also cyclophilins (Cyp) already have been described as interacting proteins for different Prx (Chevallet et al., 2003; Collin et al., 2003; Finkemeier et al., 2005; Rouhier et al., 2001), co-regulated transcripts identified by ‘Arabidopsis Coexpression Data Mining Tools’ from Leeds University (<http://www.arabidopsis.leeds.ac.uk/act/coexpanalyser.php>; Manfield et al., 2006) were searched especially for members of these protein families. For PrxII C/D two Trx and two Grx were found within co-regulated transcripts. Besides the chloroplastic Trx Lillium4 (At2g33270; correlation coefficient 0.903214), also cytosolic Trx h1 (At3g51030; correlation coefficient 0.894956) was identified. The identified Grx – both not cytosolic ones – exhibited slightly lower correlation

coefficients (At5g58530; 0.834717 and At3g28850; 0.722284). The biochemically investigated Grx CxxC4 was not among these proteins. For PrxII B the identified co-regulated transcripts contained no members of the just mentioned protein families.

### 3.2.6. Future perspectives

As described in the preceding parts of this section, the comparative biochemical characterisation of PrxII B and PrxII C in combination with bioinformatic analyses revealed various differences in biochemical properties and transcript regulations. These distinct properties strongly point towards specific functions. The next step will be the characterisation of these functionalities *in vivo*. To achieve this goal, the utilisation of transgenic plants with altered protein levels, e.g. by means of T-DNA insertion, sense- and antisense-constructs, RNAi or miRNA technology, tentatively promises at least an assignment of roles in antioxidant defence or redox-signalling. Preliminary data were obtained from T-DNA insertion lines of PrxII C (SALK\_069621, insertion located in the promoter region) and PrxII D (SALK\_138035, insertion located in an intron) and indicate such an involvement.

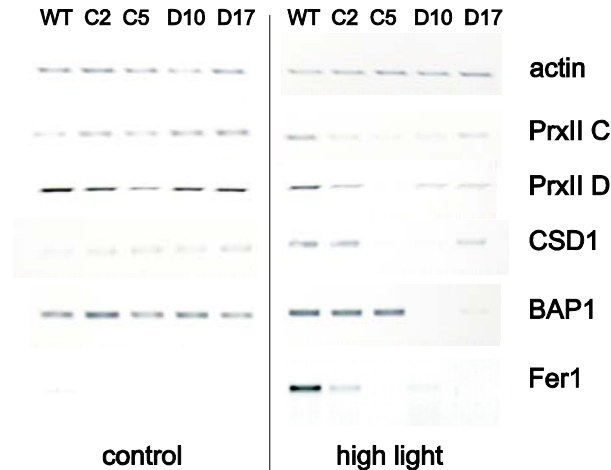


**Fig. 3.47: Effect of modified PrxII C or PrxII D expression on transcript regulation under control and high light conditions.** Leaf discs were incubated under regular light conditions and high light ( $800 \mu\text{mol quanta m}^{-2} \text{s}^{-1}$ ) for four hours. C-2 and C-5 are PrxIIC and D-10 and D-17 are PrxIID T-DNA insertion lines revealing a *knock-down* of the transcript of interest. The cDNA samples were standardised on actin transcript amounts. Following RT-PCRs with gene-specific primers, the amplified products were separated in agarose gels stained with ethidium bromide and documented with an imaging system. The scans were inverted for better visualisation. The experiment was performed twice with similar results.

Whereas upon control conditions the down-regulation of PrxII C and PrxII D was hardly visible it was strongly pronounced upon stress conditions such as high light (Fig. 3.47). This regulation was accompanied by a transcript decrease of specific ROS-markers for  $^1\text{O}_2$  and  $\text{H}_2\text{O}_2$  such as BAP1 (At3g61190) and Fer1 (At5g01600), respectively (Op den Camp et al., 2003) as well as a cytosolic SOD (CSD1, At5g23310) (Fig. 3.47). The down-regulation of Prx caused an alleviation of oxidative stress-mediated effects during short term treatments of four hours. This hints to an involvement in ROS-linked signal transduction since in a converse manner a role in antioxidative defence would be expected to result in an enhanced sensitivity towards oxidative stress. Likewise, the influence on components of the antioxidative network as on CSD1 (Fig. 3.47) might also be assigned to the involvement of PrxII C and PrxII D in signalling pathways.

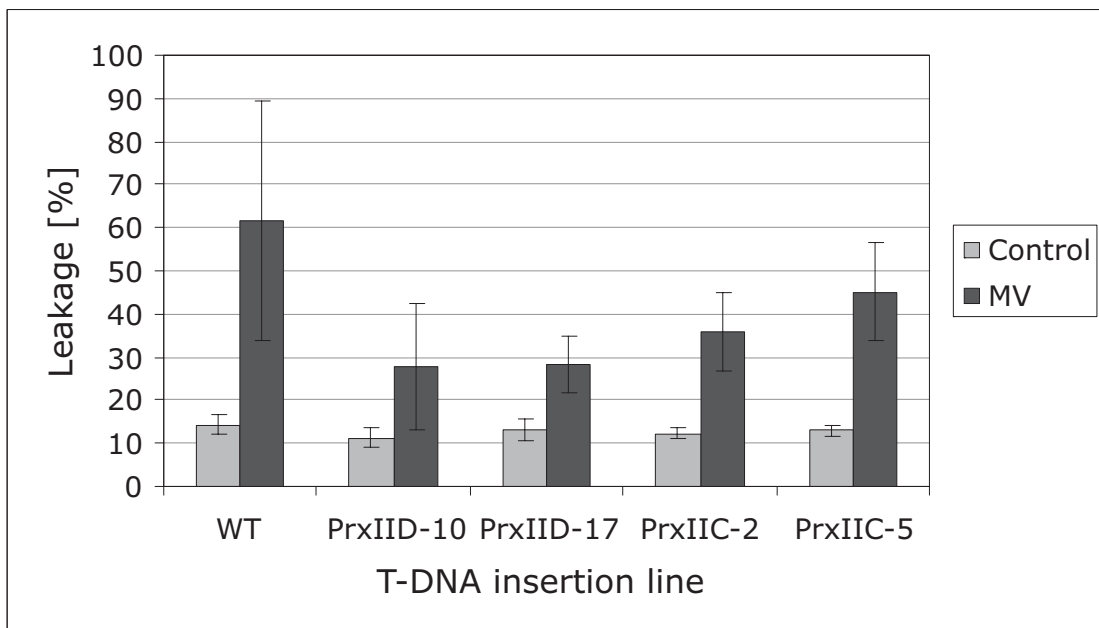


**Fig. 3.48: Measurement of ion leakage as indicator for membrane damage as a consequence of ROS generation in T-DNA insertion lines compared to wild type.**

Leaf slices were incubated for 18 h in water (control) and  $0.5 \mu\text{M}$  methyl viologen (MV), respectively. Afterwards conductivity [ $\mu\text{S}$ ] of the solutions was determined (experimental solution). To quantify the whole ion content of the leaf tissue, the discs were heated after the experiment and the conductivity of the resulting solution was determined as 100%. The ion leakage as consequence of differential treatment was given as percentage of whole ion content. The experiment was performed twice with similar results.

Additionally, susceptibility to oxidative stress mediated by methyl viologen (MV) treatment was much more pronounced in wild type plants than observed from T-DNA

insertion lines (Fig. 3.48). The impact of this effector, generating  $O_2^{\bullet-}$  as a consequence of a redox-cycling process (Smith, 1985), was investigated by measuring ion leakage in a leaf disc experiment. The leaf discs exhibited a decreased sensitivity towards oxidative stress following MV treatment in comparison to wild-type (Fig. 3.48). If these two Prx had an important role in protection against oxidative threats, their down-regulation should cause a loss of ROS-detoxification capacity and this would be expected to increase the sensitivity to MV-mediated oxidative stress.

The lower amount of PrxII C and PrxII D represented by decreased transcripts in the corresponding *knock-down* lines seemed to result in an enhancement of antioxidative capacity in comparison to wild type plants rather than an impaired plant resistance (Fig. 3.47 and Fig. 3.48). These observations tentatively indicate a role of cytosolic PrxII C and PrxII D in redox-linked signalling. It will be of special interest to shed more light on the exact signalling pathways as different modulations of signal transduction are discussed for Prx in plants (compare section 1.3.1.).

#### 4. Literature

**Ackerson CJ, Jadzinsky PD, Jensen GJ, Kornberg RD (2006)** Rigid, specific, and discrete gold nanoparticle/antibody conjugates. *J. Am. Chem. Soc.* 128, 2635-2640.

**Alonso JM, Stepanova AN, Leisse TJ, Kim CJ, Chen H, Shinn P, Stevenson DK, Zimmerman J, Barajas P, Cheuk R, Gadrinab C, Heller C, Jeske A, Koesema E, Meyers CC, Parker H, Prednis L, Ansari Y, Choy N, Deen H, Geralt M, Hazari N, Hom E, Karnes M, Mulholland C, Ndubaku R, Schmidt I, Guzman P, Aguilar-Henonin L, Schmid M, Weigel D, Carter DE, Marchand T, Risseuw E, Brogden D, Zeko A, Crosby WL, Berry CC, Ecker JR (2003)** Genome-wide insertional mutagenesis of *Arabidopsis thaliana*. *Science* 301, 653-657.

**Alphey MS, Bond CS, Tetaud E, Fairlamb AH, Hunter WN (2000)** The structure of reduced trypanothione peroxidase reveals a decamer and insight into reactivity of 2-Cys-peroxiredoxins. *J. Mol. Biol.* 300, 903-916.

**Alscher RG, Erturk N, Heath LS (2002)** Role of superoxide dismutases (SODs) in controlling oxidative stress in plants. *J. Exp. Bot.* 53, 1331-1341.

**Apel K, Hirt H (2004)** Reactive oxygen species: metabolism, oxidative stress, and signal transduction. *Annu. Rev. Plant Biol.* 55, 373-399.

**Asada K (1992)** Ascorbate peroxidase. A hydrogen peroxide scavenging enzyme in plants. *Physiol. Plant.* 85, 235-241.

**Asada K (2006)** Production and scavenging of reactive oxygen species in chloroplasts and their functions. *Plant Physiol.* 141, 391-396.

**Asada K, Takahashi M (1987)** Production and scavenging of active oxygen in photosynthesis. *In* Kyle, D.J., Osmond, C.B., Arntzen, C.J. (Eds.), *Photoinhibition*, Elsevier, Amsterdam, 227-287.

**Audette M, Chen X, Houée-Levin C, Potier M, Le Maire M (2000)** Protein gamma-radiolysis in frozen solutions is a macromolecular surface phenomenon: fragmentation of lysozyme, citrate synthase and alpha-lactalbumin in native or denatured states. *Int. J. Radiat. Biol.* 76, 673-681.

**Babior BM (1997)** Superoxide: a two-edged sword. *Braz. J. Med. Biol. Res.* 30, 141-155.

**Baier M, Dietz KJ (1996)** Primary structure and expression of plant homologues of animal and fungal thioredoxin-dependent peroxide reductases and bacterial alkyl hydroperoxide reductases. *Plant Mol. Biol.* 31, 553-564.

**Baier M, Dietz KJ (1997)** The plant 2-Cys peroxiredoxin BAS1 is a nuclear-encoded chloroplast protein: its expressional regulation, phylogenetic origin, and implications for its specific physiological function in plants. *Plant J.* 12, 179-190.

**Baier M, Dietz KJ (1999 a)** Protective function of chloroplast 2-cysteine peroxiredoxin in photosynthesis. Evidence from transgenic Arabidopsis. *Plant Physiol.* 119, 1407-1414.

**Baier M, Dietz KJ (1999 b)** Alkyl hydroperoxide reductases: the way out of the oxidative breakdown of lipids in chloroplasts. *Trends Plant Sci.* 4, 166-168.

**Baker LM, Poole LB (2003)** Catalytic mechanism of thiol peroxidase from *Escherichia coli*. Sulfenic acid formation and overoxidation of essential CYS61. *J. Biol. Chem.* 278; 9203-9211.

**Banmeyer I, Marchand C, Verhaeghe C, Vucic B, Rees JF, Knoop B (2004)** Overexpression of human peroxiredoxin 5 in subcellular compartments of Chinese hamster ovary cells: effects on cytotoxicity and DNA damage caused by peroxides. *Free Radic. Biol. Med.* 36, 65-77.

**Barranco-Medina S, Kakorin S, Lázaro JJ, Dietz KJ (2008 a)** Thermodynamics of the dimer-decamer transition of reduced human and plant 2-cys peroxiredoxin. *Biochemistry* 47, 7196-7204.

**Barranco-Medina S, Krell T, Bernier-Villamor L, Sevilla F, Lázaro JJ, Dietz KJ (2008 b)** Hexameric oligomerization of mitochondrial peroxiredoxin PrxIIIF and formation of an ultrahigh affinity complex with its electron donor thioredoxin Trx-o. *J. Exp. Bot.* 59, 3259-3269.

**Barranco-Medina S, López-Jaramillo FJ, Bernier-Villamor L, Sevilla F, Lázaro JJ (2006)** Cloning, overexpression, purification and preliminary crystallographic studies of a mitochondrial type II peroxiredoxin from *Pisum sativum*. *Acta Crystallogr. Sect. F Struct. Biol. Cryst. Commun.* 62, 695-698.

**Bennion BJ, Daggett V (2004)** Counteraction of urea-induced protein denaturation by trimethylamine N-oxide: a chemical chaperone at atomic resolution. *Proc. Natl. Acad. Sci. USA* 101, 6433-6438.

**Berberich T, Uebeler M and Feierabend J (1998)** *Plant Phys.-plant gene register* 118, 98-167.

**Berlett BS, Stadtman ER (1997)** Protein oxidation in aging, disease, and oxidative stress. *J. Biol. Chem.* 272, 20313-20316.

**Bernier-Villamor L, Navarro E, Sevilla F, Lázaro JJ (2004)** Cloning and characterization of a 2-Cys peroxiredoxin from *Pisum sativum*. *J. Exp. Bot.* 55, 2191-2199.

**Besson-Bard A, Pugin A, Wendehenne D (2008)** New insights into nitric oxide signaling in plants. *Annu. Rev. Plant Biol.* 59, 21-39.

**Bethke PC, Badger MR, Jones RL (2004)** Apoplastic synthesis of nitric oxide by plant tissues. *Plant Cell.* 16, 332-341.

- Blum H, Beier H, Gross HJ (1987)** Improved silver staining of plant proteins, RNA and DNA in polyacrylamide gels. *Electrophoresis* 8, 93-99.
- Bonanni B, Alliata D, Bizzarri AR, Cannistraro S (2003)** Topological and electron-transfer properties of yeast cytochrome c adsorbed on bare gold electrodes. *Chemphyschem.* 4, 1183-1188.
- Bonifacic M, Asmus KD (1976)** Free radical oxidation of organic disulfides. *J. Phys. Chem.* 80, 2426–2430.
- Bowler C, Slooten L, Vandenbranden S, De Rycke R, Botterman J, Sybesma C, Van Montagu M, Inzé D (1991)** Manganese superoxide dismutase can reduce cellular damage mediated by oxygen radicals in transgenic plants. *EMBO J.* 10, 1723-1732.
- Bradford, M. (1976).** A rapid and sensitive method for the quantification of microgram quantities of protein utilizing the principles of protein-dye binding. *Anal. Biochem.* 72, 58-254.
- Bréhélin C, Meyer EH, de Souris JP, Bonnard G, Meyer Y (2003)** Resemblance and dissemblance of Arabidopsis type II peroxiredoxins: similar sequences for divergent gene expression, protein localization, and activity. *Plant Physiol.* 132, 2045-2057.
- Broin M, Rey P (2003)** Potato plants lacking the CDS32 plastidic thioredoxin exhibit overoxidation of the BAS1 2-Cysteine peroxiredoxin and increased lipid peroxidation in thylakoids under photooxidative stress. *Plant Physiol.* 132, 1335-1343.
- Bryk R, Griffin P, Nathan C (2000)** Peroxynitrite reductase activity of bacterial peroxiredoxins. *Nature* 407, 211-215.
- Burmeister WP (2000)** Structural changes in a cryo-cooled protein crystal owing to radiation damage. *Acta Crystallogr. D Biol. Crystallogr.* 56, 328-341.
- Carter JD, Cheng NN, Qu Y, Suarez GD, Guo T (2007)** Nanoscale energy deposition by x-ray absorbing nanostructures. *J. Phys. Chem. B.* 111, 11622-11625.
- Carugo O, Djinović Carugo K (2005)** When x-rays modify the protein structure: radiation damage at work. *Trends Biochem. Sci.* 30, 213-219.
- Chae HZ, Chung SJ, Rhee SG (1994)** Thioredoxin-dependent peroxide reductase from yeast. *J. Biol. Chem.* 269, 27670-27678.
- Chae HZ, Kim IH, Kim K, Rhee SG (1993)** Cloning, sequencing, and mutation of thiol-specific antioxidant gene of *Saccharomyces cerevisiae*. *J. Biol. Chem.* 268, 16815-16821.
- Chang TS, Cho CS, Park S, Yu S, Kang SW, Rhee SG (2004)** Peroxiredoxin III, a mitochondrion-specific peroxidase, regulates apoptotic signaling by mitochondria. *J. Biol. Chem.* 279, 41975-41984.

**Chauhan R, Mande SC (2002)** Site-directed mutagenesis reveals a novel catalytic mechanism of *Mycobacterium tuberculosis* alkylhydroperoxidase C. *Biochem. J.* 367, 255-261.

**Cheong NE, Choi YO, Lee KO, Kim WY, Jung BG, Chi YH, Jeong JS, Kim K, Cho MJ, Lee SY (1999)** Molecular cloning, expression, and functional characterization of a 2Cys-peroxiredoxin in Chinese cabbage. *Plant Mol. Biol.* 40, 825-834.

**Chevallet M, Wagner E, Luche S, van Dorselaer A, Leize-Wagner E, Rabilloud T (2003)** Regeneration of peroxiredoxins during recovery after oxidative stress: only some overoxidized peroxiredoxins can be reduced during recovery after oxidative stress. *Biol. Chem.* 278, 37146-37153.

**Choi HJ, Kang SW, Yang CH, Rhee SG, Ryu SE (1998)** Crystallization and preliminary X-ray studies of hORF6, a novel human antioxidant enzyme. *Acta Crystallogr. D Biol. Crystallogr.* 54, 436-437.

**Choi YO, Cheong NE, Lee KO, Jung BG, Hong CH, Jeong JH, Chi YH, Kim K, Cho MJ, Lee SY. (1999)** Cloning and expression of a new isotype of the peroxiredoxin gene of Chinese cabbage and its comparison to 2Cys-peroxiredoxin isolated from the same plant. *Biochem. Biophys. Res. Commun.* 258, 768-771.

**Cigarrán S, Barrios L, Caballín MR, Barquinero JF (2004)** Effect of DMSO on radiation-induced chromosome aberrations analysed by FISH. *Cytogenet Genome Res.* 104, 168-172.

**Collin V, Issakidis-Bourguet E, Marchand C, Hirasawa M, Lancelin JM, Knaff DB, Miginiac-Maslow M (2003)** The Arabidopsis plastidial thioredoxins: new functions and new insights into specificity. *J. Biol. Chem.* 278, 23747-23752.

**Collins BM, Cubeddu L, Naidoo N, Harrop SJ, Kornfeld GD, Dawes IW, Curmi PM, Mabbutt BC (2003)** Homomeric ring assemblies of eukaryotic Sm proteins have affinity for both RNA and DNA. Crystal structure of an oligomeric complex of yeast SmF. *J. Biol. Chem.* 278, 17291-17298.

**Cordoba-Pedregosa M, Gonzalez-Reyes JA, Canadillas M, Navas P, Cordoba F (1996)** Role of apoplastic and cell-wall peroxidases on the stimulation of root elongation by ascorbate. *Plant Physiol.* 112, 1119-1125.

**Corpas FJ, Barroso JB, del Río LA (2001)** Peroxisomes as a source of reactive oxygen species and nitric oxide signal molecules in plant cells. *Trends Plant Sci.* 6, 145-150.

**Crawford NM (2006)** Mechanisms for nitric oxide synthesis in plants. *J. Exp. Bot.* 57, 471-478.

**Cumming RC, Dargusch R, Fischer WH, Schubert D (2007)** Increase in expression levels and resistance to sulfhydryl oxidation of peroxiredoxin isoforms in amyloid beta-resistant nerve cells. *J. Biol. Chem.* 282, 30523-30534.

- Dalton DA, Diaz del Castillo L, Kahn ML, Joyner SL, Chatfield JM (1996)** Heterologous expression and characterization of soybean cytosolic ascorbate peroxidase. *Arch. Biochem. Biophys.* 328, 1-8.
- Dat J, Vandenabeele S, Vranová E, Van Montagu M, Inzé D, Van Breusegem F. (2000)** Dual action of the active oxygen species during plant stress responses. *Cell Mol. Life Sci.* 57, 779-795.
- Davletova S, Rizhsky L, Liang H, Shengqiang Z, Oliver DJ, Coutu J, Shulaev V, Schlauch K, Mittler R (2005)** Cytosolic ascorbate peroxidase 1 is a central component of the reactive oxygen gene network of Arabidopsis. *Plant Cell.* 17, 268-281.
- De Leonardis S, Dipierro N., Dipierro S (2000)** Purification and characterization of an ascorbate peroxidase from potato tuber mitochondria *Plant. Physiol. Biochem.* 38: 773-779.
- Declercq JP, Evrard C, Clippe A, Stricht DV, Bernard A, Knoops B (2001)** Crystal structure of human peroxiredoxin 5, a novel type of mammalian peroxiredoxin at 1.5 Å resolution. *J. Mol. Biol.* 311, 751-759.
- del Río LA, Corpas FJ, Sandalio LM, Palma JM, Gómez M, Barroso JB (2002)** Reactive oxygen species, antioxidant systems and nitric oxide in peroxisomes. *J. Exp. Bot.* 53, 1255-1272.
- del Río LA, Sandalio LM, Corpas FJ, Palma JM, Barroso JB (2006)** Reactive oxygen species and reactive nitrogen species in peroxisomes. Production, scavenging, and role in cell signaling. *Plant Physiol.* 141, 330-335.
- Delledonne M, Murgia I, Ederle D, Sbicego PF, Biondani A, Polverari A, Lamb C (2002)** Reactive oxygen intermediates modulate nitric oxide signaling in the plant hypersensitive disease resistance response. *Plant Physiol. Biochem.* 40, 605-610.
- Delledonne M, Zeier J, Marocco A, Lamb C (2001)** Signal interactions between nitric oxide and reactive oxygen intermediates in the plant hypersensitive disease resistance response. *Proc. Natl. Acad. Sci. USA* 98, 13454-13459.
- Denicola A, Souza JM, Radi R (1998)** Diffusion of peroxynitrite across erythrocyte membranes. *Proc. Natl. Acad. Sci. USA* 95, 3566-3571.
- Desikan R, Hancock J, Neill S (2005)** Reactive oxygen species as signalling molecules. *In: Smirnoff, N. (Ed.) Antioxidants and reactive oxygen species in plants.* Blackwell Publishing, 169-196.
- Dietz KJ (2003 a)** Plant peroxiredoxins. *Annu. Rev. Plant Biol.* 54, 93-107.
- Dietz KJ (2003 b)** Redox control, redox signaling, and redox homeostasis in plant cells. *Int. Rev. Cytol.* 228, 141-193.
- Dietz KJ (2007)** The dual function of plant peroxiredoxins in antioxidant defence and redox signaling. *Subcell. Biochem.* 44, 267-294.

**Dietz KJ, Bogorad L (1987)** Plastid development in *Pisum sativum* leaves during greening: I. A comparison of plastid polypeptide composition and *in organello* translation characteristics. *Plant Physiol.* 85, 808-815.

**Dietz KJ, Horling F, König J, Baier M (2002)** The function of the chloroplast 2-cysteine peroxiredoxin in peroxide detoxification and its regulation. *J. Exp. Bot.* 53, 1321-1329.

**Dietz KJ, Jacob S, Oelze ML, Laxa M, Tognetti V, de Miranda SM, Baier M, Finkemeier I (2006)** The function of peroxiredoxins in plant organelle redox metabolism. *J. Exp. Bot.* 57, 1697-1709.

**Dinçer A, Aydemir T (2001)** Purification and characterization of catalase from chard (*Beta vulgaris* var. *cicla*). *J. Enzyme Inhib.* 16, 165-175.

**Dizdaroglu M (2005)** Base-excision repair of oxidative DNA damage by DNA glycosylases. *Mutat. Res.* 591, 45-59.

**Dubois LH, Zegarski BR, Nuzzo RG (1987)** Fundamental studies of the interactions of adsorbates on organic surfaces. *Proc. Natl. Acad. Sci. USA* 84, 4739-4742.

**Dubois LH, Zegarski BR, Nuzzo RG (1990)** Fundamental studies of microscopic wetting on organic surfaces. 2. Interaction of secondary adsorbates with chemically textured organic monolayers. *J. Am. Chem. Soc.* 112, 570-579.

**Dubuisson M, Vander Stricht D, Clippe A, Etienne F, Nauser T, Kissner R, Koppenol WH, Rees JF, Knoops B (2004)** Human peroxiredoxin 5 is a peroxynitrite reductase. *FEBS Lett.* 571, 161-165.

**Edwards K, Johnstone C, Thompson C (1991)** A simple and rapid method for the preparation of plant genomic DNA for PCR analysis. *Nucleic Acids Res.* 19, 1349.

**Feierabend J (2005)** Catalases in plants: molecular and functional properties and role in stress defence. In: Smirnoff, N. (Ed.) *Antioxidants and reactive oxygen species in plants*. Blackwell Publishing, 101-140.

**Ferreri C, Manco I, Faraone-Mennella MR, Torreggiani A, Tamba M, Chatgililoglu C (2004)** A biomimetic model of tandem radical damage involving sulfur-containing proteins and unsaturated lipids. *Chembiochem.* 5, 1710-1712.

**Fick J (2005)** Charakterisierung von biokompatiblen Oberflächen mittels Vibrations-Summenfrequenzspektroskopie und Neutronenreflektometrie. Dissertation, Naturwissenschaftlich-Mathematische Gesamtfakultät, Ruprecht-Karls-Universität Heidelberg.

**Filali-Mouhim A, Audette M, St-Louis M, Thauvette L, Denoroy L, Penin F, Chen X, Rouleau N, Le Caer JP, Rossier J, Potier M, Le Maire M (1997)** Lysozyme fragmentation induced by gamma-radiolysis. *Int. J. Radiat. Biol.* 72, 63-70.

**Finkemeier I, Goodman M, Lamkemeyer P, Kandlbinder A, Sweetlove LJ, Dietz KJ (2005)** The mitochondrial type II peroxiredoxin F is essential for redox homeostasis and root growth of *Arabidopsis thaliana* under stress. *J. Biol. Chem.* 280, 12168-12180.

**Flohé L, Budde H, Bruns K, Castro H, Clos J, Hofmann B, Kansal-Kalavar S, Krumme D, Menge U, Plank-Schumacher K, Sztajer H, Wissing J, Wylegalla C, Hecht HJ (2002)** Tryparedoxin peroxidase of *Leishmania donovani*: molecular cloning, heterologous expression, specificity, and catalytic mechanism. *Arch. Biochem. Biophys.* 397, 324-335.

**Foyer CH, Halliwell C (1976)** The presence of glutathione reductase in chloroplasts: a proposed role in ascorbic acid metabolism. *Planta* 133, 21-25.

**Foyer CH, Noctor G (2000)** Oxygen processing in photosynthesis: regulation and signalling. *New Phytol.* 146, 359-388.

**Foyer CH, Noctor G (2003)** Redox sensing and signaling associated with reactive oxygen in chloroplasts, peroxisomes and mitochondria. *Physiol. Plant.* 119, 355-364.

**Foyer CH, Noctor G (2005)** Redox homeostasis and antioxidant signaling: a metabolic interface between stress perception and physiological responses. *Plant Cell.* 17, 1866-1875.

**Fridovich I (1975)** Superoxide dismutases. *Adv. Enzymol. Relat. Areas Mol. Biol.* 41, 35-97.

**Fridovich I (1986)** Biological effects of the superoxide radical. *Arch. Biochem. Biophys.* 247, 1-11.

**Friedrich W, Knipping P, von Laue M (1912)** Interferenz-Erscheinungen bei Röntgenstrahlen. *Sitzungsber. Bayer. Akad. Wiss.* 2, 303-322.

**Frugoli JA, Zhong HH, Nuccio ML, McCourt P, McPeck MA, Thomas TL, McClung CR (1996)** Catalase is encoded by a multigene family in *Arabidopsis thaliana* (L.) Heynh. *Plant Physiol.* 112, 327-336.

**Fucci L, Oliver CN, Coon MJ, Stadtman ER (1983)** Inactivation of key metabolic enzymes by mixed-function oxidation reactions: possible implication in protein turnover and ageing. *Proc. Natl. Acad. Sci. USA* 80, 1521-1525.

**Furuya M, Haramura M, Tanaka A (2006)** Reduction of nonspecific binding proteins to self-assembled monolayers on gold surface. *Bioorg. Med. Chem.* 14, 537-543.

**Gama F, Bréhélin C, Gelhaye E, Meyer Y, Jacquot JP, Rey P, Rouhier N (2008)** Functional analysis and expression characteristics of chloroplastic Prx IIE. *Physiol. Plant.* 133, 599-610.

**Garman EF, McSweeney SM (2007)** Progress in research into radiation damage in cryo-cooled macromolecular crystals. *J. Synchrotron Radiat.* 14, 1-3.

**Gechev TS, Van Breusegem F, Stone JM, Denev I, Laloi C (2006)** Reactive oxygen species as signals that modulate plant stress responses and programmed cell death. *Bioessays* 28, 1091-1101.

**Georgiou G, Masip L (2003)** Biochemistry. An overoxidation journey with a return ticket. *Science* 300, 592-594.

**Giulivi C, Traaseth NJ, Davies KJ (2003)** Tyrosine oxidation products: analysis and biological relevance. *Amino Acids* 25, 227-232.

**Godon C, Lagniel G, Lee J, Buhler JM, Kieffer S, Perrot M, Boucherie H, Toledano MB, Labarre J (1998)** The H<sub>2</sub>O<sub>2</sub> stimulon in *Saccharomyces cerevisiae*. *J. Biol. Chem.* 273, 22480-22489.

**Goergens A (2005)** Erzeugung ortsgerichtet mutierter Varianten von Proteinen zur dualen Kopplung an funktionalisierte Oberflächen. Diplomarbeit, Technische Fakultät, Universität Bielefeld.

**Gourlay LJ, Bhella D, Kelly SM, Price NC, Lindsay JG (2003)** Structure-function analysis of recombinant substrate protein 22 kDa (SP-22). A mitochondrial 2-Cys peroxiredoxin organized as a decameric toroid. *J. Biol. Chem.* 278, 32631-32637.

**Harris N, Dodge AD (1972)** The effect of paraquat on flax cotyledon leaves: Physiological and biochemical changes. *Planta (Berl.)* 104, 210-219.

**Hattori F, Oikawa S (2007)** Peroxiredoxins in the central nervous system. *Subcell. Biochem.* 44, 357-374.

**Hawkins CL, Davies MJ (2001)** Generation and propagation of radical reactions on proteins. *Biochim. Biophys. Acta.* 1504, 196-219.

**Hillas PJ, del Alba FS, Oyarzabal J, Wilks A, Ortiz De Montellano PR (2000)** The AhpC and AhpD antioxidant defense system of *Mycobacterium tuberculosis*. *J. Biol. Chem.* 275, 18801-18809.

**Hirotsu S, Abe Y, Okada K, Nagahara N, Hori H, Nishino T, Hakoshima T (1999)** Crystal structure of a multifunctional 2-Cys peroxiredoxin heme-binding protein 23 kDa/proliferation-associated gene product. *Proc. Natl. Acad. Sci. USA* 96, 12333-12338.

**Hofmann B, Hecht HJ, Flohé L (2002)** Peroxiredoxins. *Biol. Chem.* 383, 347-364.

**Horemans N, Foyer CH, Asard H (2000)** Transport and action of ascorbate at the plant plasma membrane. *Trends Plant Sci.* 5, 263-267.

**Horling F, Baier M, Dietz KJ (2001)** Redox-regulation of the expression of the peroxide-detoxifying chloroplast 2-cys peroxiredoxin in the liverwort *Riccia fluitans*. *Planta.* 214, 304-313.

**Horling F, König J, Dietz KJ (2002)** Type II peroxiredoxin C, a member of the peroxiredoxin family of *Arabidopsis thaliana*: its expression and activity in comparison with other peroxiredoxins. *Plant Physiol. Biochem.* 40, 491-499.

**Horling F, Lamkemeyer P, König J, Finkemeier I, Kandlbinder A, Baier M, Dietz KJ (2003)** Divergent light-, ascorbate-, and oxidative stress-dependent regulation of expression of the peroxiredoxin gene family in *Arabidopsis*. *Plant Physiol.* 131, 317-325.

**Hosoya-Matsuda N, Motohashi K, Yoshimura H, Nozaki A, Inoue K, Ohmori M, Hisabori T (2005)** Anti-oxidative stress system in cyanobacteria. Significance of type II peroxiredoxin and the role of 1-Cys peroxiredoxin in *Synechocystis* sp. strain PCC 6803. *J. Biol. Chem.* 280, 840-846.

**Immenschuh S, Iwahara S, Satoh H, Nell C, Katz N, Muller-Eberhard U (1995)** Expression of the mRNA of heme-binding protein 23 is coordinated with that of heme oxygenase-1 by heme and heavy metals in primary rat hepatocytes and hepatoma cells. *Biochemistry* 34, 13407-13411.

**Ishikawa T, Takeda T, Shigeoka S (1996)** Purification and characterization of cytosolic ascorbate peroxidase from komatsuna (*Brassica rapa*) *Plant Science* 120, 11-18.

**Jabs T, Dietrich RA, Dangl JL (1996)** Initiation of runaway cell death in an *Arabidopsis* mutant by extracellular superoxide. *Science* 273, 1853-1856.

**Jabs T, Tschope M, Colling C, Hahlbrock K, Scheel D (1997)** Elicitor-stimulated ion fluxes and  $O_2^-$  from the oxidative burst are essential components in triggering defense gene activation and phytoalexin synthesis in parsley. *Proc. Natl. Acad. Sci. USA* 94, 4800-4805.

**Jackson C, Dench J, Moore AL, Halliwell B, Foyer CH, Hall DO (1978)** Subcellular localisation and identification of superoxide dismutase in the leaves of higher plants. *Eur. J. Biochem.* 91, 339-344.

**Jacob C, Holme AL, Fry FH (2004)** The sulfinic acid switch in proteins. *Org. Biomol. Chem.* 2, 1953-1956.

**Jacob S (2005)** Funktion des cytosolischen Peroxiredoxins PrxIIC in der antioxidativen Abwehr und im Redox-Signaling von *Arabidopsis thaliana*. Diplomarbeit, Fakultät für Biologie, Universität Bielefeld.

**Jacobsen FS, Morgen RW, Christman MF, Ames BN (1989)** An alkyl hydroperoxide reductase from *Salmonella typhimurium* involved in the defense of DNA against oxidative damage. Purification and properties. *J. Biol. Chem.* 264, 1488-1496.

**Janatpour K, Denning L, Nelson K, Betlach B, Mackenzie M, Holland P (2005)** Comparison of x-ray vs. gamma irradiation of CPDA-1 red cells. *Vox Sang.* 89, 215-219.

**Jang HH, Kim SY, Park SK, Jeon HS, Lee YM, Jung JH, Lee SY, Chae HB, Jung YJ, Lee KO, Lim CO, Chung WS, Bahk JD, Yun DJ, Cho MJ, Lee SY (2006)** Phosphorylation and concomitant structural changes in human 2-Cys peroxiredoxin isotype I differentially regulate its peroxidase and molecular chaperone functions. *FEBS Lett.* 580, 351-355.

**Jang HH, Lee KO, Chi YH, Jung BG, Park SK, Park JH, Lee JR, Lee SS, Moon JC, Yun JW, Choi YO, Kim WY, Kang JS, Cheong GW, Yun DJ, Rhee SG, Cho MJ, Lee SY (2004)** Two enzymes in one; two yeast peroxiredoxins display oxidative stress-dependent switching from a peroxidase to a molecular chaperone function. *Cell* 117, 625-635.

**Jara M, Vivancos AP, Calvo IA, Moldón A, Sansó M, Hidalgo E (2007)** The peroxiredoxin Tpx1 is essential as a H<sub>2</sub>O<sub>2</sub> scavenger during aerobic growth in fission yeast. *Mol. Biol. Cell* 18, 2288-2295.

**Jeong JS, Kwon SJ, Kang SW, Rhee SG, Kim K (1999)** Purification and characterization of a second type thioredoxin peroxidase (type II TPx) from *Saccharomyces cerevisiae*. *Biochemistry* 38, 776-783.

**Jönsson TJ, Lowther WT (2007)** The peroxiredoxin repair proteins. *Subcell. Biochem.* 44, 115-141.

**Joshi H, Shirude PS, Bansal V, Ganesh KN, Sastry M (2004)** Isothermal titration calorimetry studies on the binding of amino acids to gold nanoparticles. *J. Phys. Chem. B*, 108, 11535-11540.

**Karyotou K, Donaldson RP (2005)** Ascorbate peroxidase, a scavenger of hydrogen peroxide in glyoxysomal membranes. *Arch. Biochem. Biophys.* 434, 248-257.

**Kempner ES (2001)** Effects of high-energy electrons and gamma rays directly on protein molecules. *J. Pharm. Sci.* 90, 1637-1646.

**Kerk NM, Feldman LJ (1995)** A biochemical model for the initiation and maintenance of the quiescent center: implications for organization of root meristems. *Plant Development* 121, 2825-2833.

**Kiba A, Nishihara M, Tsukatani N, Nakatsuka T, Kato Y, Yamamura S (2005)** A peroxiredoxin Q homolog from gentians is involved in both resistance against fungal disease and oxidative stress. *Plant Cell Physiol.* 46, 1007-1015.

**Kim H, Lee TH, Park ES, Suh JM, Park SJ, Chung HK, Kwon OY, Kim YK, Ro HK, Shong M (2000)** Role of peroxiredoxins in regulating intracellular hydrogen peroxide and hydrogen peroxide-induced apoptosis in thyroid cells. *J. Biol. Chem.* 275, 18266-18270.

**Kim K, Kim IH, Lee KY, Rhee SG, Stadtman ER (1988)** The isolation and purification of a specific "protector" protein which inhibits enzyme inactivation by a thiol/Fe(III)/O<sub>2</sub> mixed-function oxidation system. *J. Biol. Chem.* 263, 4704-4711.

**Kim MS, Kim HS, Kim YS, Baek KH, Oh HW, Hahn KW, Bae RN, Lee IJ, Joung H, Jeon JH (2007)** Superoxide anion regulates plant growth and tuber development of potato. *Plant Cell Rep.* 26, 1717-1725.

**Kissner R, Nauser T, Bugnon P, Lye PG, Koppenol WH (1997)** Formation and properties of peroxynitrite as studied by laser flash photolysis, high-pressure stopped-flow technique, and pulse radiolysis. *Chem. Res. Toxicol.* 10, 1285-1292.

**Kitano K, Niimura Y, Nishiyama Y, Miki K (1999)** Stimulation of peroxidase activity by decamerization related to ionic strength: AhpC protein from *Amphibacillus xylanus*. *J. Biochem.* 126, 313-319.

**Klotz LO (2002)** Oxidant-induced signaling: effects of peroxynitrite and singlet oxygen. *Biol. Chem.* 383, 443-456.

**Knoops B, Clippe A, Bogard C, Arsalane K, Wattiez R, Hermans C, Duconseille E, Falmagne P, Bernard A (1999)** Cloning and characterization of AOEB166, a novel mammalian antioxidant enzyme of the peroxiredoxin family. *J. Biol. Chem.* 274, 30451-30458.

**Knox JP, Dodge AD (1985)** Singlet oxygen and plants. *Phytochemistry* 24, 889-896.

**König J, Baier M, Horling F, Kahmann U, Harris G, Schürmann P, Dietz KJ (2002)** The plant-specific function of 2-Cys peroxiredoxin-mediated detoxification of peroxides in the redox-hierarchy of photosynthetic electron flux. *Proc. Natl. Acad. Sci. USA* 99, 5738-5743.

**König J, Lotte K, Plessow R, Brockhinke A, Baier M, Dietz KJ (2003)** Reaction mechanism of plant 2-Cys peroxiredoxin. Role of the C terminus and the quaternary structure. *J. Biol. Chem.* 278, 24409-24420.

**Korytowski W, Pilas B, Sarna T, Kalyanaraman B (1987)** Photoinduced generation of hydrogen peroxide and hydroxyl radicals in melanins. *Photochem. Photobiol.* 45, 185-190.

**Koshiya T (1993)** Cytosolic ascorbate peroxidase in seedlings and leaves of maize. *Plant Cell Physiol.* 34, 713-721.

**Kovtun Y, Chiu WL, Tena G, Sheen J (2000)** Functional analysis of oxidative stress-activated mitogen-activated protein kinase cascade in plants. *Proc. Natl. Acad. Sci. USA* 97, 2940-2945.

**Kristensen P, Rasmussen DE, Kristensen BI (1999)** Properties of thiol-specific antioxidant protein or calpromotin in solution. *Biochem. Biophys. Res. Commun.* 262, 127-131.

**Kropotov AV, Grudinkin PS, Pleskach NM, Gavrilov BA, Tomilin NV, Zhivotovsky B (2004)** Downregulation of peroxiredoxin V stimulates formation of etoposide-induced double-strand DNA breaks. *FEBS Lett.* 572, 75-79.

- Kruft V, Eubel H, Jansch L, Werhahn W, Braun HP (2001)** Proteomic approach to identify novel mitochondrial proteins in Arabidopsis. *Plant Physiol.* 127, 1694-1710.
- Kwak JM, Mori IC, Pei ZM, Leonhardt N, Torres MA, Dangel JL, Bloom RE, Bodde S, Jones JD, Schroeder JI (2003)** NADPH oxidase AtrbohD and AtrbohF genes function in ROS-dependent ABA signaling in Arabidopsis. *EMBO J.* 22, 2623-2633.
- Lahrman U (2007)** Untersuchung zur biochemischen Aktivität und Proteinakkumulation des cytosolischen Typ II Peroxiredoxins C aus *Arabidopsis thaliana*. Bachelorarbeit, Technische Fakultät, Universität Bielefeld.
- Lamb C, Dixon RA (1997)** The oxidative burst in plant disease resistance. *Annu. Rev. Plant Physiol. Plant Mol. Biol.* 48, 251-275.
- Lamkemeyer P, Laxa M, Collin V, Li W, Finkemeier I, Schöttler MA, Holtkamp V, Tognetti VB, Issakidis-Bourguet E, Kandlbinder A, Weis E, Miginiac-Maslow M, Dietz KJ (2006)** Peroxiredoxin Q of *Arabidopsis thaliana* is attached to the thylakoids and functions in context of photosynthesis. *Plant J.* 45, 968-981.
- Laxa M, König J, Dietz KJ, Kandlbinder A (2007)** Role of the cysteine residues in *Arabidopsis thaliana* cyclophilin CYP20-3 in peptidyl-prolyl cis-trans isomerase and redox-related functions. *Biochem J.* 401, 287-297.
- Le Maire M, Thauvette L, de Foresta B, Viel A, Beauregard G, Potier M (1990)** Effects of ionizing radiations on proteins. Evidence of non-random fragmentations and a caution in the use of the method for determination of molecular mass. *Biochem. J.* 267, 431-439.
- Lee W, Choi KS, Riddell J, Ip C, Ghosh D, Park JH, Park YM (2007)** Human peroxiredoxin 1 and 2 are not duplicate proteins: the unique presence of CYS83 in Prx1 underscores the structural and functional differences between Prx1 and Prx2. *J. Biol. Chem.* 282, 22011-22022.
- Lehtonen ST, Markkanen PM, Peltoniemi M, Kang SW, Kinnula VL (2005)** Variable overoxidation of peroxiredoxins in human lung cells in severe oxidative stress. *Am. J. Physiol. Lung Cell Mol. Physiol.* 288, 997-1001.
- Leiros HK, McSweeney SM, Smalås AO (2001)** Atomic resolution structures of trypsin provide insight into structural radiation damage. *Acta Crystallogr. D Biol. Crystallogr.* 57, 488-497.
- Leiros HK, Timmins J, Ravelli RB, McSweeney SM. (2006)** Is radiation damage dependent on the dose rate used during macromolecular crystallography data collection? *Acta Crystallogr. D Biol. Crystallogr.* 62, 125-132.
- Lemaire SD (2004)** The glutaredoxin family in oxygenic photosynthetic organisms. *Photosynth Res.* 79, 305-318.

- Lim MJ, Chae HZ, Rhee SG, Yu DY, Lee KK, Yeom YI (1998)** The type II peroxiredoxin gene family of the mouse: molecular structure, expression and evolution. *Gene* 216, 197-205.
- Lim YS, Cha MK, Kim HK, Uhm TB, Park JW, Kim K, Kim IH (1993)** Removals of hydrogen peroxide and hydroxyl radical by thiol-specific antioxidant protein as a possible role in vivo. *Biochem Biophys Res Commun.* 192, 273-280.
- Littlefield LG, Sayer AM, Frome EL (1989)** Comparisons of dose-response parameters for radiation-induced acentric fragments and micronuclei observed in cytokinesis-arrested lymphocytes. *Mutagenesis* 4, 265-270.
- López-Huertas E, Corpas FJ, Sandalio LM, Del Río LA (1999)** Characterization of membrane polypeptides from pea leaf peroxisomes involved in superoxide radical generation. *Biochem. J.* 337, 531-536.
- Luwe M (1996)** Antioxidants in the apoplast and symplast of beech (*Fagus sylvatica* L.) leaves: seasonal variations and responses to changing ozone concentration in air. *Plant Cell Environ.* 19, 321-328.
- Manfield IW, Jen CH, Pinney JW, Michalopoulos I, Bradford JR, Gilmartin PM, Westhead DR (2006)** Arabidopsis Co-expression Tool (ACT): web server tools for microarray-based gene expression analysis. *Nucleic Acids Res.* 34, 504-509.
- Matsui Y, Sakai K, Murakami M, Shiro Y, Adachi S, Okumura H, Kouyama T (2002)** Specific damage induced by X-ray radiation and structural changes in the primary photoreaction of bacteriorhodopsin. *J. Mol. Biol.* 324, 469-481.
- McCord JM, Fridovich I (1969)** The utility of superoxide dismutase in studying free radical reactions. I. Radicals generated by the interaction of sulfite, dimethyl sulfoxide, and oxygen. *J. Biol. Chem.* 244, 6056-6063.
- Mehler AH (1951)** Studies on reactions of illuminated chloroplasts. I. Mechanism of the reduction of oxygen and other Hill reagents. *Arch. Biochem.* 33, 65-77.
- Meissner U, Schröder E, Scheffler D, Martin AG, Harris JR (2007)** Formation, TEM study and 3D reconstruction of the human erythrocyte peroxiredoxin-2 dodecahedral higher-order assembly. *Micron.* 38, 29-39.
- Meskauskiene R, Nater M, Goslings D, Kessler F, op den Camp R, Apel K (2001)** FLU: a negative regulator of chlorophyll biosynthesis in *Arabidopsis thaliana*. *Proc. Natl. Acad. Sci. USA* 98, 12826-12931.
- Meyer AJ, Brach T, Marty L, Kreye S, Rouhier N, Jacquot JP, Hell R (2007)** Redox-sensitive GFP in *Arabidopsis thaliana* is a quantitative biosensor for the redox potential of the cellular glutathione redox buffer. *Plant J.* 52, 973-986.
- Michelet L, Zaffagnini M, Marchand C, Collin V, Decottignies P, Tsan P, Lancelin JM, Trost P, Miginiac-Maslow M, Noctor G, Lemaire SD (2005)** Glutathionylation of chloroplast thioredoxin f is a redox signaling mechanism in plants. *Proc. Natl. Acad. Sci. USA* 102, 16478-16483.

**Miller G, Shulaev V, Mittler R (2008)** Reactive oxygen signaling and abiotic stress. *Physiol. Plant.* 133, 481-489.

**Miller I, Crawford J, Gianazza E (2006)** Protein stains for proteomic applications: which, when, why? *Proteomics* 6, 5385-5408.

**Mittler R, Herr EH, Orvar BL, van Camp W, Willekens H, Inzé D, Ellis BE (1999)** Transgenic tobacco plants with reduced capability to detoxify reactive oxygen intermediates are hyperresponsive to pathogen infection. *Proc. Natl. Acad. Sci. USA* 96, 14165-14170.

**Mittler R, Poulos TL (2005)** Ascorbate peroxidase, In: Smirnoff, N. (Ed.) *Antioxidants and reactive oxygen species in plants*, Blackwell Publishing 2005, 87-100.

**Mittler R, Vanderauwera S, Gollery M, Van Breusegem F (2004)** Reactive oxygen gene network of plants. *Trends Plant Sci.* 9, 490-498.

**Møller IM (2001)** Plant mitochondria and oxidative stress: Electron Transport, NADPH turnover, and metabolism of reactive oxygen species. *Annu. Rev. Plant. Physiol. Plant Mol. Biol.* 52, 561-591.

**Møller IM, Jensen PE, Hansson A (2007)** Oxidative modifications to cellular components in plants. *Annu. Rev. Plant Biol.* 58, 459-481.

**Monteiro G, Horta BB, Pimenta DC, Augusto O, Netto LE (2007)** Reduction of 1-Cys peroxiredoxins by ascorbate changes the thiol-specific antioxidant paradigm, revealing another function of vitamin C. *Proc. Natl. Acad. Sci. USA* 104, 4886-4891.

**Moon JC, Hah YS, Kim WY, Jung BG, Jang HH, Lee JR, Kim SY, Lee YM, Jeon MG, Kim CW, Cho MJ, Lee SY (2005)** Oxidative stress-dependent structural and functional switching of a human 2-Cys peroxiredoxin isotype II that enhances HeLa cell resistance to H<sub>2</sub>O<sub>2</sub>-induced cell death. *J. Biol. Chem.* 280, 28775-28784.

**Murashige T, Skoog F (1962)** A revised medium for rapid growth and bio assays with tobacco tissue cultures. *Physiol Plant* 15, 473-497.

**Murray J, Garman E (2002)** Investigation of possible free-radical scavengers and metrics for radiation damage in protein cryocrystallography. *J. Synchrotron Radiat.* 9, 347-354.

**Nagy N, Malik G, Fisher AB, Das DK (2006)** Targeted disruption of peroxiredoxin 6 gene renders the heart vulnerable to ischemia-reperfusion injury. *Am. J. Physiol. Heart Circ. Physiol.* 291, H2636-H2640.

**Nakamura C., Hasegawa M., Shimada K., Shirai M. und Miyake J (2000)** Direct triazine herbicide detection using a self-assembled photosynthetic reaction center from purple bacterium. *Biotechnol. Bioprocess. Eng.* 5, 413-417.

**Nath S, Ghosh SK, Kundu S, Praharaj S, Panigrahi S, Pal T (2006)** Is gold really softer than silver? *J. Nanoparticle Res.* 8, 111-116.

- Navrot N, Collin V, Gualberto J, Gelhaye E, Hirasawa M, Rey P, Knaff DB, Issakidis E, Jacquot JP, Rouhier N (2006)** Plant glutathione peroxidases are functional peroxiredoxins distributed in several subcellular compartments and regulated during biotic and abiotic stresses. *Plant Physiol.* 142, 1364-1379.
- Neill SJ, Bright J, Desikan R, Hancock J, Harrison J, Wilson I (2008)** Nitric oxide evolution and perception. *J. Exp. Bot.* 59, 25-35.
- Neill SJ, Desikan R, Clarke A, Hurst RD, Hancock JT (2002)** Hydrogen peroxide and nitric oxide as signalling molecules in plants. *J. Exp. Bot.* 53, 1237-1247.
- Neill SJ, Desikan R, Hancock JT (2003)** Nitric oxide signalling. *New Phytol.* 159, 11-35.
- Neumann CA, Fang Q (2007)** Are peroxiredoxins tumor suppressors? *Curr. Opin. Pharmacol.* 7, 375-380.
- Nieba L, Nieba-Axmann SE, Persson A, Hämäläinen M, Edebratt F, Hansson A, Lidholm J, Magnusson K, Karlsson AF, Plückthun A (1997)** BIACORE analysis of histidine-tagged proteins using a chelating NTA sensor chip. *Anal. Biochem.* 252, 217-228.
- Niyogi KK (1999)** Photoprotection revisited: Genetic and molecular approaches. *Annu. Rev. Plant Physiol. Plant Mol. Biol.* 50, 333-359.
- Noctor G, Foyer CH (1998)** Ascorbate and glutathione: Keeping active oxygen under control. *Annu. Rev. Plant Physiol. Plant Mol. Biol.* 49, 249-279.
- Noctor G, Gomez L, Vanacker H, Foyer CH (2002)** Interactions between biosynthesis, compartmentation and transport in the control of glutathione homeostasis and signalling. *J. Exp. Bot.* 53, 1283-1304.
- Nogoceke E, Gommel DU, Kiess M, Kalisz HM, Flohé L (1997)** A unique cascade of oxidoreductases catalyses trypanothione-mediated peroxide metabolism in *Crithidia fasciculata*. *Biol. Chem.* 378, 827-836.
- Noguera-Mazon V, Krimm I, Walker O, Lancelin JM (2006)** Protein-protein interactions within peroxiredoxin systems. *Photosynth. Res.* 89, 277-290.
- Okumura Y, Oka T, Kataoka M, Taniguchi Y, Sasaki YC (2004)** Picometer-scale dynamical observations of individual membrane proteins: the case of bacteriorhodopsin. *Phys. Rev. E Stat. Nonlin. Soft Matter Phys.* 70, 021917.1-021917.7.
- O'Neill P, Stevens DL, Garman EF (2002).** Physical and chemical considerations of damage induced in protein crystals by synchrotron radiation: a radiation chemical perspective. *J. Synchrotron Radiat.* 9, 329-332.
- op den Camp RG, Przybyla D, Ochsenbein C, Laloi C, Kim C, Danon A, Wagner D, Hideg E, Göbel C, Feussner I, Nater M, Apel K (2003)** Rapid induction of

distinct stress responses after the release of singlet oxygen in *Arabidopsis*. *Plant Cell* 15, 2320-2332.

**Orozco-Cardenas M, Ryan CA (1999)** Hydrogen peroxide is generated systemically in plant leaves by wounding and systemin via the octadecanoid pathway. *Proc. Natl. Acad. Sci. USA* 96, 6553-6557.

**Orozco-Cárdenas ML, Ryan CA (2002)** Nitric oxide negatively modulates wound signaling in tomato plants. *Plant Physiol.* 130, 487-493.

**Overmyer K, Tuominen H, Kettunen R, Betz C, Langebartels C, Sandermann H Jr, Kangasjärvi J (2000)** Ozone-sensitive *Arabidopsis rcd1* mutant reveals opposite roles for ethylene and jasmonate signaling pathways in regulating superoxide-dependent cell death. *Plant Cell.* 12, 1849-1862.

**Padh H (1990)** Cellular functions of ascorbic acid. *Biochem. Cell. Biol.* 68, 1166-1173.

**Pagnussat GC, Simontacchi M, Puntarulo S, Lamattina L (2002)** Nitric oxide is required for root organogenesis. *Plant Physiol.* 129, 954-956.

**Papinutto E, Windle HJ, Cendron L, Battistutta R, Kelleher D, Zanotti G (2005)** Crystal structure of alkyl hydroperoxide-reductase (AhpC) from *Helicobacter pylori*. *Biochim. Biophys. Acta.* 1753, 240-246.

**Park SH, Chung YM, Lee YS, Kim HJ, Kim JS, Chae HZ, Yoo YD (2000)** Antisense of human peroxiredoxin II enhances radiation-induced cell death. *Clin. Cancer Res.* 6, 4915-4920.

**Parsonage D, Youngblood DS, Sarma GN, Wood ZA, Karplus PA, Poole LB (2005)** Analysis of the link between enzymatic activity and oligomeric state in AhpC, a bacterial peroxiredoxin. *Biochemistry* 44, 10583-10592.

**Pauly N, Pucciariello C, Mandon K, Innocenti G, Jamet A, Baudouin E, Hérouart D, Frendo P, Puppo A (2006)** Reactive oxygen and nitrogen species and glutathione: key players in the legume-Rhizobium symbiosis. *J. Exp. Bot.* 57, 1769-1776.

**Pei ZM, Murata Y, Benning G, Thomine S, Klüsener B, Allen GJ, Grill E, Schroeder JI (2000)** Calcium channels activated by hydrogen peroxide mediate abscisic acid signalling in guard cells. *Nature* 406, 731-734.

**Peltier JB, Emanuelsson O, Kalume DE, Ytterberg J, Friso G, Rudella A, Liberles DA, Soderberg L, Roepstorff P, von Heijne G, van Wijk KJ (2002)** Central functions of the lumenal and peripheral thylakoid proteome of *Arabidopsis* determined by experimentation and genome-wide prediction. *Plant Cell* 14, 211-236.

**Pena-Ahumada A, Kahmann U, Dietz KJ, Baier M (2006)** Regulation of peroxiredoxin expression versus expression of Halliwell-Asada-Cycle enzymes during early seedling development of *Arabidopsis thaliana*. *Photosynth. Res.* 89, 99-112.

**Penna C, Mancardi D, Tullio F, Pagliaro P (2008)** Postconditioning and intermittent bradykinin induced cardioprotection require cyclooxygenase activation and prostacyclin release during reperfusion. *Basic Res. Cardiol.* 103, 368-377.

**Pérez-Ruiz JM, Spínola MC, Kirchsteiger K, Moreno J, Sahrawy M, Cejudo FJ, (2006)** Rice NTRC is a high-efficiency redox system for chloroplast protection against oxidative damage. *Plant Cell.* 18, 2356-2368.

**Peskin AV, Low FM, Paton LN, Maghzal GJ, Hampton MB, Winterbourn CC (2007)** The high reactivity of peroxiredoxin 2 with H<sub>2</sub>O<sub>2</sub> is not reflected in its reaction with other oxidants and thiol reagents. *J. Biol. Chem.* 282, 11885-11892.

**Pignocchi C, Foyer CH (2003)** Apoplastic ascorbate metabolism and its role in the regulation of cell signalling. *Curr. Opin. Plant Biol.* 6, 379-389.

**Planchet E, Kaiser WM (2006)** Nitric oxide (NO) detection by DAF fluorescence and chemiluminescence: a comparison using abiotic and biotic NO sources. *J. Exp. Bot.* 57, 3043-3055.

**Polle A, Wieser G, Havranek WM (1995)** Quantification of ozone influx and apoplastic ascorbate content in needles of Norway spruce trees (*Picea abies* L., Karst) at high altitude. *Plant Cell Environ.* 18, 681-688.

**Quan LJ, Zhang B, Shi WW, Li HY (2008)** Hydrogen peroxide in plants: a versatile molecule of the reactive oxygen species network. *J. Integr. Plant Biol.* 50, 2-18.

**Rabilloud T, Berthier R, Vinçon M, Ferbus D, Goubin G, Lawrence JJ (1995)** Early events in erythroid differentiation: accumulation of the acidic peroxidoxin (PRP/TSA/NKEF-B). *Biochem J.* 312, 699-705.

**Ravelli RB, McSweeney SM (2000)** The 'fingerprint' that X-rays can leave on structures. *Structure* 8, 315-328.

**Renneberg H (1982)** Glutathione metabolism and possible biological roles in the higher plant. *Phytochemistry* 21, 2771-2781.

**Rentel MC, Knight MR (2004)** Oxidative stress-induced calcium signaling in Arabidopsis. *Plant Physiol.* 135, 1471-1479.

**Rho BS, Hung LW, Holton JM, Vigil D, Kim SI, Park MS, Terwilliger TC, Pédalacq JD (2006)** Functional and structural characterization of a thiol peroxidase from *Mycobacterium tuberculosis*. *J. Mol. Biol.* 361, 850-863.

**Romero-Puertas MC, Laxa M, Mattè A, Zaninotto F, Finkemeier I, Jones AM, Perazzolli M, Vandelle E, Dietz KJ, Delledonne M (2007)** S-nitrosylation of peroxiredoxin II E promotes peroxynitrite-mediated tyrosine nitration. *Plant Cell* 19, 4120-4130.

**Romero-Puertas MC, Perazzolli M, Zago ED, Delledonne M (2004)** Nitric oxide signalling functions in plant-pathogen interactions. *Cell. Microbiol.* 6, 795-803.

**Rouhier N, Gelhaye E, Corbier C, Jacquot JP (2004)** Active site mutagenesis and phospholipid hydroperoxide reductase activity of poplar type II peroxiredoxin. *Physiol. Plant.* 120, 57-62.

**Rouhier N, Gelhaye E, Sautiere PE, Brun A, Laurent P, Tagu D, Gerard J, de Faÿ E, Meyer Y, Jacquot JP (2001)** Isolation and characterization of a new peroxiredoxin from poplar sieve tubes that uses either glutaredoxin or thioredoxin as a proton donor. *Plant Physiol.* 127, 1299-1309.

**Rouhier N, Jacquot JP (2005)** The plant multigenic family of thiol peroxidases. *Free Radic. Biol. Med.* 38, 1413-1421.

**Saha A, Mandal PC, Bhattacharyya SN (1995)** Radiation-induced inactivation of enzymes-a review *Rad. Phys. Chem.* 46, 123-145.

**Saito S, Yamamoto-Katou A, Yoshioka H, Doke N, Kawakita K (2006)** Peroxynitrite generation and tyrosine nitration in defense responses in tobacco BY-2 cells. *Plant Cell Physiol.* 47, 689-697.

**Salin ML (1988)** Toxic oxygen species and protective systems of the chloroplasts. *Physiol. Plant.* 72, 681-689.

**Sandalio LM, Fernández VM, Rupérez FL, Del Río LA (1988)** Superoxide free radicals are produced in glyoxysomes. *Plant Physiol.* 87, 1-4.

**Sasaki YC (2004)** Single protein molecular dynamics determined with ultra-high precision. *Biochem. Soc. Trans.* 32, 761-763.

**Sasaki YC, Okumura Y, Adachi S, Suda H, Taniguchi Y, Yagi N (2001)** Picometer-scale dynamical x-ray imaging of single DNA molecules. *Phys. Rev. Lett.* 87, 248102.1-248102.4.

**Sasaki YC, Okumura Y, Miyazaki T, Higurashi T (2006)** Observations of x-ray radiation pressure force on individual gold nanocrystals. *App. Phys. Lett.* 89, 053121.1-053121.3.

**Sasaki YC, Suzuki Y, Yagi N, Adachi S, Ishibashi M, Suda H, Toyota K, Yanagihara M (2000)** Tracking of individual nanocrystals using diffracted x rays. *Phys. Rev. E Stat. Phys. Plasmas Fluids Relat. Interdiscip. Topics* 62, 3843-3847.

**Sawyer DT, Valentine JS (1981)** How super is superoxide? *Acc. Chem. Res.* 14, 393.

**Sayed AA, Williams DL (2004)** Biochemical characterization of 2-Cys peroxiredoxins from *Schistosoma mansoni*. *J. Biol. Chem.* 279, 26159-26166.

**Scandalios JG (1993)** Oxygen stress and superoxide dismutases. *Plant Physiol.* 101, 7-12.

**Scandalios JG (2002 a)** The rise of ROS. *Trends Biochem. Sci.* 27, 483-486.

**Scandalios JG (2002 b)** Oxidative stress responses - what have genome-scale studies taught us? *Genome Biol.* 3, 1019.1-1019.6.

**Scandalios JG (2005)** Oxidative stress: molecular perception and transduction of signals triggering antioxidant gene defenses. *Braz. J. Med. Biol. Res.* 38, 995-1014.

**Schillmiller AL, Howe GA (2005)** Systemic signaling in the wound response. *Curr. Opin. Plant Biol.* 8, 369-377.

**Schröder E, Isupov MN, Naran A, Littlechild JA (1999)** Crystallization and preliminary X-ray analysis of human thioredoxin peroxidase-B from red blood cells. *Acta Crystallogr. D Biol. Crystallogr.* 55, 536-538.

**Schröder E, Littlechild JA, Lebedev AA, Errington N, Vagin AA, Isupov MN (2000)** Crystal structure of decameric 2-Cys peroxiredoxin from human erythrocytes at 1.7 Å resolution. *Structure* 8, 605-615.

**Sekiya M, Mulcahy G, Irwin JA, Stack CM, Donnelly SM, Xu W, Collins P, Dalton JP (2006)** Biochemical characterisation of the recombinant peroxiredoxin (FhePrx) of the liver fluke, *Fasciola hepatica*. *FEBS Lett.* 580, 5016-5022.

**Sharma P, Dubey RS (2004)** Ascorbate peroxidase from rice seedlings: properties of enzyme isoforms, effects of stresses and protective roles of osmolytes. *Plant Science* 167, 541-550.

**Sharma SS, Dietz KJ (2006)** The significance of amino acids and amino acid-derived molecules in plant responses and adaptation to heavy metal stress. *J. Exp. Bot.* 57, 711-726.

**Shen C, Nathan C (2002)** Nonredundant antioxidant defense by multiple two-cysteine peroxiredoxins in human prostate cancer cells. *Mol. Med.* 8, 95-102.

**Shetty V, Spellman DS, Neubert TA (2007)** Characterization by tandem mass spectrometry of stable cysteine sulfenic acid in a cysteine switch peptide of matrix metalloproteinases. *J. Am. Soc. Mass. Spectrom.* 18, 1544-1551.

**Shimizu N, Hirata K, Hasegawa K, Ueno G, Yamamoto M (2007)** Dose dependence of radiation damage for protein crystals studied at various X-ray energies. *Synchrotron Radiat.* 14, 4-10.

**Slesak I, Libik M, Karpinska B, Karpinski S, Miszalski Z (2007)** The role of hydrogen peroxide in regulation of plant metabolism and cellular signalling in response to environmental stresses. *Acta Biochim. Pol.* 54, 39-50.

**Smirnoff N (2000)** Ascorbate biosynthesis and function in photoprotection. *Philos. Trans. R Soc. Lond. B Biol. Sci.* 355, 1455-1464.

**Smith LL (1985)** Paraquat toxicity. *Philos. Trans. R. Soc. Lond. B Biol. Sci.* 311, 647-57.

- Smith-Pearson PS, Kooshki M, Spitz DR, Poole LB, Zhao W, Robbins ME (2008)** Decreasing peroxiredoxin II expression decreases glutathione, alters cell cycle distribution, and sensitizes glioma cells to ionizing radiation and H<sub>2</sub>O<sub>2</sub>. *Free Radic. Biol. Med.* 45, 1178-1189.
- Southworth-Davies RJ, Garman EF (2007)** Radioprotectant screening for cryocrystallography. *J. Synchrotron Radiat.* 14, 73-83.
- Stacy RA, Nordeng TW, Culiáñez-Macià FA, Aalen RB (1999)** The dormancy-related peroxiredoxin anti-oxidant, PER1, is localized to the nucleus of barley embryo and aleurone cells. *Plant J.* 19, 1-8.
- Stadtman ER (1992)** Protein oxidation and aging. *Science* 257, 1220-1224.
- Stadtman ER (1995)** Role of oxidized amino acids in protein breakdown and stability. *Methods Enzymol.* 258, 379-393.
- Stadtman ER, Levine RL (2003)** Free radical-mediated oxidation of free amino acids and amino acid residues in proteins. *Amino Acids.* 25, 207-218.
- Stork T, Laxa M, Dietz MS, Dietz KJ (2008)** Functional characterisation of the peroxiredoxin gene family members of *Synechococcus elongatus* PCC 7942. *Arch. Microbiol.* Oct 31. [Epub ahead of print]; PMID: 18974976.
- Ströher E (2008)** Exploring components of the chloroplast thiol-disulfide redox-network in *Arabidopsis thaliana*. PhD thesis, Faculty of Biology, Bielefeld University.
- Ströher E, Dietz KJ (2008)** The dynamic thiol-disulphide redox proteome of the *Arabidopsis thaliana* chloroplast as revealed by differential electrophoretic mobility. *Physiol. Plant.* In press.
- Ströher E, Wang XJ, Roloff N, Klein P, Husemann A, Dietz KJ (2009)** Redox-dependent regulation of the stress-induced zinc-finger protein SAP12 in *Arabidopsis thaliana*. *Molecular Plant Advance Access* published on December 9, 2008; doi:10.1093/mp/ssn084
- Stuart-Audette M, Blouquit Y, Faraggi M, Sicard-Roselli C, Houée-Levin C, Jollès P (2003)** Re-evaluation of intramolecular long-range electron transfer between tyrosine and tryptophan in lysozymes. Evidence for the participation of other residues. *Eur. J. Biochem.* 270, 3565-3571.
- Sweetlove LJ, Heazlewood JL, Herald V, Holtzapffel R, Day DA, Leaver CJ, Millar AH (2002)** The impact of oxidative stress on *Arabidopsis* mitochondria. *Plant J.* 32, 891-904.
- Takahama U, Oniki T (1994)** Effects of ascorbate on the oxidation of derivatives of hydroxycinnamic acid and the mechanism of oxidation of sinapic acid by cell wall-bound peroxidases. *Plant Cell Physiol.* 35, 593-600.
- Takahashi MA, Asada K (1983)** Superoxide anion permeability of phospholipid membranes and chloroplast thylakoids. *Arch. Biochem. Biophys.* 226, 558-566.

**Tanaka A, Tanaka R (2006)** Chlorophyll metabolism. *Curr. Opin. Plant Biol.* 9, 248-255.

**Tang Q, Xu CH, ShiSQ, Zhou LM (2004)** Formation and characterisation of protein patterns on the surfaces with different properties. *Synthetic Metals* 147, 247-252.

**Taylor NL, Day DA, Millar AH (2002)** Environmental stress causes oxidative damage to plant mitochondria leading to inhibition of glycine decarboxylase. *J. Biol. Chem.* 277, 42663-42668.

**Telfer A, Dhami S, Bishop SM, Phillips D, Barber J (1994)** beta-Carotene quenches singlet oxygen formed by isolated photosystem II reaction centers. *Biochemistry* 33, 14469-14474.

**Torreggiani A, Tamba M, Manco I, Faraone-Mennella MR, Ferreri C, Chatgililoglu C (2006)** Investigation of radical-based damage of RNase A in aqueous solution and lipid vesicles. *Biopolymers.* 81, 39-50.

**Torres MA, Dangl JL, Jones JD (2002)** Arabidopsis gp91phox homologues AtrbohD and AtrbohF are required for accumulation of reactive oxygen intermediates in the plant defense response. *Proc. Natl. Acad. Sci. USA* 99, 517-522.

**Trivelli X, Krimm I, Ebel C, Verdoucq L, Prouzet-Mauléon V, Chartier Y, Tsan P, Lauquin G, Meyer Y, Lancelin JM (2003)** Characterization of the yeast peroxiredoxin Ahp1 in its reduced active and overoxidized inactive forms using NMR. *Biochemistry* 42, 14139-14149.

**Trujillo M, Budde H, Piñeyro MD, Stehr M, Robello C, Flohé L, Radi R (2004)** *Trypanosoma brucei* and *Trypanosoma cruzi* tryparedoxin peroxidases catalytically detoxify peroxynitrite via oxidation of fast reacting thiols. *J. Biol. Chem.* 279, 34175-34182.

**Turner JE, Magee JL, Wright HA, Chatterjee A, Hamm RN, Ritchie RH (1983)** Physical and chemical development of electron tracks in liquid water. *Radiat. Res.* 96, 437.

**Turrens JF (1997)** Superoxide production by the mitochondrial respiratory chain. *Biosci. Rep.* 17, 3-8.

**Turrens JF (2003)** Mitochondrial formation of reactive oxygen species. *J. Physiol.* 552, 335-344.

**Valko M, Leibfritz D, Moncol J, Cronin MT, Mazur M, Telser J (2007)** Free radicals and antioxidants in normal physiological functions and human disease. *Int. J. Biochem. Cell. Biol.* 39, 44-84.

**Vandenabeele S, Van Der Kelen K, Dat J, Gadjev I, Boonefaes T, Morsa S, Rottiers P, Slooten L, Van Montagu M, Zabeau M, Inze D, Van Breusegem F. (2003)** A comprehensive analysis of hydrogen peroxide-induced gene expression in tobacco. *Proc. Natl. Acad. Sci. USA* 100, 16113-16118.

- Vanderauwera S, Zimmermann P, Rombauts S, Vandenabeele S, Langebartels C, Gruissem W, Inzé D, Van Breusegem F (2005)** Genome-wide analysis of hydrogen peroxide-regulated gene expression in *Arabidopsis* reveals a high light-induced transcriptional cluster involved in anthocyanin biosynthesis. *Plant Physiol.* 139, 806-821.
- Vanin AF, Svistunenko DA, Mikoyan VD, Serezhenkov VA, Fryer MJ, Baker NR, Cooper CE (2004)** Endogenous superoxide production and the nitrite/nitrate ratio control the concentration of bioavailable free nitric oxide in leaves. *J. Biol. Chem.* 279, 24100-24107.
- Verdoucq L, Vignols F, Jacquot JP, Chartier Y, Meyer Y (1999)** *In vivo* characterization of a thioredoxin h target protein defines a new peroxiredoxin family. *J. Biol. Chem.* 274, 19714-19722.
- Vranová E, Inzé D, Van Breusegem F (2002)** Signal transduction during oxidative stress. *J. Exp. Bot.* 53, 1227-1236.
- Wagner E, Luche S, Penna L, Chevallet M, Van Dorsselaer A, Leize-Wagner E, Rabilloud T (2002)** A method for detection of overoxidation of cysteines: peroxiredoxins are oxidized *in vivo* at the active-site cysteine during oxidative stress. *Biochem. J.* 366, 777-785.
- Wang S, Du D (2002)** Studies on the electrochemical behavior of hydroquinone at L-cysteine self-assembled monolayers modified gold electrode. *Sensors* 2, 41-49.
- Wang X, Phelan SA, Forsman-Semb K, Taylor EF, Petros C, Brown A, Lerner CP, Paigen B (2003)** Mice with targeted mutation of peroxiredoxin 6 develop normally but are susceptible to oxidative stress. *J. Biol. Chem.* 278, 25179-25190.
- Wang Y, Feinstein SI, Manevich Y, Ho YS, Fisher AB (2004)** Lung injury and mortality with hyperoxia are increased in peroxiredoxin 6 gene-targeted mice. *Free Radic. Biol. Med.* 37, 1736-1743.
- Wardman P (1989)** Reduction Potentials of One-Electron Couples Involving Free Radicals in Aqueous Solution. *J. Phys. Chem. Ref. Data* 18, 1637-1755.
- Weik M, Bergès J, Ravès ML, Gros P, McSweeney S, Silman I, Sussman JL, Houée-Levin C, Ravelli RB (2002)** Evidence for the formation of disulfide radicals in protein crystals upon x-ray irradiation. *J Synchrotron Radiat.* 9, 342-346.
- Weik M, Ravelli RB, Kryger G, McSweeney S, Ravès ML, Harel M, Gros P, Silman I, Kroon J, Sussman JL (2000)** Specific chemical and structural damage to proteins produced by synchrotron radiation. *Proc. Natl. Acad. Sci. U S A.* 97, 623-628.
- Wendehenne D, Pugin A, Klessig DF, Durner J (2001)** Nitric oxide: comparative synthesis and signaling in animal and plant cells. *Trends Plant Sci.* 6, 177-183.
- Wilson ID, Neill SJ, Hancock JT (2008)** Nitric oxide synthesis and signalling in plants. *Plant Cell Environ.* 31, 622-631.

- Wingler A, Lea PJ, Quick WP, Leegood RC (2000)** Photorespiration: metabolic pathways and their role in stress protection. *Philos. Trans. R Soc. Lond. B Biol. Sci.* 355, 1517-1529.
- Wisniewski JP, Cornille P, Agnel JP, Montillet JL (1999)** The extensin multigene family responds differentially to superoxide or hydrogen peroxide in tomato cell cultures. *FEBS Lett.* 447, 264-268.
- Wojtaszek P (2000)** Nitric oxide in plants. To NO or not to NO. *Phytochemistry.* 54, 1-4.
- Wong CM, Zhou Y, Ng RW, Kung Hf HF, Jin DY (2002)** Cooperation of yeast peroxiredoxins Tsa1p and Tsa2p in the cellular defense against oxidative and nitrosative stress. *J. Biol. Chem.* 277, 5385-5394.
- Wood ZA, Poole LB, Hantgan RR, Karplus PA (2002)** Dimers to doughnuts: redox-sensitive oligomerization of 2-Cysteine peroxiredoxins. *Biochemistry* 41, 5493-5504.
- Wood ZA, Poole LB, Karplus PA (2003 a)** Peroxiredoxin evolution and the regulation of hydrogen peroxide signaling. *Science* 300, 650-653.
- Wood ZA, Schröder E, Robin Harris J, Poole LB (2003 b)** Structure, mechanism and regulation of peroxiredoxins. *Trends Biochem. Sci.* 28, 32-40.
- Wormuth D, Heiber I, Shaikali J, Kandlbinder A, Baier M, Dietz KJ (2007)** Redox regulation and antioxidative defence in Arabidopsis leaves viewed from a systems biology perspective. *J. Biotechnol.* 129, 229-248.
- Yamamoto H, Miyake C, Dietz KJ, Tomizawa K, Murata N, Yokota A (1999)** Thioredoxin peroxidase in the Cyanobacterium *Synechocystis sp.* PCC 6803. *FEBS Lett.* 447, 269-273.
- Yamasaki H (2005)** The NO world for plants: achieving a balance in an open system. *Plant Cell Environ.* 28, 78-84.
- Yamashita H, Avraham S, Jiang S, London R, Van Veldhoven PP, Subramani S, Rogers RA, Avraham H (1999)** Characterization of human and murine PMP20 peroxisomal proteins that exhibit antioxidant activity *in vitro*. *J. Biol. Chem.* 274, 29897-29904.
- Yeo WS, Lee SJ, Lee JR, Kim KP (2008)** Nitrosative protein tyrosine modifications: biochemistry and functional significance. *BMB Rep.* 41, 194-203.
- Zaffagnini M, Michelet L, Marchand C, Sparla F, Decottignies P, Le Maréchal P, Miginiac-Maslow M, Noctor G, Trost P, Lemaire SD (2007)** The thioredoxin-independent isoform of chloroplastic glyceraldehyde-3-phosphate dehydrogenase is selectively regulated by glutathionylation. *FEBS J.* 274, 212-226.
- Zhang P, Liu B, Kang SW, Seo MS, Rhee SG, Obeid LM (1997)** Thioredoxin peroxidase is a novel inhibitor of apoptosis with a mechanism distinct from that of Bcl-2. *J. Biol. Chem.* 272, 30615-30618.

**Zhao W, Fan GC, Zhang ZG, Bandyopadhyay A, Zhou X, Kranias EG (2008)** Protection of peroxiredoxin II on oxidative stress-induced cardiomyocyte death and apoptosis. *Basic Res. Cardiol.* Nov 22. [Epub ahead of print]; PMID: 19030911.

**Zheng Y, Hunting DJ, Ayotte P, Sanche L (2008)** Radiosensitization of DNA by gold nanoparticles irradiated with high-energy electrons. *Radiat. Res.* 169, 19-27.

**Zhou Y, Zhang W, Easton R, Ray JW, Lampe P, Jiang Z, Brunkan AL, Goate A, Johnson EM, Wu JY (2002)** Presenilin-1 protects against neuronal apoptosis caused by its interacting protein PAG. *Neurobiol. Dis.* 9, 126-138.

**Zimmermann P, Hirsch-Hoffmann M, Hennig L, Gruissem W (2004)** GENEVESTIGATOR. Arabidopsis microarray database and analysis toolbox. *Plant Physiol.* 136, 2621-2632.

## Appendices

## Appendix A

**Tab. A1: List of primers used for the screening of T-DNA insetion lines.** In addition to the primer combinations and sequences, the optimal annealing temperatures are given.

primer pair	sequence forward sequence reverse	annealing temperature [°C]
PrxB Pro-f Lba1	CATAGCCATAGATCTCAA TGGTTCACGTAGTGGGCCATCG	55
PrxB Pro-f Prx Pro-r	CATAGCCATAGATCTCAA AACTCCACAGAGATCTCC	59
PrxC Pro-f Lba1	ATGTGACTCATTGACGTGAACA TGGTTCACGTAGTGGGCCATCG	55
PrxC Pro-f PrxC Pro-r	ATGTGACTCATTGACGTGAACA CTCTGTCTTCAAACCACAGAGATCTCT	65
PrxD Pro-f Lba1	ATGAAGGAAGATTGACAAGAAGA TGGTTCACGTAGTGGGCCATCG	55
PrxD Pro-f Prx7-r	ATGAAGGAAGATTGACAAGAAGA CAAGTCAATACACTTGCTTGTTGAT	57

**Appendix B****Tab. A2: List of primers used for RT-PCRs of T-DNA insertion lines.** In addition to the gene codes and primer sequences, the optimal annealing temperatures and utilised numbers of cycles are given.

gene	gene code	sequence forward sequence reverse	annealing temperature [°C]	cycles
actin	At5g09810	GGAGCTGAGATTCCGTTG GGTGCAACCATTGATCTT	52	28
PrxII C	At1g65970	GTTGAATCTGGTGGCGAGTT GCCAAGCAAGTCAAACACAT	50	34
PrxII D	At1g65940	GAAACATTATCATTTCGCTTGTTG CAAGTCAATACACTTGCTTGTTGAT	50	40
CSD1	At5g23310	GCTGCTACGTTTCCAAAGAA CGGAATTTTCTCCTGTTTCTGTC	50	27
BAP1	At3g61190	CTAAACCGGAGACCCATC AGTGACCTTCAGGTGAATAC	52	32
Fer1	At5g01600	ATGGCCTCAAACGCACTCTCGTC CTAGTCCCTTCATAGCAACG	52	29

## Appendix C

**Tab. A3: List of primers used for introduction of restriction sites and site directed mutagenesis.** In addition to the primer combinations and sequences, the optimal annealing temperatures are given.

primer pair	sequence forward sequence reverse	annealing temperature [°C]
2CP3-BamHI-f 2CP3-KpnI-r	TAGTGGGATCCATGATCTTCCACTGGTT TAGTAGGTACCCTAAATAGGTGAAGTACTC	55
2CP3-BamHI-f 2CP3-DKS-r	TAGTGGGATCCATGATCTTCCACTGGTT CAAGCCCTCCACATGTCCTTGCTGTTTGGACC	55
2CP3-DKS-f 2CP3-KpnI-r	GGTCCAAACAGCAAGGACATGTGGAGGGCTTG TAGTAGGTACCCTAAATAGGTGAAGTACTC	55

## Danksagung

An dieser Stelle möchte ich all jenen danken, die wesentlich zum Gelingen dieser Arbeit beigetragen haben. Hierbei gilt mein besonderer Dank:

- Herrn Prof. Dr. Karl-Josef Dietz dafür, dass er diese Arbeit ermöglicht hat: für die Überlassung des Themas, die hervorragende wissenschaftliche Betreuung und die wertvollen Anregungen und Diskussionen.
- Frau Dr. Andrea Kandlbinder für die gemeinsamen Exkursionen in die Welt der Physik sowie die zahlreichen Hilfen im täglichen Labor- und Büroalltag.
- Herrn Dr. Uwe Kahmann für die Anfertigung der elektronenmikroskopischen Aufnahmen, Carola Eck für die schnelle Bearbeitung meiner Proben sowie Dr. Armin Brechling und Jawad Slieh für die Zusammenarbeit am SFB-Teilprojekt D9.
- Der aktuellen Laborbesetzung Dr. Elke Ströher, Xinjia Wang und Meenakumari Muthuramalingam für die tolle Zusammenarbeit und die vielen lustigen Stunden.
- Allen aktuellen und ehemaligen Mitgliedern des Lehrstuhls ‚Biochemie und Physiologie der Pflanzen‘ für das nette Miteinander und die ständige Hilfsbereitschaft, insbesondere Frau Dr. Iris Finkemeier für die Einführung in die spannende Welt der Peroxiredoxine.
- Der Uni Gärtnerei, Bio-EDV und der mechanischen Werkstatt.
- Vielen Dank ‚meiner Herde‘ Marie-Luise Oelze, Nils Roloff, Ines Lücking, Ulli Sütthoff, Daniel Schnitzer und Stefan Birkmann nicht nur für die Kaffeepausen... Ihr seid wahnsinnig – und das ist auch gut so!
- Frau Dr. Elke Ströher nicht nur für die vielen gemeinsamen Stunden im Labor in netter Arbeitsatmosphäre sondern vielmehr dafür, dass du immer da warst! Danke!
- Annabel Steinfelder denn geteiltes Leid ist halbes Leid ;o) Vielen Dank für deine Unterstützung!
- Vielen Dank auch an alle ‚hinter den Kulissen‘: Sabine Voth, Denise Wittgrebe, Daniela Nagel, Senta Wegener und Janine Lichte: für euer Verständnis und den Ausgleich zum Laborleben; Wiebke Stärk und Ralf Dederichs für die spannenden Stunden beim Eishockey.
- Jörg Ulrich für die moralische Unterstützung, die kleinen und großen Aufheiterungen und dafür, dass du mich die ganze Zeit ertragen hast!
- Zuletzt und doch zu allererst meinen Eltern Gottfried und Roswitha Jacob und meinem Bruder Markus, für euren Rückhalt, euer Vertrauen und für die tausend (für mich ganz großen) Kleinigkeiten!

## **Erklärung**

Hiermit erkläre ich, dass ich die vorliegende Arbeit selbst angefertigt habe und nur die angegebenen Quellen und Hilfsmittel verwendet habe. Alle aus der Literatur ganz oder annähernd entnommenen Stellen habe ich als solche kenntlich gemacht.

Weiterhin erkläre ich, dass die vorliegende Dissertation weder vollständig noch teilweise einer anderen Fakultät mit dem Ziel vorgelegt worden ist, einen akademischen Titel zu erwerben. Hiermit bewerbe ich mich erstmals um den Doktorgrad der Naturwissenschaften der Universität Bielefeld.

Simone Jacob

Bielefeld, den 16. Dezember 2008